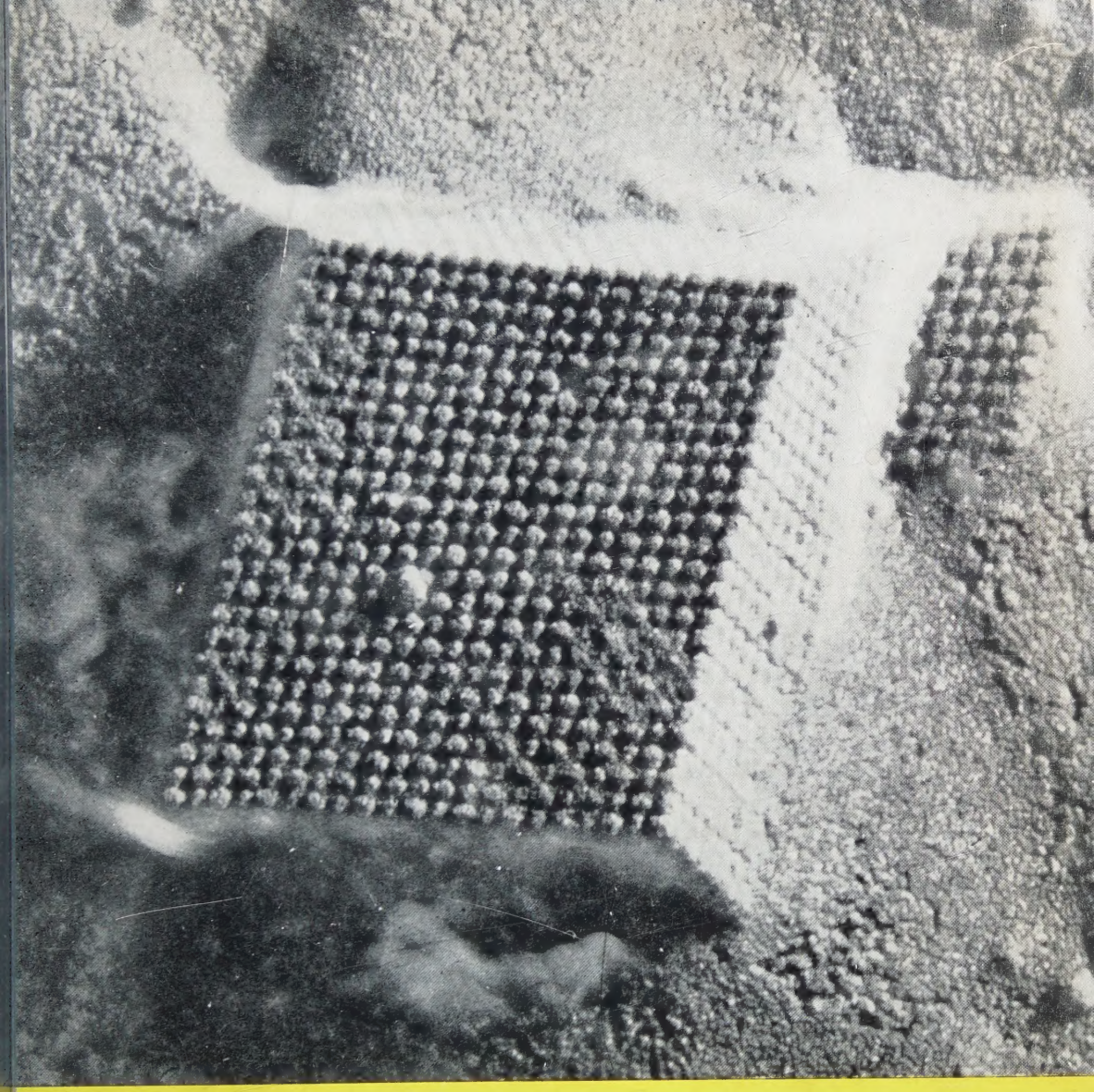

Journal of

Ultrastructure Research

Volume 2, Number 1

November 1958

Editors: FRITIOF S. SJÖSTRAND *Editor-in-Chief*

ARNE ENGSTRÖM

Academic Press Inc., Publishers, New York and London

Manuscripts as well as queries concerning details of editorial policy and rules regarding the preparation of papers should be sent to the Editorial Office, Journal of Ultrastructure Research, Department of Anatomy, Karolinska Institutet, Stockholm 60, Sweden

---

JOURNAL OF ULTRASTRUCTURE RESEARCH

PUBLISHED BY

Academic Press Inc., 111 Fifth Avenue, New York 3, N.Y., U.S.A.

Volume 1, 4 issues, $15.00

Subscription orders should be sent to the office of the publishers

---

Front cover: Electron micrograph showing a crystal of the rhombic type of tobacco necrosis virus. LABAW, L. W. and WYCKOFF, R. W. G., *J. Ultrastructure Research 2*, 9 (1958).

Prefixation Use of Hyaluronidase to Improve *in situ* Preservation for Electron Microscopy[1]

W. PALLIE and D. C. PEASE

School of Medicine, Department of Anatomy, University of California at Los Angeles, and Veterans Administration Center, Los Angeles, California

Received May 24, 1958

A brief, 2–5-minute exposure to relatively strong hyaluronidase in normal saline or Ringer solutions is regarded as a desirable prefixation treatment whenever connective tissue might be expected to retard the penetration of osmium tetroxide. The rapid physical effect of hyaluronidase was observed objectively following its topical application to exposed pial blood vessels which then quickly became dilated. Its effect on the subsequent penetration of osmic acid was assessed by the rate of darkening of underlying tissues. Following hyaluronidase prefixation treatment, arterial walls having as many as five layers of smooth muscle and a corresponding number of fenestrated elastic laminae were well preserved in all their thickness. Sweat glands embedded in dense connective tissue were uniformly fixed throughout blocks of moderate size. Comparison of material with and without hyaluronidase treatment did not reveal that any formed elements had been extracted or lost. No deleterious effects upon cytological preservation could be observed.

In recent years it has become apparent that osmium tetroxide is the general purpose fixative of choice for cellular material for electron microscopy. It is now commonly employed in either a buffered solution (*3*) and/or an isosmotic solution (*2*, *6*, *10*).

In principle the fixation procedure employed should bring the fixative into very rapid contact with living tissue. Penetration of a tissue block must be fast enough to insure that the deeper cells are exposed quickly to adequate amounts of fixative. Both Palade (*3*) and Sjöstrand and Rhodin (*8*), who first produced fixation of the quality we now recognize as the standard, emphasized that extremely minute blocks of tissue must be excised, if adequate preservation is to be achieved by this method. The problem is particularly acute with osmium tetroxide for, as light microscopists have known for generations, this substance has notoriously poor capacity for penetration. The difficulties have handicapped electron microscopists seriously when they have wished to fix tissues *in situ*, for organ capsules, and even basement membranes, may function as formidable barriers. Thus, Pease (*5*) emphasized the necessity of

[1] Supported by a grant from the United States Public Health Service.

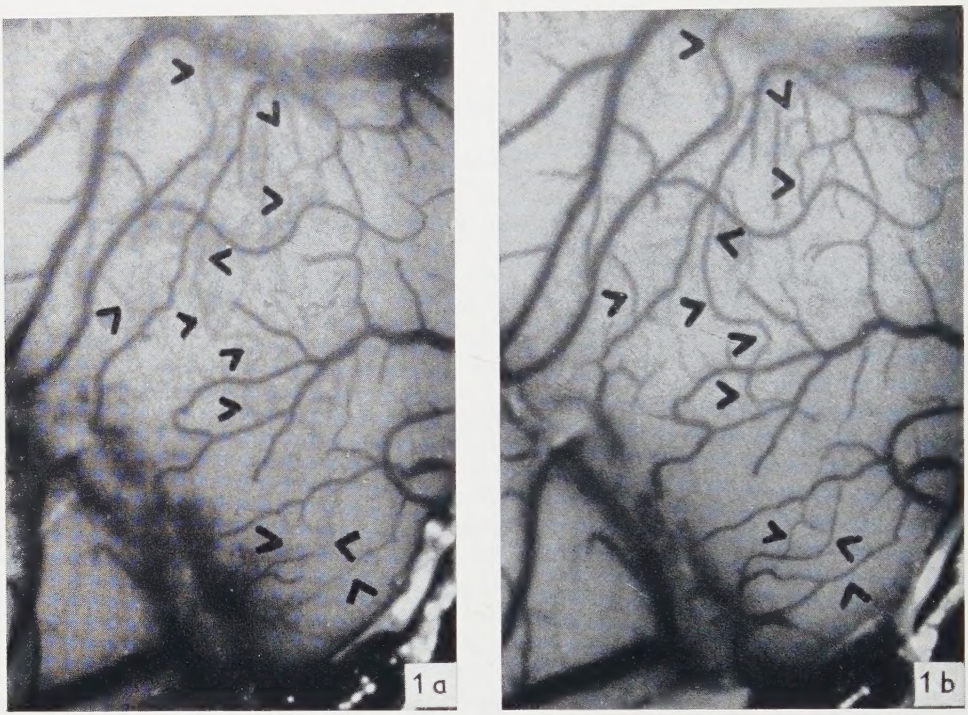

FIG. 1*a*. Pial vessels of an area of living cat's brain exposed by removing the arachnoid and more superficial layers while the animal was under pentobarbital anesthesia.
FIG. 1*b*. The same area following a 5-minute exposure to a "strong" hyaluronidase solution as described in the text. As a result of this treatment, arterial vessels become greatly dilated, an effect which is particularly evident when their vivid red color may be observed. Here the dilatation is most obvious in the smallest vessels at loci indicated by the arrows. Not only do the arterioles appear to have increased diameters after treatment, but their course may be straightened.

removing the capsule from the kidney to achieve adequate *in situ* preservation of its cortex. Likewise, Schultz, Maynard and Pease (7) achieved better preservation of cerebral cortex after removing the overlying pia. There are many situations, though, where the connective tissue cannot be removed mechanically, particularly in glandular organs where the parenchyma is diffusely embedded in much more or less dense stroma. In our own experience sweat glands have been a most difficult object to preserve adequately, presumably for this reason. Thus, even though an excellent fixative is now available to electron microscopists, its optimum use sometimes requires skill and ingenuity.

The enzyme, hyaluronidase, has been used effectively as a prefixative treatment with some dense tissues to aid the penetration of standard fixatives, as well as staining and impregnating agents employed in the preparation of tissues for conventional

FIG. 2. A relatively low power electron micrograph of a muscular artery whose media consists of five muscle layers. It was fixed well and uniformly by the topical application of osmium tetroxide after a 5-minute prefixation application of hyaluronidase solution. Micron marks accompany this and subsequent figures. × 12,500.

microscopy (*4*, *9*). Moreover, such preparations were reported to show minimal distortion when phase contrast appearances of living tissue were compared. It, therefore, seemed desirable to explore the use of this enzyme with connective tissues prior to their fixation by osmium tetroxide for electron microscopy. Becher and Hoegen (*1*) have, in fact, used hyaluronidase as a macerating agent to isolate individual cells which were then examined as whole mounts by electron microscopy. No doubt their technique would have been too harsh for the quality preservation desired for modern work with sections, but they were aware of the possibility of this usage.

We were particularly anxious to have objective criteria, first, of a physical effect of hyaluronidase on the tissue concerned, and second, of an improved penetration of osmium tetroxide. Naturally, too, we were concerned with adverse side effects that might result from the treatment. The *in situ* preservation of middle-sized arteries in living animals afforded a reasonably dramatic demonstration of the effectiveness and usefulness of hyaluronidase.

A major project in this laboratory has concerned itself with the structure of intracranial arteries in cats, dogs and monkeys. Our standard procedure has been to remove a large temporal bone flap of animals under sodium pentobarbital anesthesia. Then the dura and arachnoid layers are cut away, exposing the pial vessels. The blood vessels then have been fixed *in situ* most commonly by percolating buffered osmium tetroxide solutions through a thin cotton pad laid upon the pial surface. Usually fixation has been continued for half an hour before undercutting the tissue. Subsequently, during dehydration stages the vessels are isolated and trimmed. In general the deeper layers of the larger vessels have not been well preserved by this treatment.

If a brief prefixation treatment with a solution of hyaluronidase is employed, an immediate effect upon the blood vessels can be observed visually, and subsequent electron microscopy demonstrates that quite large vessels are well and completely fixed. We use lyophilized hyaluronidase[1] dissolved in 2–10 ml of normal saline or Ringer solution, although probably this is an unnecessarily strong solution. It is percolated through a thin cotton pad on the pia for a period of not more than 5

[1] "Wydase", 150 U.S.P. (TR) units, manufactured by the Wyeth Laboratories, Inc., Philadelphia, Pa.

FIG. 3. Part of the media of a muscular artery prepared as described but with the addition of phosphotungstic acid to heighten the contrast of certain elements. The connective tissue framework of the artery, as well as cytological detail in the muscle, was well preserved. *b.m.*, basement membrane; *coll.*, collagen; *elast.*, elastin; *nuc.*, nucleus. × 23,500.

FIG. 4. Endothelial cells well preserved in spite of the fact that fixative had to penetrate through a substantially thick media, and the thick internal elastic membrane visible here. An area demonstrating pinocytotic vesicles at the surface of a muscle cell is encircled. × 31,000.

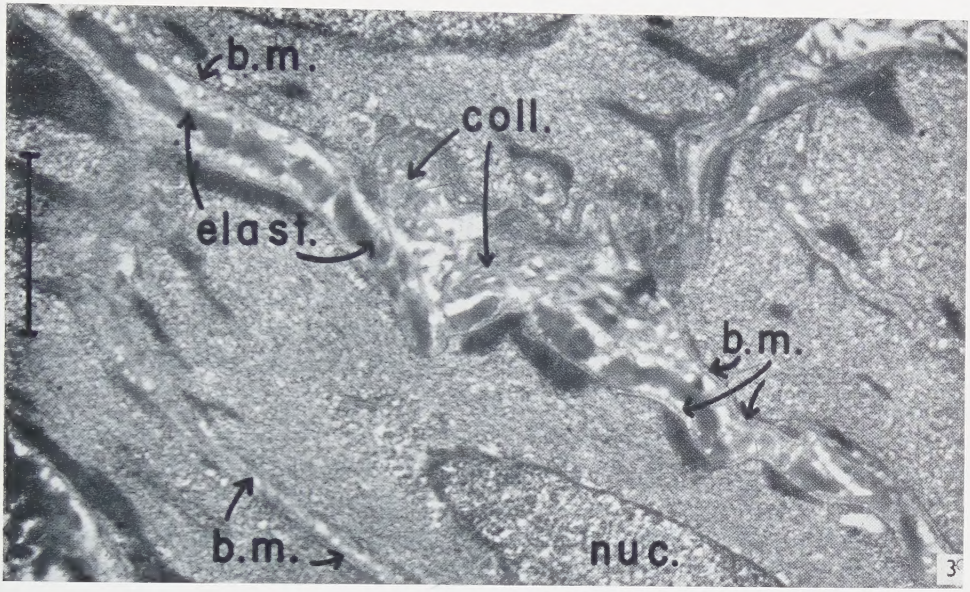

3

4

minutes before fixation is begun in the usual manner.[1] A dramatic result which can be observed directly after this topical application of the enzyme solution is the marked dilatation of blood vessels. To some extent this is shown in black and white in Fig. 1 in which numerous small vessels hardly visible before the enzyme treatment became obvious channels of substantial size after treatment with hyaluronidase. In life the dilatation is startingly evident, for it affects large as well as small vessels which then become brilliantly red during the treatment. The course of the reaction may be gauged by this color change, and two or three minutes exposure to hyaluronidase is all that is necessary to produce the effect. When fixation subsequently is commenced with osmium tetroxide, it can also be observed that the blackening of the tissues occurs more rapidly than usual. This is particularly evident in the underlying nervous tissue of the cerebral cortex.

The final evaluation of tissue preservation cannot be done entirely without subjective opinion. Fig. 2, however, reproduces a transverse section of an arterial wall at low magnification which demonstrates good fixation of the deepest layers in spite of the fact that the fixative had to penetrate through five successive layers of smooth muscle and, additionally, through or around the fenestrated elastic membranes and other connective tissue components between each of these layers. The authors know of no comparable micrograph of a well-preserved, medium-sized artery in the literature. Indeed, the paucity of publications dealing with muscular arteries is suggestive of the special difficulties people may have had with these structures.

From studies of arteries alone, we have no doubt that hyaluronidase improves the penetration of osmium tetroxide fixative solutions, but additionally we have had experience with other tissues. Cerebral cortex has been studied in this laboratory by Schultz, Maynard and Pease (*7*). Under normal circumstances the pia and/or its underlying basement membrane is a substantial barrier to its *in situ* preservation. Previously, we felt obliged to strip away the pia in order to obtain adequate preservation of the underlying nervous tissue. In the preparations described above, however, we often have observed, incidentally, cortical tissue sectioned with the arteries. Invariably this has been well preserved if reasonably near the surface. Another example that might be cited concerns the efforts of one of us (D. C. P.) over a period of several years, to preserve adequately sweat glands from the rat foot pad. These are embedded in a mass of dense collagenous tissue. Although tantalizing bits of

[1] It seems likely that blood plasma and/or tissue exudate quickly destroys the effectiveness of hyaluronidase. In applying a hyaluronidase solution, therefore, it is essential that exudates be wiped away or flushed with excess hyaluronidase solution before the final topical application of the wet pad. In practice we are careful to begin with a reasonable dry field, and usually we replace the first hyaluronidase pad with a second one after the first minute or two of application. We have also had the experience of having the hyaluronidase effect on vasodilation blocked by the previous application of Ringer solution. We, therefore, avoid washing exposed surfaces before the topical application of hyaluronidase.

gland were found well preserved from time to time, consistent results were not obtained until hyaluronidase prefixation treatments were employed. Then it was not difficult to obtain moderately large masses of gland uniformly fixed throughout the block.

The action of hyaluronidase is presumably one of liquifying tissue mucopolysaccharides. We have sought in our micrographs to find evidence of the destruction of organized macromolecular aggregates, but without success. Fig. 3 shows part of the tunica media of a muscular artery. It is quite apparent that collagen, elastin and the material of basement membranes have all survived the treatment. Similarly, the formed connective tissue elements about sweat glands including their basement membranes are seemingly unaltered. Indeed, as far as we can see by comparison with untreated material, nothing is missing. The mucopolysaccharides that constitute the osmium tetroxide barrier must be so diffusely distributed that their depolymerization does not detract from the visualization of the formed elements that remain. They must be, in effect, the "background material".

We have been unable to detect any adverse cytological effect of the hyaluronidase pretreatment. Thus, the smooth muscle in Fig. 3 is well preserved, as are also the endothelial cells of Fig. 4, although these cell types are not sufficiently complex to be altogether satisfactory test objects. Sweat glands are cytologically specialized in several ways. Their apical surfaces have microvilli, there are secretion droplets within their cytoplasm, and the basal surface is elaborately infolded to increase its area. All of these features, as well as those of the usual organelles, are seemingly unaffected by the hyaluronidase treatment.

Thus, we have come to employ hyaluronidase solutions before fixation whenever we suspect that a connective tissue barrier may hinder the rapid penetration of osmium tetroxide.

REFERENCES

1. Becher, H. and Hoegen, K., *Z. wiss. Mikroskop.* **62**, 41 (1954).
2. Caulfield, J. B., *J. Biophys. Biochem. Cytol.* **3**, 287 (1957).
3. Palade, G. E., *J. Exptl. Med.* **95**, 285 (1952).
4. Pallie, W., Corner, G. W. and Weddell, G., *Anat. Record* **118**, 789 (1954).
5. Pease, D. C., *Anat. Record* **121**, 701 (1955).
6. Rhodin, J., Correlation of Ultrastructural Organization and Function in Normal and Experimentally Changed Proximal Convoluted Tubule Cells of the Mouse Kidney. Thesis. Stockholm, 1954.
7. Schultz, R. L., Maynard, Edith A. and Pease, D. C., *Amer. J. Anat.* **100**, 369 (1957).
8. Sjöstrand, F. S. and Rhodin, J., *Exptl. Cell Research* **4**, 426 (1953).
9. Weddell, G. and Pallie, W., *Quart. J. Microscop. Sci.* **95**, 389 (1954).
10. Zetterqvist, H., The Ultrastructural Organization of the Columnar Absorbing Cells of the Mouse Jejunum. Thesis, Stockholm, 1956.

The Electron Microscopy of Tobacco Necrosis Virus Crystals

L. W. LABAW and R. W. G. WYCKOFF

National Institute of Arthritis and Metabolic Diseases,
National Institutes of Health,
Public Health Service,
Department of Health, Education, and Welfare,
Bethesda 14, Maryland

Received May 27, 1958

Earlier electron microscopic studies of crystals of the tobacco necrosis viruses have been extended with the help of carbon replication.

Two types of crystal have been observed in different preparations. One (the octahedral) is apparently cubic in symmetry but with a platy habit due to the development of a pair of large (111) faces. The molecules appear to be cubic close-packed with a tetramolecular unit having $a_0 = 370$ Å. The rhombic type has less than cubic symmetry. Unlike the crystals previously studied, none of its faces has all molecules in exactly the same plane. Attention is drawn to the granular nature of the molecules and to the kinds of molecular disorder apparent in these crystals.

Electron micrographs were published several years ago showing the molecular order to be seen on the surface of crystals of a tobacco necrosis virus protein (*5*). Since then the methods for making preparations of such protein crystals (*3*) have been greatly improved through the introduction of evaporated carbon films (*2*, *6*). The better photographs to be obtained by applying these newer methods to certain tobacco necrosis virus crystals are described below.

The materials used here have consisted of several purified virus preparations supplied for the earlier work by Dr. K. M. Smith, Director of the Virus Research Unit of the Agricultural Research Council in Cambridge, England. They are of more than one type and yield crystals of different symmetry and habit. Unfortunately the preparations are now too old to permit the closer correlation of crystalline structure and specific viral activity ultimately to be desired.

The molecular particles in all the preparations studied have been spheres with a diameter of ca 250 Å. Most commonly the crystals have been the flat, rhombic plates photographed earlier (*5*). A typical example with its dominant face nearly square in outline is shown in Fig. 1. In view of their general habit and relatively low symmetry, these crystals are designated as being of the rhombic type.

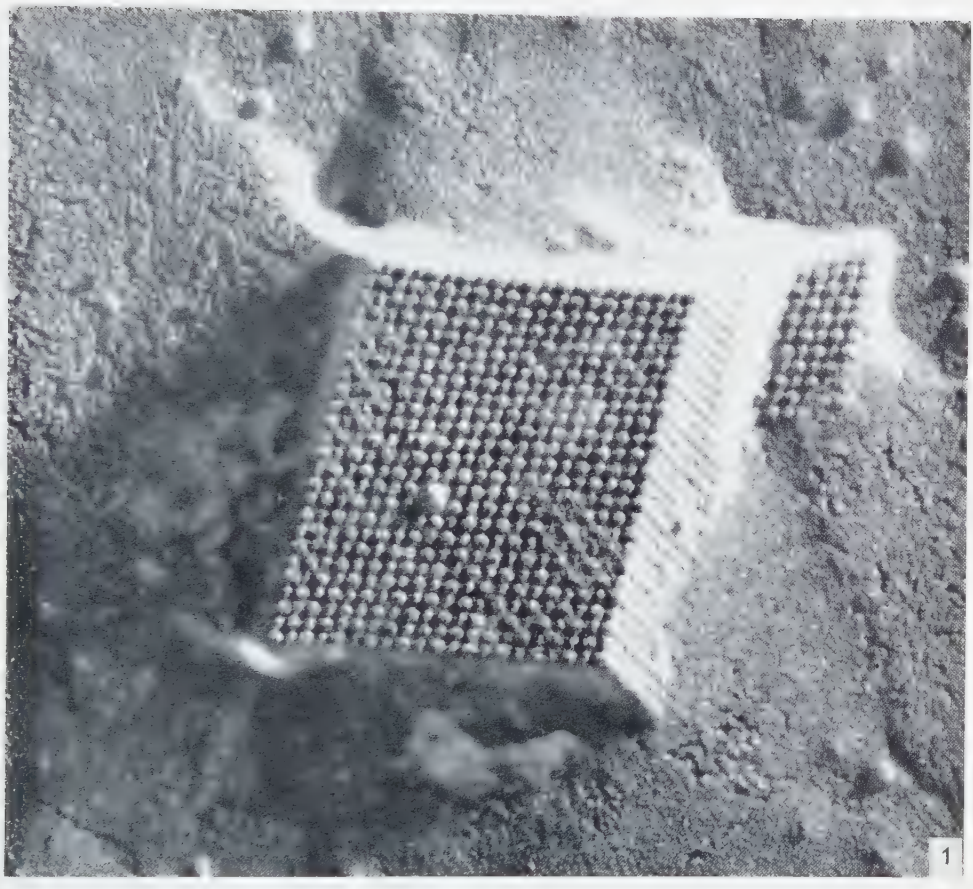

FIG. 1. A crystal of the rhombic type of tobacco necrosis virus in which the molecular order is unusually good. × 84,000.

Fig. 2 illustrates the second kind of tobacco necrosis virus crystal. These isotropic crystals are dominated by a pair of large (111) faces and it is therefore convenient to refer to them as of the octahedral type. Crystals of the octahedral type have never been seen in microscopic preparations made from the purified virus preparations which we have that give the rhombic type crystal. The frequency of occurrence of the rhombic type in microscopic preparations made from the purified virus preparations on hand which give predominately the octahedral type crystal is less than 10%. This is comparable to that shown in the optical micrograph opposite page 132 of Dr. Smith's book (*7*). It therefore seems possible that they are characteristic of two biologically distinct viruses. Both types of crystal grow from purified solutions

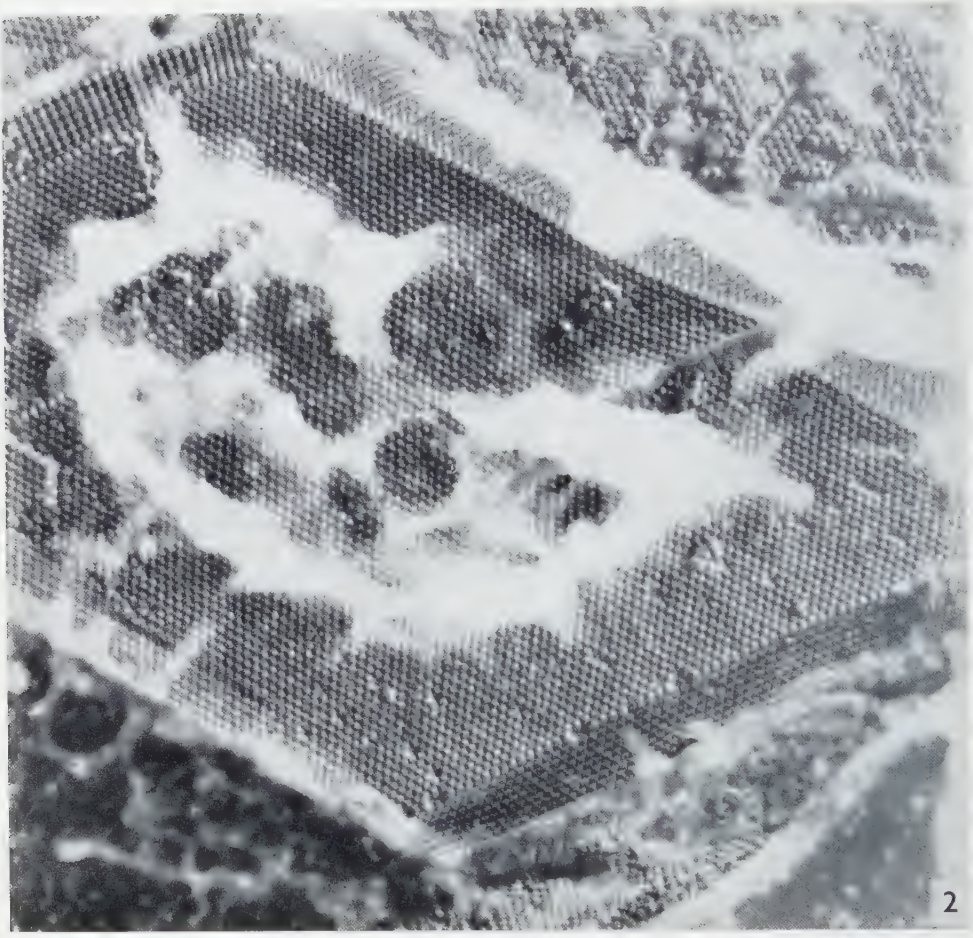

Fig. 2. A larger crystal of the octahedral type of tobacco necrosis virus. The opaque regions on the top face are due to adhering, undissolved parts of the crystal. × 53,500.

that are approximately 20% saturated with respect to ammonium sulfate under essentially the same conditions required for many other plant virus proteins, i.e., storage in the icebox at ca 4°C (*1*, *7*).

Photographs made of a large number of the octahedral type crystals and measurements on them indicate that the molecular arrangement is the cubic close packing already found for several proteins and virus proteins. Though the dominant faces have always been (111), smaller (100) and (110) faces are also present. The (111) and (100) faces are to be recognized by their planar close-packed hexagonal and

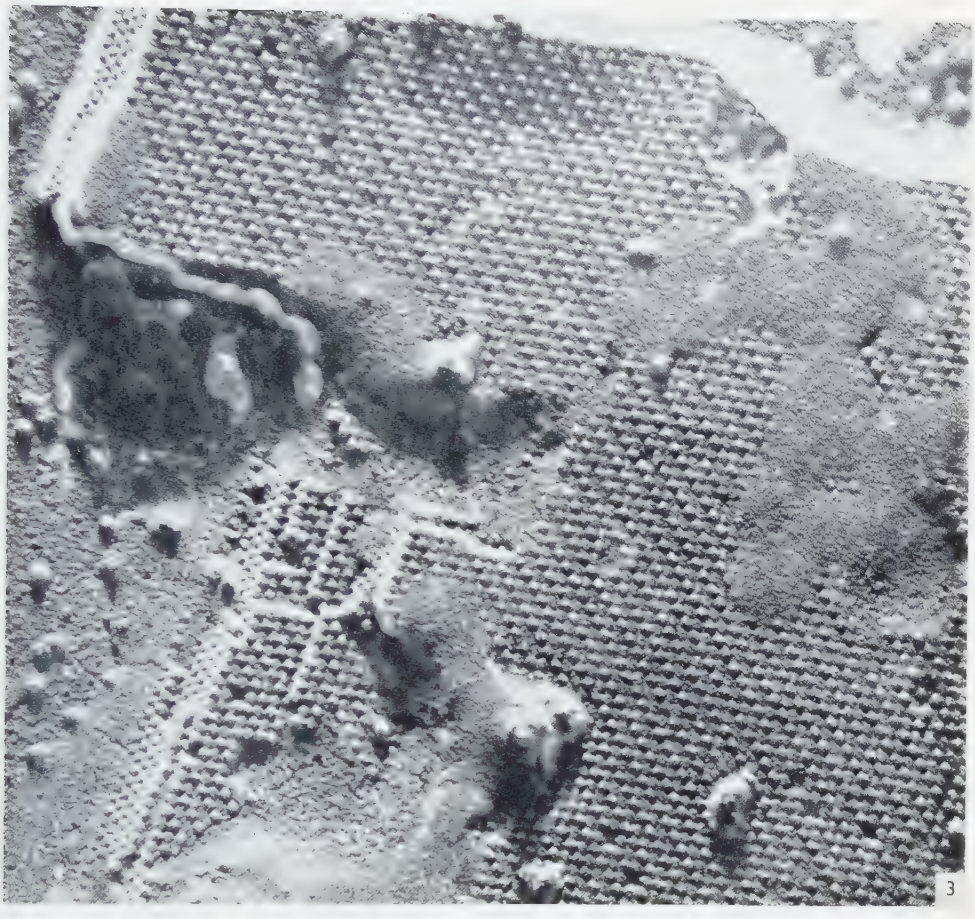

FIG. 3. Part of a crystal of the rhombic type to which more salt is adhering. The diagonal molecular rows brought out by this salt are clear. × 63,500.

cubic molecular nets; the (110) faces have rows of contacting molecules separated from one another by $\sqrt{2}$ times the molecular diameter. Unlike crystals of the southern bean mosaic virus (*4*), faces with crystallographically complex indices have not been observed. Measurements of molecular separations have been made on both the (111) and the (100) faces to establish the dimensions of the unit cell. Even with a cubic crystal such measurements can be constant in different directions only if a face is exactly normal to the axis of the microscope. As a result most measured molecular separations will be less than the true molecular diameter. This limitation inherent in

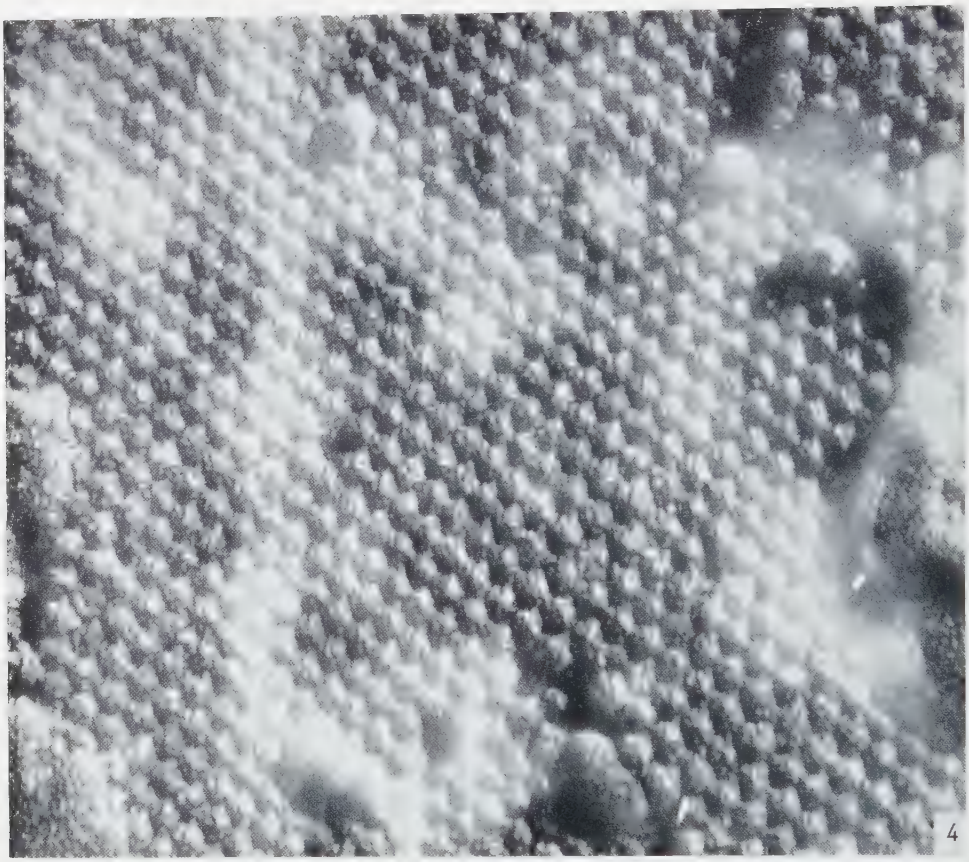

FIG. 4. A small portion of the principal face of an octahedral type crystal seen at the higher magnification that shows the granular texture of each molecule. × 190,000.

electron microscopic measurements must always be borne in mind when deducing from them the molecular dimensions and symmetry of a crystal. In the present case the average molecular separation measured on several crystals which seemed to have faces parallel to the photographic plate was ca 245 Å. The maximum value, which should approximate the true separation, was for each of these crystals close to 260 Å; this corresponds to a tetramolecular close-packed unit having the edge length 370 Å.

The lower symmetry of the rhombic type crystals is evident in all electron micrographs made of them. The rhombus that outlines the principal face of Fig. 1 has angles of ca 80° and ca 100° and its molecules do not form an exactly square and coplanar net. On the right side face of Fig. 1 the molecules of alternate vertical rows stand out above the others. Differences in molecular height can be detected also on

Fig. 5. Part of a crystal of the octahedral type showing a defect in molecular order that extends up and down the middle of the photograph. × 81,000.

the principal face of this crystal by viewing the photograph in the direction of the face diagonal striking its obtuse angle. If appreciable quantities of salt remain on the crystal (Fig. 3) this molecular alternation on the principal face is seen more clearly. The additional observations and measurements needed to establish the more complicated molecular arrangement of these crystals are now being made; the resulting structure will be described later.

A particularly interesting feature of the molecules on all these tobacco necrosis virus crystals has been their well-defined granular texture even on the cleanest attainable crystal faces. The significance of this granularity, which is noticeable though less marked on crystals of other proteins grown from strong salt solutions, is not entirely clear. Fig. 4, which shows part of a crystal face at high magnification, suggests

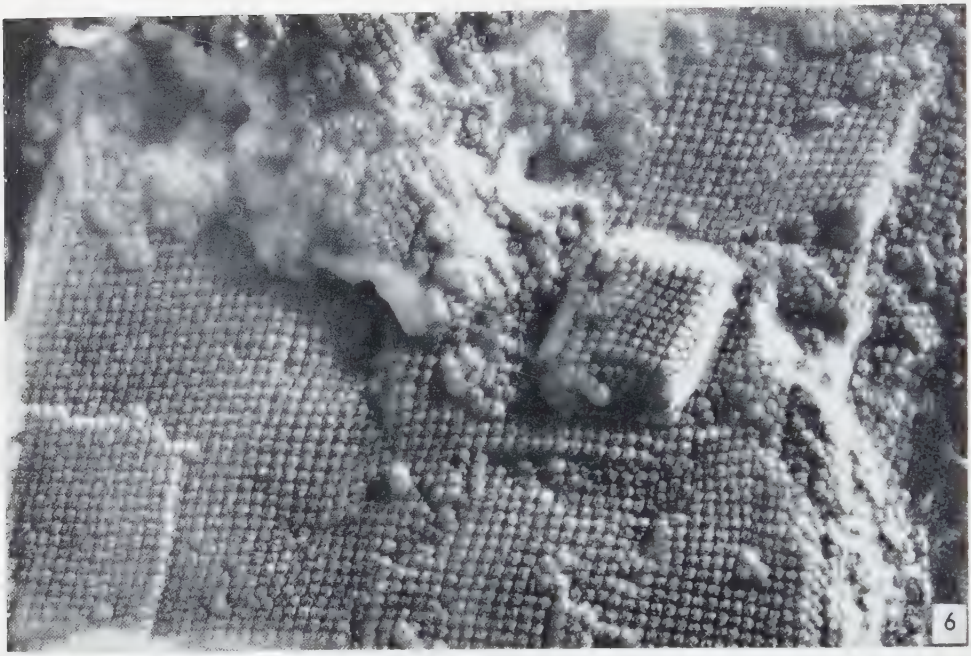

FIG. 6. Part of a crystal of the rhombic type upon which several defects in molecular order are clearly visible. × 69,000.

that it cannot be attributed to a polyhedral shape such as is possessed by the larger particles of a *Tipula paludosa* virus (*8*). It may be due to the salt that probably is an essential ingredient of these crystals. A number of photographs have been closely examined to see if the granularity is regularly repeated on neighboring molecules. This has not been the case over large areas of a crystal face though small regions have been found which may be the remains of such a repetition.

The crystals of these two forms of the tobacco necrosis virus differ noticeably in the perfection of their molecular order. Many more imperfections of the sort apparently so important to the growth of crystals composed of small molecular particles have been noted in the rhombic type of crystal. Nevertheless such a defect as that visible in the middle of Fig. 5 is encountered in the octahedral type crystals: it appears to be the surface manifestation of a dislocation whose internal course can be traced downwards for a considerable distance along molecular layers of the lower (111) face.

Few crystals of the rhombic type are entirely without defects. Some produce the pitted, undulating appearance of such a face as that of Fig. 6. Others are more or less typical dislocations. One of these is presumably responsible for the tilt in the upper right part of the crystal of Fig. 6. Another may be the cause of the molecular

skewing of the square overgrowth below and to the left of this elevation. Still others within the body of the crystal may result in the additional imperfections below the overgrowth. Occasionally such growths on the large otherwise flat crystalline faces may take the form of terraces that, as in a picture already published (*9*), give the impression of a spiraling dislocation.

REFERENCES

1. Bawden, F. C., Plant Viruses and Virus Diseases. Chronica Botanica Company, 1950.
2. Bradley, D. E., *Brit. J. Appl. Phys.*, **5**, 65, 96 (1954).
3. Labaw, L. W. and Wyckoff, R. W. G., *Exptl. Cell Research* **3**, Suppl., 395 (1955).
4. —— *Arch. Biochem. Biophys.* **67**, 225 (1957).
5. Markham, R., Smith, K. M. and Wyckoff, R. W. G., *Nature* **159**, 574 (1947).
6. Robert, L., Bussot, J. and Buzon, J., 1[er] *Congr. intern. microscopie électronique*, *Paris*, 1950, p. 528.
7. Smith, K. M., Recent Advances in the Study of Plant Viruses. J. and A. Churchill Ltd., 1951.
8. Smith, K. M. and Williams, R. C., *Endeavour* **17**, 12 (1958).
9. Wyckoff, R. W. G. and Labaw, L. W., Les techniques récentes en microscopie électronique. *Colloq. intern. centre natl. recherche sci., Toulouse*, 1955, p. 135.

The Carbon Replica Technique in the Study of the Ultrastructure of Leaf Surfaces

B. E. JUNIPER and D. E. BRADLEY

Department of Botany, University of Oxford, and Research Laboratory, Associated Electrical Industries Limited, Aldermaston Court, Aldermaston, Berks.

Received June 20, 1958

The surface properties of leaves may be a contributory factor in the efficiency of action of the variety of chemicals which are applied to foliage.

The examination of leaf surfaces in the electron microscope by carbon replicas reveals many different structures. These appear to confirm measurements made on the relative wettability of the surfaces.

The possible causes of the variation of these structures over a single leaf in the case of field specimens are discussed, and the effects of variations in environmental conditions, achieved in the growth cabinet, on the leaf surface are demonstrated.

In recent years, considerable attention has been paid to the characteristics of leaf surfaces. The efficiency of weedkillers, insecticides and fertilizers applied to foliage may all depend on the adhesion of water droplets on the leaf surfaces, and thus ultimately on the leaf surface itself.

There exists a continuous gradation between leaf surfaces which, for all practical purposes, are completely wettable, to ones which are unwettable. By the normal techniques of light microscopy, no morphological difference can be seen to account for these differences in behaviour, even between the extremes of this series.

The carbon replica technique (*1*, *2*) reveals on leaf structures an interesting diversity of submicroscopic structures which supports observations made on their response to wetting.

THE REPLICA TECHNIQUE

Relatively little work has been carried out on leaf surfaces using the electron microscope. Unless thin sections are used, it is necessary to employ some form of replica method. Mueller *et al.* (*4*) and Schieferstein and Loomis (*5*) have used a double-stage plastic replica method which, in the light of current work, may be unsatisfactory in certain cases. The reason for this is that many leaves are covered with

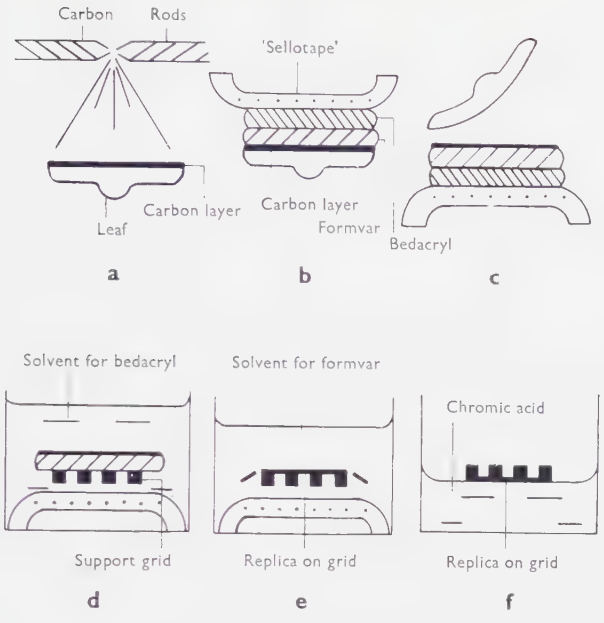

FIG. 1

a layer of wax, and the method of Mueller *et al.* involves the wetting of the surface with a neutral wetting agent, which must dissolve the wax and destroy some of the surface structure of the leaf. This seems to be borne out by their results. The method described here avoids the difficulty of having to wet the surface by employing evaporated carbon as the material for the single-stage replica. The technique is described with reference to Fig. 1.

The leaf is cut into pieces of convenient size, and mounted on a glass slide with cellulose adhesive tape. The slide is placed in a vacuum chamber and about 15 mμ of carbon is deposited in the usual way (*1*; Fig. 1*a*). The leaf is then removed from the vacuum and the carbon film is backed with two layers of plastic. The first, *Formvar*, is deposited from a 2% solution in chloroform and the second, *Bedacryl 122X*, from a 5–7% solution in benzene. When thoroughly dry, a strip of cellulose adhesive tape is now pressed onto the *Bedacryl* layer (Fig. 1*b*). The leaf can now be pulled away from the tape, leaving behind the combined carbon and plastic film (Fig. 1*c*). In some cases, it is necessary to freeze the assembly to facilitate the removal of the leaf. Next, the tape is placed in a bath of acetone which dissolves the *Bedacryl*, thus releasing the *Formvar*/carbon layer. A specimen support grid (3.05 mm, 200 mesh/in) can now be slipped between the tape and the *Formvar*/carbon film (Fig. 1*d*). The strip of tape with the grid in position, as described, is removed from the acetone and

allowed to dry. The grid can then be lifted from the tape without damaging the overlying film. The *Formvar* is finally washed away in a chloroform bath (Fig. 1*e*), or by any other suitable washing method, leaving the carbon replica on the grid. It is sometimes necessary to clean this in a bath of chromic acid (Fig. 1*f*) to remove any dirt picked up from the leaf. The replica is finally shadowed at a fairly high angle (45° is suitable).

Two interesting points arise from this method. Firstly, the leaf does not gas sufficiently in the vacuum to prevent the proper deposition of the carbon, which requires a pressure of less than 10^{-3} mm of mercury. This is probably explained by the fact that the cutin/wax layer effectively seals the leaf except for the stomatal and petiolar apertures and where it has been cut. But for this the method would probably fail. The second point is that the backed carbon layer does not adhere strongly to the leaf, and the stripping process is easily carried out. This could be explained by the partial softening of the wax layer, by the solvents used in the backing plastics, and by the wax/cell wall interface forming a natural fracture layer on the leaf surface.

The method is simple and reliable and there are no obvious inconsistencies between the results and such evidence as is given by the light microscope.

INTERPRETATION OF THE ELECTRON MICROGRAPHS

The technique described above produces two different types of specimen, either a true replica or a pseudo-replica. The latter consists of a carbon replica with some or all of the original surface protrusions from the leaf embedded in it. Treatment with chromic acid and strong organic solvents may remove much of the undissolved wax layer. However the distinction is academic and a pseudo-replica may be as informative as a true replica. An example is shown in Fig. 2. The actual undissolved portions of such a replica will appear as dense white regions in a negative print. In both cases white outlines to features are caused by large vertical thicknesses in the carbon film and must be interpreted accordingly.

THE SUBMICROSCOPIC MORPHOLOGY OF LEAF SURFACES

Marked structural differences can be detected between surfaces which are wettable and those which are not. The former generally appear to be smooth as in *Rumex obtusifolius* (Fig. 3*a*), or covered with coarse ridges or undulations arising under the actual surface as in *Aesculus hippocastanum* (Fig. 3*b*). The character of such surfaces would not lead one to expect that there would be any difficulty in wetting them,

---

FIG. 2. *Kleinia articulata*. Shadowed 2:1 with palladium. ×15,500.
All micrographs represent carbon replicas of the adaxial leaf surfaces of the species listed.

and it seems likely that they are most susceptible to the effects of fertilizers, weed-killers etc. applied to the foliage.

Surfaces which are difficult to wet have been found to show a great variety of structures. These range from the "tooth paste" forms of *Chrysanthemum segetum* (Fig. 6*b*) to the "loofah" tubes of the *Brassicas* (Fig. 4) and the delicate forms found on the surface of *Kleinia articulata* (Fig. 2). The leaf of *C. segetum* is particularly resistant to wetting and the plant to herbicides in general, presumably due to the trapping of air between the spray droplets and the leaf surface, by the wax blanket. It is important to note, however, that none of these structures could be resolved by conventional techniques in the light microscope.

These structures are surprisingly uniform over the surface of a leaf. Comparison of plants living in a growth cabinet with plants living outside seems to indicate that the surfaces of field material are often damaged, and that microclimatic changes affect the wax structures. The kind of field variation observed is shown in the adaxial surface of a leaf of *Trifolium pratense* (Fig. 5*a*). There are, however, minor changes in the leaf surface, even under controlled conditions, which require explanation. Fig. 5*b* shows part of the adaxial surface of young *Hordeum sativum*. Stripes about 30 μ long by 1 μ wide, of which the illustration is a part, occur frequently on the surface parallel to the long axis of the leaf. It seems unlikely that so narrow a region could be caused by mechanical damage and it is possible that the difference is caused by the lateral stretching of the wax layer during growth. Variation may also occur in the vicinity of stomata. An example of this is shown in the micrograph of a stoma of garden pea, *Pisum sativum*, variety *Alaska* (Fig. 5*c*). The wax platelets are more sparsely distributed than over the rest of the surface.

Differences have also been found between the abaxial and adaxial surfaces of leaves. As far as the present work goes, these are usually differences of degree and could as previously mentioned be the result of microclimatic variation between the lower and upper surfaces.

The response of the leaf to changes in environmental conditions is rapid and striking. Fig. 7*a–c* show the result in peas of reducing the light intensity from approximately 5000 ft. candles, 460 lux, (full summer daylight 7000–8000 ft. candles) to 400 ft. candles, 36 lux. The wettability is also increased with reduced light. Moreover, after being grown in total darkness, when virtually no wax structures are developed, a pea leaf returned to light can change to a condition similar to that in Fig. 7*a* within seven days. Similarly recovery from mechanical damage has been observed in *Chrysanthemum segetum*. Fig. 6*a* shows a severely damaged surface of

---

FIG. 3. *a: Rumex obtusifolius*. Shadowed 2:1 with gold/palladium. *b: Aesculus hippocastanum*, young. Shadowed 2:1 with gold/palladium. 7750 (Fig. 3*a*); 3900 (Fig. 3*b*).


a


b

Fig. 4. *Brassica oleracea* var. *capitata*. Cabbage, *January King*. Shadowed 1:1 with palladium. × 15,250.

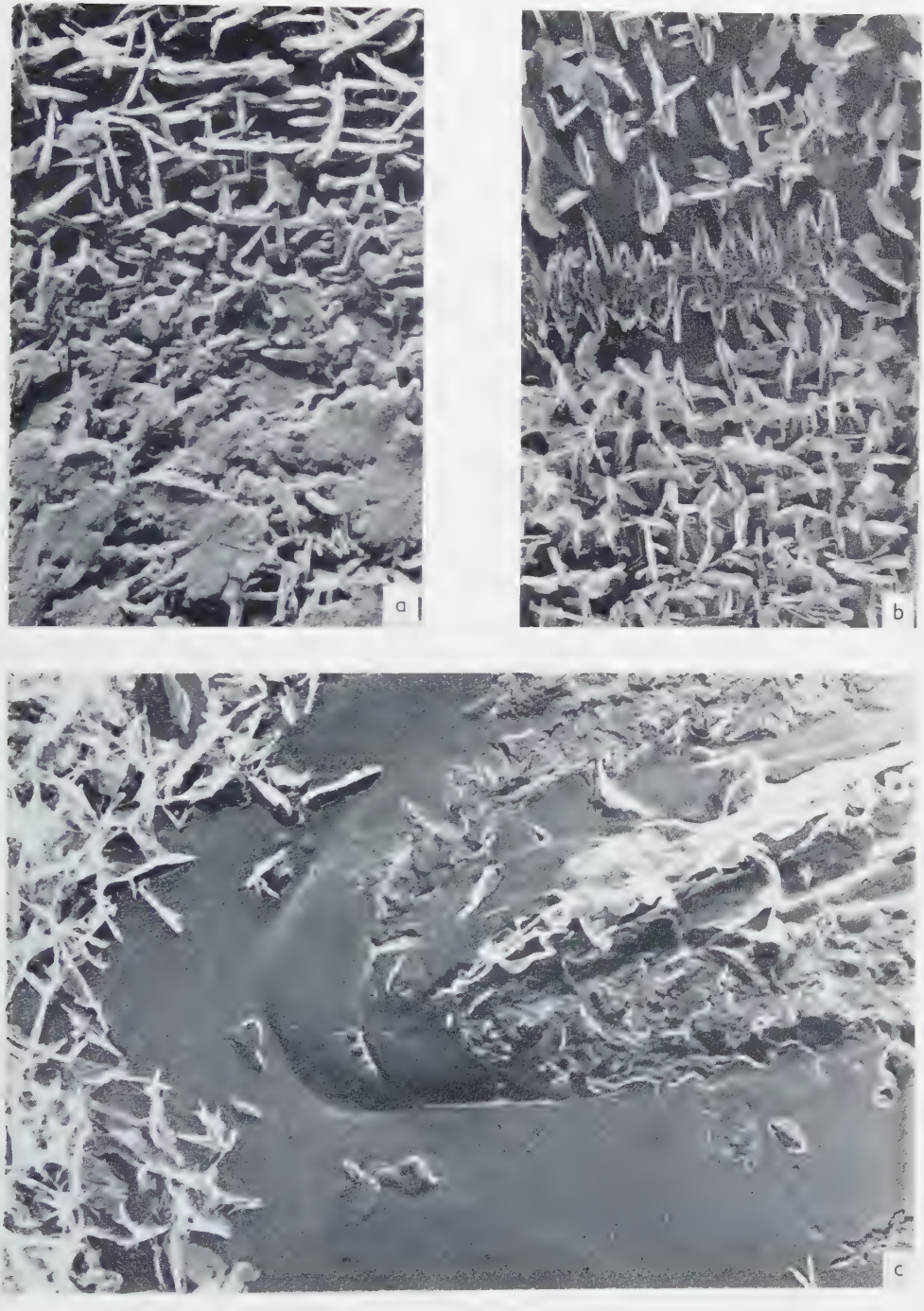

Fig. 5. *a: Trifolium pratense*. Shadowed 2:1 with gold/palladium. *b: Hordeum sativum*. Shadowed 1:1 with palladium. *c: Pisum sativum* variety *Alaska*. Shadowed 1:1 with palladium. ×7650.

a leaf immediately after brushing with a squirrel-hair brush. Fig. 6*b* shows the surface of the corresponding leaf damaged in a similar fashion and completely recovered within fourteen days.

A common agricultural technique practised in conjunction with the use of other herbicides is to treat the soil prior to, or after germination with low doses of trichloracetic acid (*T.C.A.*) or 2,2-dichlorpropionic acid (*Dalapon*). One effect of this is to make certain plant species, in particular some serious agricultural weeds, more susceptible to herbicides. The effect under the electron microscope is a progressive reduction in size and density of the wax structures on the surface with an increase in the concentration of the *T.C.A.* or *Dalapon* (*3*). There is also a corresponding fall in the contact angle, which is a measure of wettability, of up to 75 . The concentration can be increased until no wax structures can be found at all under the electron microscope. The effect of a low concentration of *Dalapon*, the equivalent of 0.68 kg/ha is shown in Fig. 7*d*. The fall in contact angle from the control was 145° to 135°.

The method of formation of these structures is not known. No pores or apertures have ever been resolved, nor would one expect them since the movement and growth of the wax almost certainly take place when it is plastic. Their chemical composition is also uncertain, except in so far as they behave like wax under the attack of specific solvents. In one instance, *Kleinia articulata*, there are indications that the structures are also soluble in water.

CONCLUSION

The technique so far developed would seem to be adaptable to other biological surfaces, except those possessing obvious protrusions or hairs, which break up the carbon film. It has the advantage that it can be used on "wet" material without apparently decreasing its efficiency. The carbon film itself is capable of resolving detail down to the 1 mμ level which is superior to the resolving power of many electron microscopes at present in use. It seems capable of resolving the most delicate structures on leaf surfaces, and the only possible introduction of artefacts would seem to be caused by shrinkage of the leaf consequent upon the evacuation of the bell-chamber.

The ultrastructure of the leaf surfaces so far studied would seem to be in complete agreement both with the observations made on their resistance to wetting and mechanical damage.

It is possible that the differences and changes in structure of the kind outlined here may be of value in selecting and developing chemicals for foliar application.

Fig. 6. *a: Chrysanthemum segetum.* Immediately after brushing. Shadowed 1:1 with palladium. *b: Chrysanthemum segetum.* Corresponding leaf after fourteen days. Shadowed 1:1 with palladium. 7650.

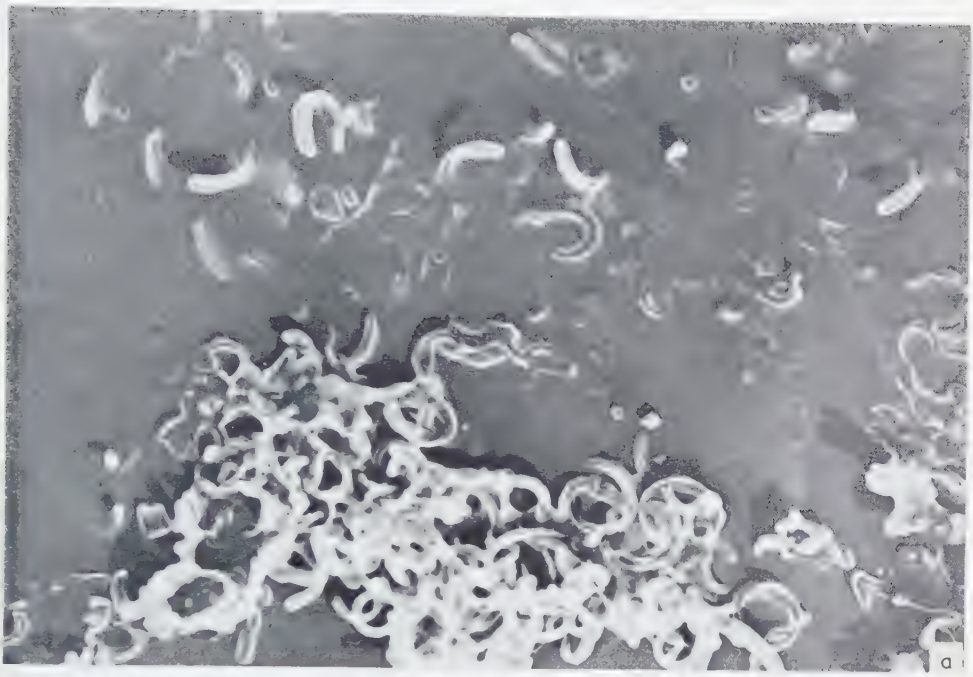
a

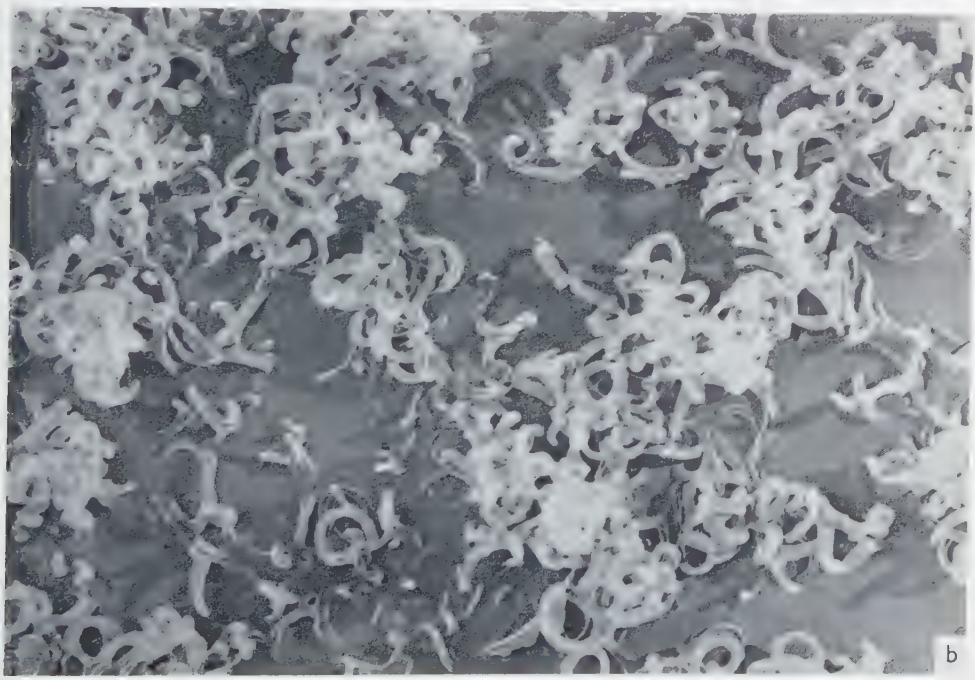
b

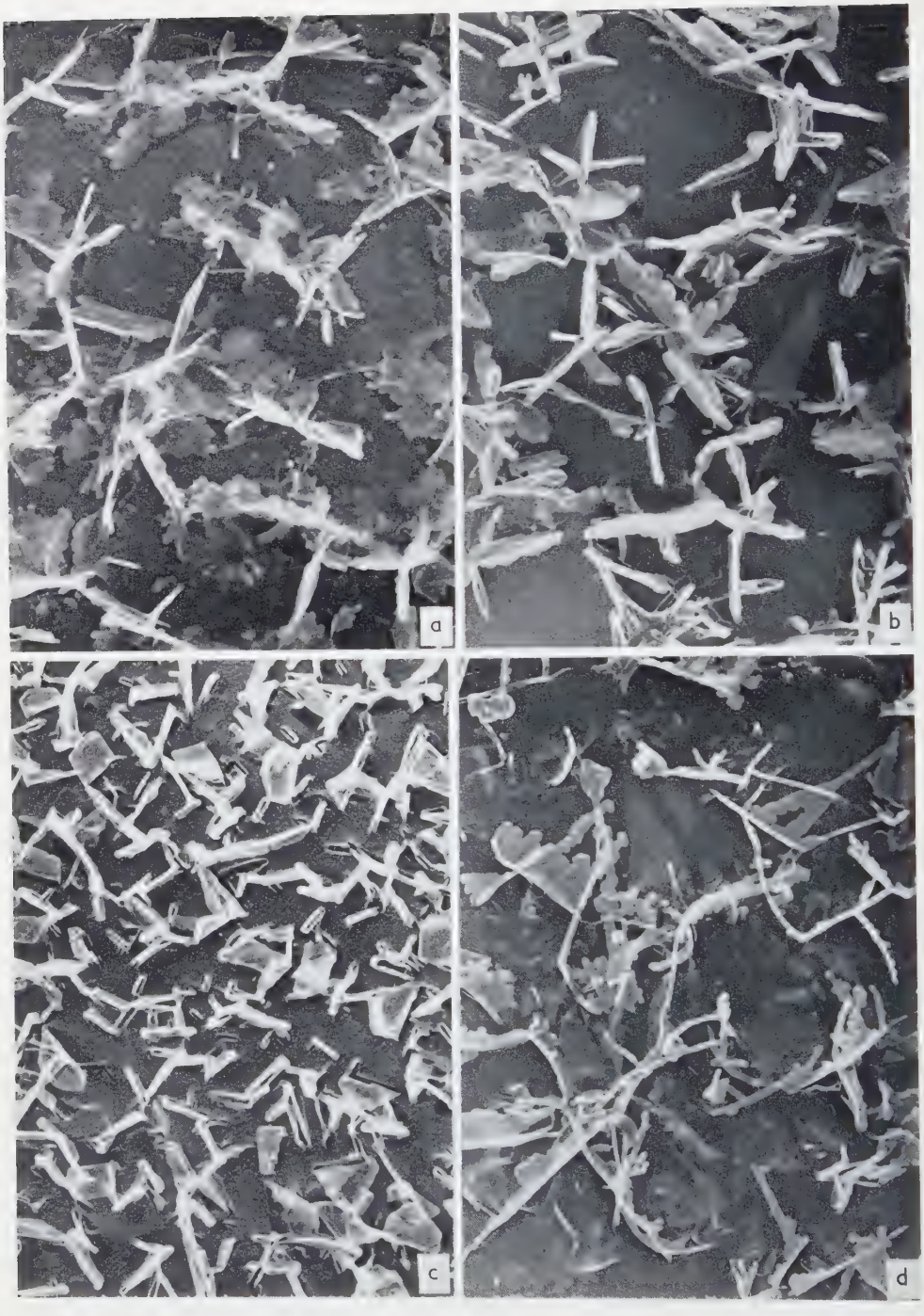
a
b
c
d

ACKNOWLEDGEMENTS

One of the authors (B. E. J.) would like to express his gratitude to Imperial Chemical Industries Ltd, for financial assistance in the above research. He would also like to thank Sir Paul Fildes, F.R.S., for electron microscope facilities, and Dr. F. A. L. Clowes for his continual advice and encouragement.

The other author (D. E. B.) would in addition like to thank Dr. T. E. Allibone, F.R.S., Director of the Research Laboratory, Associated Electrical Industries, for permission to publish this paper.

We should both like to thank Miss Joan Sampson of the Sir William Dunn School of Pathology, Oxford, for taking the majority of the electron micrographs.

REFERENCES

1. Bradley, D. E., *Brit. J. Appl. Phys.* **5**, 65 (1954).
2. Bradley, D. E. and Juniper, B. E., *Nature* **180**, 330 (1957).
3. Juniper, B. E., *New Phytologist*, in press.
4. Mueller, L. E., Carr, P. H. and Loomis, W. E., *Amer. J. Botany* **41**, 593 (1954).
5. Schieferstein, R. H. and Loomis, W. E., *Plant Physiol.* **31**, 240 (1956).

Fig. 7. *a: Pisum sativum* variety *Alaska*. Grown under controlled conditions at 5000 ft. candles Shadowed 1:1 with palladium. *b:* The same at 1500 ft. candles. *c:* The same at 400 ft. candles. *d:* The same at 1500 ft. candles, soil treated prior to germination with 0.56 gm m^2 *Dalapon*. 7750.

The Ultrastructure of Lung Tissue from Newborn and Embryo Mice

G. L. WOODSIDE and A. J. DALTON

Department of Zoology, University of Massachusetts, and National Cancer Institute, National Institutes of Health

Received June 16, 1958

Lung tissue from embryo, newborn and adult mice was studied by means of the electron microscope. Discontinuities were not found in either the endothelial lining of the capillaries or the epithelial cell lining of the alveoli. Capillary endothelial cells of newborn and embryo mice were similar in appearance to those of adult mice. Surface configurations of certain of the epithelial and endothelial cells were suggestive of pinocytosis. Numerous microvilli projected from some of the epithelial cells into the alveoli. The outer nuclear membrane of alveolar epithelial cells was found to be in direct continuity with membranes of the ergastoplasm.

Certain epithelial cells contained characteristic inclusion bodies. Some alveolar cells may have been undergoing degeneration, as indicated by the general appearance of the cytoplasm as well as the presence of the inclusion bodies. Structures similar to the cristae of normal mitochondria could be seen in many of these bodies in newborn, adult lungs and occasionally in lungs of 18-day embryos. Inclusion bodies were not found in embryos younger than 18 days. There might be a relationship between mitochondria and these inclusion bodies.

In many areas of the lungs of newborn mice a homogeneous basement membrane was apparently just being formed. Collagen and elastic fibers were frequently found in newborn and late embryo as well as in adult lung tissue. Newborn mouse lung tissue was found to contain areas of striated muscle. There was evidence that in newborn mice many alveoli were just developing. Microvilli from adjacent epithelial cells frequently projected into such areas. Evidence for and against the possibility of the existence of two cell types in alveolar epithelium has been presented and discussed.

Lung tissue of adult mammals has been studied with the aid of the electron microscope by a number of workers. It was found by Low (*23*) and confirmed by Schulz (*41*) that the alveolar walls of the rat lung were completely covered by a pulmonary epithelium with cell bodies located chiefly in the thicker areas. These observations were extended to include a similar nucleated pulmonary alveolar epithelium of other mam-

mals including man (*24*). The lining was found to be complete except possibly where "free cells" were in contact with alveolar walls. In a subsequent paper (*25*) the work of Porter and Kallman (*37*) was confirmed by the finding that prolonged exposure to the fixing fluid caused pronounced changes in the tissue including increased clarity of cell membranes. Low concluded that adequate osmication of lung tissue is to be found in the first fifteen minutes of fixation. Kisch (*21*) found a number of plasmasomes (mitochondria) and osmiophilic inclusions in cells of the lungs of bats and guinea pigs. Frequently vacuoles were present and very often the osmiophilic substance was present in the form of a ring. Occasional plasmasomes containing some dark material and lamelli-form inner structures suggested to Kisch that the so-called lipochondria might be the end product of transformed plasmasomes. What might have been similar osmiophilic cell inclusions which were stratified concentrically were first described by Schlipkoter (*38*).

Contrary to the report by Swigart and Kane (*42*) for the rat, the presence in the alveoli of adult mice of an uninterrupted thin epithelial cell layer was reported by Karrer (*14*). He also found that the endothelium of the lung capillaries was uninterrupted and that sometimes it was no more than 100 Å thick. An apparently structureless basement membrane was observed between epithelium and endothelium. It was continuous with intercellular layers between single endothelial cells. In a subsequent paper (*16*) the basement membrane was found to be thickened in certain places where it also contained collagen fibrils. He reported finding two types of alveolar epithelial cells in mouse lungs: "One protruded into the alveolar lumen with its thick portion containing the nucleus. The other was often located in a nitch of the alveolar wall and contained peculiar dark inclusions amidst numerous mitochondria."

It was also found (*15, 17*) that the ciliated cells of bronchiolar epithelium contained few mitochondria and but little endoplasmic reticulum, whereas non-ciliated cells contained many large mitochondria and well-developed endoplasmic reticulum. The latter he found to be in general agranular. Inclusion bodies similar to those described by Karrer were reported by Policard *et al.* (*35*), but apparently they contained only vacuoles. These observations were expanded by Policard *et al.* (*34*). The osmiophilic bodies were found to be oval and to be 0.9 micron along the major axis. They contained lamellae corresponding to the cristae of mitochondria and these authors believed that the osmiophilic bodies were derived from mitochondria. Occasionally incomplete osmiophilic bodies occurred as transparent cavities in the cytoplasm perhaps containing remnants of the former contents as dense fragments. The cavities sometimes exceeded one micron in diameter. Similar osmiophilic cell inclusions were described by Kikuth *et al.* (*20*) in the lungs of rats. Schulz (*41*) found in CO_2 treated rats that certain mitochondria showed characteristic alterations of the internal membranes. These he described as band-shaped transformations. He had

previously reported (*39*) that in the CO_2 experiments the mitochondria were more numerous than in normal alveolar cells of the rat, that they might be up to two microns long and were distributed over the whole cell in contrast to normal alveolar cells where the mitochondria were predominately located around the nucleus. In experiments involving an oversupply of oxygen Schulz found that the mitochondria usually showed a vesicular stage or a vacuolar transformation. Such mitochondria had largely or completely lost their lamellar structure. Schulz (*40*) also reported that the lungs of animals with mitral stenosis contained larger numbers of cyst-like structures which he thought might possibly have been derived from mitochondria. These were sometimes located close to the epithelial nucleus and in them were found concentrically stratified bands and lines.

It is evident from a study of the work already reported that uncertainty as to the origin of these cytoplasmic inclusions in alveolar epithelial cells still exists. It occurred to us that the lungs of newborn and late embryo mice should prove to be a promising source of material for a study of these inclusion bodies. When the lungs rapidly assume their functioning condition at the time of birth the possibility of extensive morphological changes certainly exists. Even in the adult a constant production and desquamation of alveolar cells has been demonstrated (*3*). If an increase in the overall number of inclusion bodies could be correlated with an increase in the number of alveolar cells being lost from the epithelium, perhaps an explanation of the cause of inclusion body formation might be suggested. It seems likely that desquamation of epithelial cells probably would not take place, at least to any great extent, until alveoli had been formed and the lungs had started to function. Even if this were not the case, the lungs of embryo mice should be compared with those of newborn and adult mice in order to study the relative frequency and general appearance of inclusion bodies. We also thought that if lungs of mouse embryos should turn out to have no inclusion bodies, we might be able by studying successively later stages, to learn something about the origin of these structures.

FIG. 1. Section through the edge of an adult lung of a DBA2 mouse showing a mesothelial cell with its microvilli, a capillary with attenuated endothelium, elastic tissue, collagen, an alveolar epithelial cell with its microvilli projecting into an alveolus, mitochondria and inclusion bodies. Chrome osmic fixation, pH 7.2. × 13,500.

All figures are electron micrographs. The line on each represents 1 micron. Labelling abbreviations for all figures are as follows:

A	alveolus	*ET*	elastic tissue	*N*	nucleus
AEC	alveolar epithelial cell	*GM*	Golgi membrane	*NI*	nucleolus
BM	basement membrane	*GV*	Golgi vesicles	*NM*	nuclear membrane
C	collagen	*IB*	inclusion body	*NP*	nuclear pore
CAP	capillary	*L*	lipid droplet	*P*	pinocytosis
CM	cell membrane	*M*	mitochondrion	*RBC*	erythrocyte
E	endothelium	*MC*	mesothelial cell	*RNP*	ribonucleoprotein granules
ER	ergastoplasm	*MV*	microvilli	*SM*	striated muscle

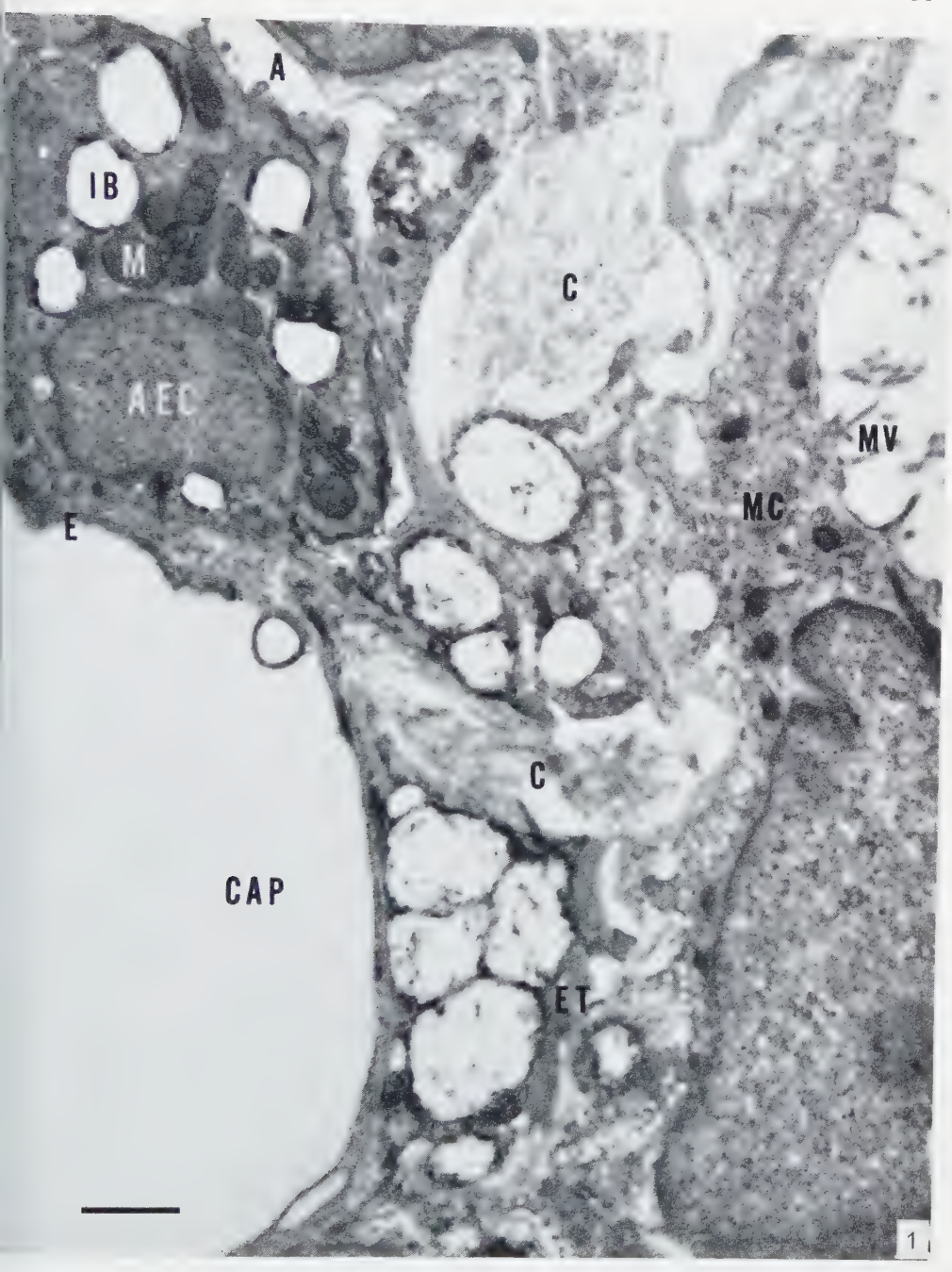
A
IB
M
C
AEC
MV
MC
E
C
CAP
ET

MATERIAL AND METHODS

All embryo and newborn mice were obtained from a (BALB/cXC3H)F_1 cross. Adult mice were either C3H, DBA2 or from the same (BALB/cXC3H)F_1 cross. For the purpose of calculating the age of embryo mice, the gestation period was determined on the basis that zero day was the day the vaginal plug was identified. Using this method, the (BALB/cXC3H)F_1 hybrid was found to have a 19 day gestation period.

Except for a few experiments with veronal acetate buffered osmic acid (*30*) the fixative used throughout the present study was a mixture of 1% osmic acid, 1% $K_2Cr_2O_7$ and 0.85% NaCl (*5*). This fixative was used at pH 7.2 for adult tissues and for most of the newborn and at from 7.2 to 7.8 for embryonic tissues.

Adult and newborn lungs were perfused with the fixative first through the right ventricle of the heart and immediately thereafter through the trachea. The perfusion was done under a dissecting microscope and the presence of the chrome osmic fixative was easily detected as the yellow fluid filled and expanded the lungs. Very small pieces of the edges of the lobes were then placed in the fixative and kept under vacuum for from fifteen minutes to one hour. Lungs of the older embryos (16, 17 or 18 days of gestation) were perfused in the same manner. After the technique had been perfected both perfusions (through the heart and through the trachea) could be completed in less than three minutes. The lungs of embryos younger than 16 days were not perfused. Instead the fixative was pipetted onto the lungs as soon as the thoracic cavity had been opened, after which very small pieces of the lung were placed in bottles of the fixative.

Following fixation the tissues were washed either in tap water or in 0.85% NaCl for from ten minutes to one hour. Tissues from adult and newborn mice were kept under vacuum during this time. After washing, tissues were placed in neutral formalin (either 10% or 20%) for from twenty minutes to one hour. Dehydration of some of the tissues was then begun by transferring them directly from the formalin to 60% alcohol. Most of the tissues, after having been removed from the formalin, were embedded in 2% agar. All tissues were dehydrated rapidly in a graded series of alcohols and embedded in a mixture of one part methyl methacrylate monomer and either five or nine parts of *n*-butyl methacrylate monomer. Best results were obtained when tissues were placed in a small amount of the monomer in a capsule and heated in an oven at 80° C for fifteen minutes. Then the rest of the monomer was added, the capsule sealed and left at 80° C for from sixteen to sixty-four hours. Ultrathin sections were cut on a Porter–Blum microtome. The sections were studied and micrographs taken with an RCA EMU-2C electron microscope.

RESULTS

The alveoli of adult and newborn lungs perfused as described above were not collapsed but were similar in appearance to the descriptions of other investigators

FIG. 2. Section through the lung of a newborn (BALB/cXC3H)F_1 mouse showing a portion of an alveolus and a capillary with endothelium considerably thicker than in the adult. Alveolar epithelial cells are also visible with microvilli projecting into the alveolus. There is a basement membrane which in places becomes very wide. The cytoplasm at the tip of one of the alveolar epithelial cells (at *X*) contains a large number of RNP granules. Chrome osmic fixation, pH 7.2. × 13,500.

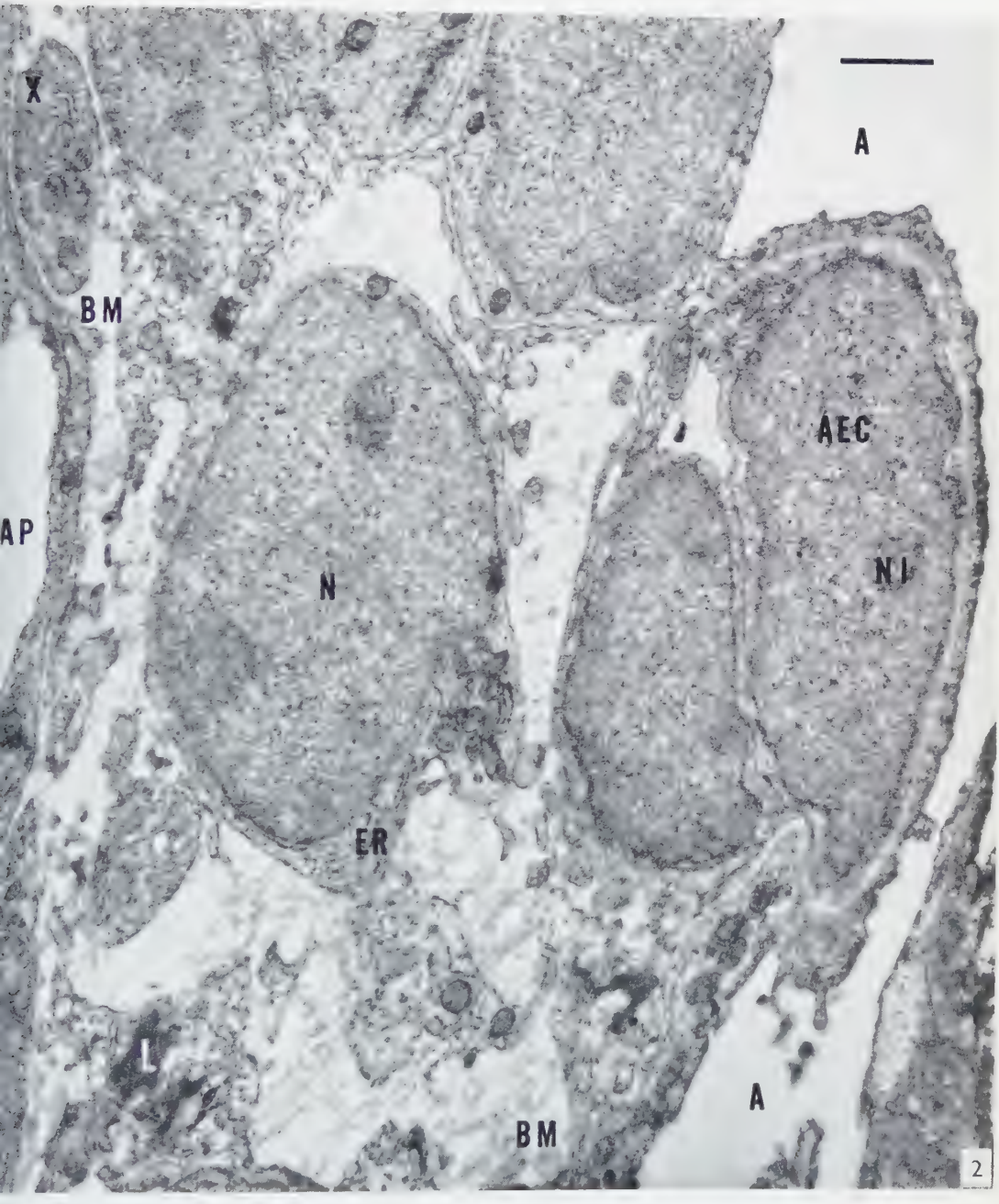
X
A
BM
AEC
AP
N
NI
ER
L
A
BM
2

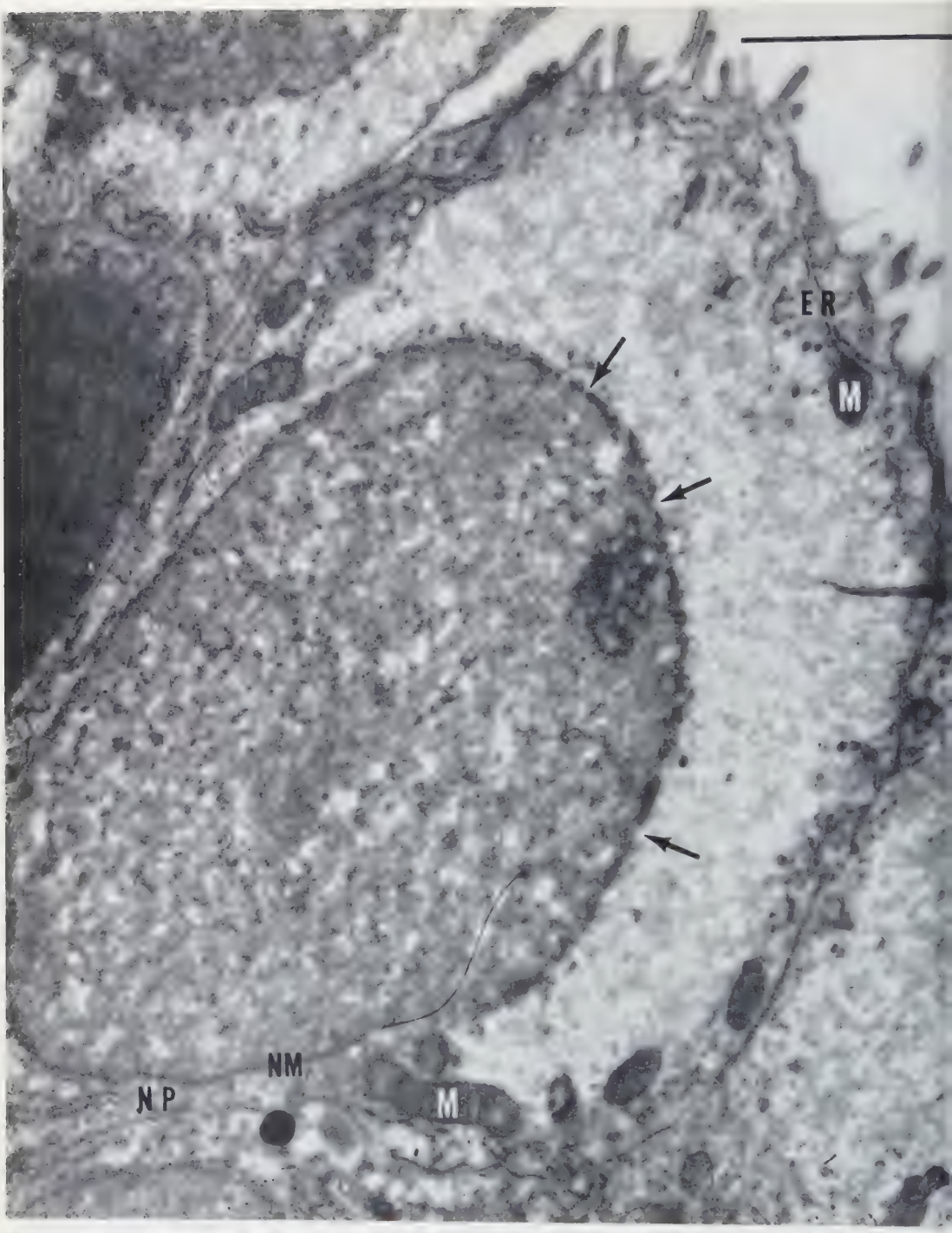

FIG. 3. Part of an alveolar epithelial cell from the lung of an 18-day (BALB cXC3H)F_1 mouse embryo. The genera
pearance of the cytoplasm suggests degeneration. Most of the mitochondria and ergastoplasm are located nea
periphery of the cell. The nuclear membrane shows a number of discontinuities (arrows), which, however, ar
interpreted as nuclear pores, but as breaks and therefore artifacts. A true nuclear pore is shown at *NP*. Ch
osmic fixation, pH 7.2. ×32,000.

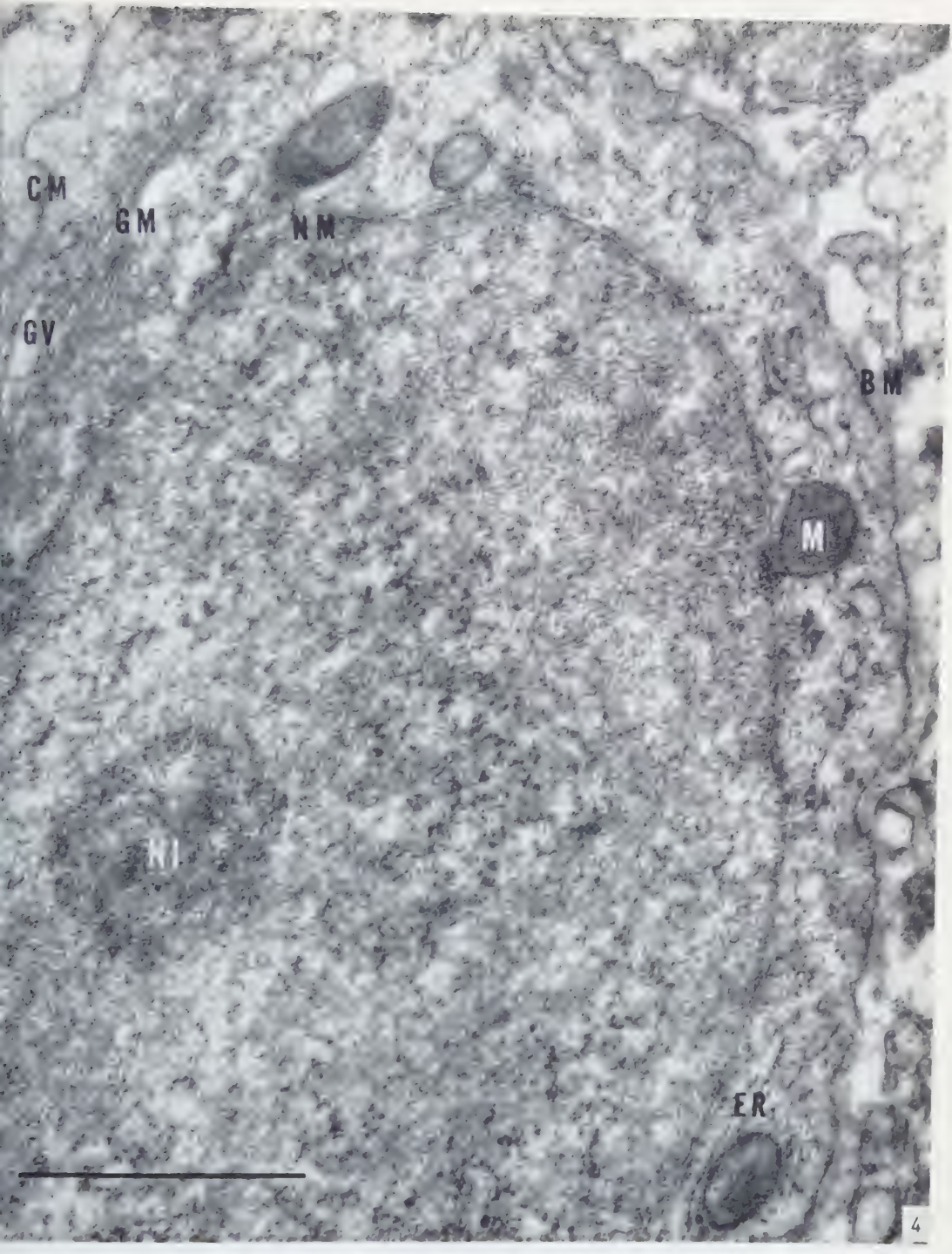

Part of a cell from the lung of a newborn (BALB cXC3H)F, mouse showing the cell membrane, nuclear mem
Golgi membranes, Golgi vesicles, nucleolus and basement membrane. Chrome osmic fixation, pH 7.2. × 43,000.

(*14*, *16*, *25*, *34*). Embryonic lung tissue was more compact. Fig. 1 shows a section of the edge of an adult lung at low magnification. Part of a mesothelial cell and its microvilli can be seen at the upper right of the figure and a capillary with its endothelial lining appears at the lower left. In the center and at top center there are elastic tissue and collagen. At the upper left is an alveolar cell bordering a small alveolus. On the surface of the alveolar epithelial cell there are a number of small microvilli and within the cell a number of mitochondria and inclusion bodies.

A section of the lung of a newborn mouse is shown in Fig. 2. A portion of an alveolus can be seen to the right and of a capillary at the extreme left. Lipid droplets occur in a stromal cell in the lower left.

Fig. 3 shows an epithelial cell from the lung of an 18-day mouse embryo (see "Material and Methods"). The appearance of the large crescent shaped area of cytoplasm free of cytoplasmic components suggests that degeneration may have set in. The ergastoplasm and mitochondria are located only near the periphery of the cell. A typical double nuclear membrane is present and appears to be broken in several places. In Fig. 4, a more normal nuclear membrane can be seen. Characteristic Golgi material can be seen in the upper left consisting of a number of small vesicles and profiles of smooth-surfaced flattened sacs. The third component of typical Golgi material, larger vacuoles, has not been found in lung tissue of newborn mice. For comparison Fig. 5 shows lung tissue from an 18-day embryo. Characteristic Golgi elements and the double nuclear membrane are shown. Two mitochondria with their outer and inner membranes and well-formed cristae can also be seen.

The fact that striated muscle occurs in the lungs of the newborn mouse is evident in Fig. 6. The nucleus of the muscle cell separates two groups of myofibrillae. As indicated earlier, samples of lung tissue were consistently taken from the outermost portions of the lobes, so that the presence of striated muscle in the material should not be confused with the occurrence of cardiac muscle in the walls of the pulmonary veins of mice. Our observations are perhaps comparable to those of Karrer (*18*).

Elastic tissue and collagen are frequently found in large amounts in the lungs of adult animals as can be observed in Fig. 7. The presence of a well-formed basement membrane is also evident. Collagen in the lung of a newborn mouse is shown at the top center of Fig. 8. Elastic tissue has also been found in newborn lungs. Interesting configurations of the ergastoplasm are visible in the center of the figure—the mem-

---

FIG. 5. Lung tissue from an 18-day (BALB cXC3H)F_1 mouse embryo showing Golgi membranes, Golgi vesicles, ergastoplasm and mitochondria. Chrome osmic fixation, pH 7.2. ×31,500.

FIG. 6. Striated muscle from lung tissue of a newborn (BALB cXC3H)F_1 mouse showing the nucleus of the muscle cell between two groups of myofibrillae. Mitochondria are numerous and contain large numbers of compact cristae. Chrome osmic fixation, pH 7.2. ×42,000.

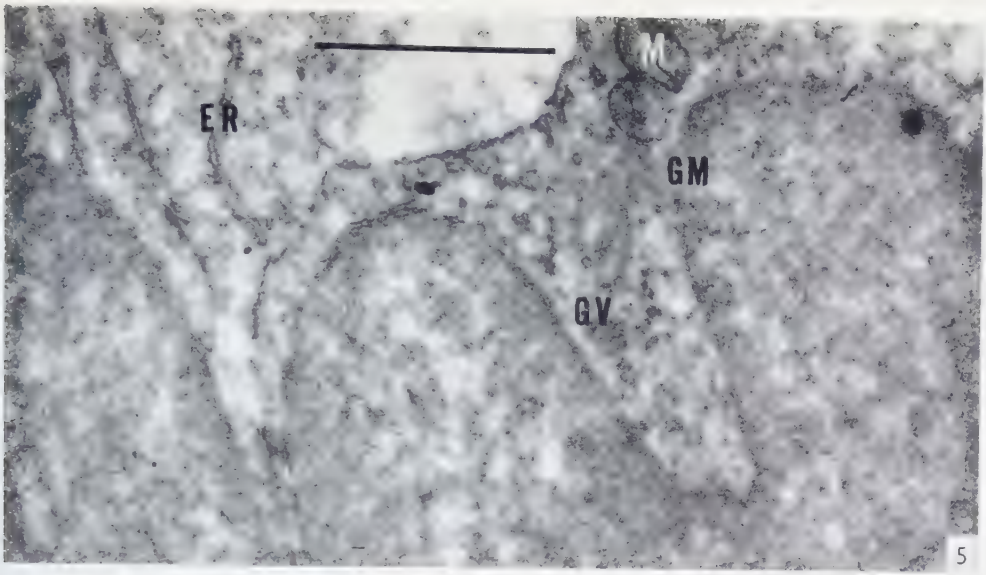

5

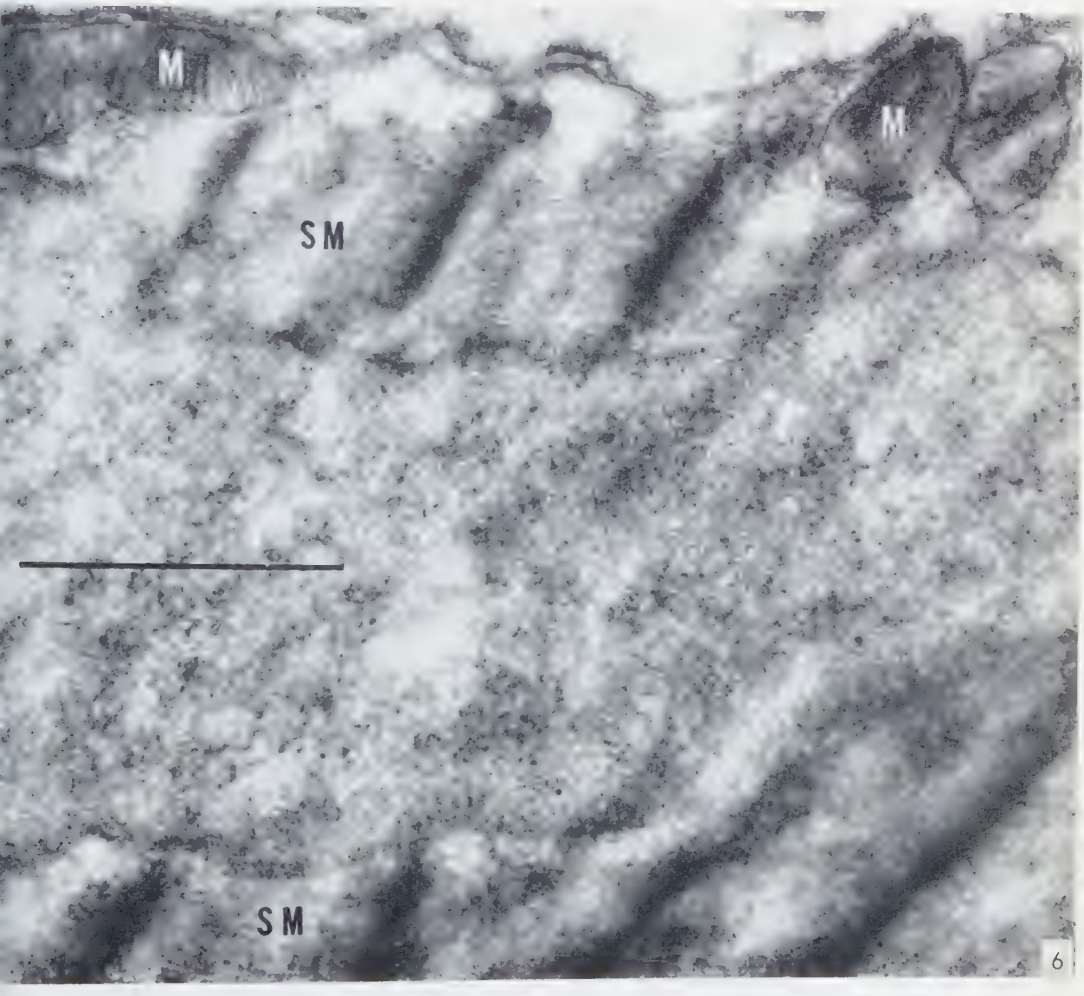

6

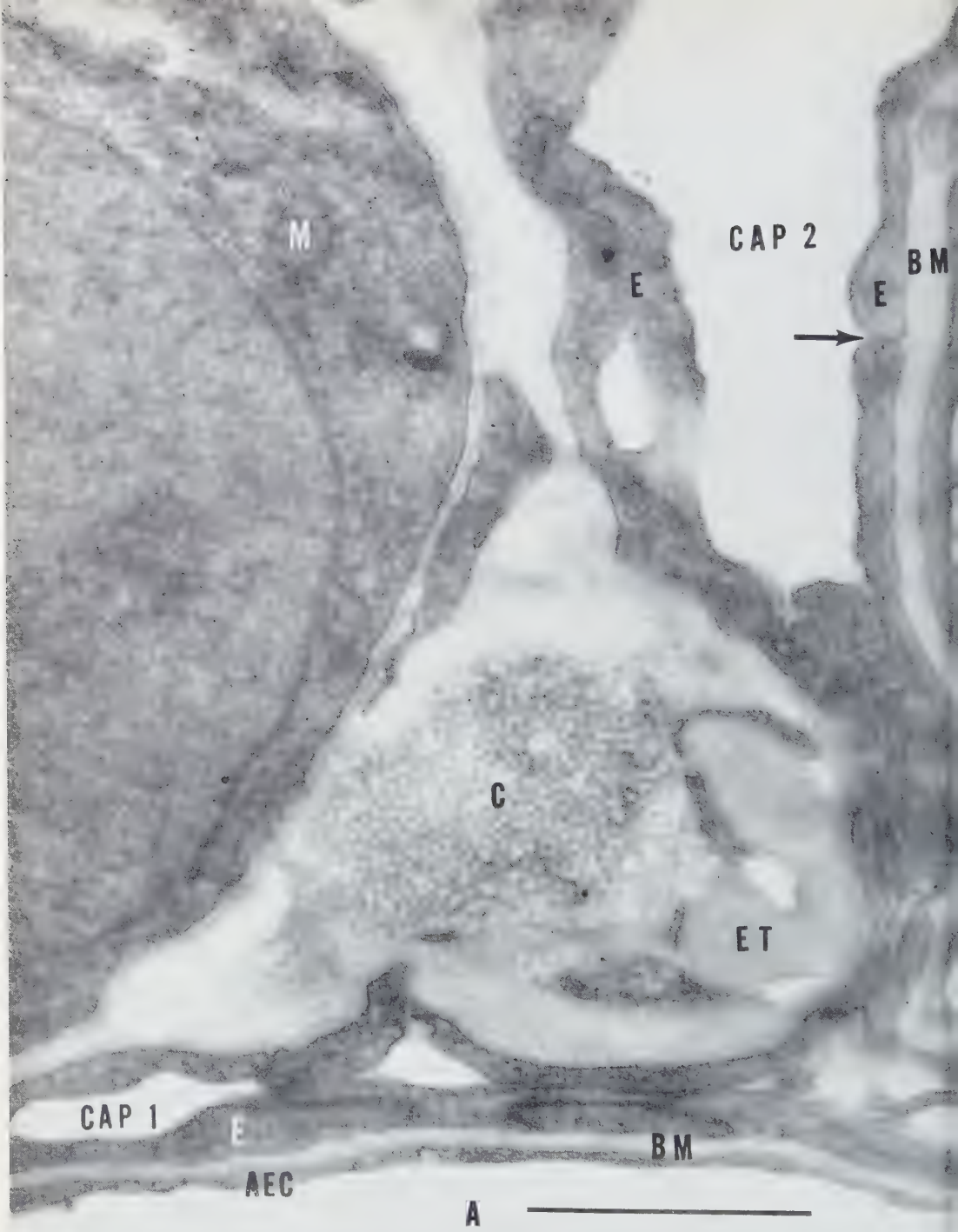

FIG. 7. Lung tissue from an adult DBA2 mouse showing a portion of an alveolus bounded by thin alveolar epithe and separated from an adjoining cell (endothelium) by a well-formed basement membrane. A collapsed capi (seen at *CAP* 1) widens out at *CAP* 2 and is bounded by well-formed endothelium. The point of contact betv two endothelial cells is indicated at the arrow. In this instance continuity between the capillary lumen and basement membrane cannot be demonstrated. Collagen and elastic tissue are seen in the knee of the capillary an separated from an alveolar epithelial cell by homogeneous basement membrane. Chrome osmic fixation, pH 7.2. 43

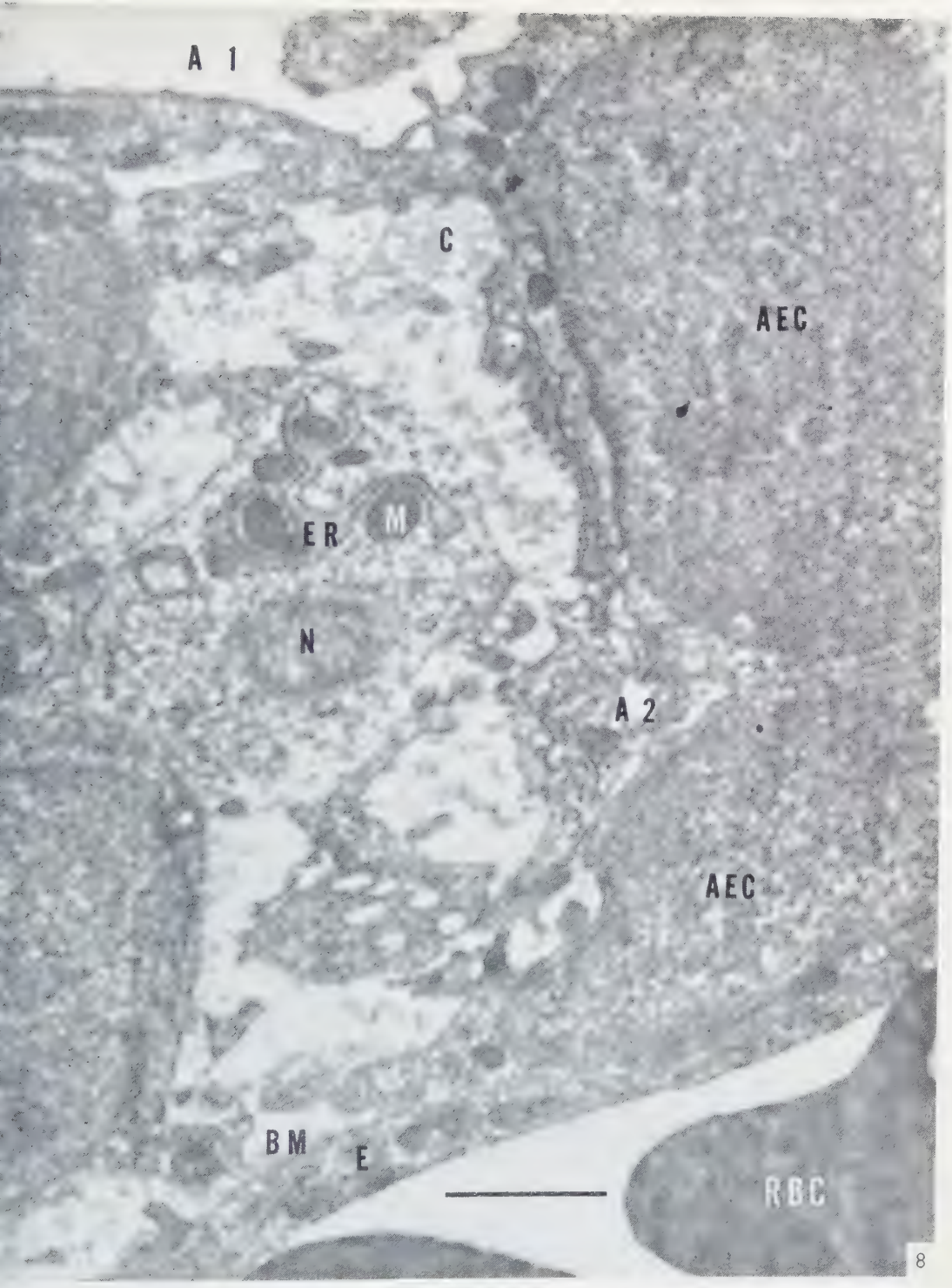

. Section of lung tissue of a newborn (BALB cXC3H)F_1 mouse showing a capillary with red blood corpuscles, helium with mitochondria, basement membrane, alveolar epithelial cells, a portion of a large alveolus, an alveolus process of formation, the tip of a nucleus and ergastoplasm closely associated with mitochondria. Collagen is e near the top of the figure. Chrome osmic fixation, pH 7.2. ×24,500.

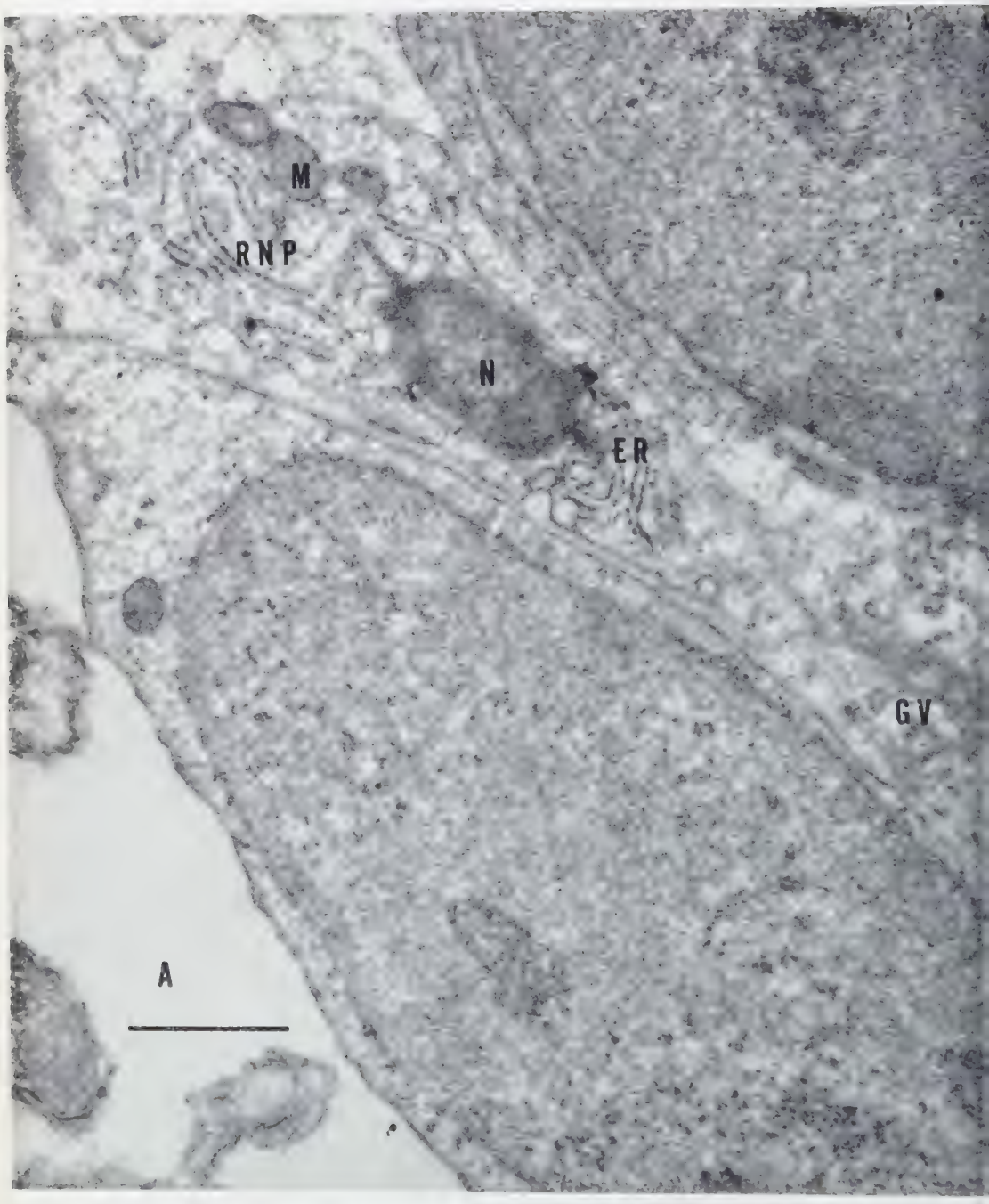

FIG. 9. Section of lung tissue of a newborn (BALB cXC3H)F_1 mouse showing part of an alveolus, the nucleus
cell cut tangentially, ergastoplasm with conspicuous RNP granules, Golgi vesicles, and mitochondria. Chrome c
fixation, pH 7.2. ×24,000.

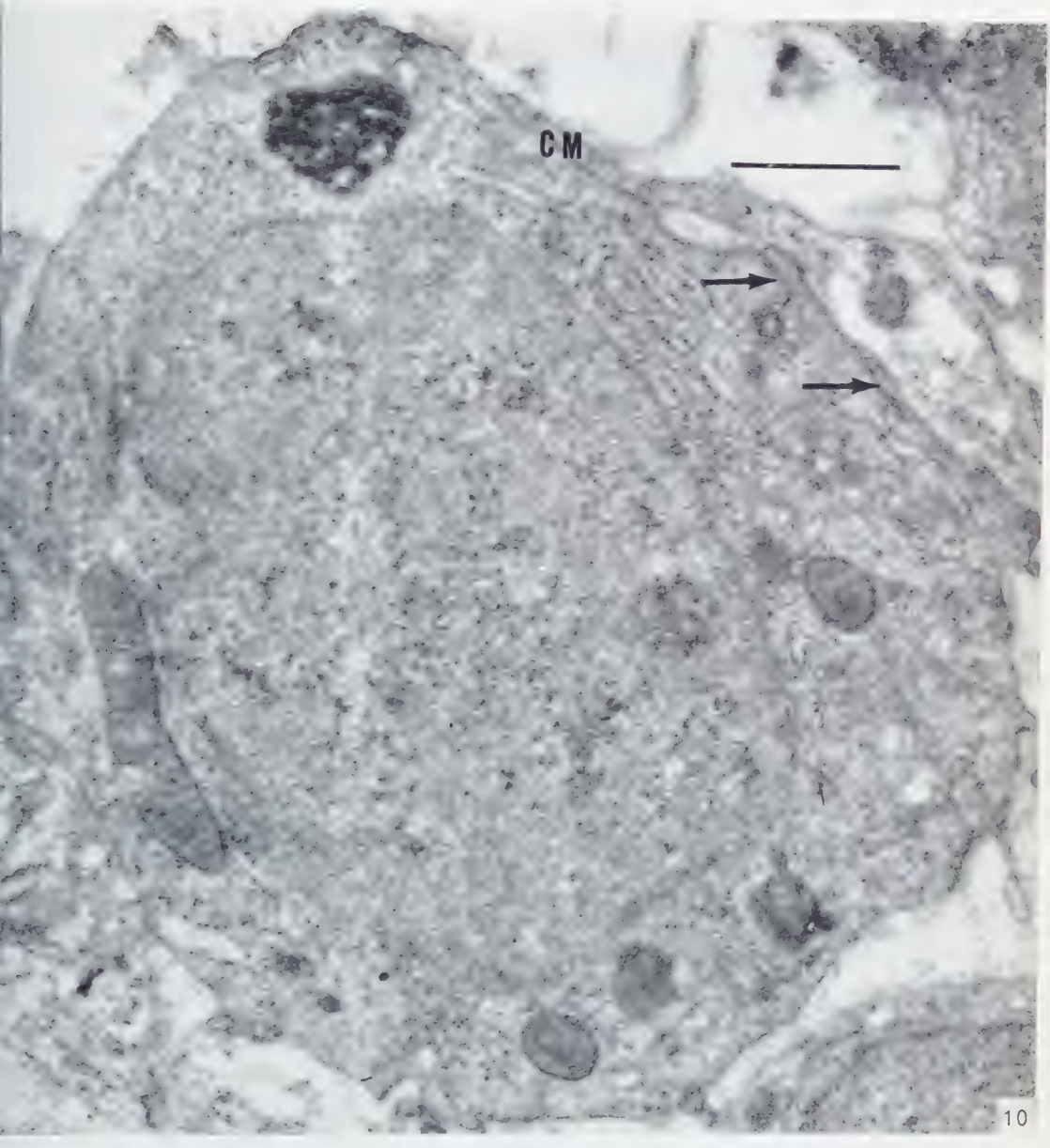

. 10. Section from the same newborn mouse as shown in Fig. 9. RNP granules, both associated with membranes free in the cytoplasm, are shown as well as a portion of the nucleus of the cell, mitochondria, and the cell membrane. At two places (arrows) vesicles formed by the fusion of plasma membrane are indicated. Chrome osmic fixation, 7.2. ×24,000.

branes with their clearly defined RNP granules practically surround a number of mitochondria. The structure below the ergastoplasm is a small portion of the nucleus.

In Fig. 9 the RNP granules of the ergastoplasm are clearly visible. As in the previous figure, the tip of a nucleus is shown cut tangentially. RNP granules, both associated with membranes and free in the cytoplasm are shown in Fig. 10. Golgi elements consisting of profiles of small vesicles and flattened sacs can be seen.

The fact that the outer nuclear membrane is in direct continuity with membranes of the ergastoplasm of alveolar epithelial cells is clearly demonstrated in Fig. 11. A portion of the nucleus with its inner nuclear membrane occupies the lower right of the figure; above can be seen an alveolus with sections of microvilli. An example of a "nuclear pore" can be seen at the top of the nucleus. It is apparent that in the region of the "pore" the double nuclear membrane becomes a single line.

Fig. 12 shows a portion of an alveolar epithelial cell from the lung of an adult mouse. Microvilli are present projecting into the alveolus. The cell also contains a number of vacuolated structures or inclusion bodies. Basement membrane and collagen fibers occur near the upper right of the figure. Fig. 13 shows more of these inclusion bodies as well as a number of normal mitochondria in an epithelial cell from the lung of an adult mouse. The appearance of the inclusion bodies in Fig. 14 suggests the possibility that the material within the cavity might have been derived from the cristae of the mitochondria. That the inclusion bodies are not confined to adult lungs is indicated in Fig. 15 which shows lung tissue taken from a newborn mouse. Two of the inclusion bodies are strongly osmiophilic whereas a third contains structures which might be interpreted as once having been cristae. Several normal mitochondria are seen to the right of the inclusion bodies. Fig. 16 (also from a newborn mouse) contains a number of normal mitochondria and three which are apparently in the process of being transformed into inclusion bodies. In each of the three, modified cristae and vacuolar spaces can be seen. The size of these three appears to be within the range of normal mitochondria.

Fig. 17 shows a portion of the cytoplasm of an alveolar epithelial cell taken from a mouse embryo of 18 days gestation (see "Material and Methods"). The detailed

---

FIG. 11. A portion of an alveolar epithelial cell from the lung of a newborn (BALB/cXC3H)F_1 mouse showing part of the nucleus and the nuclear membrane, the outer layer of which is continuous with ergastoplasm. At one point (arrow) a "nuclear pore" can be seen. A single thin membrane is evident at this point, and there is no continuity between the nucleoplasm and cytoplasm. Sections of microvilli occur in the alveolus, and there are suggestions of pinocytosis. Chrome osmic fixation, pH 7.2. ×42,000.

FIG. 12. Part of an alveolar epithelial cell from the lung of an adult DBA2 mouse. Numerous microvilli project into the alveolus. The cell is bounded by a basement membrane beyond which can be seen an area of collagen. Ergastoplasm occurs in many parts of the cell, and numerous mitochondria with typical cristae are present. Vacuolated inclusion bodies are distributed among the mitochondria. Chrome osmic fixation, pH 7.2. ×31,000.

11

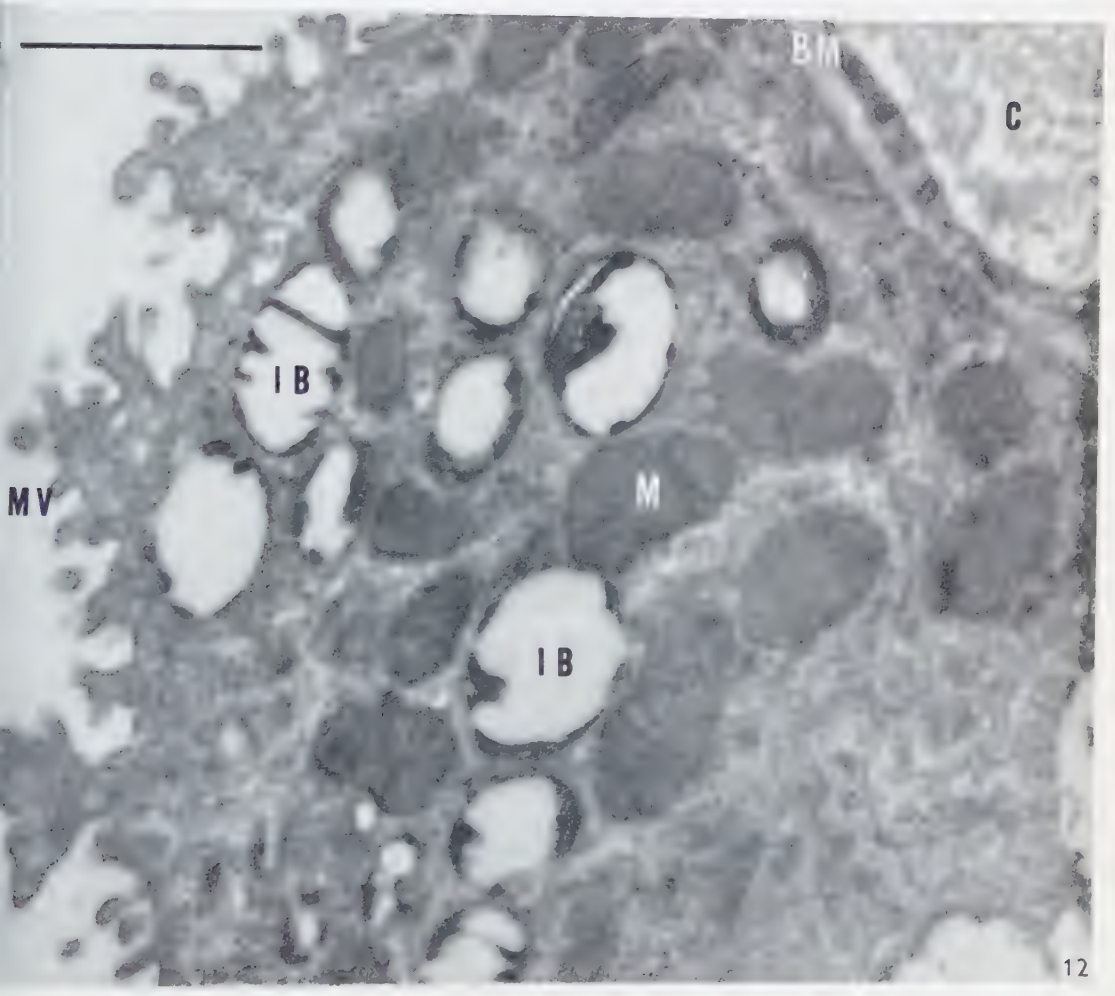

12

structure of a number of mitochondria is shown and in the upper left what appears to be a very early stage in the formation of an inclusion body. The beginning of vacuole formation is indicated. Fig. 18 is from another embryo of the same age. Above the nucleus of an alveolar epithelial cell can be seen three normal mitochondria flanked by two inclusion bodies.

DISCUSSION

Capillary endothelium

The present study confirms the findings of Karrer (*14*, *16*) relating to the appearance of the capillary endothelium in the lung of the adult mouse and extends them to newborn and embryo mice. No pores have been found in the endothelium. Approximation of the plasma membranes of two endothelial cells has been found, but there was no evidence that an actual opening in capillary walls occurs. In the adult lung the endothelium is frequently a very thin structure (*6*) whereas in the newborn it is often considerably less attenuated. Characteristic mitochondria are present in the endothelium and are especially numerous in tissue from embryo and newborn mice. In no case have we ever found inclusion bodies in the capillary endothelium of the lung. The mitochondria always seem to have a normal appearance, even the earliest stages of possible transformation to inclusion bodies having never been observed. Occasionally evidence of pinocytosis is present.

Basement membrane

Karrer (*14*, *16*) discusses the properties of the basement membrane of the adult mouse lung. In most respects the present work as it relates to adult lung tissue confirms his findings. He shows collagen fibrils, but states that no elastic tissue could be recognized in relation to the basement membrane in his preparations. Low (*24*) had previously described elastic tissue in this region and our observations agree with his. Both collagen fibrils and elastic tissue have also been found in the lungs of newborn and late embryo mice. The appearance of the basement membrane in lungs of newborn mice often suggests that it is just being formed.

Alveolar epithelium

Continuity. The present study confirms the earlier evidence (*14*, *16*, *23*, *24*) that the alveoli of the mouse lung are lined with a thin continuous epithelial layer. This is in contrast to the findings of Policard *et al.* (*35*) who felt that the lining was dis-

FIG. 13. Section of lung tissue from an adult DBA2 mouse showing a portion of an alveolar epithelial cell containing large numbers of mitochondria and a few inclusion bodies. Smooth membranes in continuity with the ergastoplasm are intimately associated with many of the mitochondria. Except at its free border, where microvilli project into the alveolus, the cell is surrounded by basement membrane. Areas of elastic tissue and collagen are present. Chrome osmic fixation, pH 7.2. 32,000.

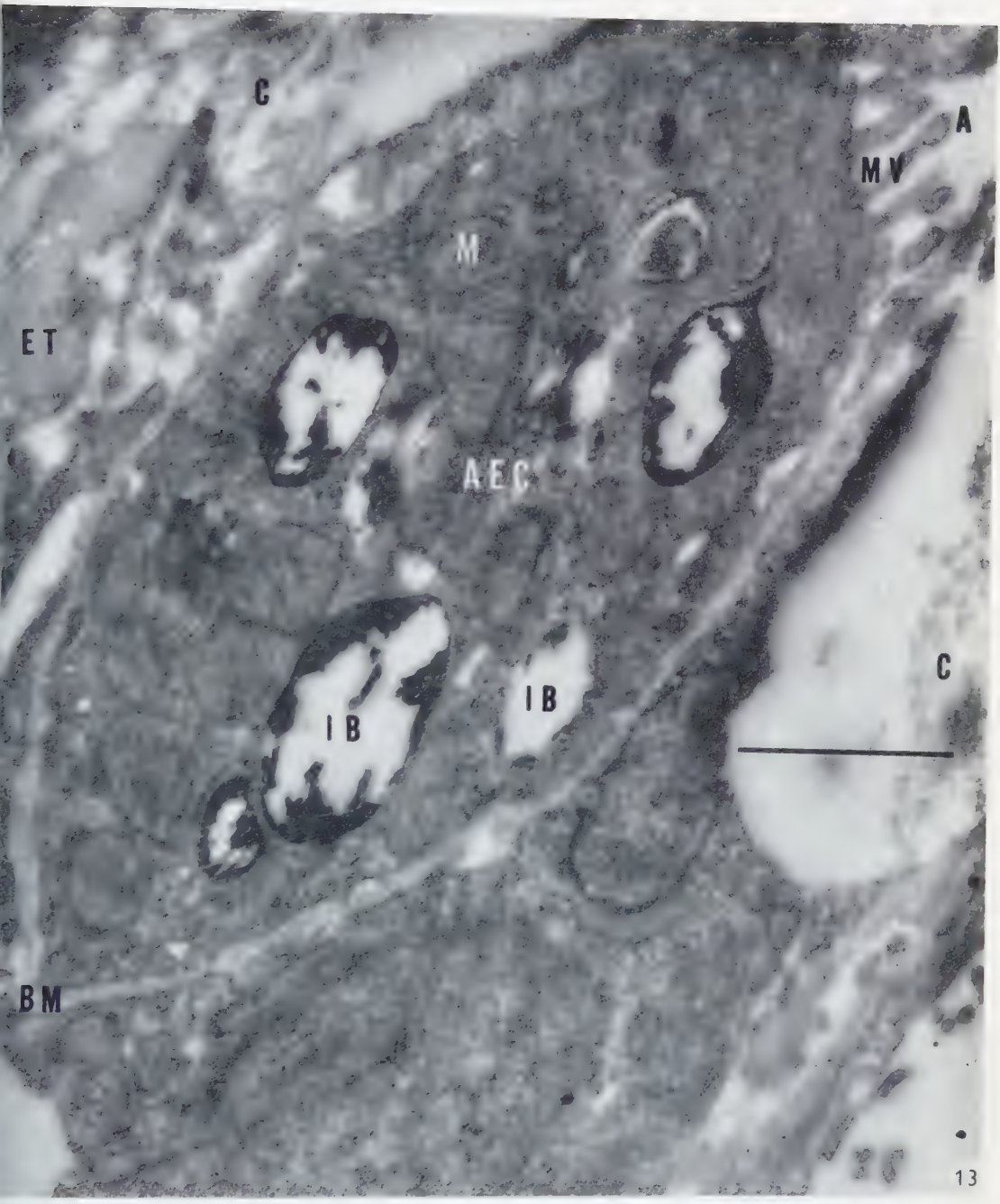
C
A
MV
M
ET
AEC
C
IB
IB
BM
13

continuous. No extensive measurements of the thickness of the membrane were made in the present study but our observations agree with the range of thickness found by Karrer (*14*, *16*).

Cell types. The possibility that the alveolar epithelium might consist of more than one type of cell has been suggested by a number of workers (*3*, *10*, *14*, *16*, *22*, *34*). If the lung is thought of as a more or less static organ in which the alveolar epithelial cells do not change, the present results could be interpreted as providing evidence of two types of alveolar epithelial cells. Confirming the work of Karrer (*16*), we have found that one type contains a large number of microvilli at the free surface. This type also usually has a large number of mitochondria and frequently inclusion bodies can be found in the cytoplasm. There is a striking similarity between these cells and the "specific cells" described by Kisch (*21*). The other type of epithelial cell possesses few if any microvilli. There are usually fewer mitochondria, and inclusion bodies are not seen.

If, however, the lung is regarded dynamically the possibility suggests itself that perhaps we are not dealing with two distinct kinds of epithelial cells; rather that one is but a morphological variant of the other. One evidence for this possibility is the demonstration of what appear to be transitional forms between normal mitochondria and inclusion bodies. However, the statement is made by Karrer (*16*): "It has been found impossible up to now to establish a relation between these inclusions and the mitochondrial profile although both occur side by side in the same alveolar cell and are comparable in size." Karrer worked with adult mouse lung tissue. In the present work with adult lungs we found relatively little evidence for transitional forms. This was even more true of the lungs of 14- through 17-day embryos in which no inclusion bodies could be found. In newborn mice and in 18-day embryos, however, a number of instances which appear to be transition forms between normal mitochondria and inclusion bodies have been found. There is some evidence that the transition from one type of cell to the other may be accompanied by a degenerative process. This is indicated by the general appearance of the cytoplasm (Fig. 3). Our material also shows that in alveolar epithelial cells, in which most of the mitochondria

---

FIG. 14. A portion of the cytoplasm of an alveolar epithelial cell from the lung of an adult DBA2 mouse showing a few normal mitochondria and a number of inclusion bodies. In addition to being vacuolated, some of the inclusion bodies contain strands of material which stretch from one side of the body to the other. In other cases the strands appear to be broken and are represented by short pieces on either side. Chrome osmic fixation, pH 7.2. ×32,000.

FIG. 15. Newborn (BALB/cXC3H)F_1 mouse lung tissue showing a portion of an alveolar epithelial cell containing some normal mitochondria and a few inclusion bodies. Two of these are markedly osmiophilic, whereas a third is vacuolated and contains remnants of internal strands. Chrome osmic fixation, pH 7.2. ×24,000.

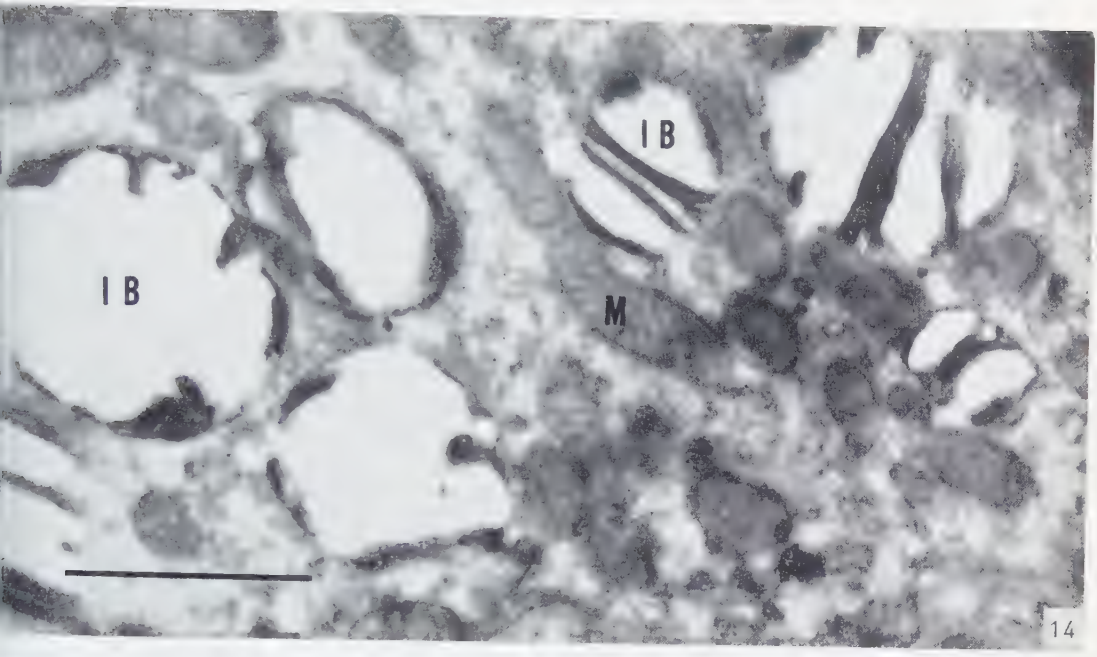

14

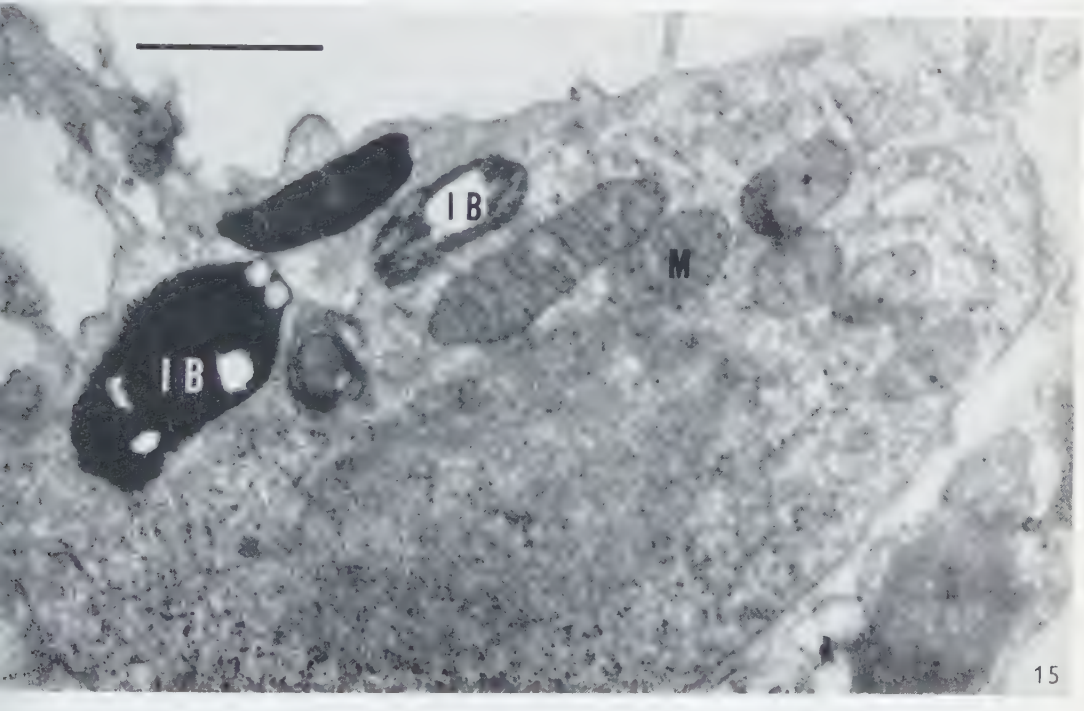

15

are normal but a few may be in the early stages of transition to inclusion bodies, very few microvilli can be found on the free surface (Fig. 18). In contrast, cells containing large numbers of inclusion bodies also have large numbers of microvilli (Fig. 12). Thus perhaps epithelial cells which are going to undergo desquamation may exhibit at least two structural transformations prior to their separation from the rest of the membrane: the development of microvilli on the free surface and the appearance of inclusion bodies among the mitochondria.

Support for the concept of structural changes in mitochondria undergoing degeneration has come from the work of Luft and Hechter (*27*). They found that cow adrenal cells fixed in 2.5% OsO_4 an hour to an hour and a half after the death of the animal exhibited many structural changes. The chromatin was clumped at the nuclear membrane and the mitochondria were more or less rounded, had only a few cristae, and contained many vesicles attached to the inner bounding membrane. Perfusion with liver-filtered, warmed, oxygenated, citrated beef blood, however, resulted in cells with finely dispersed chromatin and elongated mitochondria containing normal cristae but practically no vesicles. This evidence suggests that cellular degenerative changes between the time of death and fixation include marked alterations in the mitochondria.

A possible significance of the vesiculated mitochondria as compared with mitochondria containing intact cristae is provided by the findings of Greene *et al.* (*7*). Two types of particles were isolated from beef heart mitochondrial fractions. One type, called the electron transport particles, were found to consist mainly of vesiculated fragments of mitochondria. The other type, called phosphorylating electron transport particles, were found to consist of mitochondrial fragments with intact cristae.

Hartman (*9*) found that after cortisone treatment the mitochondria of motor nerve cells contained vacuoles. After large doses the mitochondria were swollen and empty with only a few short crests to distinguish them from simple cytoplasmic vacuoles. It had been pointed out by Cowdry (*4*) that in aging cells the number of mitochondria decreases and finally disappears. Payne (*33*) discovered that in pituitary and adrenal cells the mitochondria became swollen and converted into pigment granules. Weiss and Lansing (*44*) found that in the anterior pituitary of the mouse the fine structure of mitochondria changed with aging. Their number decreased, their diameter became

---

FIG. 16. Section of a portion of the cytoplasm of an alveolar epithelial cell from the lung of a newborn (BALB cXC3H)F_1 mouse. Many ergastoplasmic profiles can be seen as well as a number of mitochondria. Typical cristae are present in most of the mitochondria, but in a few (*M*2) the interior of the mitochondrion is occupied by numerous strands which extend from one side to the other across vacuolated spaces. In still other mitochondria (*M*3) very small vacuoles are present, but more or less typical cristae can be recognized. Microvilli extend into the alveolus, and the cell membrane at one place shows evidence of fusion (arrow). Chrome osmic fixation, pH 7.2. ×43,000.

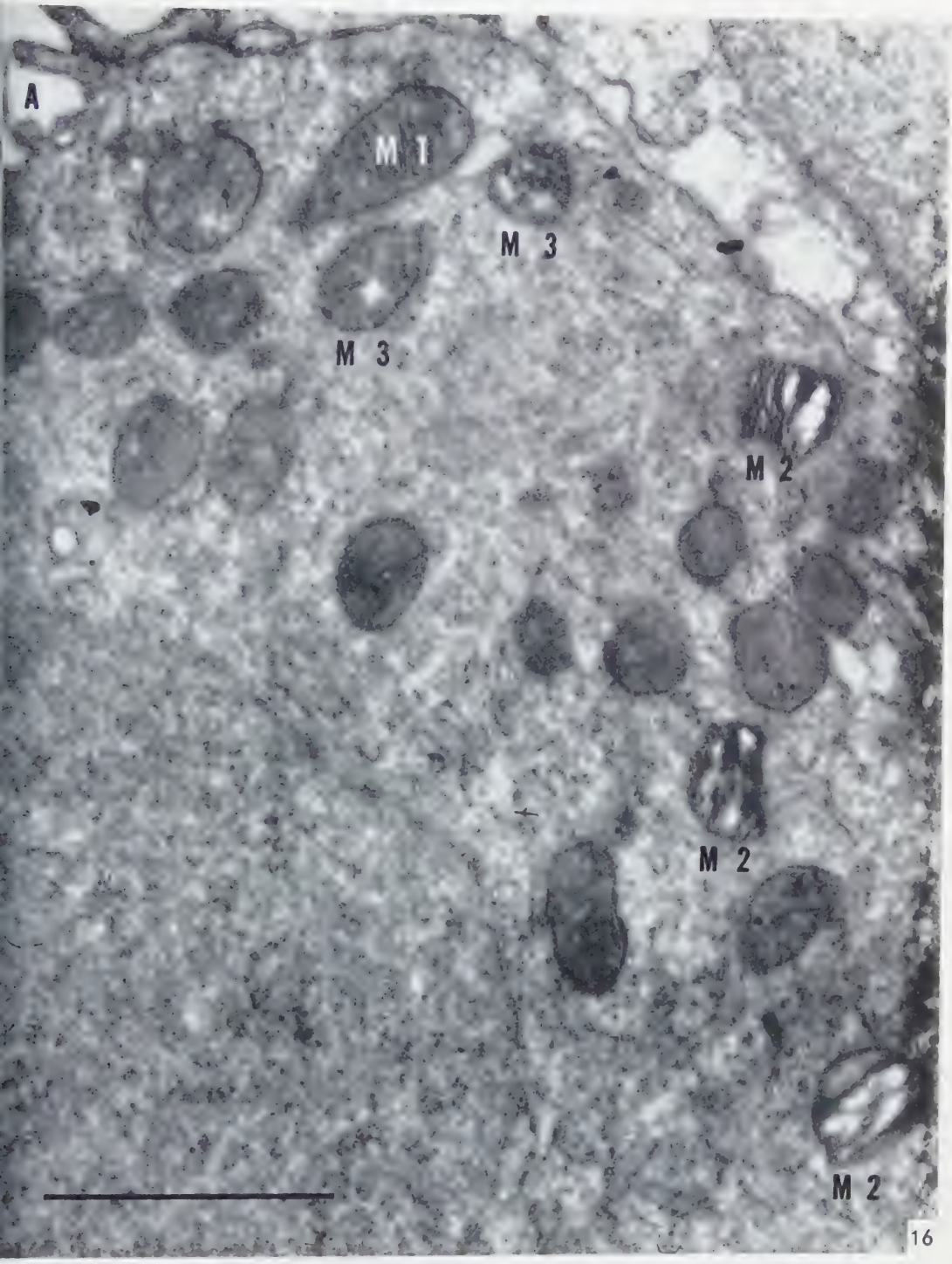

16

FIG. 17. Mitochondria in an alveolar epithelial cell from the lung of an 18-day (BALB/cXC3H)F_1 mouse embryo. At $M1$ less dense areas between the cristae suggest the early formation of vacuoles, whereas the mitochondria at $M2$ and $M3$ seem to be normal in appearance. Chrome osmic fixation, pH 7.2. $\times$ 76,000.

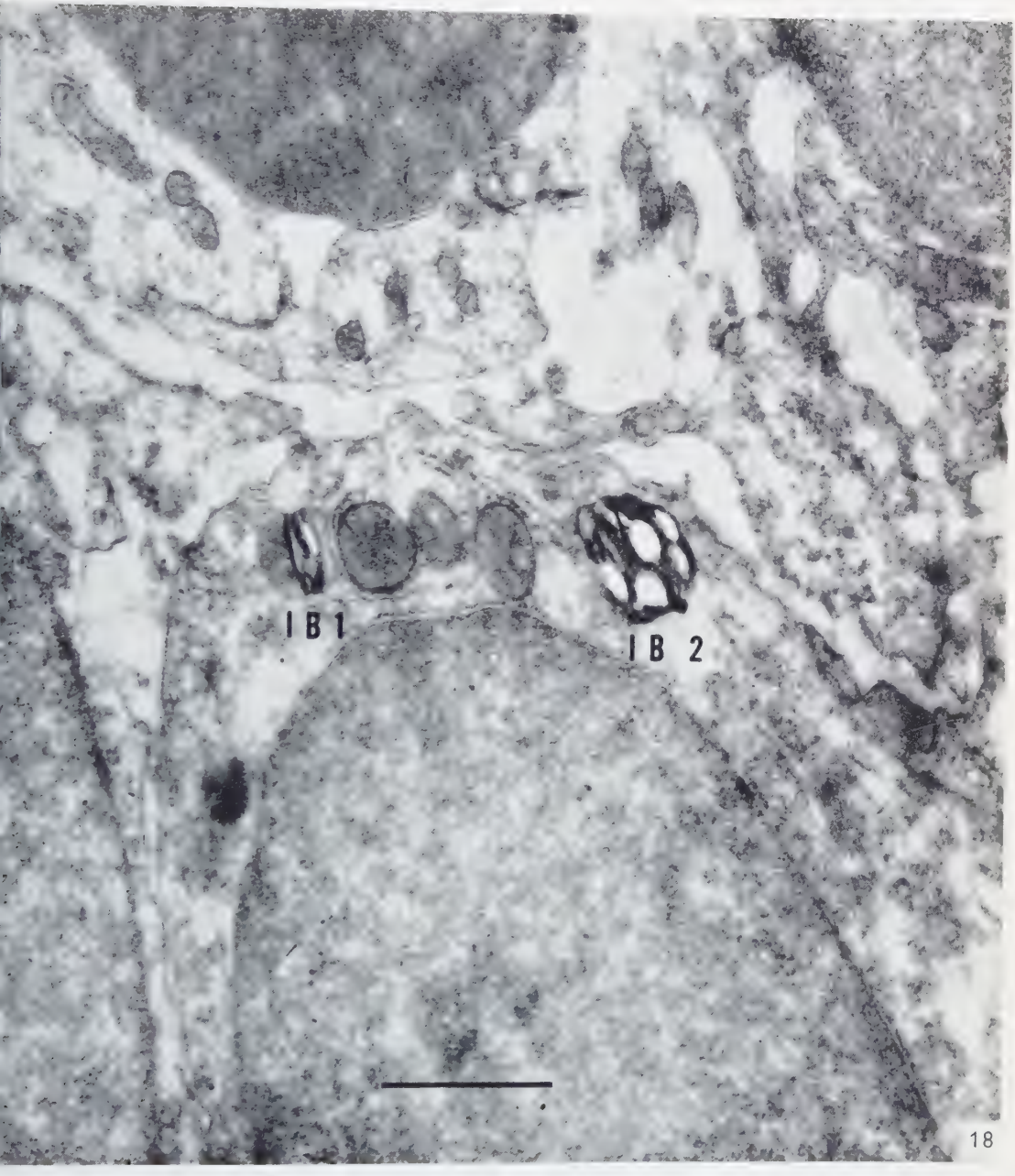

18. Mitochondria and inclusion bodies in an alveolar epithelial cell of an 18-day (BALB/cXC3H)F_1 mouse
ryo. One of the inclusion bodies (*IB*1) suggests a very early stage in the transformation of a mitochondrion; some
nal cristae are visible on either side of a region of more dense filaments which extend from one border of the
cture to the other. Less dense areas among these filaments suggest early vacuole formation. The other inclusion
(*IB*2) is not only larger than either the mitochondria or the first inclusion body, but also contains a number
acuoles in addition to dense filaments. Chrome osmic fixation, pH 7.2. ×24,000.

two to five times greater than in young cells, they were vacuolated, and their cristae were represented by small stumps only.

It seems to us that the degenerating mitochondria found by Howatson and Ham (*12*) in a small percentage of Novikoff tumor cells are probably different from the inclusion bodies under discussion. They contained granular material but no vacuoles. It is also doubtful whether the changes induced in isolated rat liver mitochondria (*28*) following irradiation with gamma rays are related to the present findings.

Indirect evidence for a change from one type of alveolar epithelial cell to another is provided by the fact that the mitotic rate of normal lung tissue is surprisingly high (*3*, *45*, *46*). High mitotic activity implies that cells are being lost and that replacement is accomplished by cell division. The cells being lost are probably sloughed off as was suggested by Bertalanffy and Leblond (*3*). Low (*24*) and Policard *et al.* (*34*) describe free alveolar cells although Karrer (*14*) could not find cells of this type. So far as we know it has not been proved that these free cells contain larger numbers of inclusion bodies. Even if this were to be proved, the problem would still remain as to whether or not the two types of alveolar epithelial cells which have been described are really but variants of one type. That the lung contains two types of cells which have different staining properties has been shown by Bertalanffy and Leblond (*3*). This in itself would suggest a difference in the metabolic activity of the two types. It seems to us that the possibility that one type is degenerating into the other should certainly be excluded before the evidence that there are two distinct morphological types can be considered to have been proved.

Mitochondria. With respect to the normal internal structure of the mitochondria of alveolar epithelial cells, our observations confirm the work of Palade (*29*, *31*), Low (*26*), Howatson and Ham (*13*), Ekholm and Sjöstrand (*6*) and others. Our evidence agrees with the finding that the cristae arise by the folding of the inner limiting membrane. Osmiophilic mitochondrial granules are frequently observed.

Golgi. Many of the epithelial cells especially in the lungs of newborn and embryo mice contain well-differentiated Golgi elements. These always contain the small vesicles and groups of lamellae or tubules but we have not found in lung tissue any examples of Golgi material containing the larger vacuoles typically associated with the other elements (*5*).

Ergastoplasm. Policard *et al.* (*34*) state that the alveolar epithelial cells are normally deprived of ergastoplasm. Our observations indicate that for adult tissue the amount of ergastoplasm is reduced but not absent. It should be emphasized, however, that typical ergastoplasm occurs normally in epithelial cells of the lungs of 14- through 18-day mouse embryos and is exceptionally well seen in newborn mice. Intra cytoplasmic membranes and vesicles both with and without RNP particles are a regular feature in such tissues. Karrer (*15*, *17*) studied bronchiolar epithelium of the mouse

and found that the ciliated cells contained a relatively small amount of endoplasmic reticulum while non-ciliated cells contained a larger amount of well-developed endoplasmic reticulum.

Nuclear envelope. Watson (*43*) stated that in resting cells of rat liver and spleen the outer nuclear membrane was continuous with the ergastoplasm. This was confirmed by Palade (*32*) for lymphocytes, monocytes, granulocytes and macrophages. He spoke of this envelope as a perinuclear cisterna. We have shown that the same arrangement prevails in the alveolar epithelial cells of mouse lung. The extension of the outer nuclear membrane into the cytoplasm as fully differentiated ergastoplasm is clearly shown.

Watson (*43*) found that in interphase cells "circular pores are formed in the double nuclear envelope by continuities between the inner and outer membranes which permit contact between the nucleoplasm and the cytoplasm unmediated by a well defined membrane". Porter (*36*) also reported that "at several points the continuity of the profile (nuclear envelope) is interrupted by pores or openings, and at these points the less dense regions of the nuclear content are continuous with the continuous phase (the matrix) of the cytoplasm". Anderson and Beams (*2*) also report the presence in Rhodnius of nuclear pores 400 Å in diameter. They were also seen by Howatson and Ham (*13*) in Novikoff hepatoma cells. One might interpret the nuclear membrane seen in Fig. 3 in this way, but it seems more probable to us that the membrane has simply been broken, thus giving the appearance of pores not unlike some of those shown by Watson and by Porter. When this figure is compared with Fig. 4 and especially with Fig. 11, it becomes evident that the normal uninjured nuclear membrane does not show true discontinuities. The inner and outer nuclear membranes appear to fuse, giving rise to a single thin membrane which extends across the "pore". That true nuclear pores seem unlikely is indicated by the biochemical evidence presented by Hogeboom and Schneider (*11*). For further discussion of this problem see Haguenau and Bernhard (*8*), Kautz and DeMarsh (*19*) and André and Rouiller (*1*).

REFERENCES

1. André, J. and Rouiller, Ch., *Proc. Stockholm Conf. Electron Microscopy*, 1956, p. 162. Almqvist & Wiksell, Stockholm, and Academic Press Inc., New York, 1957.
2. Anderson, E. and Beams, H. W., *J. Biophys. Biochem. Cytol.* **2**, 439 (1956).
3. Bertalanffy, F. D. and Leblond, C. P., *Anat. Record* **115**, 515 (1953).
4. Cowdry, E. V., *Carnegie Inst. Wash. Publ. Contrib. Embryol.* **8**, 39 (1918).
5. Dalton, A. J. and Felix, M. D., *in* Fine Structure of Cells, *Symposium VIIIth Intern. Congr. Cell Biol., Leiden*, 1954, p. 274. P. Noordhoff Ltd., Groningen, 1955.
6. Ekholm, R. and Sjöstrand, F. S., *J. Ultrastructure Research* **1**, 178 (1957).

7. Greene, D. E., Lester, R. L. and Ziegler, D. M., *Biochim. et Biophys. Acta* **23**, 516 (1957).
8. Haguenau, F. and Bernhard, W., *Bull. du cancer* **42**, 537 (1955).
9. Hartman, J. F., *J. Biophys. Biochem. Cytol.* **2**, 375 (1956).
10. Hesse, F. E. and Loosli, C. G., *Anat. Record* **105**, 299 (1949).
11. Hogeboom, G. H. and Schneider, W. C., *Science* **118**, 419 (1953).
12. Howatson, A. F. and Ham, A. W., *Cancer Research* **15**, 62 (1955).
13. —— *Can. J. Biochem. and Physiol.* **35**, 549 (1957).
14. Karrer, H. E., *Bull. Johns Hopkins Hosp.* **98**, 65 (1956).
15. —— *J. Biophys. Biochem. Cytol.* **2**, 115 (1956).
16. —— *ibid.* **2**, 241 (1956).
17. —— *Exptl. Cell Research* **10**, 237 (1956).
18. —— *J. Appl. Phys.* **28**, 1381 (1957).
19. Kautz, J. and DeMarsh, Q. B., *Exptl. Cell Research* **8**, 394 (1955).
20. Kikuth, H. W., Schlipkoter, H. W. and Schroeteler, P., *Proc. Stockholm Conf. Electron Microscopy*, 1956, p. 246. Almqvist & Wiksell, Stockholm, and Academic Press Inc., New York, 1957.
21. Kisch, B., *Exptl. Med. Surg.* **13**, 101 (1955).
22. Loosli, C. G., Adams, W. E. and Thornton, T. M., *Anat. Record* **105**, 697 (1949).
23. Low, F. N., *Anat. Record* **113**, 437 (1952).
24. —— *ibid.* **117**, 241 (1953).
25. —— *ibid.* **120**, 827 (1954).
26. —— *J. Biophys. Biochem. Cytol.* **2**, 337 (1956).
27. Luft, J. and Hechter, O., *J. Biophys. Biochem. Cytol.* **3**, 615 (1957).
28. Okada, S. and Peachey, L. D., *J. Biophys. Biochem. Cytol.* **3**, 239 (1957).
29. Palade, G. E., *Anat. Record* **114**, 427 (1952).
30. —— *J. Exptl. Med.* **95**, 285 (1952).
31. —— *J. Histochem. and Cytochem.* **1**, 188 (1953).
32. —— *J. Biophys. Biochem. Cytol.* **1**, 567 (1955).
33. Payne, F., *Anat. Record* **96**, 77 (1946).
34. Policard, A., Collet, A. and Pregermain, S., *Proc. Stockholm Conf. Electron Microscopy*, 1956, p. 244. Almqvist & Wiksell, Stockholm, and Academic Press Inc., New York, 1957.
35. Policard, A., Collet, A. and Giltaire Ralyte, L., *Presse méd.* **62**, 1775 (1954).
36. Porter, K. R., *Harvey Lectures, Ser.* **51**, p. 175. Academic Press Inc., New York, 1957.
37. Porter, K. R. and Kallman, F., *Exptl. Cell Research* **4**, 127 (1953).
38. Schlipkoter, H. W., *Deut. med. Wochschr.* **79**, 1658 (1954).
39. Schulz, H., *Naturwissenschaften* **43**, 205 (1956).
40. —— *Virchow's Arch. pathol. Anat. u. Physiol.* **328**, 582 (1956).
41. —— *Proc. Stockholm Conf. Electron Microscopy*, 1956, p. 240. Almqvist & Wiksell, Stockholm, and Academic Press Inc., New York, 1957.
42. Swigart, R. H. and Kane, D. J., *Anat. Record* **118**, 57 (1954).
43. Watson, M. L., *J. Biophys. Biochem. Cytol.* **1**, 257 (1955).
44. Weiss, J. M. and Lansing, A. I., *Proc. Soc. Exptl. Biol. Med.* **82**, 460 (1953).
45. Woodside, G. L. and Kelton, D. E., *Anat. Record* **122**, 484 (1955).
46. —— *ibid.* **125**, 571 (1956).

The Fine-Structure of the Mitotic Spindle in Sea Urchin Eggs[1]

P. R. Gross, D. E. Philpott, and S. Nass

Biology Department, New York University, New York, and Marine Biological Laboratory, Woods Hole, Massachusetts

Received June 30, 1958

The mitotic apparatus of dividing eggs of *Arbacia punctulata* has been observed with the electron microscope in ultrathin sections of the cells fixed in subzero ethanol, sea water-OsO_4, and buffered, isotonic OsO_4. Marked differences in appearance obtain among the different preparations. In general, ethanol tends to aggregate and coarsen fine-structure, and OsO_4 to disperse it. Features of spindle ultrastructure common to all preparations, and hence assumed to reflect conditions *in vivo* are: (1) very large numbers of small, dense particles, assumed to be ribonucleoprotein; (2) general fine-structure identical with that of the ground cytoplasm elsewhere in the cell; (3) exclusion from the forming and completed spindle of all cytoplasmic particulates larger than a few hundred Å; and (4) a fibrous (or finely tubular) component, probably connecting kinetochores with the centriolar region, the fibers being associated along their entire length with the RNP particles.

The reality of the mitotic apparatus as a fibrous structure in the dividing cell appears, after some lingering doubts, to be finally established. A major line of evidence in this development has been the demonstration of birefringence in the spindle and asters (e.g., *12*, *13*, *30*). Equally important, perhaps, has been the demonstration that the mitotic apparatus may be isolated as a unit by selective solubilization of the cytoplasm in dividing sea urchin eggs (*17*).

Establishment of the highly-gelled, fibrous nature of the mitotic spindle makes possible a rational attack upon the problems surrounding the mechanisms of its formation. Two lines of attack have recently developed, one employing chemical investigation of isolated spindles as well as the isolation treatments themselves (*15*, *16*), the other beginning with consideration of the labile colloidal systems of the cytoplasm presumed to be involved in sol-gel transformations (*2*, *3*, *5–8*).

Study of the ultrastructure of the mitotic apparatus by contemporary methods has, unfortunately, been attempted in only a few cases. This is the more surprising in

[1] The substance of this paper was presented in a lecture at the New York Academy of Sciences on November 11, 1957, a long abstract of which was published in Trans. N. Y. Acad. Sci., Ser. II, *20*, 154–172 (1957).

view of the improved techniques now available to electron microscopists and of the fundamental nature of the problem.

Mazia (*15*) has published electron micrographs of sections of isolated spindles, but the general quality of these is inadequate for the purpose of defining spindle ultrastructure, particularly since the procedures used in spindle isolation may well solubilize important components, providing, in the electron micrographs, a deceptively simple structure.

Electron micrographs of high quality have been made by Porter (*23*, *24*) for certain tumour cells, and by Harven and Bernhard (*10*) for certain vertebrate tissue cells. Other studies have been reported by Beams *et al.* (*4*), Rozsa and Wyckoff (*25*), Sedar and Wilson (*26*), Selby (*27*), and Tanaka *et al.* (*31*). Kurosumi (*14*) has very recently published a paper on mitosis in the sea urchin *Heliocidaris crassispina*. The earlier observations suffer from inadequate resolution and poor orientation, while the more recent ones provide (except for those of Kurosumi) only as much information as can be obtained from populations of cells in which mitotic figures are not plentiful and correct orientation in sections is even more rare.

Thus the literature now available must be regarded only as a beginning in the study of mitotic ultrastructure. The very extensive accounts of spindle fine-structure provided by Mazia rest on grounds other than morphologic.

The features of marine invertebrate eggs which make them such desirable objects for physiologic and biochemical studies on cell division serve also in morphologic investigations. Thus, in a properly handled population of *Arbacia punctulata* eggs, 95% of the cells will be in mitosis, and of these, say 50% might be at or near metaphase of the first cleavage, the remainder lagging or leading very slightly. Examination of such cell populations with ordinary techniques of electron microscopy should yield, *a priori*, a high proportion of observations on cells with mitotic figures present, in the chosen stage, and perhaps most important, properly oriented.

The results presented herein represent an effort toward systematic investigation of such a type. They represent, however, an additional purpose: the electron micrographs of isolated spindles presented by Mazia (*15*) can be interpreted in terms of one of several conflicting theories of spindle ultrastructure; and yet, these micrographs may be misleading, since the isolated spindles have been treated in a way that might result in the extraction of important chemical components. We have, therefore, in these studies, employed not only the conventional OsO_4 fixation, but also the same treatment used by Mazia and Dan (*17*) to "kill" their cells prior to solubilization of the cytoplasm surrounding the spindle. We have then simply avoided removing the cytoplasm, and having "fixed" the cells with subzero ethanol (*vide infra*), osmicated afterward, as Mazia (*15*) has done with the isolated spindles. Our observations in this area should serve, therefore, as a morphologic control on the Mazia-

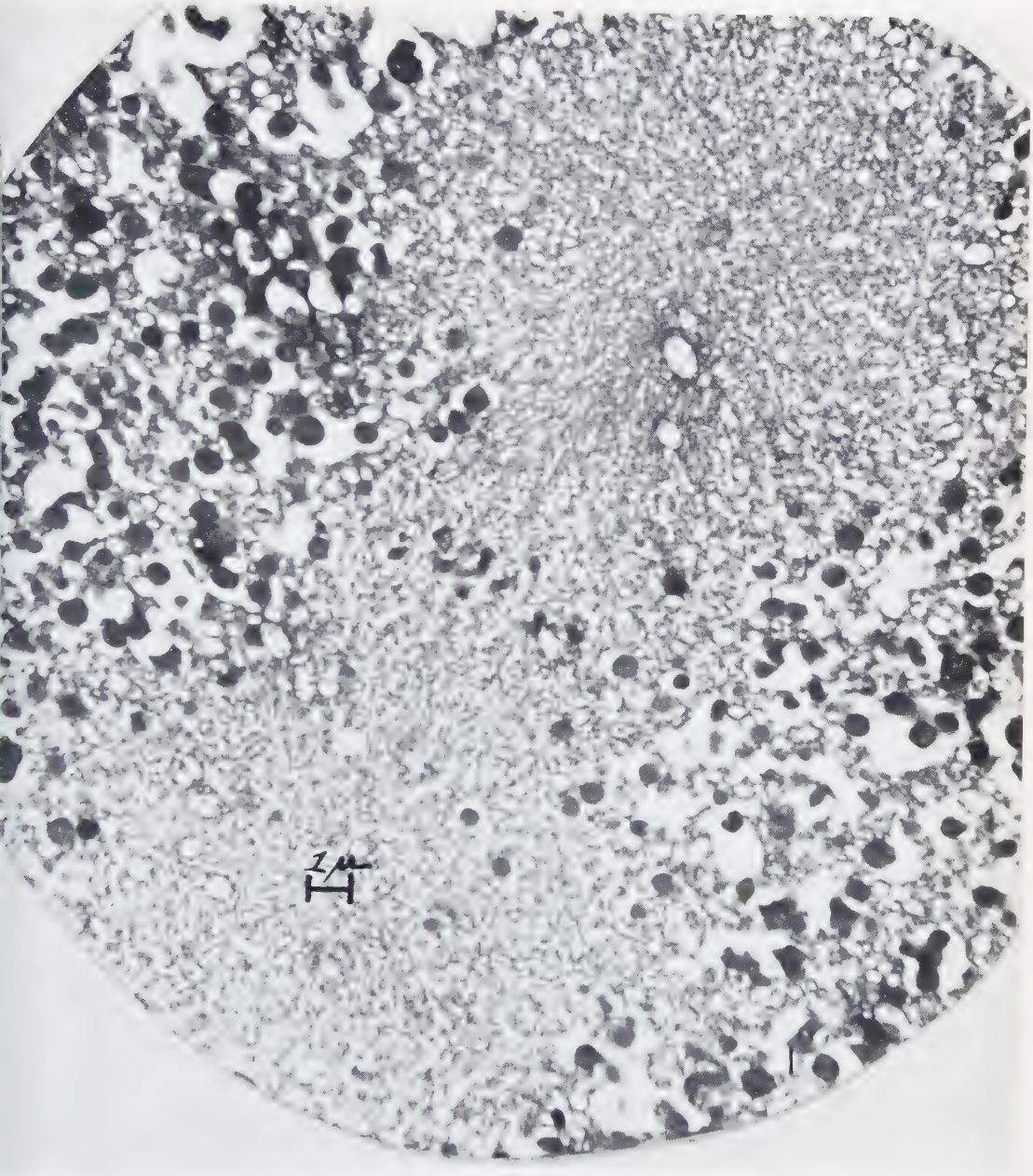

1. Survey view of metaphase figure in first cleavage division of *Arbacia* egg. Fixation: 30% ethanol at −10°C. osmication. "Chromosomal" fibers visible. Extensive shrinkage of cytoplasmic inclusion bodies. ×6000.

Dan isolation procedure, and on their interpretations of spindle ultrastructure as based upon observations of the isolated material. Published details of newer methods of isolation, not requiring alcoholization, and being developed in Mazia's laboratory, are awaited in this regard with interest.

METHODS

The cells studied were fertilized eggs of *Arbacia punctulata*, obtained and treated in ordinary fashion (*11*). Two types of fixation were employed: ethanol and OsO_4.

Ethanol fixation. Mazia and Dan (*17*) discovered that cells in mitosis may be killed, without destruction of the sensitive spindle, in 30% ethanol at − 10 C. This fixative, furthermore, effects a minimum of denaturation of cytoplasmic proteins, and hence, it is proposed, a minimum rearrangement of spindle ultrastructure. After fixation, Mazia and Dan isolate the mitotic apparatus by solubilization of the cytoplasm with detergents, or more recently (*16*), with ATP, leaving intact the spindle and associated structures. In our procedure, eggs in the desired stage of mitosis are fixed in 30% ethanol at − 10 C for 30 minutes. At the end of this period, the fixative is replaced with subzero 30% ethanol containing 1% osmium tetroxide. The osmium penetrates and stains adequately within about 30 minutes, during the last fifteen of which the cells are removed from the ice-salt bath and permitted to warm toward room temperature. Toward the end of the staining period, the solution begins to accumulate reduction products of the OSO_4 and is changed. Fixation and osmication completed, the cells are dehydrated by passage through an alcohol series. Embedding and cutting are described below.

OsO_4 fixation. Cells in the desired stage of mitosis are lightly centrifuged, the sea water decanted, and the fixative added, after which the eggs are resuspended by gently shaking. The fixatives used were: (1) 1% OsO_4 dissolved in sea water without additional buffering, pH 7.2, and (2) 1% OsO_4 in an artificial, isotonic sea water, heavily buffered with veronal-acetate-HCl to pH 7.4. This solution is prepared by a modification of the fixative used by Sjöstrand and described in Zetterqvist (32). The final osmolarity was 1.0.

All dehydrated specimens were embedded in a mixture of four parts of *n*-butyl methacrylate and one of methyl methacrylate, in gelatin capsules. With benzoyl peroxide as catalyst, the plastic was thermally polymerized at 55 C to sufficient hardness. The plastic blocks were cut on the microtome described by Philpott (*21*), and the ribbons floated on 30% acetone which was later enriched to 50% to facilitate flattening. Specimen grids were 100 mesh copper, and the support was either formvar or carbon.

The electron micrographs were made with an RCA model EMU-2C instrument fitted with a 250 micron condenser aperture and a 65 micron objective aperture.

While a reasonably complete set of stages for the first cleavage has been obtained, no attempt will here be made to discuss the mitotic cycle systematically; such a course would be at variance with the purpose of the present communication, which is to describe the ultrastructure of the mitotic spindle in the *Arbacia* egg.

FIG. 2. Survey view of metaphase figure in first cleavage division of *Arbacia* egg. Fixation: Veronal-acetate buffered 1% OsO_4 in isotonic salt solution. Mitochondria at *m*, yolk granules at *y*, pigment vacuole at *p*, chromosomes (?) at *ch*. This micrograph should be compared with Fig. 1. Note absence of spindle fibers, and of condensed chromosomes. × 6000.

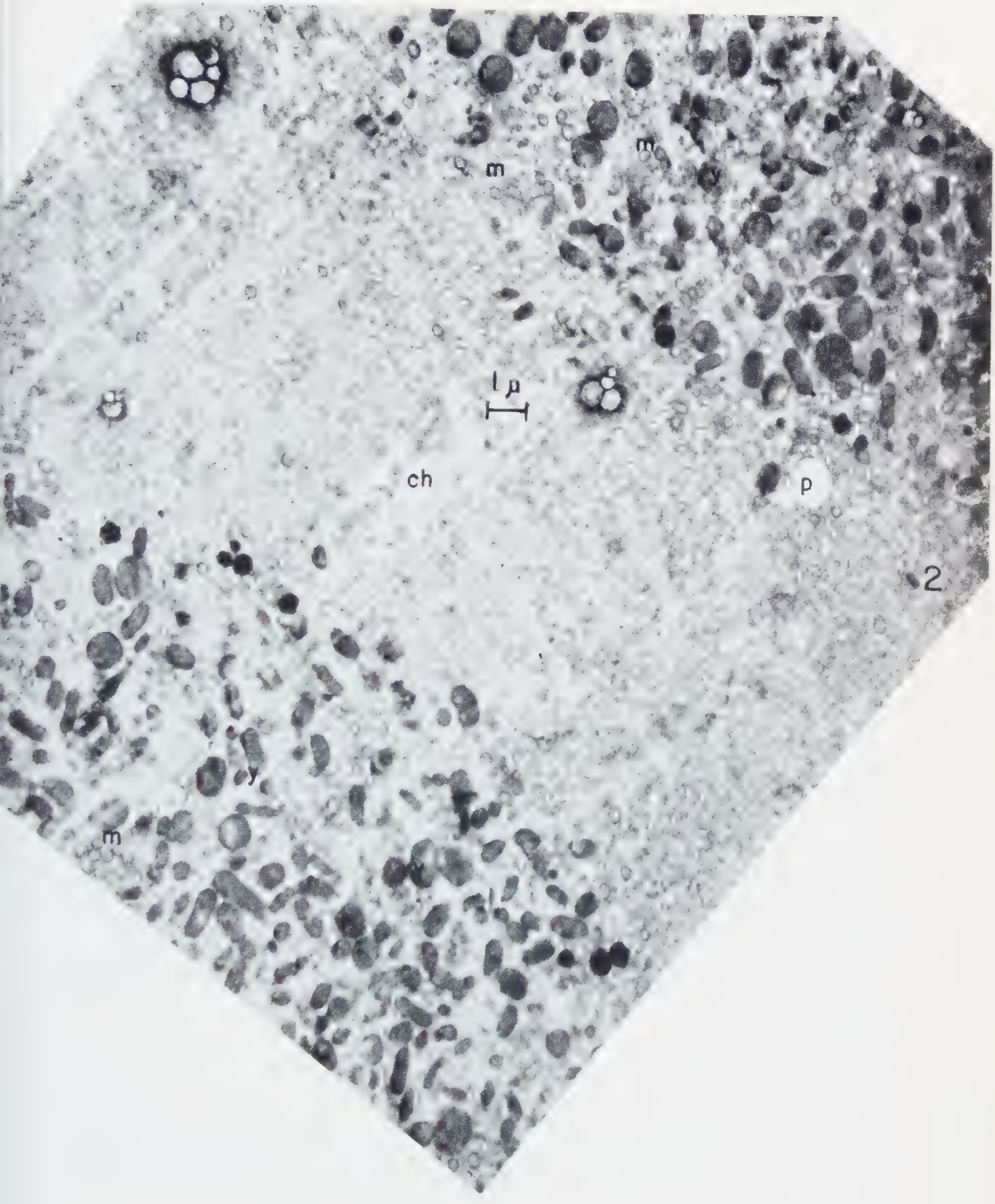
m
m
1 μ
ch
p
2
m

RESULTS

Both the cold ethanol and the OsO_4 techniques permitted observations of the mitotic apparatus; i.e., the spindle, although easily dispersed with various metabolic poisons and with high hydrostatic pressures, was not dissolved or grossly disorganized in either fixative. The two techniques gave, however, very different results at the ultrastructural level, and these were in general opposite in effect: the alcohol treatment showed a tendency to shrink, condense, and coarsen structures, and the OsO_4 tended to disperse and make homogeneous structures even large enough (e.g., astral "rays" and spindle "fibers") to be seen optically in the living cell. This may be a fortunate result, since it appears quite possible that the situation *in vivo* is intermediate between that obtaining in OsO_4-fixed specimens and that seen in alcohol-fixed material.

Fig. 1 is a survey view, at low magnification, of a metaphase cell fixed in subzero alcohol. The section is quite thick. Fixation of cytoplasmic structures is poor, and the ethanol solution has clearly caused much shrinkage of the large cytoplasmic particulates (pigment vacuoles, yolk granules, etc.). The mitochondria cannot be identified after this treatment. The mitotic apparatus, however, is remarkably similar at this magnification to that seen with the light microscope in living or fixed cells. "Chromosomal" fibers are visible, and these, on closer examination, are seen as bundles of several finer fibers. The chromosomes are visible as typical condensed metaphase bodies.

Fig. 2 is a survey view, for comparison, of a cell in the metaphase of the first cleavage, fixed in buffered, isotonic OsO_4. The ground cytoplasm is here homogeneous and finely dispersed; mitochondria are clearly visible, with their characteristic internal structure preserved. The yolk particles are not shrunken. Two pigment vacuoles are shown (the pigment is extracted during fixation, leaving a hole surrounded by the vacuolar membrane). There are, of course, a great many pigment vacuoles in this egg, but at fertilization, these move out to the periphery, leaving very few in the region immediately surrounding the spindle (*11*). Oil globules are seen as dense, crenated, structureless bodies of diameter 0.5–1.0 microns. Most striking is the relative homogeneity of the spindle; no fibers are seen at this magnification, and the chromosomes themselves are invisible. This last is not surprising in view of the difficulty of seeing the metaphase chromosomes in the living cell, and in view of the finding of Mitchison and Swann (*18*) that the metaphase chromosomes are invisible when sought with the interference microscope, having as they do the same refractive index as the spindle itself. That the chromosomes are nevertheless present is shown by their gradual reappearance in early anaphase, when they progressively lose density relative to the spindle, and begin to vesiculate anticipating telophase.

These observations, even at low magnification, permit one conclusion: the spindle

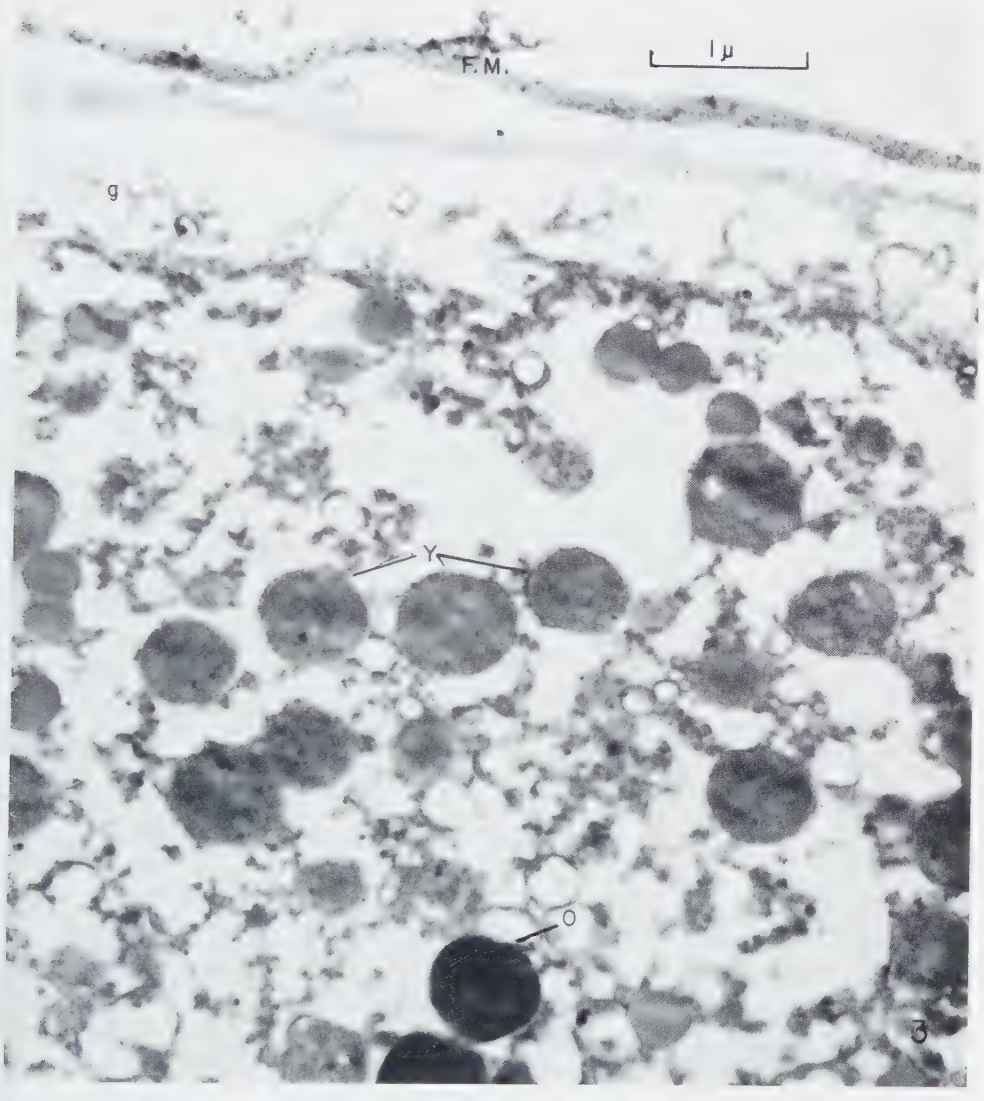

FIG. 3. Region at periphery of fertilized *Arbacia* egg. Fixation: subzero ethanol. *F.M.*, fertilization membrane; *g*, remnants of lysed cortical granules; *O*, oil droplet; *Y*, yolk granules. To show general quality of fixation in ethanol (30%) at -10°C. $\times$21,000.

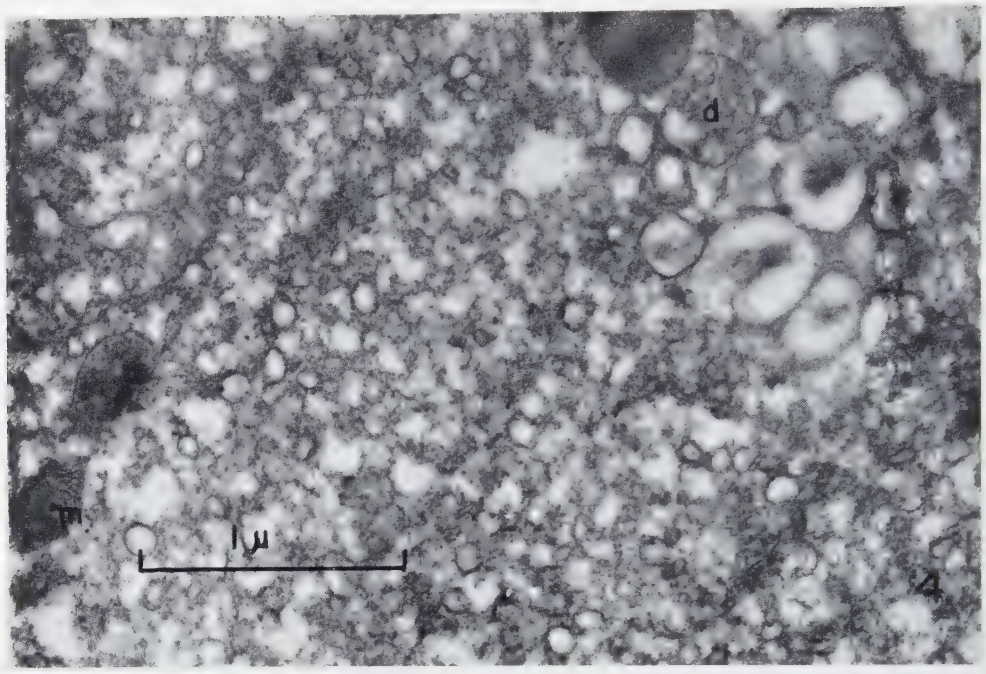

FIG. 4. Peripheral region, clear zone of centrifuged egg, unfertilized. To show quality of OsO_4 fixation Small vesicles in ground cytoplasm. Abundant RNP particles ("Palade particles"), 160 Å in diameter. Mitochondrion at *m*, dictyosome vesicles at *d*. × 35,000.

has a fine-structure largely similar to, or identical with, that of the ground substance of the cytoplasm as a whole. This conclusion is supported by the more detailed observations now to be described.

The quality of fixation of cytoplasmic structures in subzero ethanol is more easily assessed from photographs made at higher magnifications and with thinner sections. One such is shown in Fig. 3. This is a micrograph of a section of the periphery of a fertilized egg. Visible are the fertilization membrane, granular and vacuolar remnants of the cortical granules (which lyse at fertilization), yolk particles with their membranes, dense oil droplets, and an array of vacuolar or vesicular structures distributed throughout the ground cytoplasm. Some of these vesicles represent, perhaps, pigment vacuoles, but most of them appear to be artifacts, as discussed below. The ground

FIG. 5. Aster and adjacent cytoplasm, metaphase of first cleavage. The edge of the aster occupies the top 30 % of the print. Fixation: unbuffered sea water – OsO_4. Yolk at *Y*, mitochondria at *M*, oil droplets at *O*. Note considerable cytoplasmic vacuolization, abundant RNP particles, identity of fine structure in astral region with that of ground cytoplasm elsewhere. × 57,000.

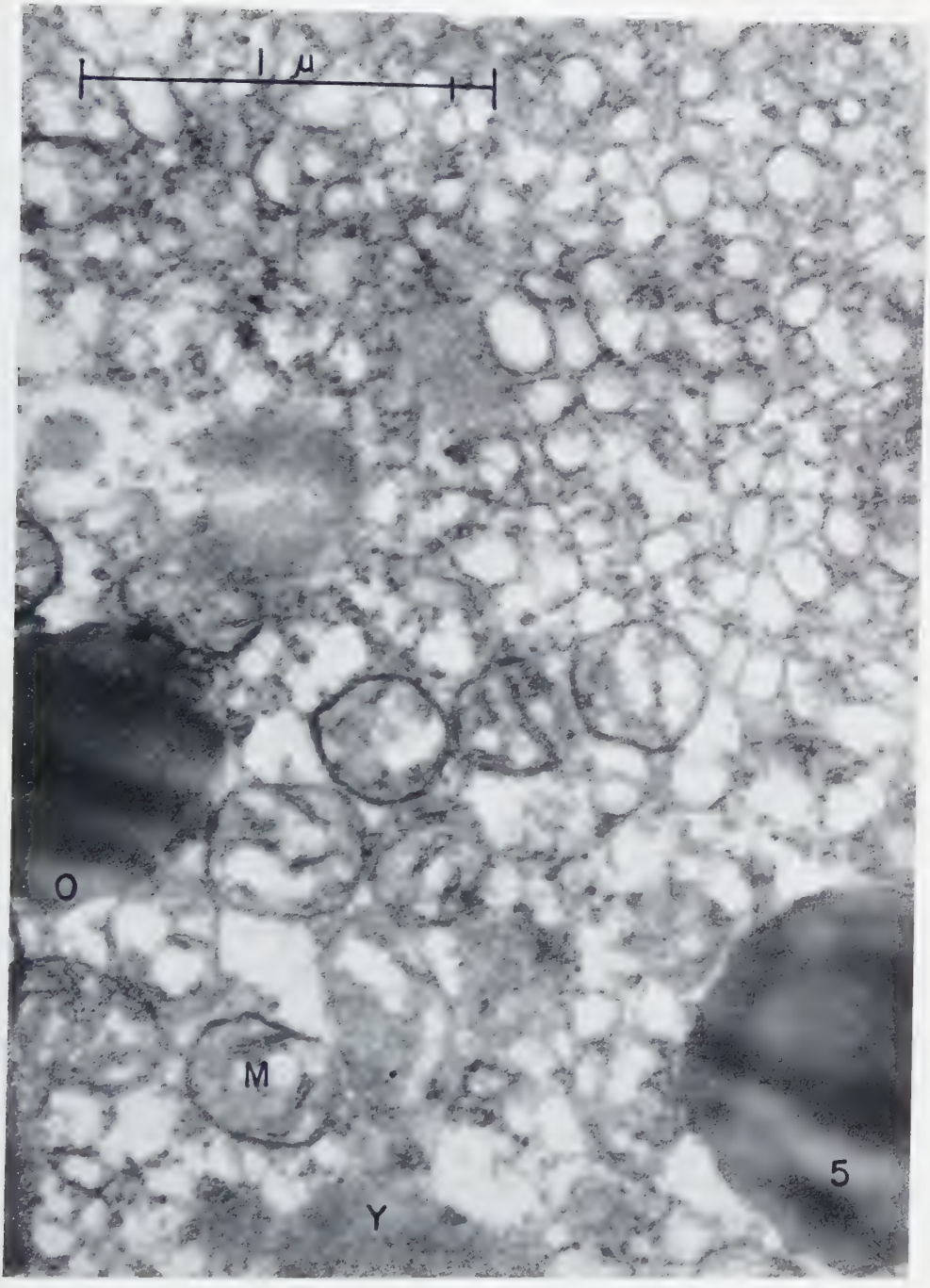
1 μ
O
M
Y
5

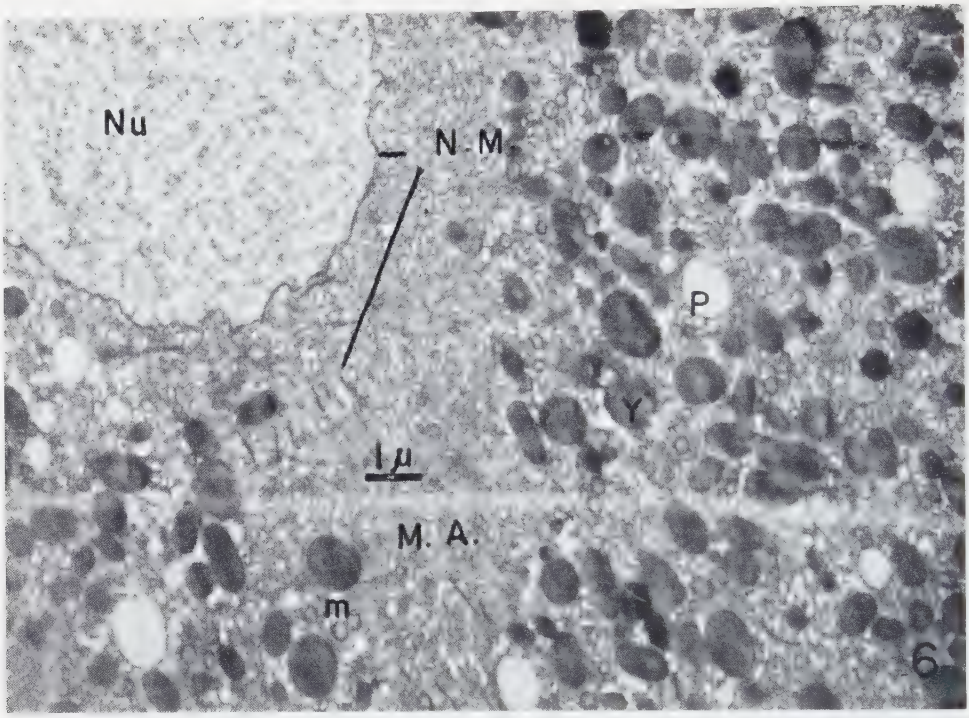

FIG. 6. Early "streak" stage, i.e., spindle forming prior to breakdown of fusion nucleus. Nucleus at *Nu*, nuclear membrane at *N.M.*, *m*, *p*, *y*, as before; *M.A.*, forming spindle. ×7500.

cytoplasm shows no extended membranous ergastoplasm, unless the many vesicles be regarded as such, but the dense ribonucleoprotein (RNP) particles associated with that component in other cells are seen in enormous numbers, albeit extensively aggregated in this fixative. Shrinkage has produced many "empty" spaces.

Figs. 4 and 5 show, for comparison, the quality of cytoplasmic fixation in OsO_4. Fig. 4 is a region of the clear zone of a centrifuged unfertilized egg, fixed with buffered OsO_4. This photograph shows only the ground substance, a small mitochondrion, and what appear to be a few dictyosomal vesicles (*9*). The ground substance is, however, finely dispersed, with only very small vacuoles, and the major visible component is the large population of free RNP particles, 160 Å in diameter, and supposed by Palade (*20*) to be responsible for cytoplasmic basophilia.

Fig. 5 is the periastral region of a metaphase cell fixed in OsO_4 in sea water (unbuffered except for the sea water bicarbonates). This fixative is inferior to the strongly buffered osmium tetroxide, since it produces very regularly a high degree of vacuolization. This extreme variability in the degree of vacuolization of the ground cytoplasm

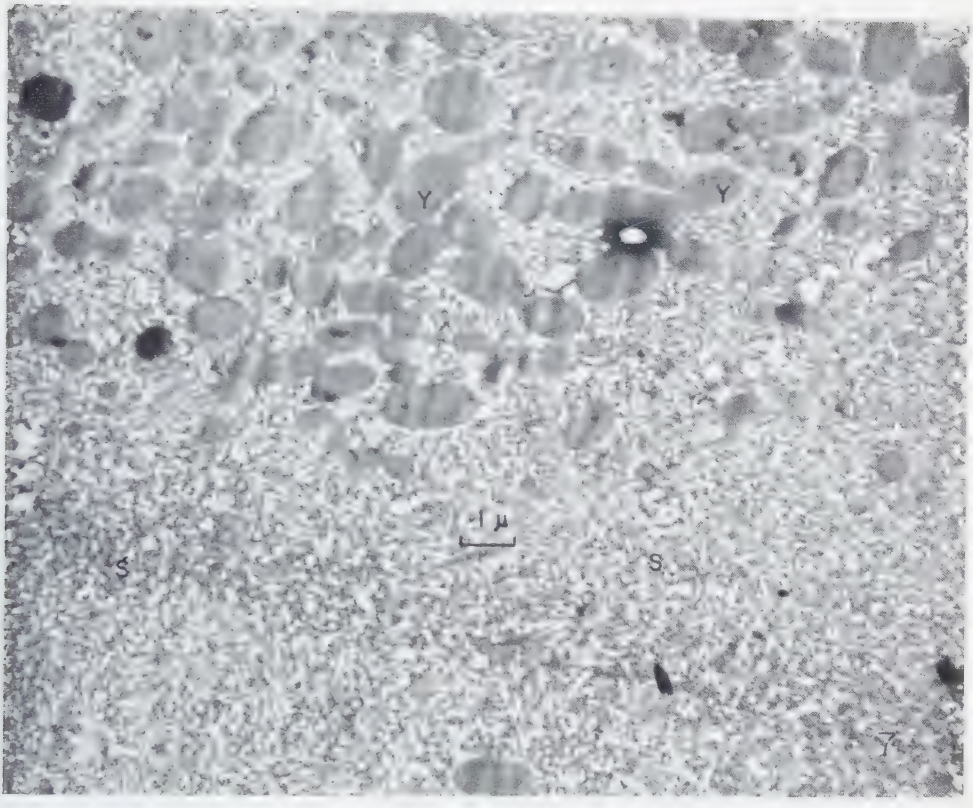

FIG. 7. Survey view of metaphase spindle. Regions of slight linear order at *S*, yolk at *Y*. Note similarity of fine-structure of spindle with ground cytoplasm elsewhere; abundant RNP particles, absence of visible chromosomes. × 7000.

makes it necessary to consider all such small vacuoles as seen in Fig. 5 as probable artifacts of fixation, and not, as is often suggested, as homologous to ergastoplasm or to the membranes thereof in vertebrate tissue cells. Despite the vacuolization, however, the cytoplasmic particulates are well preserved, as is the fine-structure of the mitochondria and yolk granules. The mitochondria show very well their double limiting membranes and their internal membranes. The ground substance is here again finely dispersed, and contains very large numbers of the free RNP particles.

Of particular interest in Fig. 5 is the astral region, seen in approximately the top 30% of the print shown. This region is identical in fine-structure with the ground cytoplasm elsewhere, except that the gelation leading to the formation of the aster has excluded from this zone all particulates larger than the 160 Å RNP particles.

That the ground cytoplasm may be in a different state of (unresolved) order in the

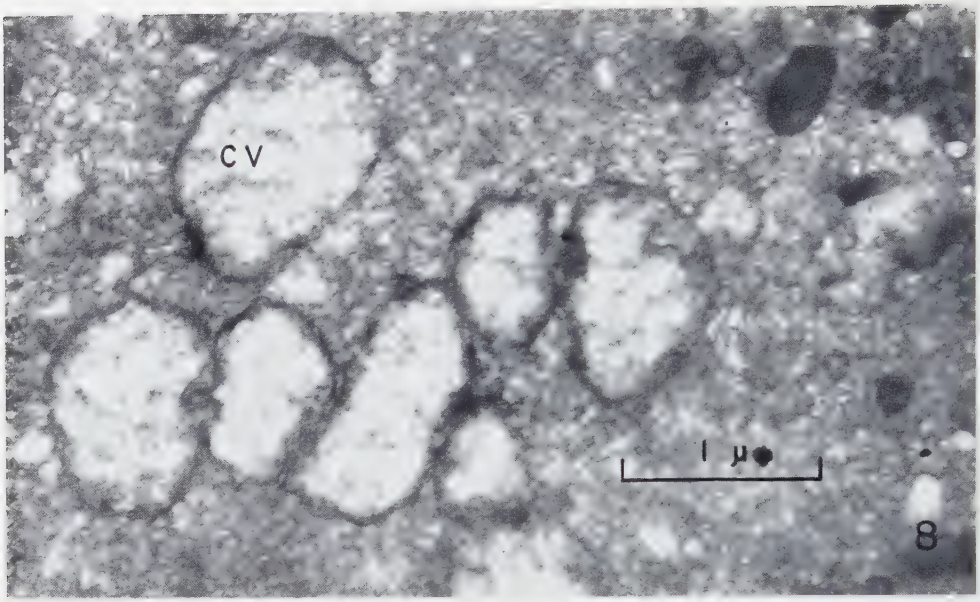

FIG. 8. Vesicular telophase chromosomes. × 26,000.

spindle region than elsewhere in the cell is suggested in Fig. 6, which shows a "streak" stage, i.e., beginning formation of the spindle prior to nuclear breakdown. Here, in a buffered-OsO_4 fixed specimen, are shown the nucleus, yolk, mitochondria, and pigment vacuoles. There appears to be no difference, at this magnification, between the ground substance surrounding the particulates and that within the forming "streak", except that the latter has somehow already excluded the larger particulates. It is to be noted that the "streak" spindle contains some linear fragments which may be, as Afzelius (*1*) has suggested, delaminated nuclear membrane. Whatever their origin, such fragments are often found in the perinuclear region, and may be responsible for the birefringence occasionally observed there.

Fig. 7 is another survey view of the metaphase spindle, fixed in buffered OsO_4. Once again, the conclusion is inescapable that the spindle contains everything except the large granules, and that these have somehow been pushed out of the mitotic figure. A tendency toward a certain degree of linear order is seen in the spindle regions marked *S*, and on closer examination this appears to be a manifestation of the presence of very fine fibers. These are, however, very scarce in the osmium-fixed material, at least with the resolutions available for these observations.

The chromosomes of the telophase figure are shown in Fig. 8. This is an early

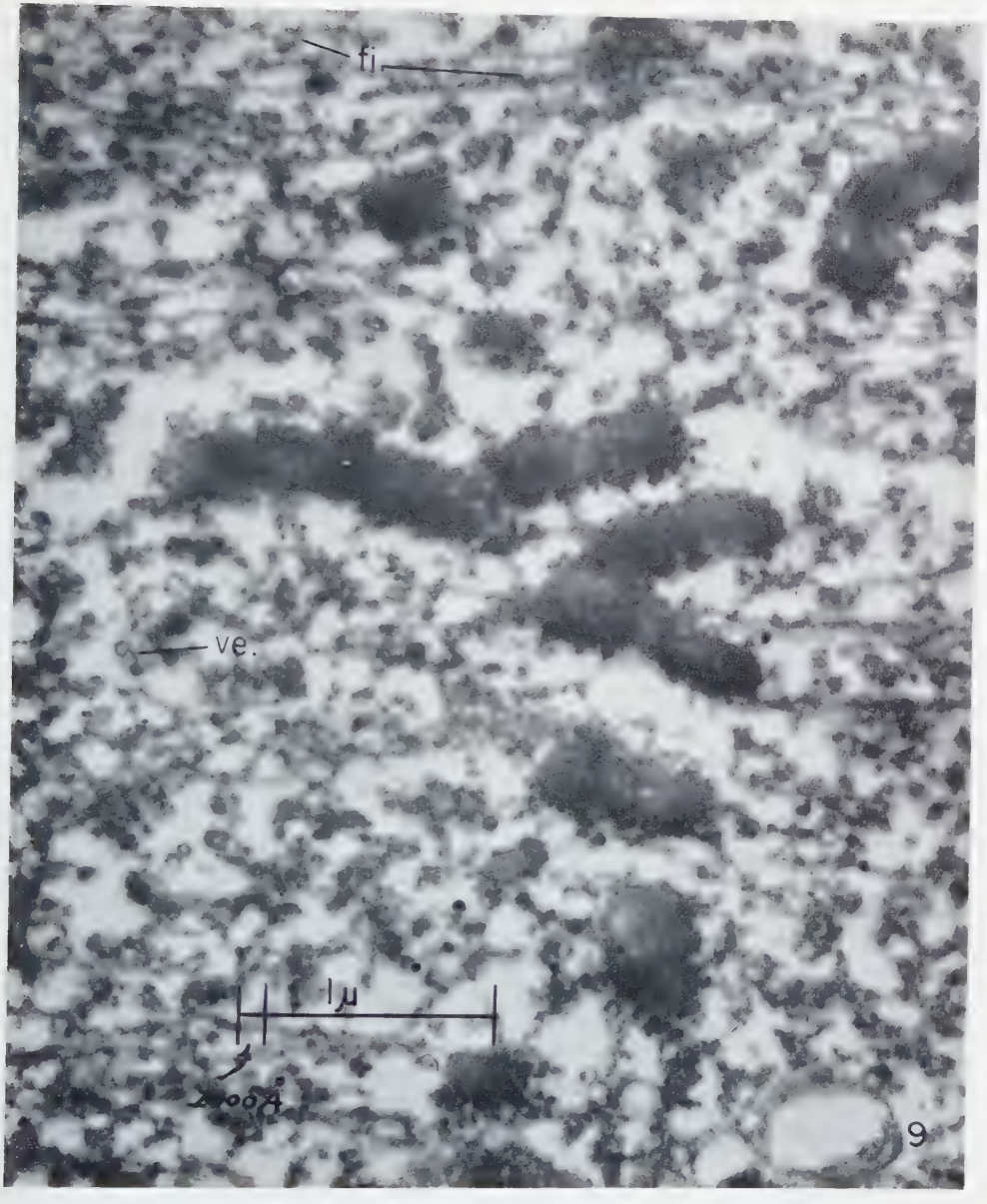

FIG. 9. Metaphase plate, ethanol-fixed egg in first cleavage mitosis. Densely osmiophilic chromosomes, chromosomal fibers. Abundance of somewhat aggregated RNP particles, separate and in association with fibrous or tubular elements (*fi.*). Small vesicles (*ve.*). × 34,000.

telophase, although the chromosome vesicles have begun to associate prior to reconstitution of the daughter nucleus.

While the metaphase chromosomes are invisible in the osmium-fixed specimens, they are clearly seen in the ethanol-fixed material, as shown in Figs. 9 and 10. Fig. 9 is a micrograph of the metaphase plate in an alcohol-fixed specimen, and together with Fig. 10, which is from a different preparation, shows several interesting features of spindle ultrastructure.

The chromosomes are very dense, and have obviously undergone differential shrinkage and condensation (cf. osmium-fixed specimens). Little detail of their internal structure is visible, except for a suggestion, pronounced at the chromosomal surfaces, of small 200–300 Å vesicles and particles (Fig. 9). The dense bodies seen in the large chromosome in Fig. 10 may be precipitated osmium. Fig. 10 shows the centromere region of one apparently metacentric chromosome, with reduced density within the centromere, and an interesting arrangement of the entering chromosomal fibers from opposite spindle poles.

These figures (9 and 10) show three structural components of the spindle itself: First, throughout the spindle, are found the small dense RNP particles. The mean diameter of these particles is here 400 Å, but in view of the tendency of these particles to aggregate during the ethanol fixation, it would appear likely that they represent clumps of the 160 Å particles found in the osmium-fixed specimens. The existence of this component in one or the other form in spindles fixed both ways makes it unlikely that this material represents a non-specific precipitate artifact. A second component of the spindle is an array of small vesicles (which are probably not profiles of tubules), some of them as small as 150 Å in diameter. Finally, and seen to advantage in the ethanol-fixed specimens, one finds fibers which run between the poles and the kinetochores or centromeres, and which apparently produce the fiber bundles seen as chromosomal fibers in thick survey sections such as the one shown in Fig. 1. These fibrous elements are ca. 200 Å wide, and show two peripheral densities and a less dense internal region, suggesting a tubular structure. Each fiber is associated with the small, dense RNP particles, but the fiber appears to be a distinct component, since the RNP ("microsomal") particles are found between and among the fibers, and indeed, occupying most of the volume of the spindle, of which the fibers constitute a miniscule fraction. At many points along the fibers, however, the RNP particles appear to merge completely with the fiber, suggesting that the latter may possibly be a product of the former.

FIG. 10. Metaphase chromosomes and spindle fibers, ethanol-fixed egg in first cleavage mitosis. Kinetochore at *cm.r.*, with chromosomal fibers (*fi.*) entering but not joining. Dense bodies in chromosome (*d.b.*) of unknown origin. Abundant RNP particles on, in, and surrounding fibrous elements. 30,000.

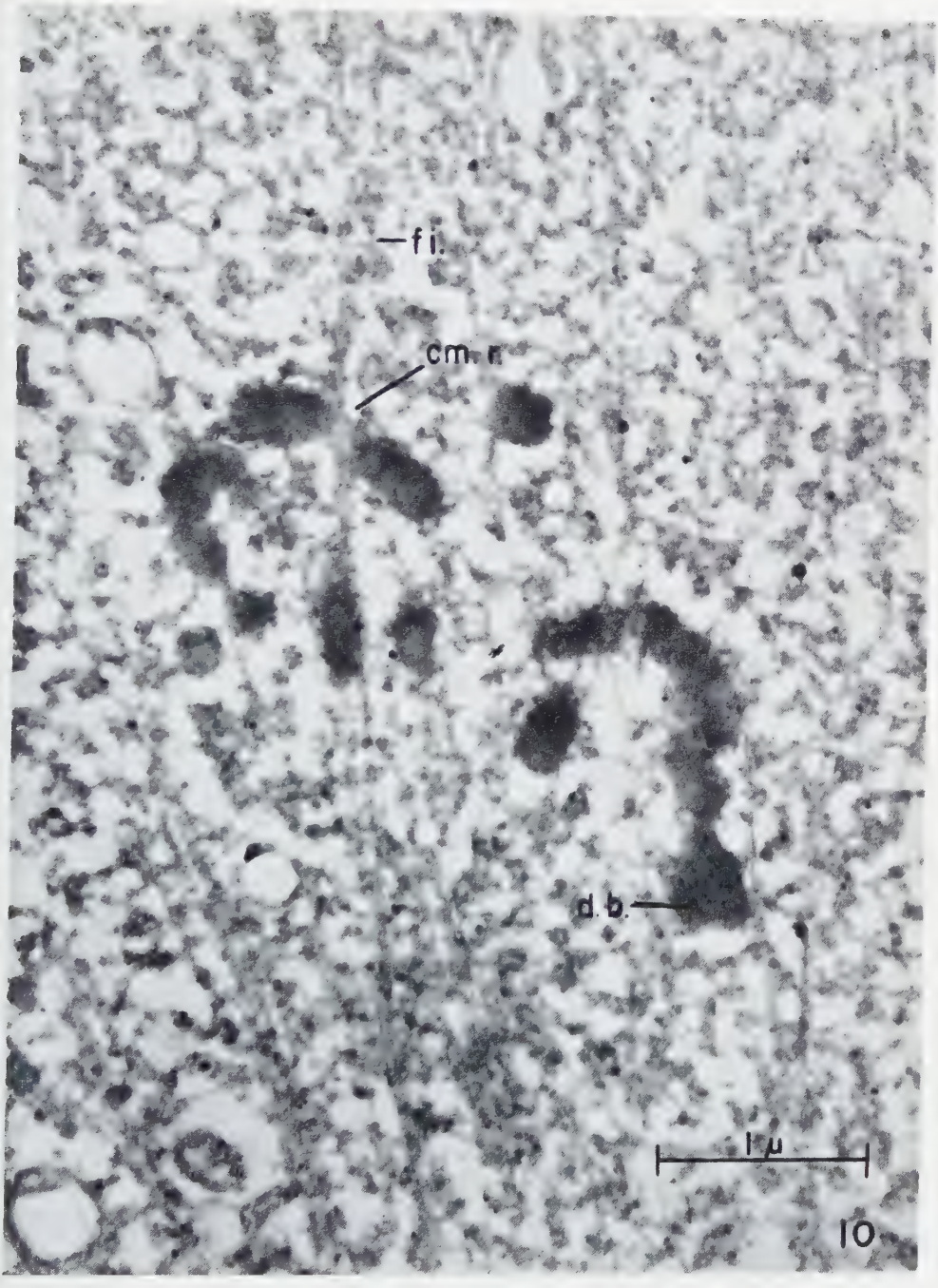
fl.
cm. n
d. b.
1 μ
10

DISCUSSION

The observations herein described suggest that the mitotic spindle *in vivo* contains all of the visible (to the electron microscope) components of the ground cytoplasm, and more particularly, the dense RNP particles, but that it excludes all cytoplasmic particulates larger than 40–50 millimicrons. This conclusion is strengthened by the interferometric observations of Mitchison and Swann (*18*), who showed that the refractive index of the spindle is lower than that of the cytoplasm as a whole, but that if allowance is made for the contribution from the larger particulates, then the R.I. of the spindle is identical with that of the ground substance. Such a correspondence in R.I. is unlikely to be fortuitous; i.e., were the spindle a condensation differing greatly in composition from the ground substance, one might well expect it to show a considerably different R.I., except in the unlikely case of identical density and refractive index increment.

The OsO_4-fixed specimens could be interpreted as showing that the spindle is, in addition, structureless. Such a conclusion could, however, hardly be correct in view of the birefringence of the spindle, of the visibility of the fibers in the living cell, and even in view of the function of the mitotic apparatus. This suggests that the osmium has a rather severe dispersive effect, at least on the mitotic apparatus. The ethanol-fixed material shows, on the other hand, distinct fibrous elements, in addition to the RNP particles (or "microsomal" particles as we (*6–8*) and Kurosumi (*14*) have called them). These fibers could be responsible for the *in vivo* optical properties of the spindle. The aggregative effect of ethanol fixation has undoubtedly coarsened and disordered these elements to some degree, but it is reasonable to suppose that, in some form, separate fibrous elements of submicroscopic dimensions do exist in the normal spindle. Whether these elements are formed by the necklace-like adlineation of the RNP particles, or are organized from soluble macromolecules by the centrioles and kinetochores cannot be answered, in our opinion, on morphologic grounds alone.

Our finding of fibrous elements in the spindle is in accord with observations of other investigators, but our interpretation of their role in the assembly and function of the spindle is somewhat different. Porter's (*23*, *24*) implication is that the fibers (his, found in tumour cells, are sometimes double) arise from the centriole and thus delineate and complete the mitotic apparatus: a similar situation is assumed by many, on less direct evidence, to obtain. The presence of a large population of cytoplasmic inclusions in the *Arbacia* egg provides evidence according to which such a picture should be discarded as too simple, although it doubtless contains elements of truth. Did the spindle arise merely as a set of fibers running between poles and chromosomes, one might expect that the larger particulates (yolk, mitochondria, oil, pigment)

would be present to some extent within the spindle itself, with fibers growing between and among them. The rather dramatic and total exclusion of these particulates from the spindle region, even in the early "streak" stage, prior to nuclear breakdown, and before any extensive fibrillization is apparent, must be interpreted in terms of a generalized gelation, involving either the RNP particles themselves or invisible, soluble macromolecules, in the region of the forming spindle. The fibrous elements seen, comprising as they do only a small fraction of the total volume of the gelled region, must then be a secondary (and possibly simultaneous), but fundamentally important development.

These results also call into question interpretations of spindle ultrastructure based upon Mazia's (*15*) electron micrographs of sections of isolated spindles. It seems clear from a comparison of our ethanol-fixed, but (relatively) unextracted spindles with his micrographs that the solubilization procedures used for mass isolation of spindles at that time resulted in extraction of much material from the structure, and perhaps in some randomization of what remained. The cytochemical complexity of the spindle as shown, for example, by Pollister and Ris (*22*), Stich (*28*, *29*), and Monné and Slautterback (*19*), is consistent with the present finding of complex submicroscopic architecture, but not with the demonstrable chemical simplicity of the isolated spindle.

These arguments do not in any way negate the possibility (we, indeed, regard it as a probability) that the isolated spindle is a "residual" structure, whose component nucleotide-protein (*16*) represents the working parts of the fully-assembled spindle. Quite possibly, the RNP particles observed by us and by Kurosumi (*14*) are simply "trapped" in the spindle region during the gelation of the spindle precursor. This question cannot, however, be decided on the basis of morphologic studies alone. The presence of the "Palade particles" everywhere in the spindles shown herein, even in and on the quantitatively minor fibrous component, may not after all be fortuitous; indeed it is likely, at least in our present view, that these RNP particles participate directly in the sol-gel transformation leading to the assembly of the mitotic spindle. We have been interested to find that Kurosumi (*14*), apparently unaware of our earlier publications in this area, has independently come to substantially the same conclusion.

The authors gratefully acknowledge support for the research program, of which this work was a part, from the American Cancer Society, the National Science Foundation, and the U.S. Public Health Service, through grant #A-2303, National Institute of Arthritis and Metabolic Diseases.

REFERENCES

1. Afzelius, B. A., *Z. Zellforsch. u. mikroskop. Anat.* **45**, 660 (1957).
2. Anderson, N. G., *Quart. Rev. Biol.* **31**, 169 (1956).
3. —— *ibid.* **31**, 243 (1956).
4. Beams, H. W., Evans, T. C., van Breemen, V. and Baker, W. W., *Proc. Soc. Exptl. Biol. Med.* **74**, 717 (1950).
5. Gross, P. R., *Biol. Bull.* **107**, 364 (1954).
6. —— *J. Cellular Comp. Physiol.* **47**, 429 (1956).
7. —— *ibid.* **49**, Suppl. 1, 243 (1957).
8. Gross, P. R. and Pearl, W., *J. Cellular Comp. Physiol.*, in press.
9. Gross, P. R. and Nass, S., unpublished observations.
10. Harven, E. de and Bernhard, W., *Z. Zellforsch. u. mikroskop. Anat.* **45**, 378 (1956).
11. Harvey, E. B., The American Arbacia and Other Sea Urchins. Princeton Univ. Press, 1956.
12. Inoué, S., *Exptl. Cell Research*, Suppl. 3, 305 (1952).
13. Inoué, S. and Dan, K., *J. Morphol.* **89**, 423 (1951).
14. Kurosumi, K., *Protoplasma* **49**, 116 (1958).
15. Mazia, D., *Symp. Soc. Exptl. Biol.* **9**, 335 (1955).
16. —— *Symposium on the Chemical Basis of Heredity*, p. 169. Johns Hopkins University Press, 1957.
17. Mazia, D. and Dan, K., *Proc. Natl. Acad. Sci. U.S.* **38**, 826 (1952).
18. Mitchison, J. M. and Swann, M. M., *Quart. J. Microscop. Sci.* **94**, 381 (1953).
19. Monné, L. and Slautterback, D. B., *Exptl. Cell Research* **1**, 477 (1950).
20. Palade, G. E., *J. Biophys. Biochem. Cytol.* **1**, 59 (1955).
21. Philpott, D. E., *Exptl. Med. Surg.* **13**, 189 (1955).
22. Pollister, A. W. and Ris, H., *Cold Spring Harbor Symposia Quant. Biol.* **12**, 147 (1947).
23. Porter, K. R., *Harvey Lectures, Ser.* **51**, 175 (1956).
24. — *in* Fine Structure of Cells, *Symp. VIIIth. Congr. Cell Biol., Leiden*, 1954, p. 236. Noordhoff Ltd., 1955.
25. Rozsa, G. and Wyckoff, R. W. G., *Biochim. et Biophys. Acta* **6**, 334 (1950).
26. Sedar, A. W. and Wilson, D. F., *Biol. Bull.* **100**, 107 (1951).
27. Selby, C. C., *Exptl. Cell Research* **5**, 386 (1953).
28. Stich, H., *Chromosoma* **4**, 429 (1951).
29. —— *Z. Naturforsch.* **6 b**, 259 (1951).
30. Swann, M. M., *J. Exptl. Biol.* **28**, 417 (1951).
31. Tanaka, H., Uchino, F., Dohi, S. and Amano, S., *Acta Haematol. Japan* **19**, 571 (1956).
32. Zetterqvist, H. The Ultrastructural Organization of the Columnar Absorbing Cells of the Mouse Jejunum. Thesis. Stockholm, 1956.

Ultrastructure of Mouse Uterine Surface Epithelium under Different Estrogenic Influences

2. Early Effect of Estrogen Administered to Spayed Animals

O. NILSSON

Department of Histology and Laboratory for Biological Ultrastructure Research, Department of Anatomy, Karolinska Institutet, Stockholm

Received September 10, 1958

Spayed mice of the C3H strain were given a single intraperitoneal injection of 1 μg estradiol-17β in 0.05 ml propylene glycol. The appearance of the uterine epithelial cells was investigated 4 hours and 20 hours after the hormone administration.

At the 4-hour level, the epithelial cells were 10–14 μ in height and 4–5 μ in width. The lumenal cell membrane was triple-layered and possessed many small, irregular microvilli. Lipid granules were observed in both the lumenal and basal parts of the epithelium. About 1–3 μ large areas with a complex structure and different types of cytoplasmic bodies were noticed. Small vacuoles, 600–900 Å large, occurred frequently in the lumenal part of the cytoplasm.

At the 20-hour level, the epithelial cells were 12–16 μ in height and 4–5 μ in width. The lumenal cell membrane was triple-layered and possessed many microvilli with a lumenal substance. Some lipid granules were observed in the cytoplasm. The cytoplasmic structures were similar to those noticed at the 4-hour level, but some differences occurred. For instance, the system of α-cytomembranes was well developed, and the Golgi apparatus showed large vacuoles.

Compared to the epithelium of spayed animals, there was noted, among other differences, a change in the structure of the cell membrane. In spayed animals, the distance between the dense layers of the lumenal surface membrane was about 70 Å and the distance between lateral, adjacent cell membranes was about 260 Å. At the 4-hour and 20-hour levels, the corresponding distances were about 40 Å and 160 Å respectively.

The estrogen-induced, early changes in the whole uterus were reported in several papers (*4*, *5*, *14–17*, and others). It was shown that a primary phase of the uterine response occurred within 4–6 hours after the administration of estrogen. It was characterized by a peak in the water imbibition, an increase in the content of certain ions, and an accelerated glycolytic activity. A secondary phase of the response

complex followed at about 20 hours and was characterized by cell growth. It was associated with, for instance, an increase of the uterine solids and an elevated oxidative metabolism.

With the light microscope, morphological changes of the uterine epithelium in the form of a hypertrophy were demonstrated 20 hours after the administration of estrogen (*15*). In an electron microscopical study, the early, estrogen-induced changes in the ultrastructure of this epithelium were described (*9*). This paper is concerned with some of the changes that appear in the uterine epithelium of spayed mice 4 hours and 20 hours after the injection of estradiol.

MATERIAL AND METHODS

The estrogen sensitivity of the animals employed was tested as follows: 20 adult mice were spayed and allowed to rest for a fortnight. They were then injected with 0.1 μg estradiol-17β in 0.5 ml propylene glycol divided into three doses, which were administered on three consecutive days. Vaginal smears were taken on the fourth day (twice) and on the fifth and sixth day. After a rest period of three weeks, the experiment was repeated, administering this time a total dose of 0.05 μg estradiol-17β under the same experimental conditions.

To control the possible influence of the route of the intraperitoneal administration, the standard dose of estradiol-17β used throughout this investigation (1 μg in 0.05 ml propylene glycol) was administered in a single injection to 10 spayed mice. Following the injection at 9 a.m., smears were taken daily at 9 a.m. and 6 p.m. for four days. In all experiments, the smears were interpreted as suggested by Emmens (*3*).

Two experimental groups of animals, each group comprising 7 mice of the C3H strain, were used in this electron microscopical study. At an age of three months, the animals were controlled for about a fortnight by daily vaginal smears, spayed, and allowed a rest period of two weeks. Control smears were taken also during this period. With the animals under an ether narcosis, intraperitoneal injections of the solutions used were made. In each group, 5 animals were given a single dose of 1 μg estradiol-17β in 0.05 ml propylene glycol, and 2 animals, which served as controls, were given only 0.05 ml propylene glycol.

The animals of one group were sacrificed for fixation 4 hours after the injection; the animals of the other group were sacrificed 20 hours after the injection. The fixative was a buffered, 1% osmium tetroxide solution (*11*, *12*) at room temperature; the preparations were embedded in butyl methacrylate (*7*). Details of the fixation and embedding procedure were communicated earlier (*8*). The sections were cut with glass knives (*6*) on an ultramicrotome designed by Sjöstrand (*13*) and examined in an RCA EMU-2C electron microscope.

FIG. 1. Survey picture of uterine epithelium at the 4-hour level. The lumenal cell surface is irregular, the lateral cell surfaces are slightly folded, and the basement membrane is winding. In the lumenal part of the cytoplasm, there are some areas with dense substance and empty spaces. Many lipid granules lie in the cells. × 10,000.

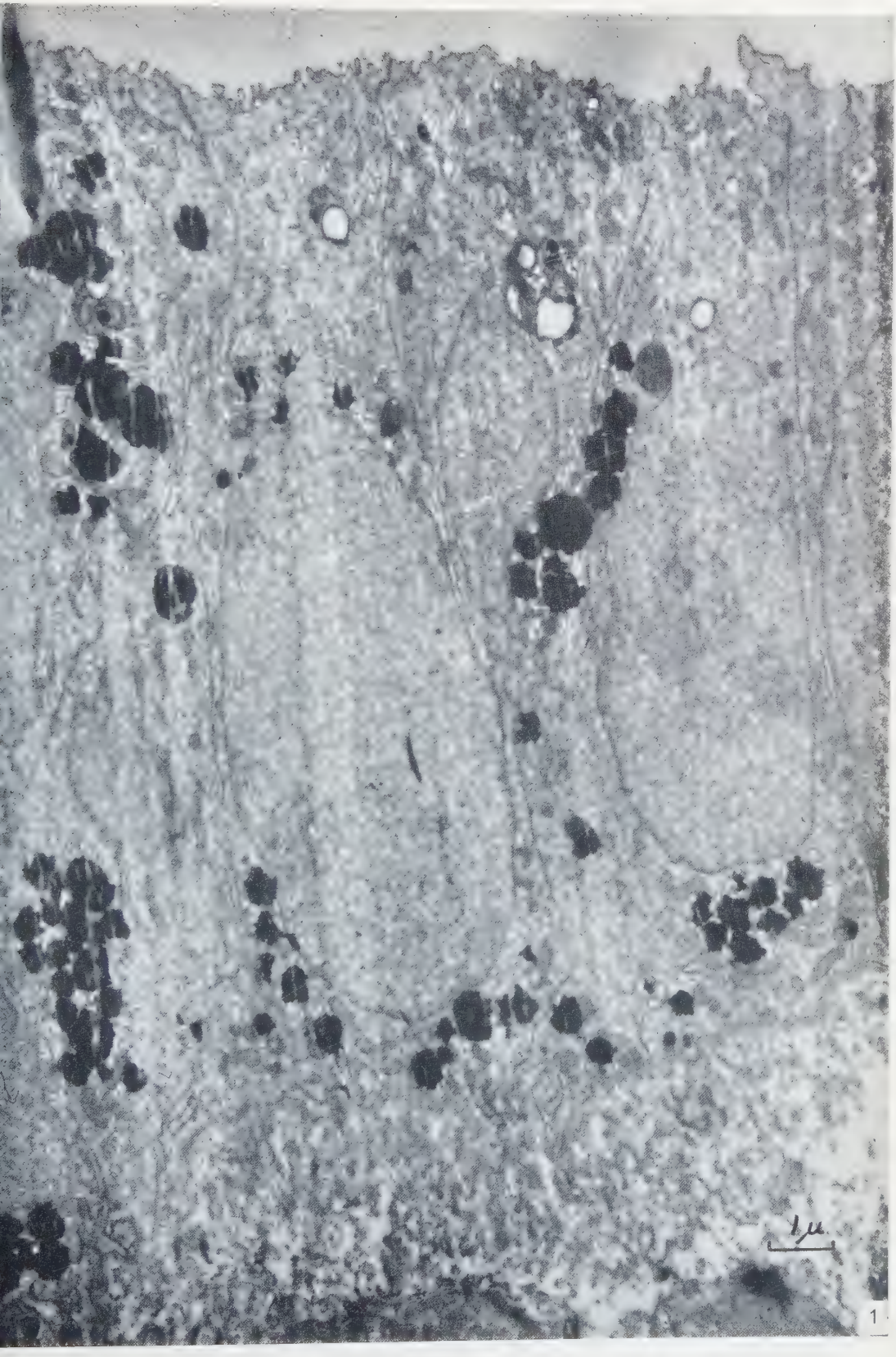
1μ

FIG. 2. Lumenal part of uterine epithelium at the 4-hour level. The lumenal cell surface is irregular. Many small v
uoles lie in the cytoplasm under the surface membrane. A vesicle with ring-shaped profiles appears in the upper, l
hand part of the epithelium. Many lipid granules are seen. ×21,000.

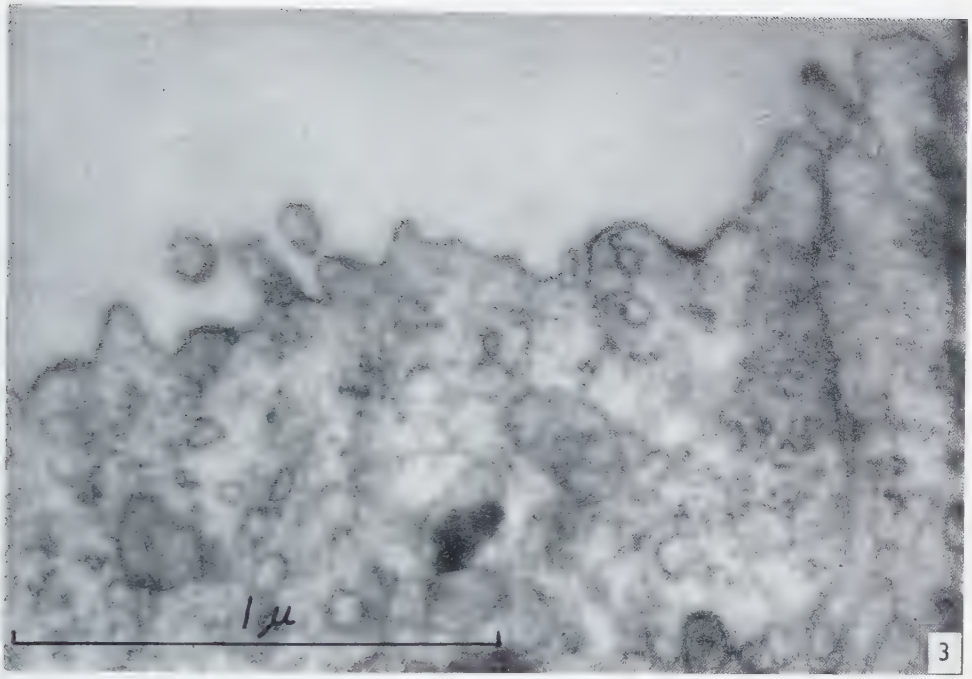

FIG. 3. Lumenal part of uterine epithelium at the 4-hour level. Mitochondria and small vacuoles lie in the cytoplasm. A cell border runs at the right-hand side. × 62,000.

The measurements of the distance between the dense layers in the lumenal surface membrane and between the lateral, adjacent membranes were made from their central parts. To calculate the distance in the lumenal membrane, electron micrographs at an initial magnification of 24,000 times were used, and to calculate the distance between the lateral membranes, electron micrographs at an initial magnification higher than 10,000 times were used. In each experimental group, sections of satisfactory quality were selected from two animals, and measurements on one or two cells from each animal were made. Measurements were performed only on those places where the layers or membranes were represented by thin, distinct, dark lines. Mean values from the cells were used to calculate the group means of the animals (Table I).

RESULTS

Hormone assays

As a result of the subcutaneous injections, it was found that all mice given 0.1 μg estradiol-17β showed cornified vaginal smears, whereas following the administration of 0.05 μg, 16 out of 20 animals exhibited a positive reaction. The intraperitoneal injection of 1 μg estradiol-17β gave in all mice a positive reaction after two days.

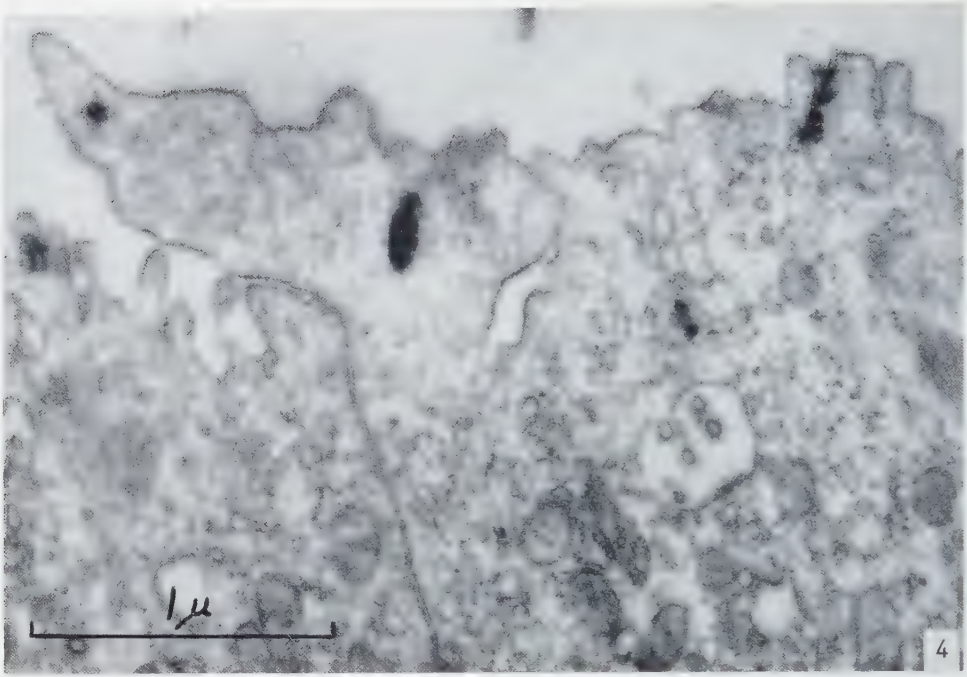

FIG. 4. Lumenal part of uterine epithelium at the 4-hour level demonstrating a bleb-like formation, which shows only cytoplasmic ground substance. In the cytoplasm, there are mitochondria, small vacuoles, and a vesicle with ring-shaped profiles. A cell border runs in the middle of the picture. × 40,000.

Control animals

The ultrastructure of the uterine epithelium from these animals did not differ from that observed in the spayed animals (*8*).

4 hours after estrogen administration

The epithelial cells were 10–14 μ in height and 4–5 μ in width; the oval nuclei lay basally in the cells (Fig. 1).

The cell membrane possessed, at the lumenal surface, projections with a maximum length of about 0.4 μ. Some of them had the slender shape of microvilli, but some were broad and deformed (Figs. 2–5). Small, bleb-like protrusions with an interior composed mainly of cytoplasmic ground substance were also noticed (Fig. 4). The lumenal cell membrane manifested a triple-layered structure at the regions where the cell membrane ran straight and perpendicularly to the section surfaces. Two dense layers were separated by a less dense layer; the distance between the two

FIG. 5. Lumenal cell membrane of a uterine epithelial cell at the 4-hour level. The triple-layered structure of the plasma membrane is discernible at some places (→). × 150,000.

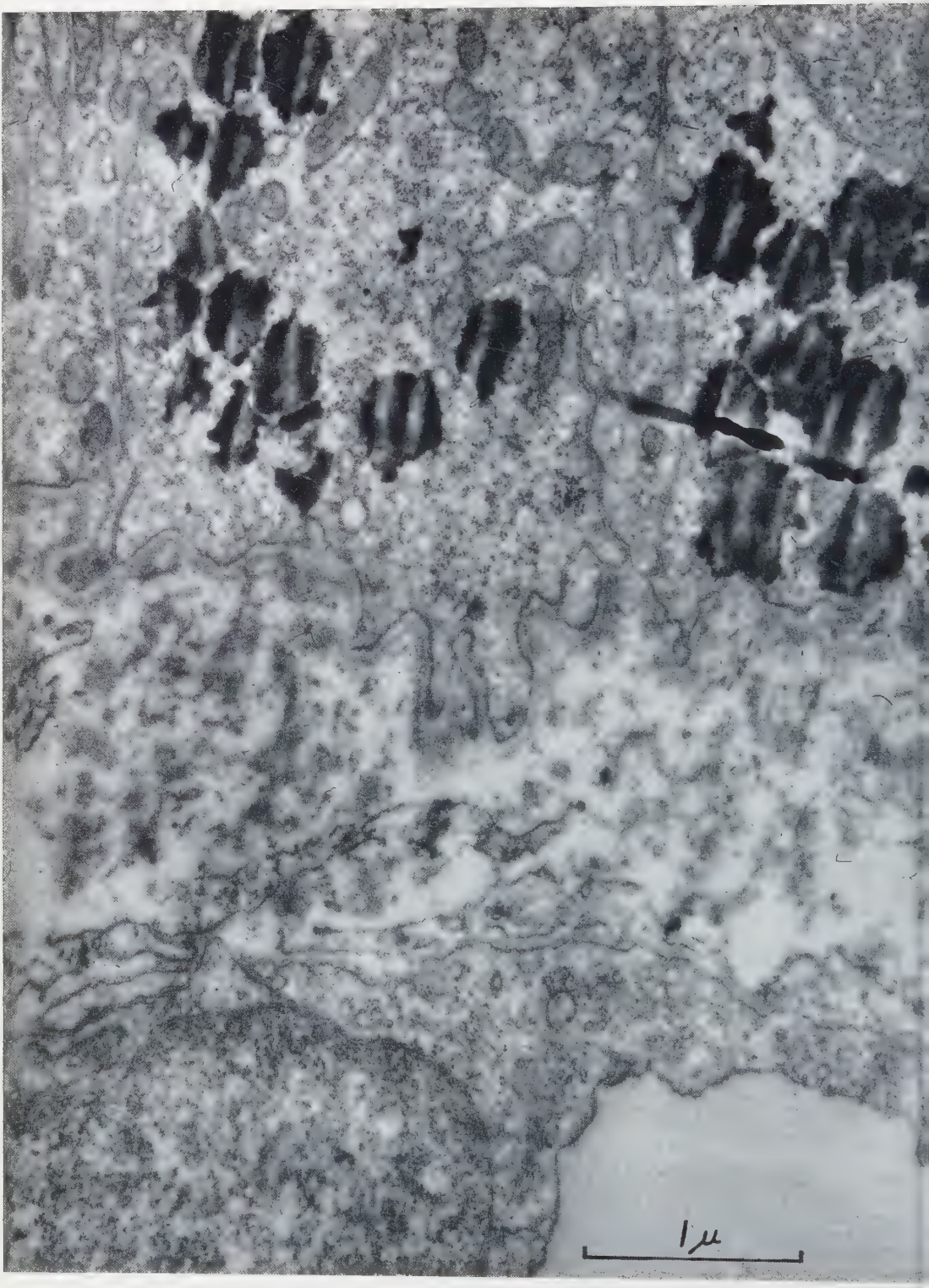
1μ

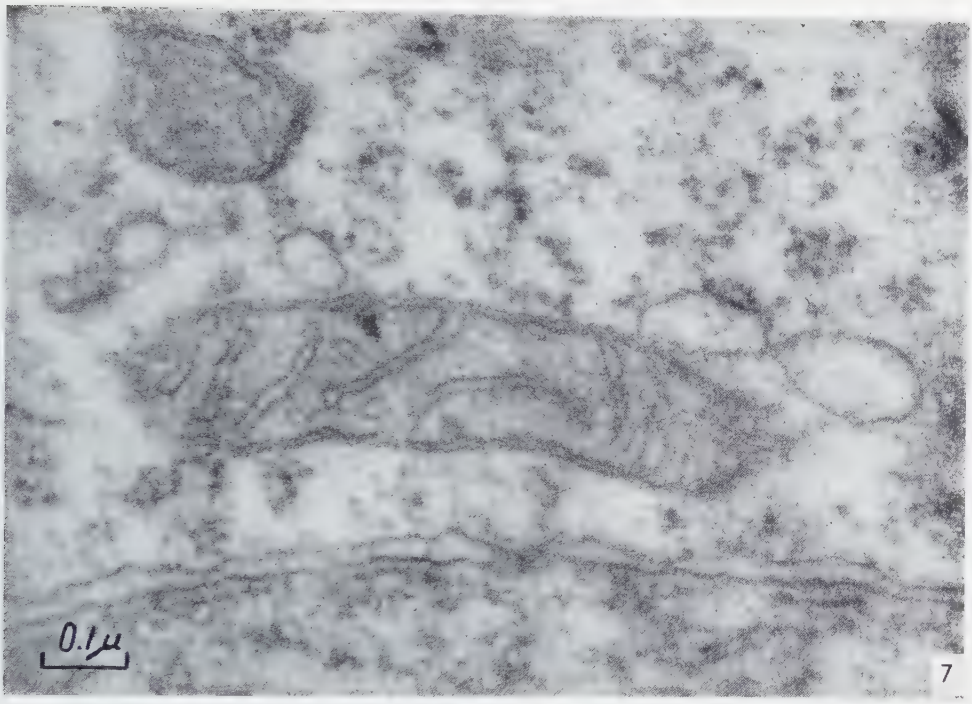

FIG. 7. Mitochondrion in a uterine epithelial cell at the 4-hour level demonstrating outer and inner membranes, circular profiles, and a dark granule. Some small vacuoles lie in the cytoplasm at the upper surface of the mitochondrion. The small particles of the cytoplasm occur in groups or form bending rows. Part of another mitochondrion is visible at the upper, left-hand side. A nuclear membrane runs in the lower part of the figure. × 107,000.

dense layers was about 40 Å (Fig. 5; Table I). The lateral cell surface sometimes appeared folded (Fig. 1). Lateral, adjacent cell surfaces ran parallel and at a distance of about 160 Å (Fig. 8; Table I). The basal cell surface was winding (Fig. 6).

The mitochondria appeared as small rods, and the inner, dark layer of the surface membrane was occasionally seen to continue into internal membranes. Small, dark granules with a maximum size of about 500 Å and circular profiles were sometimes observed inside the mitochondria (Fig. 7).

The system of α-cytomembranes occurred as small, rounded or elongated profiles in the cytoplasm (Figs. 8 and 10).

FIG. 6. Basal part of endometrium at the 4-hour level. In the epithelial cells, many mitochondria and lipid granules are seen. A portion of a nucleus appears in the upper, right-hand corner of the picture. The cell borders are irregular, and the basement membrane runs windingly. In the connective tissue, a vessel can be recognized. The cell that forms the vessel lies in the lower part of the picture; the lumen of the vessel appears at the lower, right-hand side. × 34,000.

TABLE I

DISTANCES BETWEEN THE DENSE LAYERS OF THE LUMENAL CELL SURFACE AND BETWEEN THE LATERAL, ADJACENT CELL SURFACES

Treatment	Animal No.	Number of Measurements	Mean ± S.D. in Å	Group Mean in Å	Ratio
Dense layers of the lumenal cell surfaces:					
Control group (spayed animals)	1	10	69.1 ± 3.44	68.6	—
	2	10	68.1 ± 3.70		
4 hours after estrogen administration	3	10	38.9 ± 3.61	39.6	0.58
	4	10	40.3 ± 2.95		
20 hours after estrogen administration	5	10	42.4 ± 4.57	42.4	0.62
	6	10	42.4 ± 5.63		
Lateral, adjacent cell surfaces:					
Control group (spayed animals)	2	10	273 ± 17.2	259	—
	7	10	244 ± 11.6		
4 hours after estrogen administration	3	10	148 ± 10.6	160	0.62
	4	10	172 ± 10.5		
20 hours after estrogen administration	6	10	181 ± 6.9	162	0.63
	8	10	142 ± 5.6		

The Golgi apparatus was situated in the apical part of the cell and showed the usual composition of smooth membranes, Golgi granules, and vacuoles (Fig. 8).

Lipid granules were observed in both the lumenal and basal parts of the epithelium (Figs. 1, 2 and 6).

Areas, 1-3 μ large, showing an intricate structure with alternating parts of dark granules and parallel membranes, were noticed in the cytoplasm (Figs. 1 and 8–10). Some parts of these areas were enclosed by concentric membranes, and appeared empty or partly filled with granules or an amorphous substance. Sometimes, they contained a finely granulated material (Fig. 10).

Bodies, the interior of which was composed of coarse granules of varying size and blackness and, sometimes, also of a dark or dense substance, were frequently

FIG. 8. Part of two uterine epithelial cells at the 4-hour level. A cell border runs in the middle of the figure, and nuclei are discernible in the lower, right- and left-hand corners. Two Golgi apparatus are situated in the middle of the picture on each side of the cell border. Lipid granules lie in the lower part of the figure; a large area composed of membranes, dense substance, and spaces lies to the left and a smaller one to the right. Granulated bodies (-) appear in the cytoplasm. A vesicle with ring-shaped profiles is visible in the upper, right-hand corner. × 48,000.

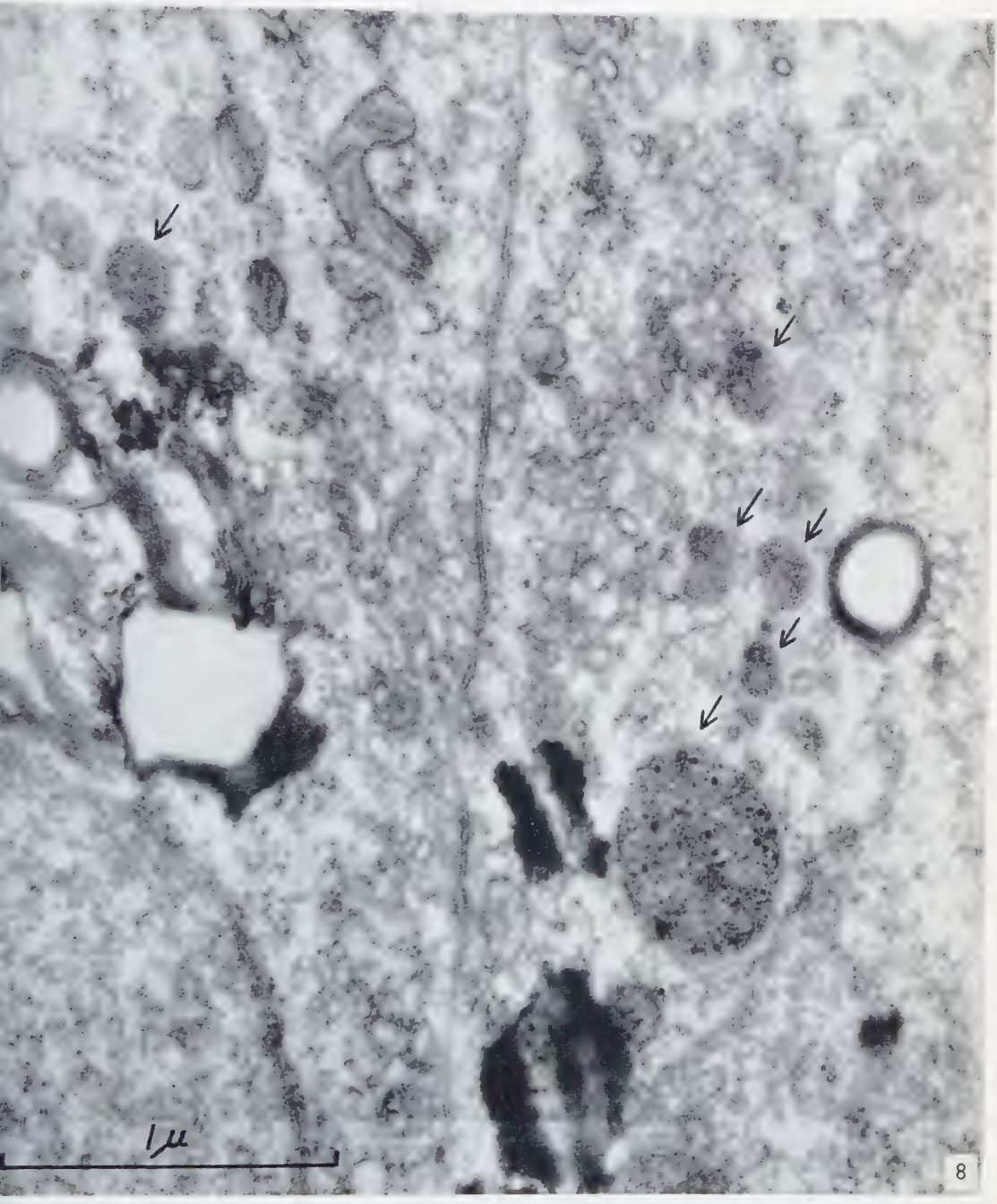
1μ
8

observed (Fig. 8). These granulated bodies mostly had a size of 0.2–0.3 μ, but bodies up to 0.6 μ in size were noticed. Some bodies showed a distinct border membrane.

Bodies of similar size and shape displayed an interior of coarse granules and concentric membranes (Fig. 9) or contained an irregular coil of membranes (Fig. 11).

Dark, homogeneous, ovoid granules with a smooth outline, the largest being about 1 μ, were noticed in the cytoplasm. Sometimes, they were connected with membrane systems. The dark granules did not seem to occur so frequently as the other cytoplasmic bodies.

Vesicles, which contained a varying amount of small, ring-shaped profiles, were seen in the cells (Figs. 2, 4 and 8). These vesicles had a maximum size of about 0.5 μ.

Small vacuoles were frequently noticed in the cytoplasm, mostly in the lumenal part of the cell (Figs. 2 and 3). They were 600–900 Å large and were bounded by a smooth membrane.

20 hours after estrogen administration

The epithelial cells were 12–16 μ in height and 4–5 μ in width; the oval nuclei lay basally in the cells.

The lumenal cell membrane was slightly bulging into the lumen, and possessed many microvilli with a maximum length of about 0.6 μ. At their surface, a lumenal substance of thin, dense strands was noticed (Figs. 12 and 13). The lumenal membrane displayed a triple-layered structure with a distance of about 40 Å between the dense layers (Fig. 13; Table I). The lateral cell surface was sometimes folded. The distance between the lateral, adjacent cell membranes was about 160 Å (Table I). The basal cell surface was winding.

The mitochondria, which resembled small rods, exhibited the triple-layered outer and inner membranes. The mitochondria sometimes contained dark granules with a maximum size of about 500 Å and small, circular profiles (Figs. 14, 15 and 17).

The system of α-cytomembranes was fairly well developed and was marked as rounded profiles or as elongated formations (Figs. 15, 16 and 18).

The Golgi apparatus had the usual appearance, but manifested large vacuoles with a maximum size of about 0.3 μ (Fig. 17).

Lipid granules were observed in the cytoplasm (Fig. 14).

Areas, 1–2 μ large, with a complex and varying composition of dark granules, membranes, and empty spaces were present. They were similar to the corresponding structures in the epithelium at the 4-hour level.

FIG. 9. Part of a uterine epithelial cell at the 4-hour level demonstrating lipid granules and an area composed of membranes, dense substance, and spaces. In the upper half of the picture, there lies a body with coarse granules and parallel membranes. A portion of a nucleus is visible in the lower, left-hand corner. × 66,000.

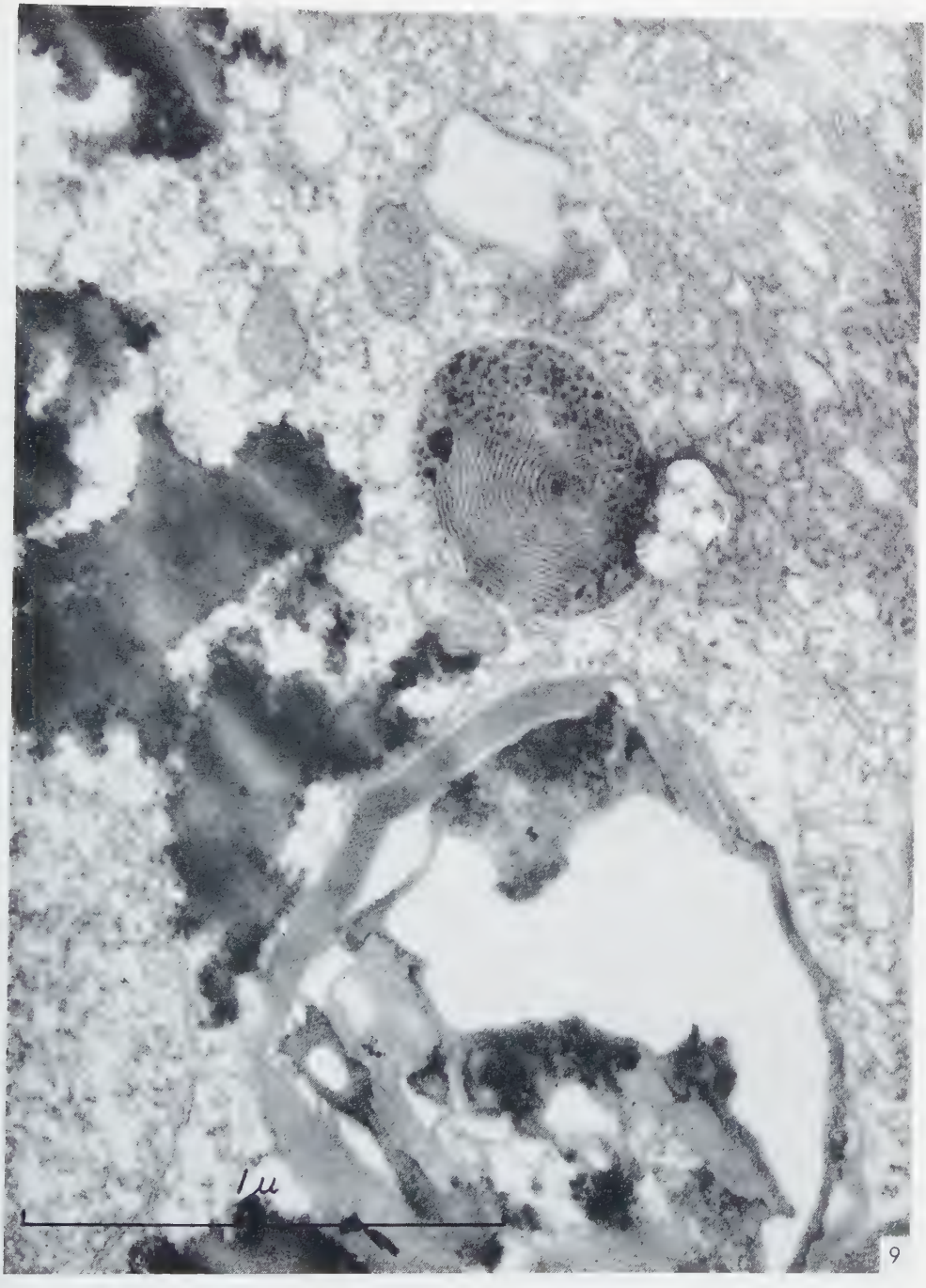
1μ
9

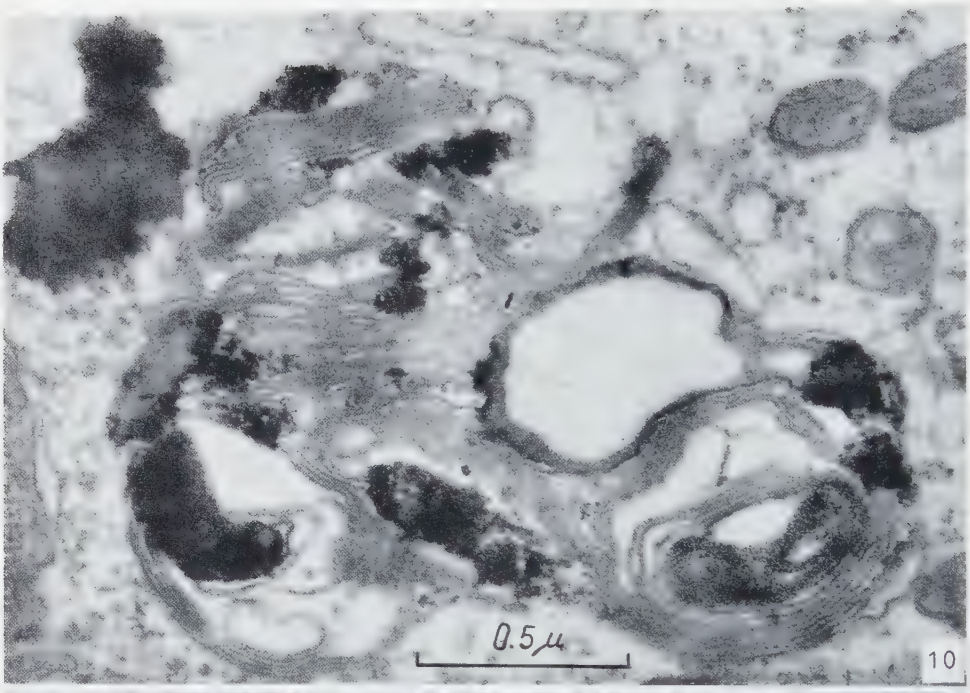
0.5 μ
10

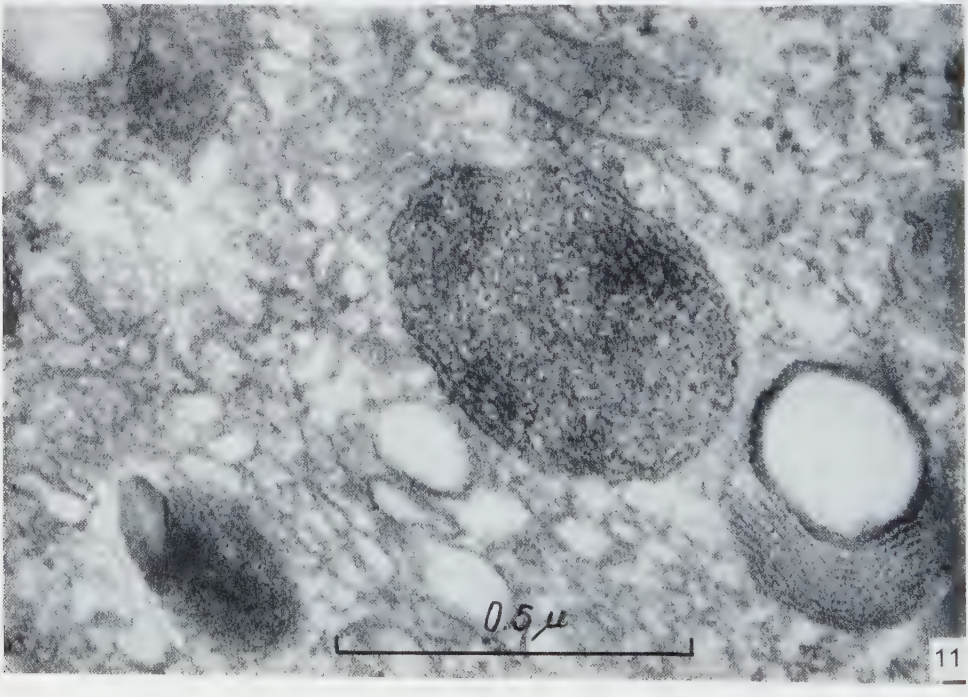
0.5 μ
11

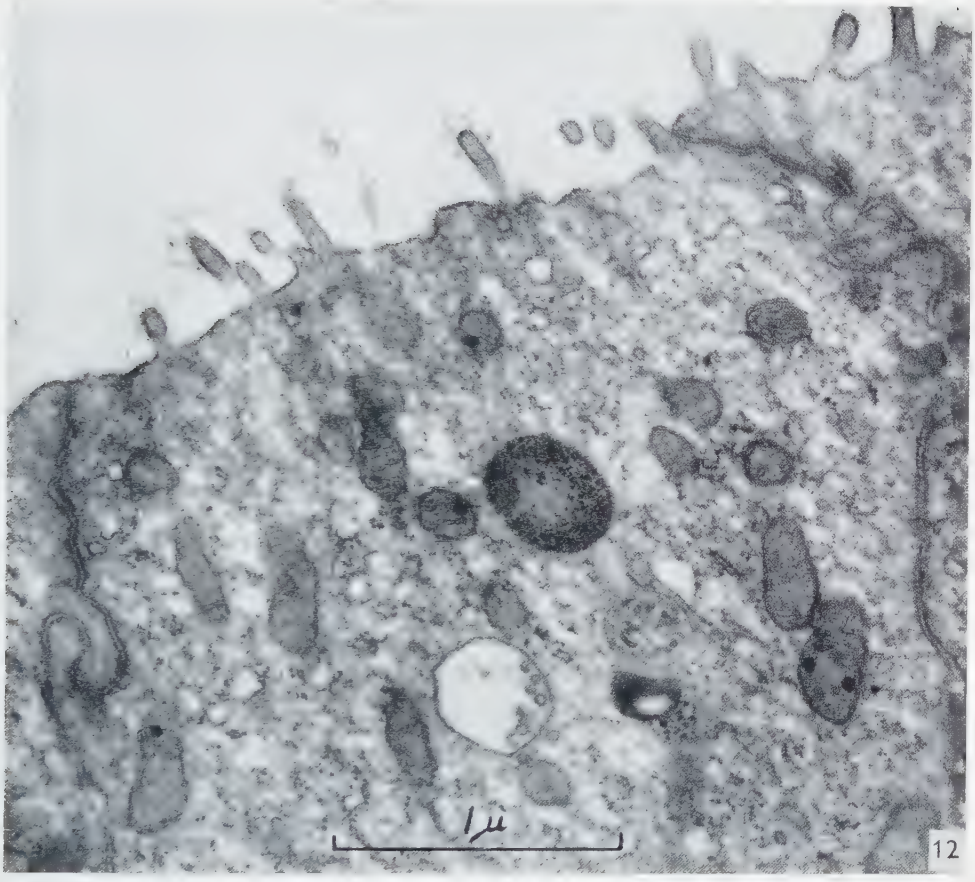

FIG. 12. Lumenal part of uterine epithelium at the 20-hour level. The lumenal cell surface is rather regular and possesses microvilli with a lumenal substance. Cell borders run at the right- and left-hand sides. Mitochondria, some containing dark granules, lie in the cytoplasm. A vesicle with ring-shaped profiles appears, and above that structure, a large, granulated body is seen. × 37,000.

FIG. 10. Area composed of membranes, dense substance, and spaces appearing in a uterine epithelial cell at the 4-hour level. Lipid granules and mitochondria are also seen, and in the lower, left-hand corner, a portion of a nucleus appears. × 55,000.

FIG. 11. Body with an irregular coil of membranes appearing in a uterine epithelial cell at the 4-hour level. In the lower, right-hand corner, there lies an area composed of membranes and of a space surrounded by a dense substance. × 92,000.

Bodies containing coarse granules of varying size and blackness, and bodies containing an irregular coil of membranes were noticed (Figs. 12, 17 and 18). Furthermore, dark ovoid granules were marked. They all had the same size and appearance as the similar structures that were noticed in the epithelium at the 4-hour level.

Vesicles, which contained small, ring-shaped profiles, were seen also in these cells (Figs. 12 and 15). The vesicles had a maximum size of about 0.5 μ. The ring-shaped profiles occurred in a varying number; once, about forty profiles were observed.

Small vacuoles were noticed in the cytoplasm (Fig. 16). They were bounded by a smooth membrane.

DISCUSSION

Although the hormonal assays with the subcutaneous administration do not meet all criteria of a valid bioassay, it is likely that the ED50 of estradiol-17β in the animals employed is around or below 0.05 μg. This ED50 value is within the variation reported for different mouse strains.

To induce the uterine changes, an intraperitoneal dose of 1 μg estradiol-17β in propylene glycol was given. This is highly above the dose necessary to induce cornified smears, and an assay also demonstrated that all the animals tested were in estrus two days after the hormone injection. This fact, together with the ultrastructural differences invariably noticed between the spayed animals and the animals of the 4-hour and 20-hour levels, makes it probable that also these animals were under the influence of the estrogen. Such changes in ultrastructure could not be induced by the injection of propylene glycol.

The aspect of the uterine epithelium from the spayed animals (*8*) showed marked changes upon the administration of estrogen. The cellular ultrastructure was investigated 4 hours and 20 hours after the injection of estradiol-17β, and the results show that both these periods are characterized by specific, structural changes.

At the 4-hour level, changes were noticed, for example, in the appearance of the lumenal cell surface and in the configuration of the plasma membrane.

In the spayed animals, the lumenal cell surface was rather regular and showed a distinct layering. The distance between the two dense layers of the lumenal cell surface was about 70 Å, and the distance between the lateral, adjacent cell membranes was about 260 Å. After estrogen administration, the surface membrane was more irregularly outlined, and even small blebs, which contained only cytoplasmic ground substance, were noticed. The layering of the lumenal cell membrane was visible only at some places, probably depending upon the irregular course of the membrane. The distance between the two layers of the surface membrane and the distance between the lateral, adjacent cell membranes was decreased to about 40 Å and 160 Å

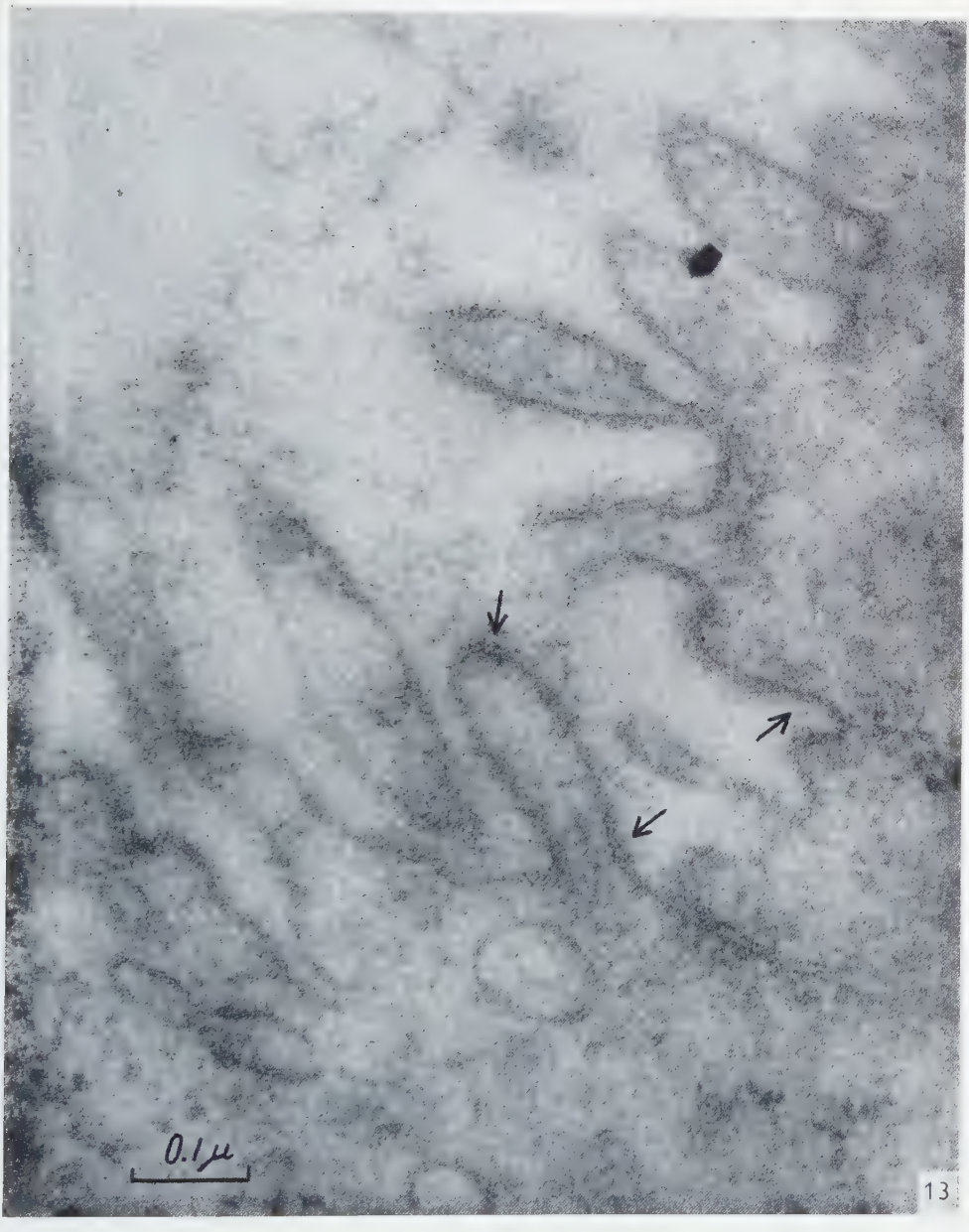

FIG. 13. Lumenal cell membrane of uterine epithelium at the 20-hour level. The triple-layered structure of the plasma membrane is discernible at some places (>), and the lumenal substance is visible. × 150,000.

respectively. These values are based on measurements on cells from a few animals of each group, and the figures cannot be regarded as statistically proven. The tendency in their changes, however, indicates that, in this material, the administration of estradiol-17β caused a structural modification of the plasma membrane in the uterine epithelial cells.

Szego (*14*) concluded that at the 4-hour level there might be an increased permeability of the uterine cell to glucose, and Bullough (*2*) reviewed some investigations that supported the view that one action of estrogen is the stimulation of the glucokinase system. He also stated that it is assumed that the system, which is under hormonal influence, may be operating primarily on the cell surface. The described morphological changes give further support to the view that the cell membrane is one of the primary sites for the hormone action.

The increase in cell height with a fairly constant cell width implies an augmentation of the cell volume. Analyses of the whole uterus have shown that the 4- and 6-hour levels are characterized by an increased cellular uptake of water (*4*, *15*, *16*). It is probable that, in the epithelial cells also, the volume increase at this early stage depends mainly upon water imbibition and that the change of the cell membrane structure facilitates the entrance of water.

At the 20-hour level, some distinctive features in the uterine epithelium were the presence of the lumenal substance, the occurrence of a rather well developed system of α-cytomembranes, and a further increase in cell height.

The appearance of the lumenal cell membrane with the regular microvilli and the lumenal substance was in accordance with the findings in the uterine epithelium of estrous animals (*8*). The distance between the two dense layers of the lumenal cell surface and the width of the intercellular space were similar to the corresponding figures estimated at the 4-hour level.

The system of α-cytomembranes was often noticed as long profiles in the cytoplasm. An augmentation of the α-cytomembranes is commonly regarded as a sign of protein synthesis. The increase of the cell height at this level was demonstrated earlier (*15*). The height increase and the augmentation of the α-cytomembranes might imply an active growth of the cell. This is in correspondence with other investigations, which demonstrated that the whole uterus at this secondary phase of the estrogen influence showed an augmentation of total oxidative metabolism and of uterine solids (*14*, *15*, *17*).

FIG. 14. Mitochondria and lipid granules in a uterine epithelial cell at the 20-hour level. In one of the mitochondria, a dark granule appears. × 92,000.

FIG. 15. Mitochondria and vesicles with ring-shaped profiles in a uterine epithelial cell at the 20-hour level. The small particles of the cytoplasm are seen, and in the lower, left-hand corner, α-cytomembranes appear. × 88,000.

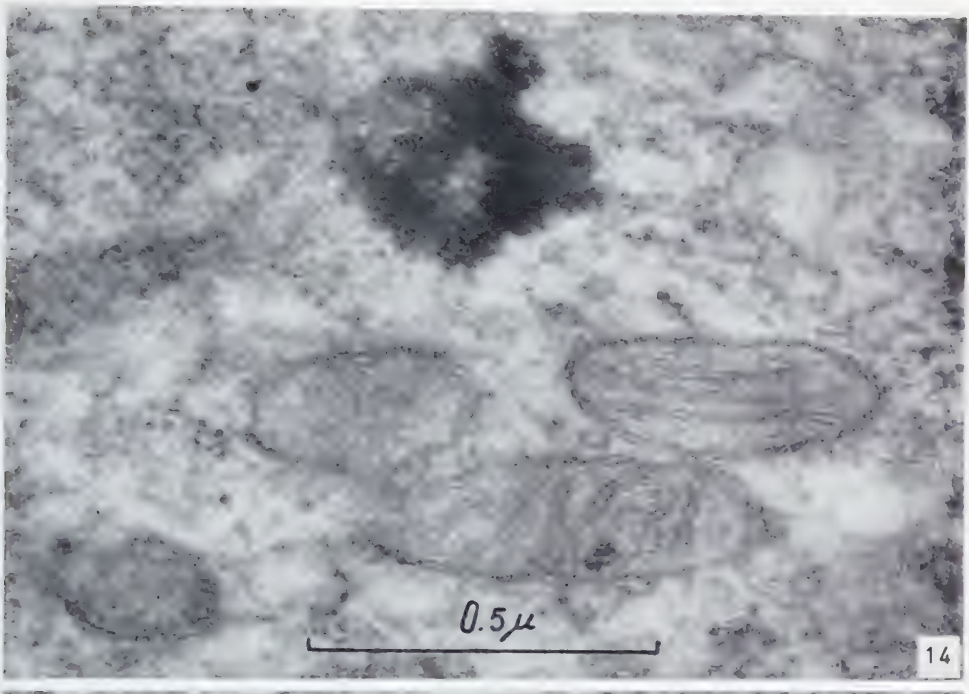
0.5μ
14

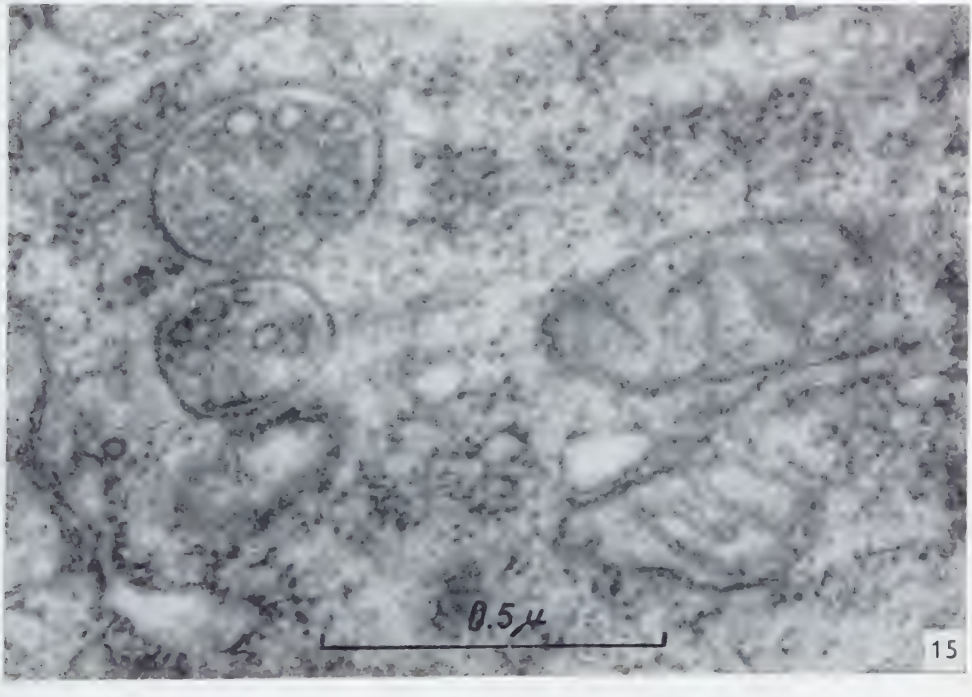
0.5μ
15

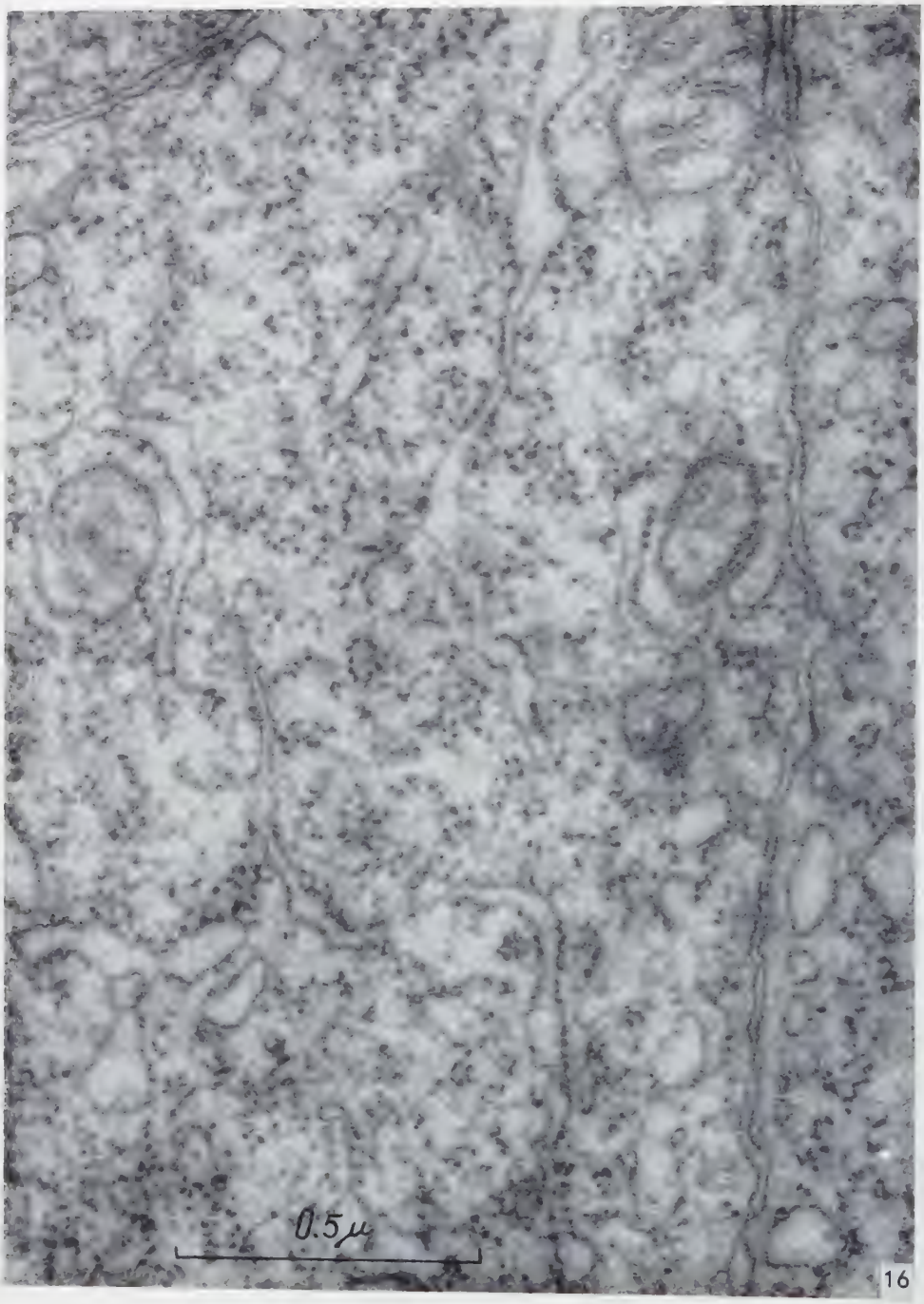

FIG. 16. System of α-cytomembranes in basal part of uterine epithelium at the 20-hour level. A portion of a nucleus lies in the upper, left-hand corner, and a cell border runs at the right-hand side. × 83,000.

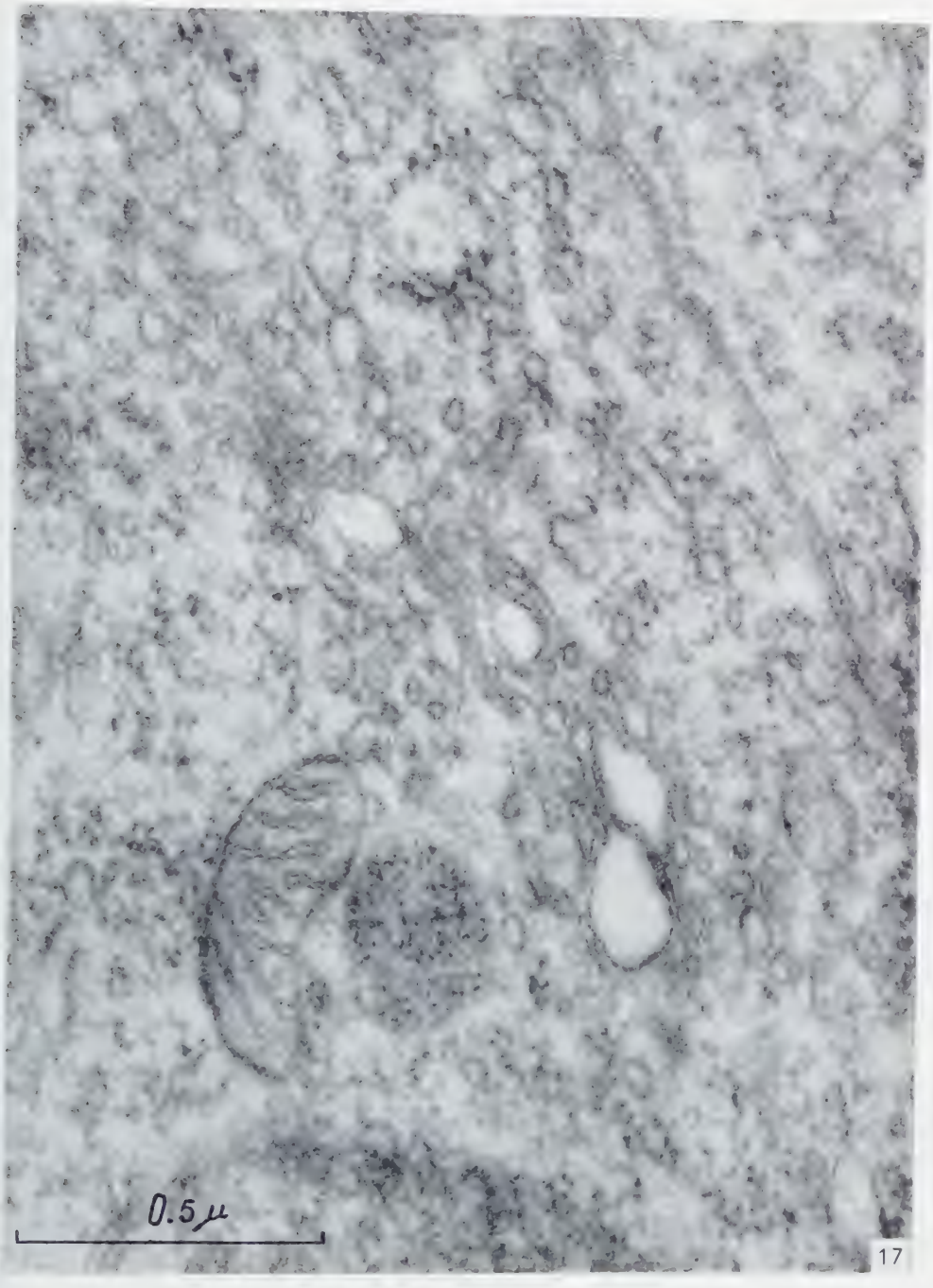

FIG. 17. Golgi apparatus in uterine epithelium at the 20-hour level demonstrating parallel membranes, Golgi granules, and vacuoles. In the lower part of the picture, there lie a mitochondrion and a granulated body, and under them, a portion of a nucleus appears. × 83,000.

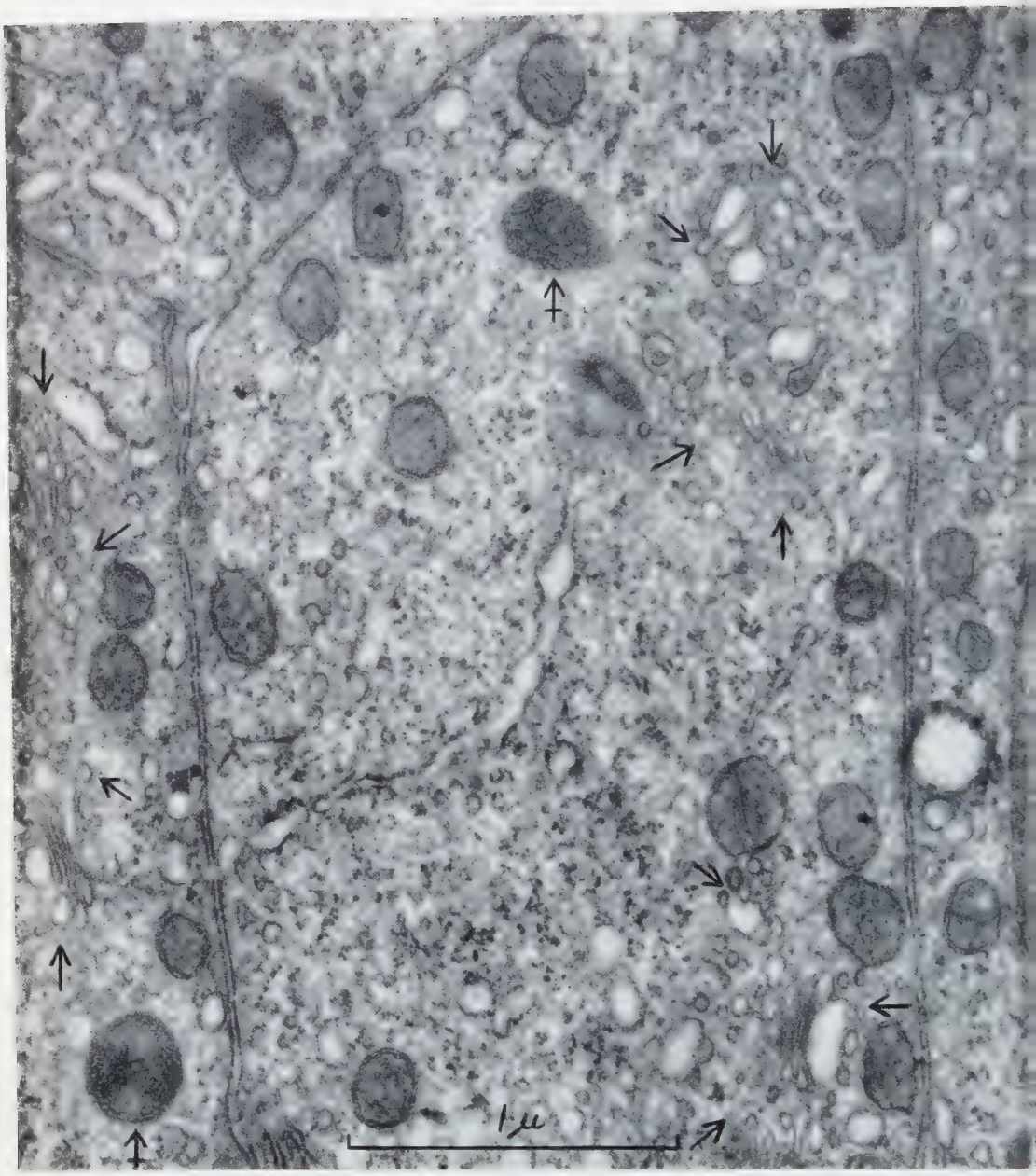

Fig. 18. Part of uterine epithelium at the 20-hour level. Several cell borders are seen, and a portion of a nucleus at the right-hand side. Many mitochondria and some cytoplasmic bodies (↔) are visible. Fragments of Golgi apparatus (→) appear, and profiles of α-cytomembranes are discernible. ×46,000.

Thus, the mouse uterine epithelial cell also seems to exhibit at least some of the changes that were found to characterize the whole uterus 4 hours and 20 hours after the administration of estrogen.

The granulated bodies, which are described in this study, were noticed also in the epithelium of spayed animals. Belt (*1*) communicated the presence of similar bodies in the rat adrenal cortex. He interpreted them as precursors to mitochondria and liposomes. The role of the granulated bodies in the uterine epithelium is still obscure. However, they are apparently influenced by estrogen, and further studies (*10*) might demonstrate their behavior at later stages after the estrogen administration.

"Professor Erik Ahlströms fond för obstetrisk-gynekologisk forskning", "Svenska Sällskapet för Medicinsk Forskning", and the Swedish State made grants towards the expenses of the investigation. AB Leo, Hälsingborg, supplied the estrogen preparation. Miss Leila Nilsson, Department of Women's Diseases, Karolinska Sjukhuset, provided much able assistance with the hormone assays.

REFERENCES

1. Belt, W. D., *J. Biophys. Biochem. Cytol.* **4**, 337 (1958).
2. Bullough, W. S., *Vitamins and Hormones* **13**, 261 (1955).
3. Emmens, C. W., *J. Endocrinol.* **1**, 373 (1939).
4. Kalman, S. M., *J. Pharmacol. Exptl. Therap.* **121**, 252 (1957).
5. Kalman, S. M. and Lowenstein, J. M., *J. Pharmacol. Exptl. Therap.* **122**, 163 (1958).
6. Latta, H. and Hartmann, J. F., *Proc. Soc. Exptl. Biol. Med.* **74**, 436 (1950).
7. Newman, S. B., Borysko, E. and Swerdlow, M., *J. Research Natl. Bur. Standards* **43**, 183 (1949).
8. Nilsson, O., *J. Ultrastructure Research* **1**, 375 (1958).
9. —— Exptl. Cell Research **14**, 434 (1958).
10. —— in preparation.
11. Palade, G. E., *J. Exptl. Med.* **95**, 285 (1952).
12. Rhodin, J., Correlation of Ultrastructural Organization and Function in Normal and Experimentally Changed Proximal Convoluted Tubule Cells of the Mouse Kidney. Thesis. Stockholm, 1954.
13. Sjöstrand, F. S., *Experientia* **9**, 114 (1953).
14. Szego, C. M., *in* Bullock, T. H. (Ed.), Physiological Triggers and Discontinuous Rate Processes, p. 152. American Physiological Society, Washington, D.C., 1957.
15. Szego, C. M. and Roberts, S., *Recent Progr. in Hormone Research* **8**, 419 (1953).
16. Talbot, N. B., Lowry, O. H. and Astwood, E. B., *J. Biol. Chem.* **132**, 1 (1940).
17. Telfer, M. A., *Arch. Biochem. Biophys.* **44**, 111 (1953).

The Fine Structure of Connective Tissue in the Tunica Propria of Bronchioles[1]

H. E. KARRER

Department of Pathobiology, School of Hygiene and Public Health, Johns Hopkins University, Baltimore, Maryland

Received June 18, 1958

The tunica propria of bronchioles of adult mice has been examined in the electron microscope. The following components are regularly encountered in the tunica propria: the basement membrane of the epithelium, the fibroblasts, the collagen fibrils, the elastic fibers, and the filaments.

The basement membrane, a thin sheet which underlies the epithelium, is believed to be part of the connective tissue.

Some fibroblasts are enveloped by a filamentous layer resembling a basement membrane. Others have thin filaments radiate from the surface.

The collagen fibrils show as many as eight bands per period. Their morphology corresponds to that found in purified fibrils.

The elastic fibers are of irregular size, form, and shape. They split up into fine filaments at their periphery.

Thin (about 10 mμ) filaments resembling those associated with fibroblasts and with elastic fibers occur also between the collagen fibrils. Some of these show a periodic beading. They are probably related to collagen.

The term connective tissue applies to a large number of elements in the animal body, the morphological appearance of which varies with their location and function. Light-optically one can distinguish the loose, "unspecialized" connective tissue which occurs in all organs and sites from the more specific, "specialized" types of such tissue, like tendon, dermis, ligamentum nuchae, cartilage, bone, and portions of large arteries. In the loose connective tissue, both the fibrous components, collagen and elastin, occur side by side in somewhat equal amounts. In the specific types of connective tissue, on the other hand, one or the other fibrous component may predominate; in addition, specific cell forms typical for the particular type of tissue may be found.

The morphological structure of different connective tissues has been studied extensively by light microscopists. More recently the ultrastructure of fibrous connective

[1] Supported by a Grant-in-Aid from the National Cancer Institute, U.S. Public Health Service (C-1230).

tissue components has been investigated further by means of X-ray diffraction (*1*, *5*, *8*) and of electron microscopy (*62*, *73*).

Valuable information has been gained from such biophysical studies of purified connective tissue fractions. However, these studies do need to be supplemented by additional electron microscopic investigations of the structure of *intact* connective tissue as it occurs in the animal, for several reasons: (1) The topographic relationships between collagen fibrils and elastic fibers and between these fibers and connective tissue cells are only evident in the intact tissue, not in tissue fractions. (2) Only in such intact tissue can one hope to observe the morphological events occurring when cells engage in the formation of fibers. (3) Morphological changes that are known to take place in connective tissues during aging or in the course of pathological processes are more easily studied in intact tissue than in purified fractions thereof.

This present study has been undertaken in view of this need for additional information on the fine structure of intact connective tissue. This study is primarily concerned with the first of the above-mentioned points, that is, with the topographic relationship between the different connective tissue components, since it is felt that these relationships are unclear and controversial. In addition, a morphological description is given of the connective tissue components as they are seen in thin sections.

The tunica propria of bronchioles which is the subject of this study represents an example of a loose, "unspecialized" connective tissue. This tissue was chosen because in it the relationships of structures are perhaps simpler and more easily understood than in specialized tissues like the elastic portion of arteries, cartilage, bone, etc. Findings made on a simple type of connective tissue can perhaps provide the more elementary information on which future studies, concerned with other types of such tissues, could be based.

MATERIAL AND METHODS

White mice 2 to 3 months of age were used as donor animals. Their lungs were perfused through the trachea and through the heart with osmium tetroxide (*27*) and were fixed for an additional one to two hours *in vitro*, at 4°C. Ascending concentrations of acetone were used for dehydration. In order to increase the contrast of collagenous and of elastic elements in the electron-optical image, most tissues were subjected to staining with phosphotungstic acid. This compound was dissolved in a concentration of 1 % in the 70 % acetone of the dehydration series, and the tissue was left in this solution for 15–30 minutes before being transferred into 100 % acetone (containing no phosphotungstic acid). The pieces of dehydrated tissue were impregnated and subsequently embedded in a mixture of 3 to 4 volumes of *n*-butyl methacrylate and of 1 volume of ethyl methacrylate containing 0.2 to 0.5 benzoyl peroxide. The methacrylate used for embedding was prepolymerized (*7*) to a very high viscosity. Polymerization was completed in approximately 48 hours in

an oven set at 74 to 80°C (*7*). Sections were cut on a Porter-Blum microtome (*48*) using glass knives prepared in the laboratory. These sections were subsequently examined in an RCA EMU 2 electron microscope.

OBSERVATIONS

In survey electron micrographs of low magnification the tunica propria of bronchioles appears as a rather narrow layer of connective tissue which supports the ciliated and non-ciliated cells of the epithelium (Fig. 1). This layer separates the bronchiolar epithelium from the lung capillaries and alveoli (Fig. 1). In rare specimens, a separation appears within this layer of connective tissue: notably the capillary and alveolar walls appear to be torn away from the connective tissue elements of the tunica propria (Fig. 2). The width of the tunica propria varies depending on the size of the bronchiole. In smaller bronchioles only a narrow layer of connective tissue (average about 500 mμ) separates the bronchiolar epithelium from the endothelium of lung capillaries and only a few isolated fibroblasts are seen within this layer (Fig. 3). In larger bronchioles the tunica propria reaches a width several times as great as that depicted in Fig. 1 and consists of loosely arranged extracellular material and of numerous fibroblasts (Fig. 6).

Within the layer of the tunica propria, the following structures can be recognized: the basement membrane of the bronchiolar epithelium, the connective tissue cells (fibroblasts), the collagen fibrils, the elastic fibers, and the filaments.

Of these structures, only the cells are recognized equally well in osmium-fixed tissues and in tissues that have been stained with phosphotungstic acid subsequent to osmium fixation. On the other hand, the basement membrane, collagen fibrils, elastic fibers, and filaments are seen much better if phosphotungstic acid treatment has been used in addition to osmium fixation.

FIG. 1. Epithelium of a bronchiole and underlying tunica propria. Non-ciliated and ciliated cells (with cilia, *Ci*) of the epithelium as well as a fibroblast (*Fib*) and collagen fibrils (*Cf*) of the tunica propria (*Tp*) are distinguished. Beyond, portions of alveolar lumina (*Al*) can be seen. × 6900.

FIG. 2. Epithelium of a bronchiole and underlying tunica propria (*Tp*) with fibroblasts (*Fib*) and collagen fibrils (*Cf*). Inside capillaries which are adjacent to an alveolus (*Al*) two white blood cells (*Wbc*) and a red blood cell (*Rbc*) are seen. The separation of these capillaries from the tunica propria is considered an artifact. × 4900.

Key to Abbreviations

Abm	alveolar basement membrane	*Cl*	capillary lumen	*M*	mitochondrion
Ae	alveolar epithelium	*Ebm*	basement membrane of epithelium	*N*	nucleus
Al	alveolus	*Ef*	elastic fiber	*Nm*	nuclear membrane
Ar	artifact	*Er*	endoplasmic reticulum	*Pm*	plasma membrane
Be	bronchiolar epithelium	*Fib*	fibroblast	*Rbc*	red blood cell
Ce	capillary endothelium	*Fil*	filament	*Tp*	tunica propria
Cf	collagen fibril	*I*	inclusion	*V*	vacuole
Ci	cilium			*Wbc*	white blood cell

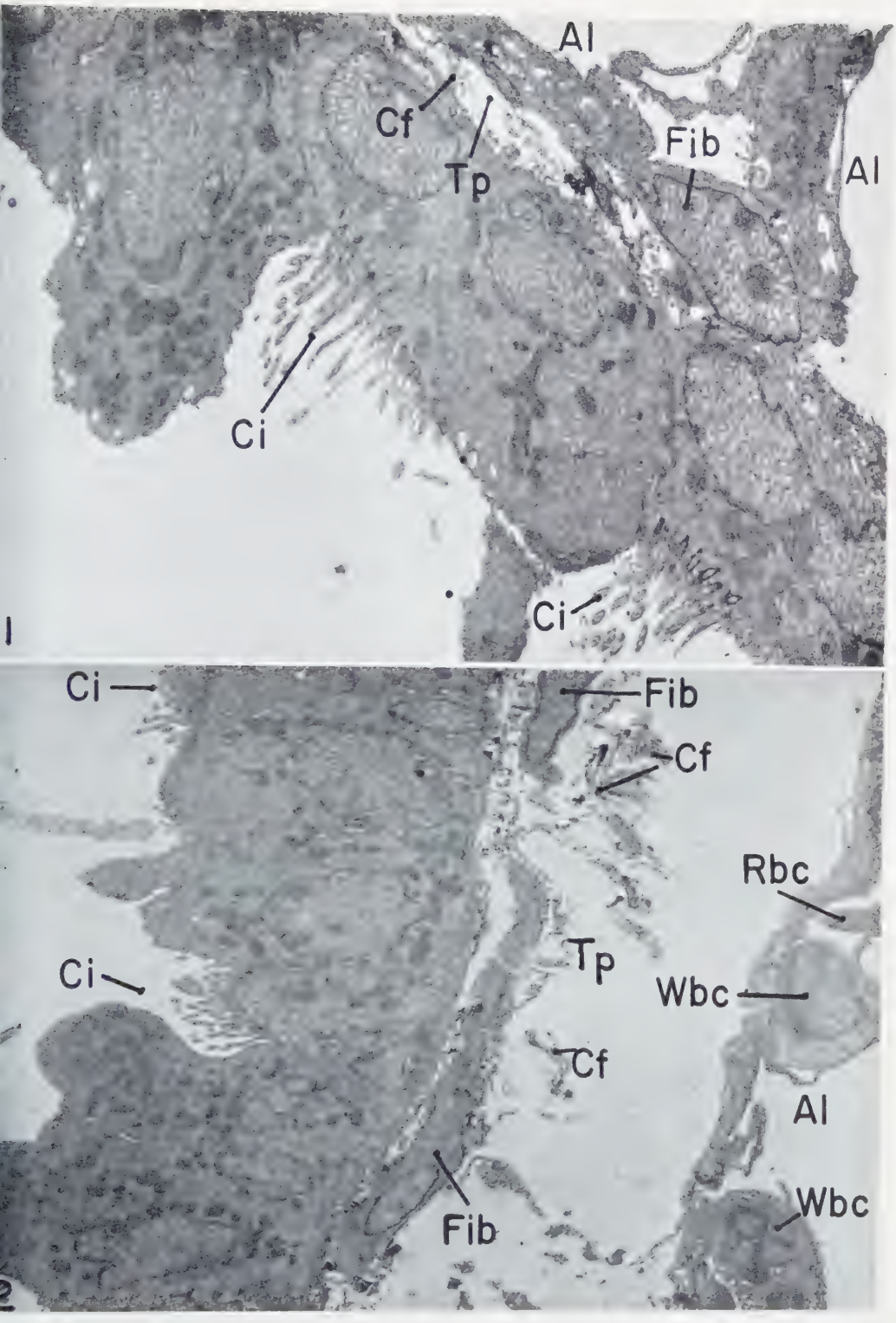
Al
Cf
Tp
Fib
Al
Ci
Ci
Ci
Fib
Cf
Rbc
Tp
Ci
Wbc
Cf
Al
Fib
Wbc

The basement membrane of bronchiolar epithelium

The basement membrane is recognized in phosphotungstic acid treated tissue as a thin layer (17 to 27 mμ) of medium electron density which runs approximately parallel to the plasma membrane of the epithelial cells. It is separated from this plasma membrane by a less dense zone approximately 15 to 27 mμ wide (Figs. 4–7, 11, 13 and 16). The basement membrane continues uninterrupted beneath the points where adjacent epithelial cells meet. It often appears without any typical fine structure and is rather ill-defined (Fig. 4, center of Fig. 5), but it is well outlined in other cases (Figs. 6 and 11).

In tissues not stained with phosphotungstic acid the basement membrane can sometimes be seen (Fig. 5) despite the very low contrast. In other unstained tissues this membrane may be completely invisible (Fig. 3). However, in such tissues the basement membrane can be simulated wherever certain artifacts (manifested by areas of decreased density) occur close to the base of the epithelium (Ar_1, Fig. 3). The narrow layer of denser material between such artifacts and the plasma membrane of the epithelium (Fig. 3) is indistinguishable from the uniformly dense material elsewhere in the tunica propria (*Tp*, Fig. 3), and it thus does not necessarily represent the basement membrane. Similar artifacts are also recognized elsewhere in the tissue (Ar_2, Fig. 3).

When the tissue is well preserved, connective tissue components of the tunica propria are usually found adjacent to the basement membrane. Thus, elastic fibers (Figs. 4, 7, 11 and 13), collagen fibrils (Figs. 6 and 7), and fibroblasts (Fig. 11) can be seen in actual contact with the basement membrane. However, these units are readily distinguished from the membrane and are not observed to fuse with it.

The fibroblasts

In thin sections the fibroblasts appear as elongated cells of irregular outlines which contain an oval or irregularly-shaped nucleus, and which are enclosed by a well-defined plasma membrane. Rarely this plasma membrane is seen composed of two

---

FIG. 3. Base of the bronchiolar epithelium (*Be*) with tunica propria (*Tp*), a capillary (*Cl*), and portion of an alveolus (*Al*). Areas of lesser density are considered artifacts (Ar_1, Ar_2). A fibroblast (*Fib*) contains numerous round and elongated profiles of endoplasmic reticulum (*Er*) and a mitochondrion (*M*). A capillary contains a white blood cell (*Wbc*). The alveolar epithelium (*Ae*) is separated from the capillary endothelium (*Ce*) by the alveolar basement membrane (*Abm*). × 56,000.

Fig. 4. Base of the bronchiolar epithelium (*Be*) and adjacent portion of the tunica propria. Adjacent to the plasma membrane (*Pm*) of the epithelial cells lies the ill-defined layer of the basement membrane (*Ebm*). Below this membrane an elastic fiber (*Ef*) and a fibroblast (*Fib*) are recognized. × 83,000.

FIG. 5. Base of the bronchiolar epithelium (*Be*) and adjacent portion of the tunica propria. The plasma membrane (*Pm*) of the epithelial cell is accompanied by an ill-defined basement membrane (*Ebm*). 56,000.

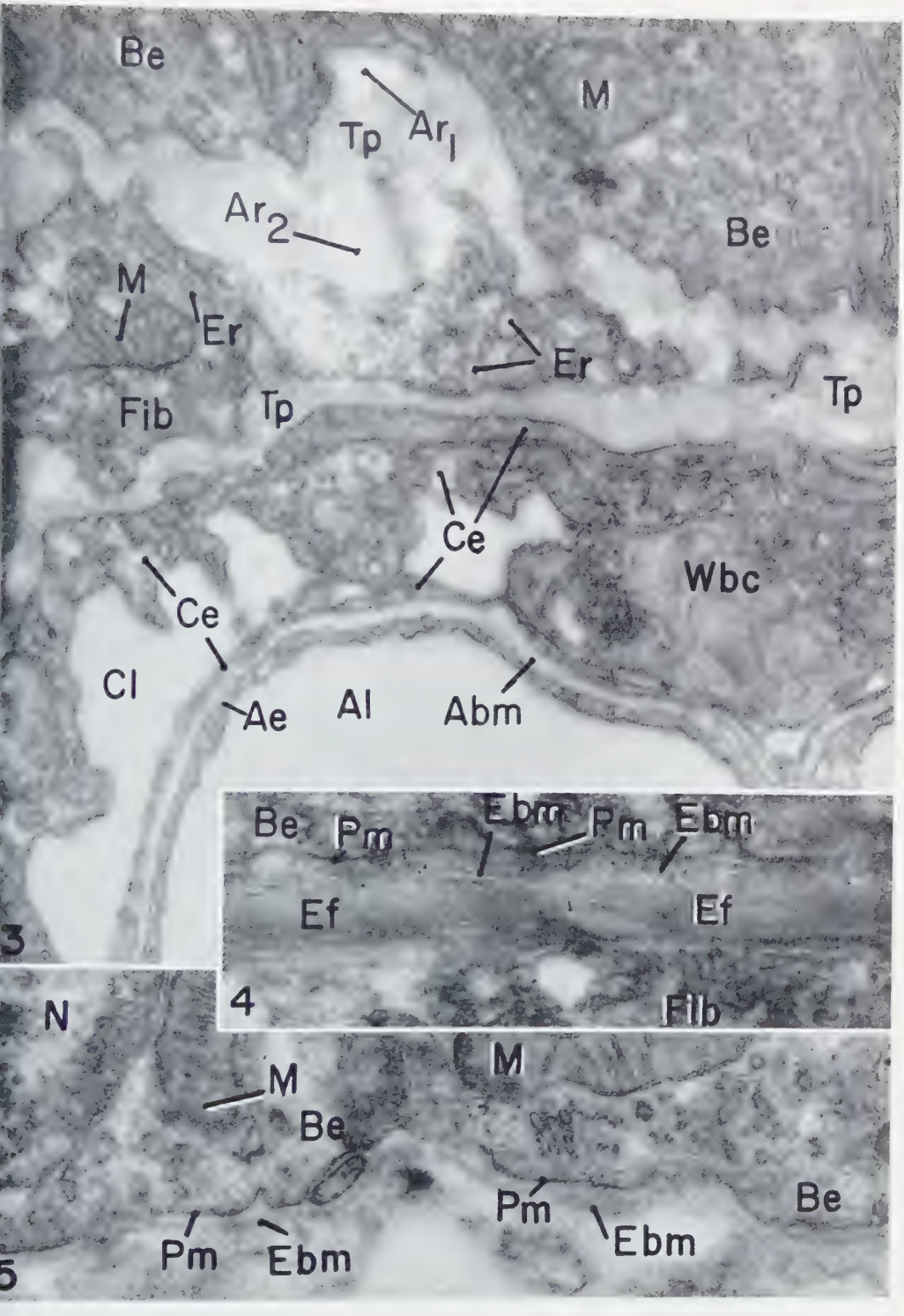
Be
Tp
Ar1
M
Ar2
Be
M
Er
Er
Tp
Fib
Tp
Ce
Wbc
Ce
Cl
Ae
Al
Abm
Be
Pm
Ebm
Pm
Ebm
Ef
Ef
3
4
Flb
N
M
M
Be
Pm
Be
Pm
Ebm
Ebm
5

separate units (*Pm*, Fig. 30). In some cells the plasma membrane is separated from the nuclear membrane by only a very narrow layer of cytoplasm (*Pm*, Figs. 14 and 26). The fibroblasts are of an appreciable thickness usually only in the central portion containing the nucleus. At their periphery they are reduced to thin protoplasmic sheets. In sections these appear as thin strands of cytoplasm delimited by a plasma membrane (Figs. 3, 6, 8 11, 13, 15, 16, 18, 19, 21 and 23). Some of these peripheral extensions may become so thin (14 mμ) that they appear as little more than two parallel plasma membranes (Fig. 23). In one instance such a thread-like extension showed a periodicity comparable to that of collagen (arrows, Fig. 23).

The fibroblasts are often found distributed singly with extracellular fibers separating the single cells from each other (Figs. 6, 11, 16 and 21). In some preparations distances between single cellular fragments as seen in thin sections may be measured in microns. On the other hand, some fibroblasts are found adjacent. The plasma membranes of two such neighboring cells are always seen as two distinct structures (*Pm*, Figs. 12, 13, 24, 27 and 28).

Next to the plasma membrane of some fibroblasts certain layers of filamentous appearance can be found. Such layers occur around thin peripheral extensions of fibroblasts (arrows, Fig. 6; double arrows, Fig. 16) as well as around the central portion of the cells (arrows, Figs. 20, 21 and 24). They are of varying width (20 to 65 mμ). Cells as little as 250 mμ apart can be observed, one of which is enveloped by such a layer, whereas the other is not (Fig. 21). These layers somewhat resemble the basement membrane of the epithelium (Figs. 6, 16, 20 and 21). In some cases they are seen to split up into delicate filaments (*Fil*, Figs. 8, 17 and 24).

FIG. 6. Base of the bronchiolar epithelium (*Be*), basement membrane (*Ebm*), and tunica propria with fibroblasts (*Fib*), collagen fibrils (*Cf*), and elastic fibers (*Ef*). Small profiles inside fibroblasts are interpreted as portions of their endoplasmic reticulum (*Er*). One fibroblast is surrounded by a narrow and ill-defined layer (arrows) which somewhat resembles the basement membrane of the epithelium (*Ebm*). Small dense "dots" (double arrows) are thought to represent cross sections of filaments. × 66,000.

FIG. 7. Base of the bronchiolar epithelium (*Be*), basement membrane (*Ebm*), and tunica propria with collagen fibrils (*Cf*), elastic fibers (*Ef*), and filaments (*Fil*). A group of collagen fibrils (Cf_3) seem to merge gradually (double arrows) with elastic material (*Ef*). Some filaments appear to be beaded. × 71,000.

Fig. 8. Portion of a fibroblast (*Fib*), collagen (*Cf*) and elastin (*Ef*). The slender extension of a fibroblast is bounded on each side by a dense plasma membrane (*Pm*). A rather dense mass, apparently made up of thin filaments (*Fil*), radiates from the surface of the fibroblast, but the dense plasma membrane may still be distinguished within this mass of filaments. Some of these filaments appear to be beaded (arrow). × 80,000.

FIG. 9. Small portion of a fibroblast (*Fib*) and adjacent fibrous structures. One collagen fibril showing characteristic periodicity seems to divide into two units at both its extremities (Cf_1). Delicate filaments (*Fil*) are in close contact with the fibroblast surface and weave around a collagen fibril (Cf_2). × 58,000.

FIG. 10. Small portion of a fibroblast and adjacent fibrous structures. Numerous distinct thin filaments (*Fil*) extend from the surface of the fibroblast and interweave with collagen fibrils (Cf_1). Portion of another collagen fibril (Cf_2) seems to be superimposed on the cell. × 58,000.

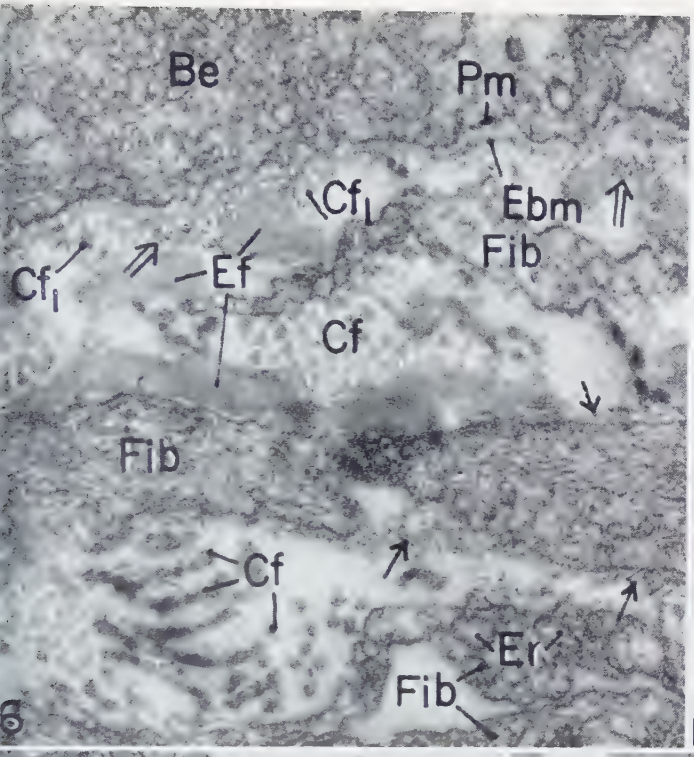
Be
Pm
Cf1
Ebm
Fib
Cf1
Ef
Cf
Fib
Cf
Er
Fib

6

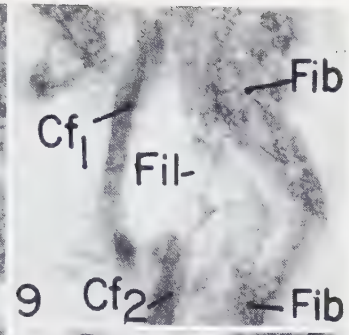
Fib
Cf1
Fil
Cf2
Fib

9

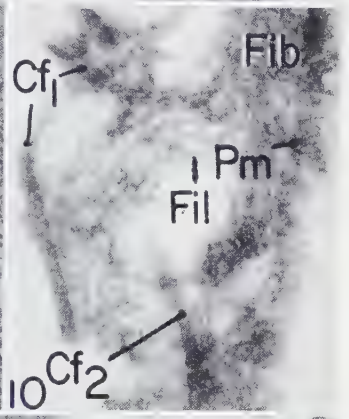
Fib
Cf1
Pm
Fil
Cf2

10

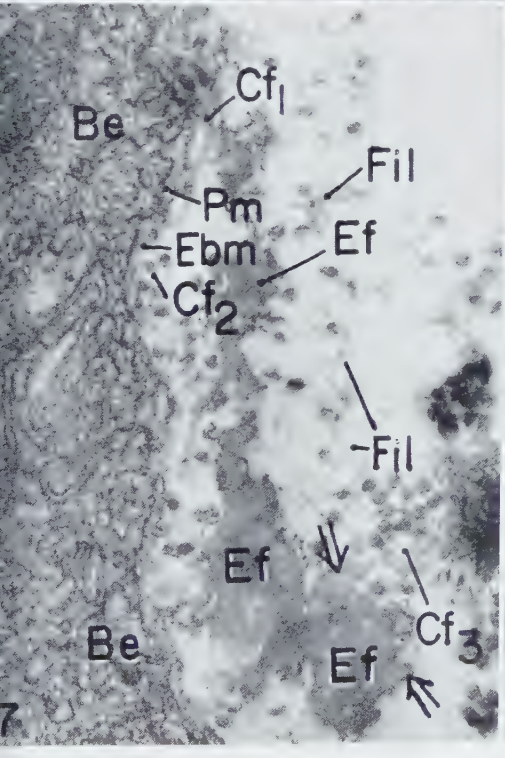
Cf1
Be
Fil
Pm
Ebm
Ef
Cf2
Fil
Ef
Cf3
Be
Ef

7

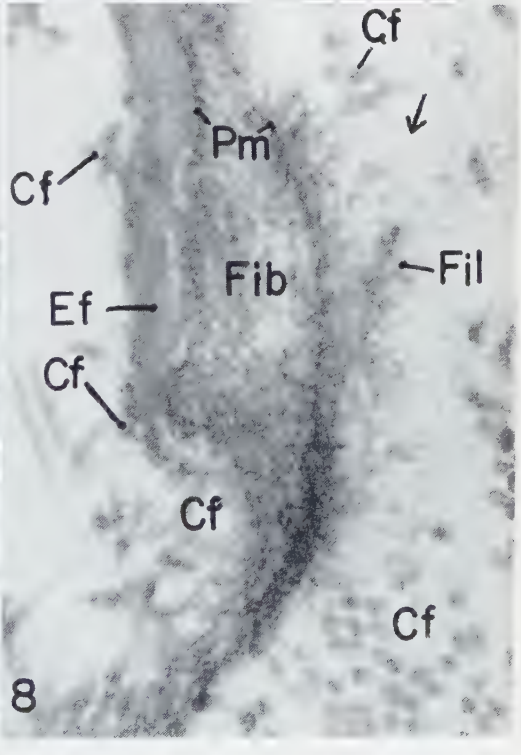
Cf
Pm
Cf
Fil
Fib
Ef
Cf
Cf
Cf

8

The cytoplasm of fibroblasts contains the following components: small elongated mitochondria (*M*, Figs. 3, 12, 24 and 25), elongated profiles of the endoplasmic reticulum with attached dense particles (Er_1, Fig. 25; *Er*, Fig. 26), profiles of the endoplasmic reticulum without attached particles (Er_2, Fig. 25), and vacuoles and vesicles of different sizes and shapes, most of which may also be portions of the endoplasmic reticulum (*V*, Figs. 11, 12, 20, 23–25, 27 and 28). The dense membrane of some of these vesicles is clearly seen to be continuous with the plasma membrane of the fibroblast (*V*, Figs. 20 and 27). On rare occasions some rather dense inclusion bodies of irregular size and shape are also found inside the fibroblasts (*I*, Fig. 12). These inclusion bodies lack a typical fine structure. Most of these cytoplasmic components are seen better if phosphotungstic acid staining is omitted (Figs. 3 and 25–28), since in stained tissue they appear somewhat masked by a diffuse granularity of marked contrast (Figs. 11–13, 16, 17, 20 and 24).

The collagen fibrils

The collagen fibrils are seen as cylindrical units which appear under considerable contrast after phosphotungstic acid staining, but which are usually ill-defined if no stain is used. In cross sections the round profiles measure 24 to 55 mμ in diameter, in longitudinal sections 27 to 47 mμ. They are easily identified if their typical periodicity (*62, 73*) and interperiod bands (*39, 41, 61*) are seen (*Cf*, Figs. 22, 23, 29 and 30). This may be observed where a long enough portion of the fibril happens to lie in the plane of the section. The fibrils lie in groups or small bundles (*Cf*, Figs. 11, 13, 14, 16, 21 and 29), but they may also occur singly (Fig. 7). They are often sandwiched in between fibroblast extensions (Figs. 13, 16, 21 and 24). Others lie isolated and well away from the nearest cells (Fig. 29), particularly in the wide tunica propria of the larger bronchioles. Some collagen fibrils are adjacent to elastic material (Figs. 7 and 22), to the basement membrane of the epithelium (Cf_1, Fig. 6; Cf_1 and Cf_2, Fig. 7), and to the plasma membrane of fibroblasts (Figs. 8–11, 13, 14, 16, 17, 21, 23 and 30). On rare occasions a collagen fibril seems to overlap the outline of a fibroblast (Cf_2, Fig. 10), but never are typical fibrils recognized inside fibroblasts.

The typical period and interperiod bands of collagen are seen wherever direction of sectioning and electron optical resolution are favorable. The a_1, a_2, b_1, b_2, c, d, e_1,

---

FIG. 11. Base of bronchiolar epithelium (*Be*) and adjacent portion of the tunica propria. The plasma membrane of the epithelium (*Pm*) is accompanied by the basement membrane (*Ebm*). A fibroblast (Fib_1) is closely associated with the basement membrane in one sector but is separated from it elsewhere by small elastic fibers (*Ef*). Portion of another fibroblast (Fib_2) is seen containing isolated vacuolar structures (*V*) which are thought to be portions of the endoplasmic reticulum. Between the two fibroblasts lie a group of collagen fibrils (*Cf*) and thin filaments (*Fil*). × 73,000.

FIG. 12. Portions of two fibroblasts (Fib_1, Fib_2) showing inclusions (*I*), vacuoles (*V*), profiles of the endoplasmic reticulum (*Er*), mitochondria (*M*), and nucleus (*N*). × 57,000.

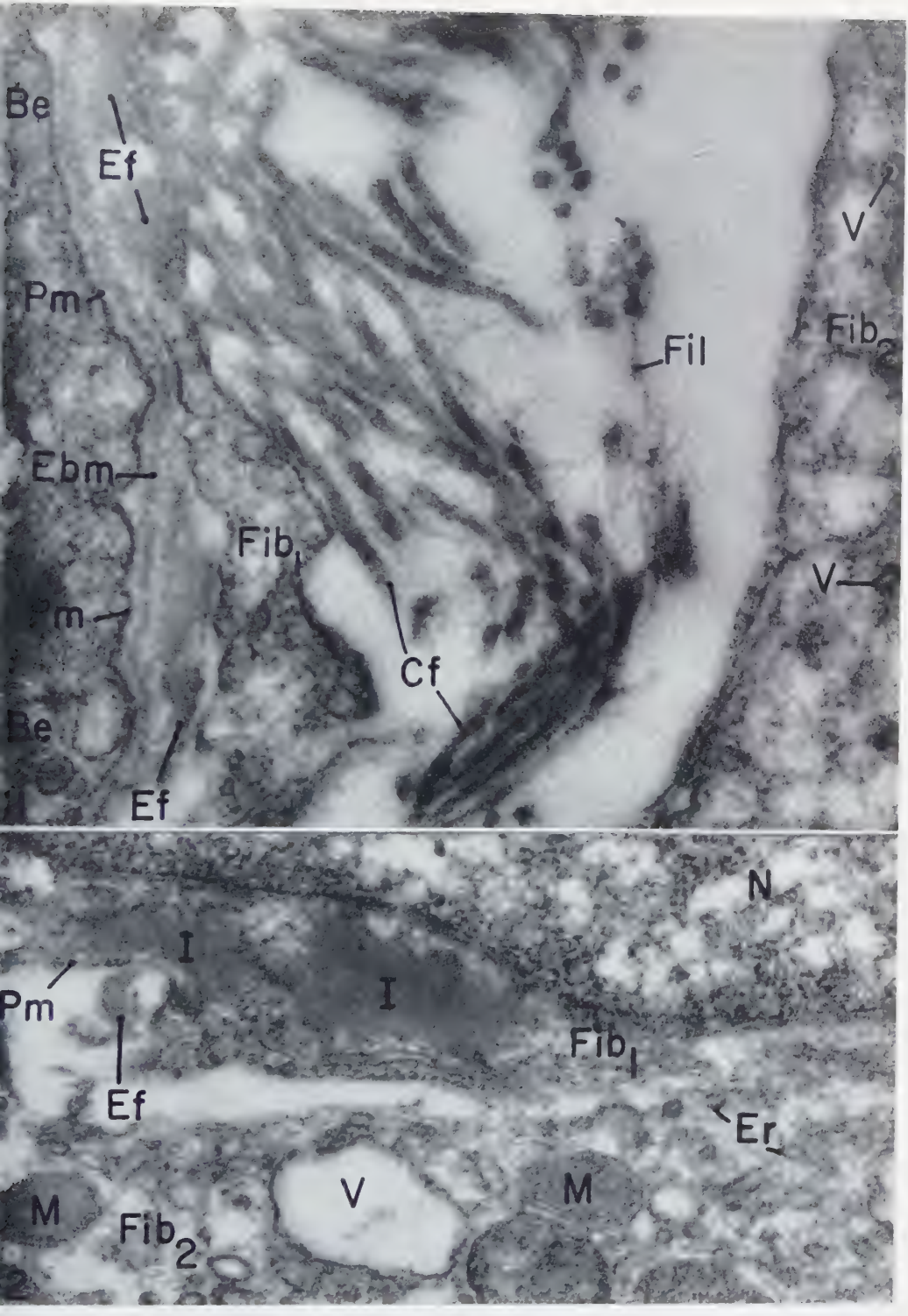
Be
Ef
Pm
Ebm
Fib1
Pm
Be
Ef
Cf
Fil
V
Fib2
V
N
I
I
Pm
Ef
Fib1
Er
M
V
M
Fib2

and e_2 bands (*61*) have been recognized (Fig. 30). The main periods, represented by the a and b bands, are spaced at regular intervals of about 60 mμ (Fig. 30). The main periods of adjacent fibrils may appear in register (arrows, Fig. 29) or not in register (double arrows, Fig. 29; Fig. 30). At the main period the diameter of a collagen fibril seems to be slightly longer than at the interperiod region (Cf_2 and Cf_3, Fig. 30) namely, about 42 mμ versus 37 mμ.

The elastic fibers

In the present report the term elastic fiber is applied to certain intercellular material, other than collagen fibrils, which has a rather variable appearance. Reasons for considering that this material represents elastic fibers will be discussed later in this report. After phosphotungstic acid staining this material appears as uniformly dense masses of irregular size, shape, and outline, which lack a periodicity, and which are scattered between fibroblasts and collagen fibrils. Without phosphotungstic acid staining this material remains nearly unrecognizable (Figs. 3 and 5) except in rather thick sections.

In sections the elastic fibers usually appear as elongated structures of indefinite length and about 100 to 200 mμ in width (*Ef*, Figs. 4, 8 and 15; Ef_1, Fig. 16; Ef_2, Fig. 13). Other fragments of elastic fibers are seen as irregularly shaped masses of varying size (*Ef*, Figs. 6, 7, 11, 14, 18–20, 22 and 24). After phosphotungstic acid staining their density appears comparable to that of collagen fibrils in cross sections (Figs. 6–8, 13 and 16). Elastic fibers generally appear homogeneous in their central portions, but sometimes ill-defined bands and dots, thought not to be artifacts, can be made out in these portions (Fig. 19). At their periphery, many elastic fibers split up into filaments (*54*; Figs. 15, 16, 18, 19 and 22) of about 11 mμ in diameter.

Like the collagen fibrils, the elastic fibers are found in close contact with the basement membrane of the epithelium (*Ef*, Figs. 4, 6 and 11; Ef_1, Fig. 13) and with the plasma membrane of fibroblasts (*Ef*, Figs. 8, 11, 15 and 18–20; Ef_1 and Ef_2, Fig. 13), but they remain on the outside of this plasma membrane. However, certain rarely

---

FIG. 13. Base of the bronchiolar epithelium (*Be*), basement membrane (*Ebm*), and portion of the tunica propria with four fibroblasts (Fib_{1-4}), collagen fibrils (*Cf*), and elastic fibers (*Ef*). Two adjacent fibroblasts (Fib_2, Fib_3) are bounded by individual plasma membranes (*Pm*). × 59,000.

FIG. 14. Portion of a fibroblast with nucleus (*N*), and extracellular collagen fibrils (*Cf*) and elastic fibers (*Ef*). The plasma membrane (*Pm*) is clearly recognizable over most of its course. In the cytoplasm a few profiles of endoplasmic reticulum (*Er*) are apparent. The collagen fibrils and elastic fibers are in immediate contact with the plasma membrane (arrows) but are all located on the outside of this membrane. × 57,000.

FIG. 15. Portion of a fibroblast (*Fib*) and adjacent elastic fiber (*Ef*). The fiber lies adjacent to the plasma membrane (*Pm*) and splits up into filaments (left). × 72,000.

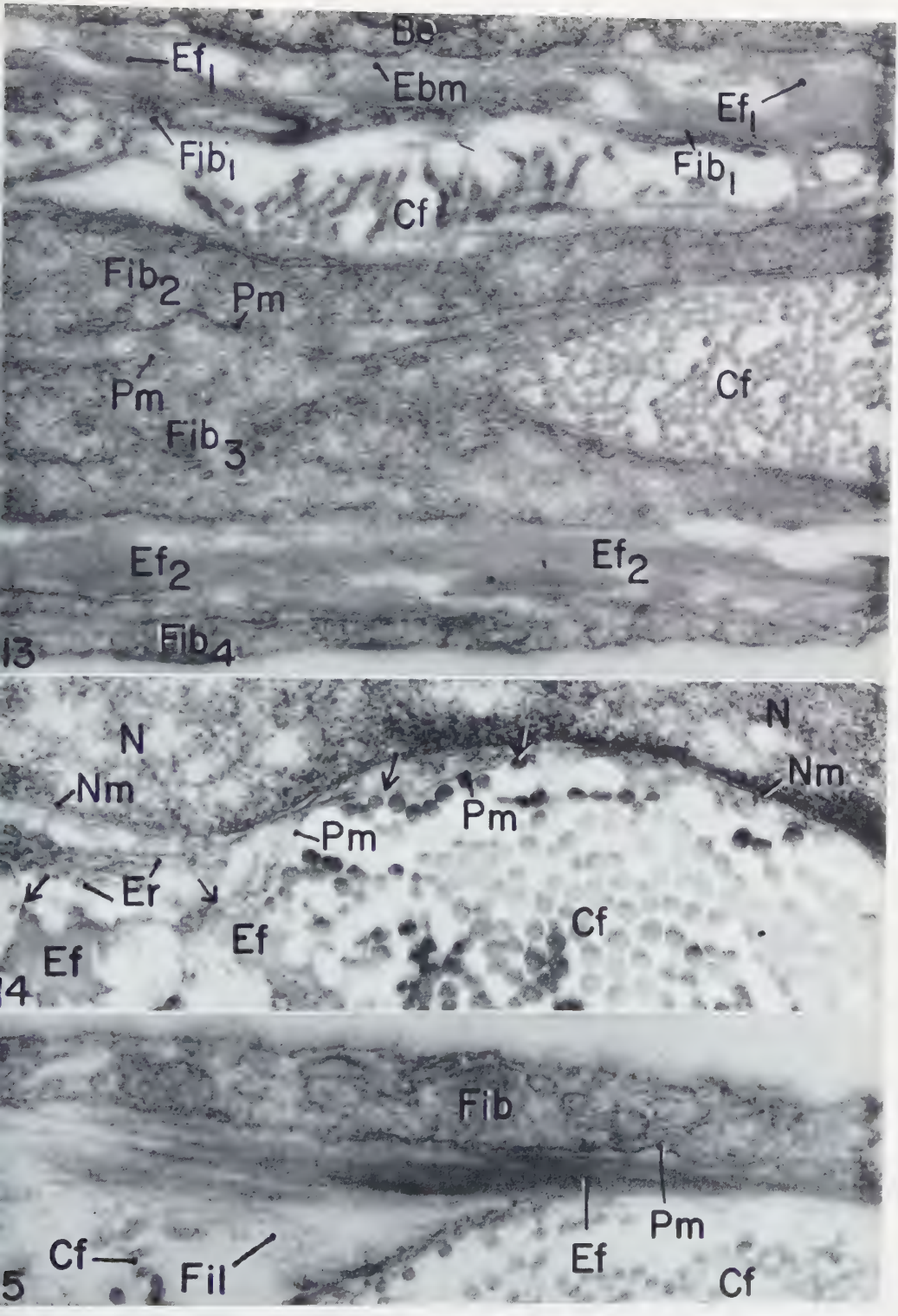
Bc
Ef1
Ebm
Ef1
Fib1
Fib1
Cf
Fib2
Pm
Pm
Cf
Fib3
Ef2
Ef2
Fib4
13
N
Nm
N
Nm
Pm
Pm
Er
Ef
Cf
Ef
14
Fib
Pm
Cf
Fil
Ef
Cf
5

observed inclusions inside fibroblasts may appear morphologically indistinguishable from the extracellular elastic fibers (*I*, Fig. 12).

Still other elastic fibers are in close contact with collagen fibrils (Figs. 6, 7 and 22). Some of them have an irregular outline with semi-circular protrusions. These protrusions resemble cross section profiles of collagen fibrils (double arrows, Fig. 7). Other elastic fibers appear to consist of globular subunits of the approximate size and shape of collagen fibril cross sections (arrows, Fig. 16).

The filaments

Extracellular thin filaments (*25*, *49*, *56*) of an estimated diameter of about 11 mμ are encountered everywhere in the tunica propria. They occur intermingled with collagen fibrils and seem to have a definite relation to them (*Fil*, Figs. 7, 11 and 29). In cross sections these filaments may appear as dense dots (double arrows, Fig. 6). Some of the filaments are beaded (*15*, *49*, *51*, *67*; *Fil*, Fig. 7; arrow, Fig. 8; Fil_1, Fig. 29), but due to lack of contrast and resolution the exact dimensions of this cross structure cannot be determined.

The filaments as described above resemble those that radiate from the surface of certain fibroblasts (*Fil*, Figs. 8–10, 17 and 24) as well as those which are continuous with elastic fibers (*Fil*, Figs. 16, 18, 19 and 22) except for the beading which has not been observed in the latter. All of these different filaments are visible only in osmium-fixed, phosphotungstic acid stained connective tissue. They have not been observed in unstained tissue.

DISCUSSION

The basement membrane of the bronchiolar epithelium

The basement membranes which underlie epithelia have been considered by most workers to be specialized portions of the connective tissue (*66*), although some such membranes, notably in invertebrates (*23*), were assumed to be products of the

---

FIG. 16. Base of the bronchiolar epithelium (*Be*), basement membrane (*Ebm*), and tunica propria with fibroblasts (*Fib*), collagen (*Cf*) and elastin (*Ef*). One fibroblast (Fib_1) is surrounded on the outside of its plasma membrane by an ill-defined and moderately dense material which somewhat resembles a basement membrane (double arrows). Two elastic fibers (Ef_1) seem to split up into a number of thin filaments (*Fil*). Another elastic fiber (Ef_2) consists of round fragments of the approximate size of collagen fibril cross sections (arrows). × 55,000.

FIG. 17. Portion of a fibroblast (*Fib*). Thin filaments (*Fil*) radiate from its whole surface. At one point two thicker units resembling collagen fibrils seem to be in close apposition to the fibroblast surface (double arrow). × 58,000.

FIG. 18. Portions of two fibroblasts (*Fib*) and surrounding fibrous structures. A small elastic fiber (*Ef*) splits up into numerous thin filaments (*Fil*). × 45,000.

FIG. 19. Fibroblasts (*Fib*) and elastin. Small fragments of elastic fibers (*Ef*) split up into numerous short filaments (*Fil*). × 45,000.

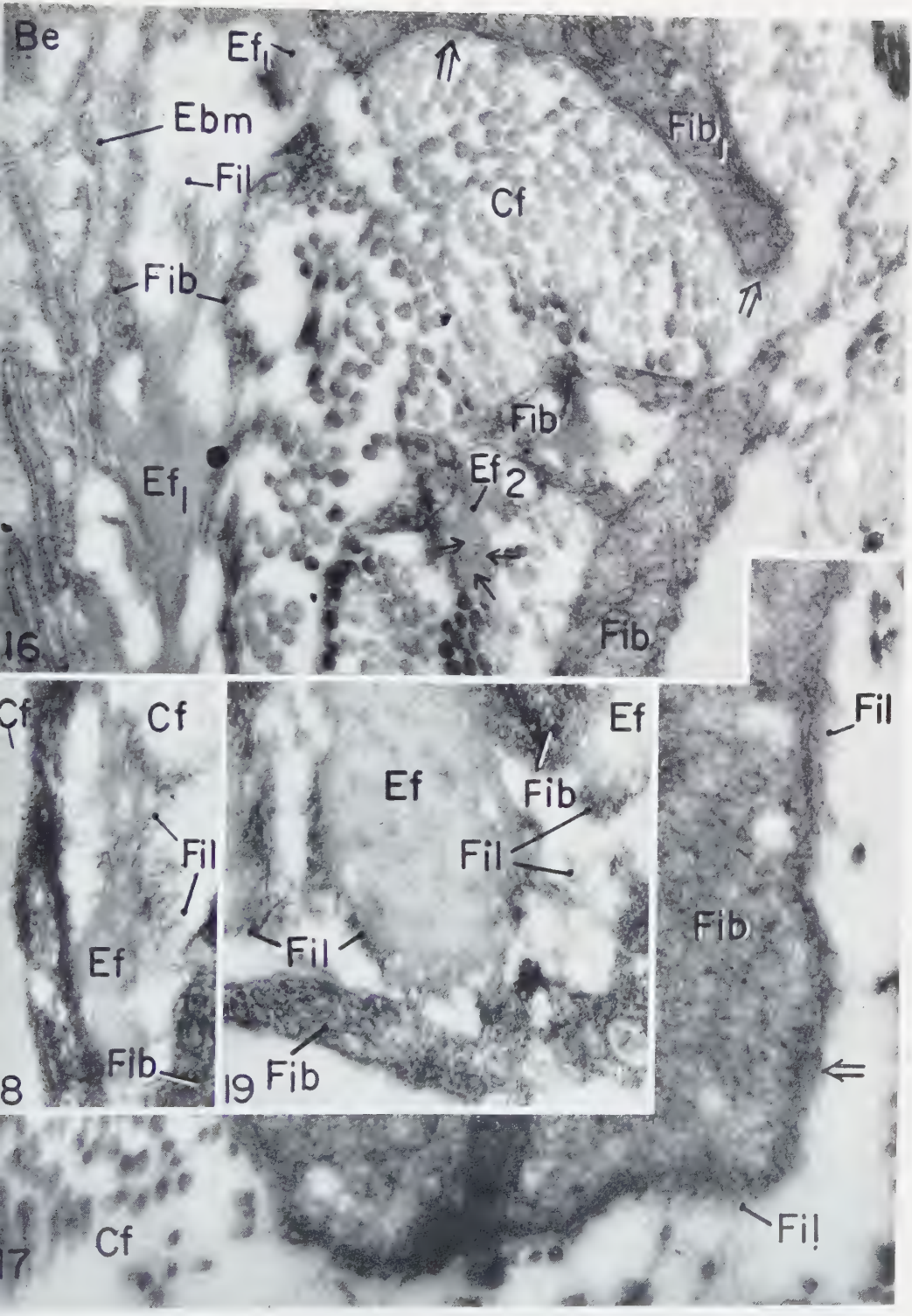
Be
Ef1
Ebm
Fil
Cf
Fib1
Fib
Fib
Ef1
Ef2
Fib
16
Cf
Cf
Fil
Ef
Fib
8
Ef
Ef
Fib
Fil
Fil
19
Fib
Fil
Fib
Cf
17
Fil

epithelium. The origin and nature of the basement membrane cannot be determined with certainty on the basis of our electron micrographs. However, its origin from connective tissue is suggested by its close topographic relationship with connective tissue cells and fibers (Figs. 4, 6, 7, 11, 13 and 16) and by its similarity to certain layers of a filamentous fine structure that surround fibroblasts (Figs. 6, 16, 20 and 24). A comparable fine structure has been seen in the basement membrane underlying the corneal epithelium (*25*).

It could be assumed that the basement membrane is related to collagen. Indeed, sheet-like collagenous structures are well known from other sites (*26*), and they can also be produced experimentally from collagen solutions (*13*). On the other hand, some workers have suggested that basement membranes as seen in the optical microscope are to be considered as "condensed" portions of the ground substance of the connective tissue (*12*). Their arguments are based on light-optical studies of the tinctorial, physiological, and chemical properties of both basement membrane and ground substance. Similar comparisons cannot be made at the electron microscopic level since there are, as yet, no histochemical or other methods available that would identify the ground substance and its "condensations" in the electron microscope. In our electron micrographs the ground substance is altogether invisible, assumedly because it appears under conditions of insufficient contrast.

The basement membrane as seen in our electron micrographs resembles other basement membranes described by various authors (*4*, *43*, *47*, *52*, *53*, *65*, *76*). Like the basement membrane of bronchioles, these other membranes are also seen as thin,

---

FIG. 20. Portion of a fibroblast (*Fib*), collagen (*Cf*), and elastin (*Ef*). A few cytoplasmic vesicles (*V*) are seen as apparent invaginations of the plasma membrane. A thin and ill-defined layer, which has a filamentous structure, accompanies the plasma membrane on its outside (arrows). It seems to continue into the spaces between collagen fibrils in the form of thin filaments (double arrow). 56,000.

FIG. 21. Portions of two fibroblasts. One fibroblast (Fib_1) is enveloped by a narrow layer of filamentous structure (arrows) which surrounds its plasma membrane (*Pm*). From this layer thin filaments (*Fil*) extend in between surrounding collagen fibrils (*Cf*). Several collagen fibrils are in immediate contact with this layer. A second fibroblast (Fib_2) is not surrounded by any such layer of filamentous material. × 83,000.

FIG. 22. Collagen (*Cf*) and elastin (*Ef*). The elastic fibers split into thin filaments (*Fil*). Several collagen fibrils (*Cf*) which are in immediate contact with these elastic fibers show the main periods and inter-period bands. × 56,000.

FIG. 23. Fragment of a fibroblast (*Fib*) and collagen fibrils (*Cf*). The fibroblast contains a few vacuoles (*V*) and terminates in a thin protoplasmic thread which is clearly defined, on either side, by a plasma membrane (*Pm*). The main period cross bands of the collagen fibril lying next to the fibroblastic extension seem to be matched in register by similar periods inside this protoplasmic extension itself (arrows). × 69,000.

FIG. 24. Three fibroblasts (Fib_{1-3}) and adjacent fibrous structures. The cytoplasm shows vacuolar structures (*V*) and a mitochondrion (*M*). Beyond the plasma membranes (*Pm*) stretches a mass of fine filamentous material (arrows) which fills the space between two fibroblasts (Fib_1, Fib_2) and which splits up at its periphery into filaments (*Fil*). A small dense structure (*Ef*) is interpreted as elastic material. × 98,000.

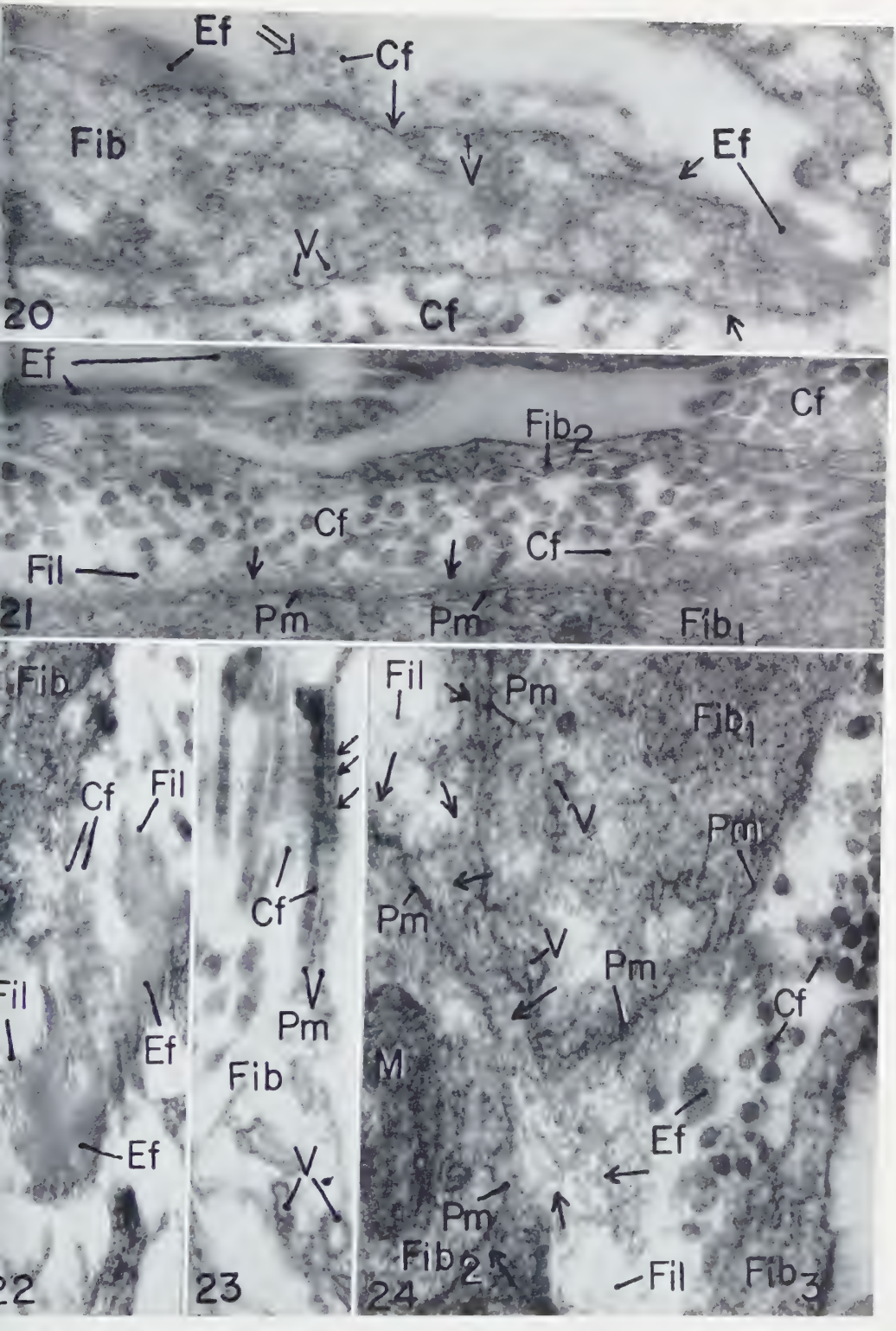
Ef
Cf
Fib
V
Ef
V
20
Cf
Ef
Cf
Fib2
Cf
Cf
Fil
Pm
Pm
Fib1
21
Fib
Cf
Fil
Ef
Ef
22
Cf
V
Pm
Fib
V
23
Fil
Pm
Fib1
V
Pm
Pm
V
Pm
Cf
M
Ef
Pm
Fib2
Fil
Fib3
24

electron-dense sheets which usually appear separated from the epithelium by a narrow, translucent space. It has been suggested that the basement membranes as seen electron-optically do not correspond to what is generally called "basement membrane" by the light microscopist (*63*).

The fibroblasts

It is assumed that most, if not all, cells seen inside the tunica propria are fibroblasts. The following morphological findings support this view since similar findings characterize fibroblasts in the light microscope (*36*): the elongated form of the cells and their peripheral attenuation to form thin protoplasmic sheets, their arrangement in loose networks, and their close topographic relationship with fibers. Connective tissue cells other than fibroblasts, which have been well characterized by light microscopy (*36*), could not be recognized in the course of this study.

The peripheral portions of fibroblasts become extremely attenuated (Figs. 13, 15, 16, 18, 21 and 23). Sheets of cytoplasm of similar thinness have been recognized in the lung (*28*). Moreover, cells grown in tissue culture are commonly attenuated to a comparable thinness. Indeed, the occurrence in the animal body of cells which are as flat as tissue culture cells shows that the thinness of the latter is by no means a unique phenomenon which obtains only under conditions of *in vitro* culture.

The significance of the periodicity seen along an attenuated portion of a fibroblast (arrows, Fig. 23) is not understood at the present time.

This report does not confirm the assumption that fibroblasts form a syncytium (*69*), since the two distinct plasma membranes of adjoining fibroblasts are always recognized (Figs. 13, 24, 27 and 28). A plasma membrane is seen even in the thinnest extensions of fibroblasts (Figs. 21 and 23) and can also be recognized where filaments seem to radiate from the cell surface (Figs. 8 and 24). The suggestion that this plasma membrane of fibroblasts consists in reality of two dense subunits with an intermediate

---

FIG. 25. Portion of a fibroblast with mitochondria (*M*) and endoplasmic reticulum (*Er*). The reticulum occurs in form of cisternae (Er_1) with attached particles and also in form of tubules or of vesicles arranged in strings (Er_2) with no adhering particles. Other single vesicles (*V*) may also be portions of the reticulum. × 56,000.

FIG. 26. Small portion of a fibroblast with nucleus (*N*) and endoplasmic reticulum (*Er*). In one sector the plasma membrane (*Pm*) is separated from the double nuclear membrane (*Nm*) by only a very narrow layer of cytoplasm (arrows). × 56,000.

FIG. 27. Portions of two adjacent fibroblasts. The plasma membranes (*Pm*) of the two cells appear as two distinct units. Several small vesicles (*V*) are seen as invaginations of one of the plasma membranes. A small portion of the nucleus of one fibroblast is included (*N*). × 56,000.

FIG. 28. Portions of two adjacent fibroblasts. The plasma membranes (*Pm*) of both cells appear as two dense lines distinct from each other. An elongated profile of the endoplasmic reticulum (*Er*) and small vesicles (*V*) are seen in the cytoplasm of one cell. × 48,000.

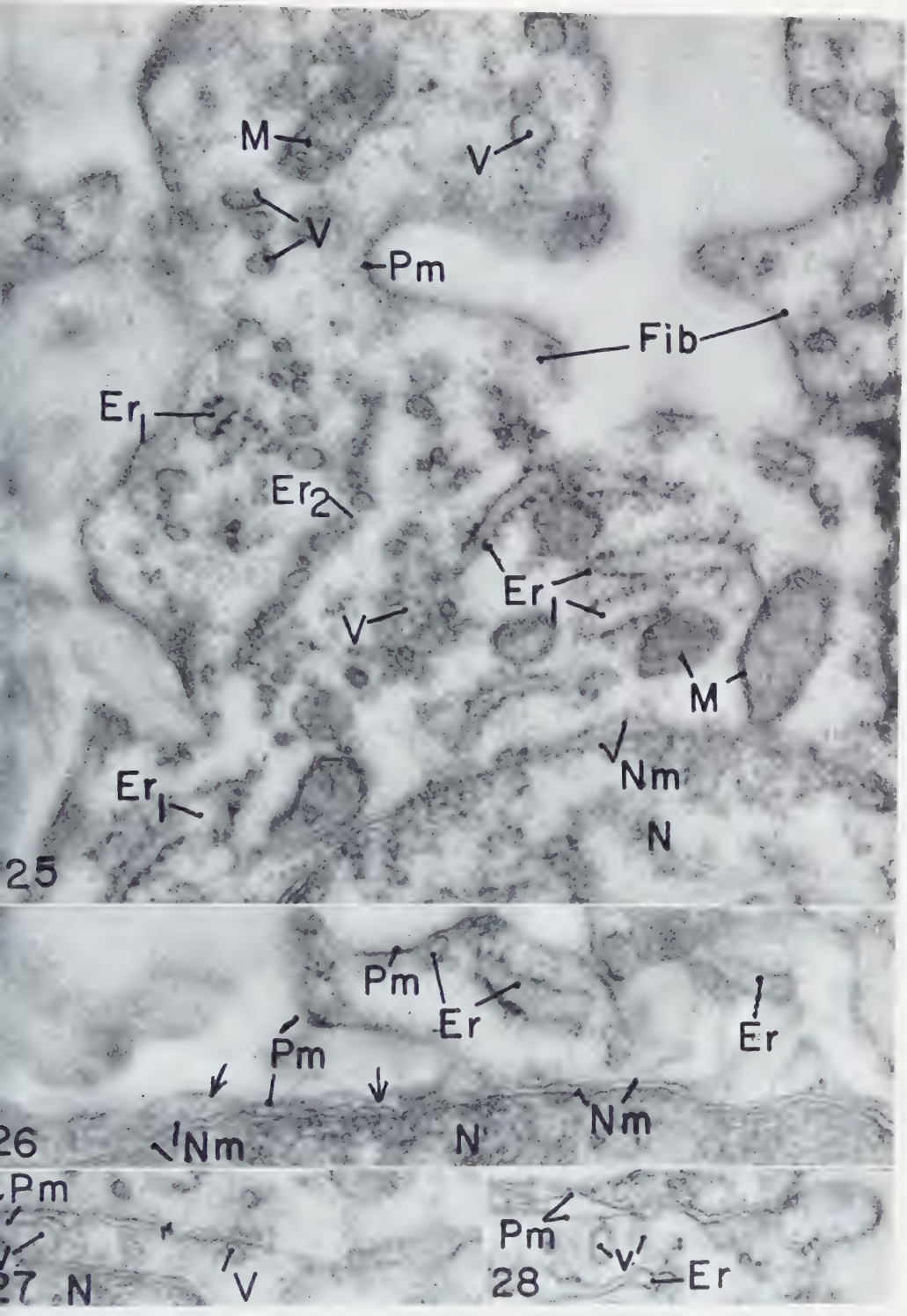
M
V
V
Pm
Fib
Er1
Er2
Er1
V
M
Nm
N
Er1
25
Pm
Er
Er
Pm
Nm
N
Nm
26
Pm
27 N
V
Pm
V
28
Er

less dense layer (Fig. 30) is in agreement with observations made on other cell types (*11*, *57*, *60*, *64*, *77*).

The ill-defined layer of material which surrounds certain fibroblasts (Figs. 6, 8, 16, 20, 21 and 24) could be considered analogous with a basement membrane. Its location suggests that this material is formed by the fibroblasts which it surrounds. Since the plasma membranes of such fibroblasts are usually distinct, this ill-defined layer on the outside of the plasma membrane (Figs. 8, 21 and 24) is thought to be extracellular material. It seems likely that such layers are temporary structures since not all fibroblasts are surrounded by them. Perhaps they represent the first morphological evidence of fiber formation at the cell surface. This view is supported by the filamentous appearance of the layers, and by their close relationship to collagen fibrils and elastic fibers (Figs. 8, 20, 21 and 24) as well as to the filaments (Figs. 8 and 10).

Within fibroblasts the usual cytoplasmic structures can be found, i.e., mitochondria, endoplasmic reticulum (*45*, *46*), small granules (*44*), vacuoles, and inclusions. However, those specific granules thought to be related to fiber formation (*24*, *55*) were not recognized. Those granules are especially abundant in rapidly multiplying fibroblasts of young tissues or of tissue cultures. Their absence argues against an intensive fibrogenesis in our material.

Phosphotungstic acid staining produces a granular or fibrillar appearance of the cytoplasm. It thereby masks the cytoplasmic structures to some extent. In such stained material certain vacuoles or units of the endoplasmic reticulum could be mistakenly interpreted as cross sectioned profiles of collagen fibrils. Usually, however, these vacuoles are recognizable as such (Figs. 11, 12 and 24) and are seen even better in unstained sections (Fig. 25). Typical cross sectioned or longitudinal profiles of collagen fibrils are never encountered in the cytoplasm.

FIG. 29. Bundle of collagen fibrils. Since most of the fibrils do not run in the exact plane of the section, their ends fade out as the fibrils leave the section plane. The main periods appear as dense cross bands which are resolved into two individual bands wherever the course of the fibrils is in the section plane (double arrows). The inter-period bands appear as less dense cross bands in between the main periods. The main periods of different collagen fibrils are in register with each other in some sectors (arrows) but are not coinciding in other sectors (double arrows). Between the fibrils thin filaments (*Fil*) are seen. Some fibrils actually seem to terminate in several such filaments. Some filaments are clearly beaded (Fil_1). × 68,000.

FIG. 30. Collagen fibrils and portion of a fibroblast. The fibroblast (*Fib*) is surrounded by a plasma membrane (*Pm*) which in some sectors seems to be composed of two dense subunits (indicated by arrows). The collagen fibril next to the plasma membrane appears in very close contact with it. Four of the collagen fibrils which happen to run in the section plane clearly show main periods and inter-period bands. The main period consists of the a and b bands, both of which appear as double in suitable spots. Of the inter-period bands the c, d, and e bands can be seen, the e band appearing as double. The "polarity" created by the band pattern is unidirectional in the two adjacent fibrils Cf_1 and Cf_2, but the "polarity" of a third fibril Cf_3 is oriented in the opposite direction. Main periods of adjacent fibrils are not in register. × 239,000.

Fil
Fil
Fil
Fil
9

Pm
Fib
Cf1
Cf2
Pm
Fib
Pm
Cf3
30

Certain vesicles which may be portions of the endoplasmic reticulum are seen as invaginations of the plasma membrane of fibroblasts. This is in agreement with observations made in other cell types (*45*).

The significance of certain intracellular inclusion bodies (*1*, Fig. 12), which have a density comparable to that of elastic fibers, is not understood at present.

The collagen fibrils

No distinction is made between reticulin and collagen fibrils by means of silver impregnation (*10*, *37*, *68*) since such a distinction is rather uncertain (*21*, *33*) and indicates differences in the ground substance rather than in the fibrils themselves (*22*). Thus, the term "collagen fibril" is applied to all cylindrical extracellular structures that exhibit the well-known periodicity (*62*, *73*) and interperiod bands (*39*, *41*, *61*) despite the fact that these fibrils would probably be classified by the light microscopist as argyrophilic or as reticulin. Nor was any silver staining done in order to render the fibrils more clearly visible (*70*, *71*) since they showed up quite well when phosphotungstic acid staining was used.

In cross section the fibrils are seen as round, uniformly dense profiles (Figs. 13, 14, 16, 21 and 24). Thus their appearance in the form of hollow cylinders (*31*, *75*) cannot be confirmed. Such an appearance may have been caused by the removal of the plastic by the authors quoted.

In longitudinal views of fibrils their somewhat greater diameter at the main period as compared with that at the inter-period (Fig. 30) has been ascribed to differential shrinkage during the drying of the fibrils (*14*, *61*, *75*). Such shrinkage would be minimized in fibrils embedded in methacrylate since water would be replaced first by the dehydrating agent (ethanol or acetone) and subsequently by the plastic. There is, indeed, only minimal shrinkage in our plastic-embedded fibrils (Fig. 30).

The periodicity and the inter-period bands as seen in whole mounts of fresh or of variously preserved collagen fibrils (*39*, *41*, *61*, *62*, *73*) are also seen in thin sections of such fibrils (*32*, *42*, *54*, *58*, *72*; Figs. 9, 22, 23, 29 and 30). This fact has been interpreted by some authors as proof of the plate-like character of the "bands" (*54*). On the contrary, other authors believe that the bands of the main period are limited to the periphery of the fibrils (*32*). The length of the main period as measured in our material is somewhat below the 640 Å average, but it nevertheless lies inside the limits of the variability established for fibrils of different tissues (*62*).

The occurrence of visible inter-period bands has been recognized as variable (*14*). In our osmium-fixed, phosphotungstic acid stained material the inter-period bands were always observed where the fibrils happened to be suitably oriented, i.e., in the section plane. In such fibrils a three-banded appearance (*50*, *74*) was never observed. On the other hand, as many as eight bands per period (Fig. 30) were not often seen

either. This could be explained on the basis of inadequate resolution and contrast. Presumably for the same reason more than eight bands (*39*) were never observed.

It is an interesting fact that some adjacent collagen fibrils can be found, the periods of which are either not in register, or which are oriented antiparallel (*39*) with each other (Fig. 30). Non-registry of adjacent fibrils seems to be real rather than due to artifacts in some cases (*39*). On the other hand, one could assume that non-registry has been caused by positional shifts of fibrils during dehydration or embedding. Such artifactitious distributional shifts of connective tissue components do occur (Fig. 2). The significance of the antiparallel arrangement of adjacent fibrils is unknown at present.

The cross bands of those fibrils which are in register are not seen as being continuous between adjacent fibrils (Figs. 29 and 30). This is in contradiction to findings presented by other authors (*2*, *59*). Presumably such "bridges" between bands of adjacent fibrils are simulated by the bands of superimposed fibrils or (in sections) by the bands of tangentially cut third fibrils.

The elastic fibers

Elastic fibers are characterized best by their light-optical appearance after staining by different, more or less specific methods. They seem less well-defined by chemical analyses than by their morphological appearance since chemical analyses tend to yield variable results which depend on the age and origin of the elastin (*34*) and on the isolation procedure used (*16*, *17*). In the electron microscope, elastic fibers seem to lack very typical morphological features (*16*). Various authors observed them as either atypical dense masses of varying size and shape (*18*, *19*) or as helically coiled structures (*35*). Within some fibers a filamentous subunit was recognized (*3*, *9*, *18*, *19*) which suggested that these fibers consist of two components, one filamentous, the other amorphous (*19*).

In this report we have described all the non-cellular, electron-optically visible material other than collagen which is found located between fibroblasts as elastic fibers. This seems somewhat arbitrary in view of the rather poor characterization of elastic fibers as seen in the electron microscope. Our reasons for designating this material as elastic are as follows. First, the occurrence of elastic fibers in the tunica propria can be expected on the basis of light-optical studies (*38*). Also, the structures designated by us as elastic fibers resemble the purified elastic fibers obtained from typical elastic tissues like ligamentum nuchae or aorta (*19*), and they appear similar to the elastic fibers of ligamentum nuchae as seen in thin sections (*9*). The observation that many of the structures split up into thin filaments (Figs. 15, 16, 18, 19 and 22) is consistent with findings of similar filaments inside isolated (*3*, *18*, *19*) and sectioned

(*9*, *54*) elastic fibers. The animals employed were young and apparently healthy, thus diminishing the chance that some of the structures designated as elastic fibers are really manifestations of pathological changes known to occur in aging elastic tissues (*20*). In order to further establish the identity of these structures, the examination in the light microscope of orcein-stained thick sections that had been cut in series with the thin ones was considered. However, in experiments with aorta tissue it was found that orcein did not adequately stain the elastin if the tissue had been fixed in osmium and stained with phosphotungstic acid. For this reason a comparison of thick and thin sections was not attempted. Elastin stains other than orcein were not investigated.

Some of our electron micrographs demonstrate the close association (*9*, *18*, *19*) of collagen fibrils with elastic fibers (Figs. 6–8 and 22). A most interesting interrelation between the two types of fibers is shown in Fig. 7 (double arrows) where collagen fibrils actually seem to fuse into a mass indistinguishable from an elastic fiber. Also, in Fig. 16 (arrows) a small elastic fiber is made up of sub-fragments that somewhat resemble slightly enlarged collagen fibril cross sections. Nevertheless, such morphological observations are insufficient to allow for the conclusion that the "transformation" of collagen into elastin (*18*, *29*, *30*) is possible. It is also doubtful whether all "purified" preparations of elastin have really been pure in view of the intricate intermingling of collagen fibrils with elastic fibers and even with portions of fibroblasts. Impurities consisting of collagen were considered as a possible cause of collagen type X-ray diffraction patterns such as were obtained with elastin (*5*). Perhaps similar impurities, consisting of collagen as well as of cell fragments, could be responsible for differences in chemical analyses of elastin from the aorta (*16*).

The filaments into which some elastic fibers seem to split up (Figs. 15, 16, 18, 19 and 22) are indistinguishable from filaments associated with the surface of certain fibroblasts (Figs. 8 and 10) or with collagen fibrils (Figs. 7, 9, 11 and 29). At least, those observed to be portions of elastic fibers may well be thought of as the ultimate visible fibrous units in these fibers.

The filaments

The thin filaments seen associated with collagen fibrils (*25*, *56*; Figs. 7, 9, 11 and 29) probably correspond to similar filaments obtained during purification procedures (*14*, *15*) or during reprecipitation (*40*, *67*) of collagen, or to those seen in whole mounts of connective tissue (*49*). Such filaments were considered to be closely related to collagen (*15*, *49*). Perhaps they are identical with the filaments (protofibrils) known to occur inside the collagen fibrils themselves. This view is supported by the observation of a periodical beading in some of these filaments (*15*, *49*, *51*, *67*; Figs. 7, 8 and

29). The relationship between these filaments interspersed amongst collagen fibrils and similar filaments which are associated with fibroblasts (Figs. 8, 10, 17 and 24) or with elastic fibers (Figs. 15, 16, 18 and 19) is not clear at the present time.

We are indebted to Dr. F. B. Bang and to Miss B. Summers for help during the preparation of the manuscript and to Mr. J. Cox for technical assistance.

REFERENCES

1. Astbury, W. T. and Bell, F. O., *Nature* **145**, 421 (1940).
2. Bahr, G. F., *Arch. Dermatol. u. Syphilis* **193**, 518 (1951).
3. —— *Z. Anat. Entwicklungsgeschichte* **116**, 134 (1951).
4. Bargmann, W., Knoop, A. and Schiebler, T. H., *Z. Zellforsch. u. mikroskop. Anat.* **42**, 386 (1955).
5. Bear, R. S., *J. Am. Chem. Soc.* **66**, 1297 (1944).
6. —— *J. Am. Leather Chemists' Assoc.* **46**, 438 (1951).
7. Borysko, E., *J. Biophys. Biochem. Cytol.* **2**, Suppl., 3 (1956).
8. Corey, R. B. and Wyckoff, R. W. G., *J. Biol. Chem.* **114**, 407 (1936).
9. Dettmer, N., *Z. Zellforsch. u. mikroskop. Anat.* **45**, 265 (1956).
10. Dettmer, N., Neckel, I. and Ruska, H., *Z. wiss. Mikroskop.* **60**, 290 (1951).
11. Ekholm, R. and Sjöstrand, F. S., *J. Ultrastructure Research* **1**, 178 (1957).
12. Gersh, I. and Catchpole, H. R., *Am. J. Anat.* **85**, 457 (1949).
13. Gross, J., *J. Biophys. Biochem. Cytol.* **2**, Suppl., 261 (1956).
14. Gross, J. and Schmitt, F. O., *J. Exptl. Med.* **88**, 555 (1948).
15. Gross, J., Sokal, Z. and Rougvie, M., *J. Histochem. and Cytochem.* **4**, 227 (1956).
16. Hall, D. A., *Nature* **168**, 513 (1951).
17. —— *Biochem. J.* **59**, 459 (1955).
18. Hall, D. A., Keech, M. K., Reed, R., Saxl, H., Tunbridge, R. E. and Wood, M. J., *J. Gerontol.* **10**, 388 (1955).
19. Hall, D. A., Reed, R. and Tunbridge, R. E., *Exptl. Cell Research* **8**, 35 (1955).
20. Hass, G. M., *Arch. Pathol.* **35**, 29 (1943).
21. Hofmann, U. and Kühn, K., *Proc. Stockholm Conf. Electron Microscopy*, 1956, p. 220. Almqvist & Wiksell, Stockholm, and Academic Press Inc., New York, 1956.
22. Irving, E. A. and Tomlin, S. G., *Proc. Roy. Soc. London B* **142**, 113 (1954).
23. Iwakin, A. A., *Z. Anat. Entwicklungsgeschichte* **75**, 444 (1925).
24. Jackson, S. F., *Symposia Soc. Exptl. Biol.* **9**, 89 (1955).
25. Jakus, M. A., *Am. J. Ophthalmol.* **38**, 40 (1954).
26. —— *J. Biophys. Biochem. Cytol.* **2**, Suppl., 43 (1956).
27. Karrer, H. E., *Bull. Johns Hopkins Hosp.* **98**, 65 (1956).
28. —— *J. Biophys. Biochem. Cytol.* **2**, Suppl., 287 (1956).
29. Keech, M. K. and Reed, R., *Proc. Stockholm Conf. Electron Microscopy*, 1956, p. 230. Almqvist & Wiksell, Stockholm, and Academic Press Inc., New York, 1956.
30. Keech, M. K., Reed, R. and Wood, M. J., *J. Pathol. Bacteriol.* **71**, 477 (1956).
31. Kennedy, J. J., *Science* **121**, 673 (1955).

32. Kuhnke, E. and Wohlfarth-Bottermann, K. E., *Proc. Stockholm Conf. Electron Microscopy*, 1956, p. 223. Almqvist & Wiksell, Stockholm, and Academic Press Inc., New York, 1956.
33. Kühn, K., Hofmann, U. and Grassmann, W., *Z. Naturforsch.* **11 b**, 581 (1956).
34. Lansing, A. I., *Transactions Second Conf. on Connective Tissues, Josiah Macy, Jr. Foundation, New York*, 1952, p. 45.
35. Lansing, A. I., Rosenthal, T. B., Alex, M. and Dempsey, E. W., *Anat. Record* **114**, 555 (1952).
36. Maximow, A., *in* Von Möllendorff, W. (Ed.), Handbuch der mikroskopischen Anatomie des Menschen, Bd. II, Teil 1, p. 250. Springer, Berlin, 1927.
37. McKinney, R. C., *Arch. exptl. Zellforsch. Gewebezücht.* **9**, 14 (1930).
38. Miller, W. S., The Lung, p. 28. Charles S. Thomas, Springfield, Ill., 1947 (second ed.)
39. Nemetschek, T., Grassmann, W. and Hofmann, U., *Z. Naturforsch.* **10 b**, 61 (1955).
40. Noda, H. and Wyckoff, R. W. G., *Biochim. et Biophys. Acta* **7**, 494 (1951).
41. Nutting, G. C. and Boraski, R., *J. Am. Leather Chemists' Assoc.* **43**, 96 (1948).
42. Ornstein, L., *J. Biophys. Biochem. Cytol.* **2**, Suppl., 297 (1956).
43. Ottoson, D., Sjöstrand, F., Stenström, S. and Svaetichin, G., *Acta Physiol. Scand.* **29**, Suppl. 106, 611 (1953).
44. Palade, G. E., *J. Biophys. Biochem. Cytol.* **1**, 59 (1955).
45. —— *ibid.* **1**, 567 (1955).
46. —— *ibid.* **2**, Suppl., 85 (1956).
47. Porter, K. R., *Anat. Record* **118**, 433 (1954).
48. Porter, K. R. and Blum, J., *Anat. Record* **117**, 685 (1953).
49. Porter, K. R. and Vanamee, P., *Proc. Soc. Exptl. Biol. Med.* **71**, 513 (1949).
50. Pratt, A. W. and Wyckoff, R. W. G., *Biochim. et Biophys. Acta* **5**, 166 (1950).
51. Randall, J. T., Fraser, R. D. B., Jackson, S., Martin, A. V. W. and North, A. C. T., *Nature* **169**, 1029 (1952).
52. Rhodin, J., Correlation of Ultrastructural Organization and Function in Normal and Experimentally Changed Proximal Convoluted Tubule Cells of the Mouse Kidney. Thesis. Stockholm, 1954.
53. —— *Exptl. Cell Research* **8**, 572 (1955).
54. Rhodin, J. and Dalhamn, T., *Exptl. Cell Research* **9**, 371 (1955).
55. Robbins, W. C., Watson, R. F., Pappas, G. D. and Porter, K. R., *J. Biophys. Biochem. Cytol.* **1**, 381 (1955).
56. Robertson, J. D., *J. Biophys. Biochem. Cytol.* **2**, 369 (1956).
57. —— *ibid.* **3**, 1043 (1957).
58. Robinson, R. A. and Cameron, D. A., *J. Biophys. Biochem. Cytol.* **2**, Suppl., 253 (1956).
59. Robinson, R. A. and Watson, M. L., *Anat. Record* **114**, 383 (1952).
60. Roth, L. E., *J. Biophys. Biochem. Cytol.* **2**, Suppl., 235 (1956).
61. Schmitt, F. O. and Gross, J., *J. Am. Leather Chemists' Assoc.* **43**, 658 (1948).
62. Schmitt, F. O., Hall, C. E. and Jakus, M. A., *J. Cellular Comp. Physiol.* **20**, 11 (1942).
63. Selby, C. C., *J. Biophys. Biochem. Cytol.* **1**, 429 (1955).
64. Sheldon, H., *J. Biophys. Biochem. Cytol.* **2**, 253 (1956).
65. Sjöstrand, F. S. and Hanzon, V., *Exptl. Cell Research* **7**, 393 (1954).
66. Steiner, K. and Hitschmann, O., *Z. Zellforsch. u. mikroskop. Anat.* **5**, 150 (1927).
67. Vanamee, P. and Porter, K. R., *J. Exptl. Med.* **94**, 255 (1951).

68. Von Herrath, E. and Dettmer, N., *Z. wiss. Mikroskop.* **60**, 282 (1951).
69. Von Möllendorff, W. and Von Möllendorff, M., *Z. Zellforsch. u. mikroskop. Anat., Abt. B* **3**, 503 (1926).
70. Wassermann, F., *Ergeb. Anat. u. Entwicklungsgeschichte* **35**, 240 (1956).
71. Wassermann, F. and Kubota, L., *J. Biophys. Biochem. Cytol.* **2**, Suppl., 67 (1956).
72. Wohlfarth-Bottermann, K. F. and Kuhnke, E., *Naturwissenschaften* **44**, 595 (1957).
73. Wolpers, C., *Virchow's Arch. pathol. Anat. u. Physiol.* **312**, 292 (1944).
74. —— *Frankfurt. Z. Pathol.* **61**, 417 (1949/50).
75. Wyckoff, R. W. G., *Transactions Third Conf. on Connective Tissues, Josiah Macy, Jr. Foundation, New York*, 1952, p. 38.
76. Yamada, E., *J. Biophys. Biochem. Cytol.* **1**, 445 (1955).
77. Zetterqvist, H., The Ultrastructural Organization of the Columnar Absorbing Cells of the Mouse Jejunum. Thesis. Stockholm, 1956.

Ultrastructure of Retinal Rod Synapses of the Guinea Pig Eye as Revealed by Three-Dimensional Reconstructions from Serial Sections

F. S. SJÖSTRAND

Laboratory for Biological Ultrastructure Research, Department of Anatomy, Karolinska Institutet, Stockholm

Received September 10, 1958

The structure of the synaptic bodies of the retinal receptors of the guinea pig eye and the synaptic connections of these receptors have been studied on three-dimensional reconstructions from serial sections. Series with up to forty ultrathin sections (average thickness 250 Å) were examined.

Two types of synaptic bodies belonging to the α- and the β-cells respectively can be distinguished. Both types contain the same basic structural components: the synaptic granules or vesicles, the synaptic vacuoles and the synaptic ribbon. The α-cells are in synaptic contact with dendrites presumably belonging to two different bipolars. The dendrites end inside an invagination of the plasma membrane of the synaptic body at its vitreal pole and make contact with two synaptic vacuoles forming a pair of vacuoles which are in mutual contact.

Extensions from three to four synaptic bodies belonging to the β-cell type enter into contact relation to each α-cell and the dendrites which are synaptically connected to the α-cell. These contacts are interpreted as synaptic contacts. It is proposed that this extensive system of interreceptor contacts might exert inhibitory effects on the transmission between α-cells and bipolars.

Some preliminary observations on the ultrastructural organization of the synaptic bodies of the retinal receptors of the guinea pig and perch eyes have been described by the author in several conference reports and survey articles. In the case of the retinal rod synapses of the guinea pig eye, a three-dimensional model was worked out from an analysis of ultrathin sections through about 800 synapses which were sectioned at different angles. This model was assumed to reveal the most basic structural features of the rod synapses in a crude way (*20*, *23*, *24*).

This method for working out a three-dimensional model was not assumed by the author to be quite reliable when dealing with a structure of the complexity of the retinal synapses. Therefore, a method for collecting and analyzing long series of

ultrathin sections has been worked out and true three-dimensional reconstructions made of the synaptic region. These reconstructions have confirmed most of the main features of the earlier model and have given information regarding further details. Furthermore, the reconstructions have made it possible to discover intimate inter-receptor contacts presumably of synaptic character.

MATERIAL AND TECHNIQUES

Eyes from guinea pigs, which had been killed by decapitation, were divided into two halves by cutting with a sharp razor blade along the equator of the eye bulb. The eye cup was then cut in thin slices which were immersed into a 1% osmium tetroxide solution buffered according to Palade (*13*) to pH 7.2 with veronal acetate buffer and made isotonic to the guinea pig erythrocytes by adding sodium chloride to the buffer solution (*18*). After 3–4 hours' fixation, the tissue was washed in Tyrode's solution for 30 minutes to one hour, dehydrated in 70%, 95% and absolute ethyl alcohol. The tissue was embedded in *n*-butyl methacrylate or a mixture of *n*-butyl and methyl methacrylate according to Newman, Borysko and Swerdlow (*12*). The preparation, fixation and most of the dehydration were performed in a cold room at +4°C.

Ultrathin serial sections were cut with a Sjöstrand ultramicrotome using specially sharpened razor blades (*18*) or freshly broken glass knives (*11*). The average thickness of the sections in long series of sections was estimated from the reconstructions to be about 250 Å.

For collecting the serial sections, a method was worked out which represents a modification of the method described by Gay and Anderson (*9*). The ribbons of sections were collected on formvar films of regular thickness (about 200 Å). The formvar film was suspended over a ring with a small handle which had been punched out of a stainless steel sheet. The handle was knicked at a defined angle. This tool was found to improve the precision in handling the sections as compared to the wire loops described by Gay and Anderson. For transferring the sections to the grids, the ring was fastened by means of its handle in a plexiglass ring on a microscope stage. The grid was placed on the flat top of a conically shaped plexiglass rod fastened to the microscope condensor lens. The plexiglass ring was adjusted in such a position that the sections were located over the hole of the grid. The microscope substage was then raised until the formvar film made contact with the grid. The grid covered with the film could then be removed. The microscope used for these manipulations was equipped with a Leitz Ultropak illuminator with an objective for observation in reflected light. An ordinary condensor lens system for illumination with transmitted light through the plexiglass rod made it possible to make use of both principles for illumination. The defined angle between the plane of the ring coated with the formvar

film and its handle made it possible to orient the plane of the formvar film parallel to that of the grid. This was achieved by fastening the handle to a plane on the plexiglass ring with a corresponding inclination. The exact orientation of the formvar film parallel to the surface of the grid is of importance in order to allow a simultaneous and uniform contact all around the hole of the grid with a minimum of distortion and wrinkling of the film.

The thin ring used for handling the formvar film makes it easy to collect the ribbon of sections onto the film by contacting the sections from the air side.

The rings are coated with a formvar film in the following way. A regular formvar film is made by dipping a microscope slide into a 0.3% solution of formvar in ethylen dichloride and floating the film off onto a water surface. The stainless steel rings are now placed onto the film. The formvar film with the stainless steel rings is transferred to a microscope slide by passing the slide from above the formvar film through the water. The slide is turned 180°, from the moment it makes contact with the air side of the formvar film till it is lifted out of the water. The side, on which the formvar film is sticking to the slide, will then be facing upwards when the slide passes through the water surface. The film is then air-dried and, due to the knicks of the handle of the stainless steel ring, the formvar film suspended over the ring dries without making contact with the surface of the microscope slide.

The most useful type of grid was found to be one with a single circular hole with a diameter of 0.7 to 1.5 mm. These grids were made by drilling holes in 0.2 mm thick, round copper plates with 3 mm diameter. It was found important that the grids were made of sufficient thick material because a slight distortion of the grid results in a rupture of the film.

The grids were dipped into a 0.3% solution of formvar in ethylen dichloride before applying the film carrying the sections. This improves the conditions for contact between the film and the grid. This contact was, furthermore, improved by quickly passing the grid with the formvar film carrying the sections through ethylen dichloride vapour. As a last step, the films were reinforced by evaporation of carbon onto the films in a shadow-casting unit.

The serial sections were examined in an RCA EMU-3A electron microscope at 100 kV. The beam current was slightly reduced by unscrewing the cathod cap about $\frac{1}{3}$ to $\frac{1}{2}$ of a turn. The sections were first examined with the condensor lens defocussed and then photographed with focussed beam at peak intensity. Molybdenum objective apertures with a diameter of 50 μ were used. Sections mounted on regular, fine mesh grids were also examined in an RCA EMU-2C electron microscope with 50–120 μ objective apertures.

The procedure for calibration of the magnification has been described earlier (*18*). The best specimen resolution of the EMG's obtained so far during this study has been about 30 Å.

RESULTS

General description of the receptor cells. The outer and inner segments and the rod and cone fibers represent three distinctly, differently built segments of the retinal receptors. The rod and cone fibers extend from the external limiting membrane to close to the outer plexiform layer where the transition to the forth part of the receptor cells, the synaptic bodies, is located. The rod and cone fibers show, as has been pointed out in an earlier paper (*19*), a striking similarity to nonmyelinated nerve fibers. The plasma membrane of the receptor cells and that of the Müller's cells, which represent the glia elements of the retina, form a triple-layered membranous structure appearing like that surrounding the nerve axon of nonmyelinated nerve fibers. Furthermore, the cytoplasm in this segment contains filaments oriented lengthwise. These filaments are similar in appearance to the axon filaments. The cell nucleus is located at different levels along the rod fibers of the rod receptor cells. Those nuclei which are located most vitreally are found to extend partially into the synaptic body.

Two types of synaptic bodies have been observed, the ovoid-shaped and the conically shaped. In the mixed retinas, the synaptic bodies of the cones belong to the latter type. In the pure rod retina of the guinea pig, these two types are also present. Two types of rods have been distinguished, α- and β-cells (*19*), and the difference in form and structure of the synaptic bodies is one structural feature that makes this distinction possible. The conically shaped synaptic bodies are characteristic of the β-cells.

The complete three-dimensional reconstruction has so far been restricted to the ovoid-shaped synaptic bodies, the "rod spherules", of the guinea pig rods. The conically shaped synaptic bodies have been reconstructed only partially.

Certain well defined structural components are present in the synaptic bodies. The difference between the two types of synaptic bodies appears to be limited to a difference in the number of such components, all types of components being represented in both types of receptors.

The same basic components of the synaptic bodies have so far been observed in the guinea pig, cat, frog, toad and perch retinae, by De Robertis and Franchi (*6*) in the mouse and by Carasso (*4*) in the toad (*Alytes obstetricans*) retinae.

The bipolar nerve cells send a number of dendrites towards the synaptic bodies of the receptor cells. According to light microscopical observations (*14*), the dendrites branch into a number of thin branchlets which, in the electron micrographs, appear intertwined in a rather complicated system of rounded, oval or elongated profiles which are closely packed. These profiles represent sections through dendrites as well as through extensions of the Müller's cells. In the guinea pig retina, this mass

of nerve cell dendrites and Müller's cell extensions fills the space between the bipolar nerve cell bodies and the receptor synapses. In the perch retina, this layer is located between the layer of horizontal cells and the rod and cone synapses.

The cytoplasm of the dendrites contains thin filaments similar to the axoplasmic filaments, scattered mitochondria with a few inner membranes, opaque large granules and vesicles (Figs. 1-23). The number of such components is rather small in the dendritic branchlets.

The plasma membrane of the dendrites and their branchlets appears as an osmiophilic layer measuring 60 Å in thickness. Where the branchlets are closely packed or in contact with extensions from the Müller's cells, a less opaque interspace separates the opaque layers of the two plasma membranes. The thickness of this less opaque interspace is strikingly constant, and the mean value of its width is 100 Å.

Dendrites from the bipolars or their branchlets approach the vitreal pole of the synaptic bodies, and their blindly ending tips extend into the synaptic body for a distance of up to about 1 μ (Fig. 11). The end tips are separated from the cytoplasm of the receptor cells through an invagination of its plasma membrane (Fig. 11). The diameter of the dendritic branchlets increases, when approaching the synaptic body, and the part located inside the vitreal pole forms a rounded vesicle-like end, the dendritic end vesicle. At the vitreal pole of the synaptic body, the dendritic branchlets are frequently slightly constricted (see, for instance, Fig. 11). The widened part of the dendritic branchlet, which is located outside the vitreal pole of the receptor, has a length of about 1 μ and a diameter that varies considerably. The largest value for the average diameter of this part was measured to 0.3 μ. These parts of the dendritic branchlets are oriented perpendicularly to the vitreal surface of the synaptic body.

In the small synaptic bodies, which exhibit an ovoid form, there are most frequently two dendrites or dendritic branchlets that enter each synaptic body. These branchlets seem to belong to different neurons. This conclusion, however, needs further testing. The reason for the uncertainty is that only one of these branchlets in each synaptic body analyzed so far has been securely traced all the way to the nerve cell body.

The structural components of the synaptic bodies. There are three characteristic structural components of the synaptic bodies: the synaptic granules or vesicles, the synaptic vacuoles and the synaptic ribbon.

The synaptic granules. Scattered all over the ground substance of the cytoplasm there are granules or small vesicles of a rather uniform diameter. They show a spherical form and are bounded by a more opaque surface layer or membrane. The opacity of the central part is greater than that of the surrounding ground substance but less than that of the surface layer. The opacity decreases gradullay towards the center. These granules measure 300–400 Å in diameter.

The synaptic vacuoles are irregularly shaped and appear frequently with outpocketings and branches. There are three synaptic vacuoles in the ovoid synaptic bodies. Two of them are in mutual contact forming a pair. These two vacuoles are, furthermore, in direct contact with the end vesicles of the dendritic branchlets (see, for instance, Fig. 8). A thin extension of each vacuole forms a stalk-like structure which extends towards the vitreal pole of the synaptic body along the surface of the corresponding dendritic end vesicle (Figs. 11–13, 19 and 20). A third vacuole extends from the vitreal pole far in a scleral direction and forms a large, sometimes hook-shaped vacuole, the convexity of which is directed sclerally. This third vacuole might perhaps branch off from one of the paired vacuoles close to the stalk-like extension of the vacuole at the vitreal pole of the synaptic body.

The stalk-like extension of each paired vacuole reaches the surface of the synaptic body at the vitreal pole. The plasma membrane bounding the synaptic body forms a narrow tube-like invagination around this extension. This invagination then envelops the vacuole (Figs. 7, 11–13, 19 and 20). The invaginations at the two paired vacuoles and those of the dendritic vesicles all merge into one common coating of all these components. Due to this coating, all the synaptic vacuoles and the end vesicles of the dendritic branchlets are bounded by double membranes appearing as two opaque osmiophilic layers separated by a less opaque interspace. The total mean thickness of this triple-layered component is 220 Å and the mean distance between the centers of the two opaque layers is 160 Å. From these dimensions, the thickness of the single opaque layers can be calculated to 60 Å and the width of the bright interspace to 100 Å.

At the surface where the two synaptic vacuoles are in mutual contact, the separating wall also consists of two opaque layers separated by a less opaque interspace. The thickness of the two opaque layers and the width of the less opaque interspace are similar to those of the other triple-layered membrane components described above. The same dimensions apply to the triple-layered wall at the contact surface between the tips of the dendritic branchlets and the synaptic vacuoles.

The synaptic vacuoles contain granules or vesicles which appear identical to the synaptic granules or vesicles. Frequently, the vacuoles appear almost empty or they contain some amorphous material.

The synaptic ribbon consists of a ribbon-shaped component that is particularly strongly osmiophilic. It is bent in a ∩-shape and is associated with the paired synaptic vacuoles. It is located in the scleral grove between the two paired synaptic vacuoles along the line where their surface membranes reach in mutual contact (Fig. 12). The two ends of the ribbon extend to points close to the surface of the synaptic body at its vitreal pole. The synaptic ribbon is not confined to one plane but can be more or less twisted in addition to the ∩-shaped curvature. The latter curvature is mainly oriented in a plane parallel to the flat surfaces of the ribbon.

The length of the ribbon is about 2–3 μ, its mean thickness 350 Å and its width 0.2 μ. It shows intimate topographic relation to the triple-layered septum which is formed by the walls of the two paired synaptic vacuoles where these are in mutual contact. The adjacent cytoplasm is here particularly opaque and fills the deepest part of the grove, which, in cross sections, has a rounded form. Close to the surface of the synaptic ribbon, the synaptic granules form a single layer of densely arranged granules. In the sections, this layer appears as a row of granules.

Other membranous components have been observed in the scleral part of the synaptic bodies. These membranes bound vesicles or tubular components. Their opacity is low and their morphology unclear. These components can easily be differentiated from the synaptic granules through their larger size and from the synaptic vacuoles through their single-layered, bounding surface membrane.

The plasma membranes of the synaptic bodies and of the Müller's cells appear as an osmiophilic layer with a mean thickness of 60 Å. With the exception of an area at their vitreal poles, the synaptic bodies are completely surrounded by Müller's cell cytoplasm. Between the opaque layers of the plasma membranes of the synaptic bodies and of the Müller's cells, a less opaque interspace of rather constant thickness is interposed. The thickness of this layer is 100 Å. At the vitreal pole, the plasma membrane of the Müller's cells passes over from the surface of the synaptic bodies to the surface of the dendritic branchlets and the extensions of the synaptic bodies of the β-type.

The cytoplasm of the Müller's cells can be easily recognized and distinguished from that of the other components of the retina. It contains uniformly distributed, opaque particles of a rather uniform size and opacity. Their mean diameter is 250 Å. These particles are easily differentiated from the 150 Å-particles present in the nerve cells, for instance, in connection with α-cytomembranes. The latter particles are arranged in groups, they are more opaque and distinctly of a smaller size (Fig. 2).

Only very few α-cytomembranes have been observed in the Müller's cells. A Golgi apparatus has been observed in Müller's cells located at the level of the synaptic bodies and the outer plexiform layer. Mitochondria have so far been observed in the Müller's cells close to their free surface at the outer limiting membrane.

The interreceptor contacts. Through the serial sectioning, it has been possible to reveal that the retinal receptors to a considerable extent are in direct mutual contact (Fig. 19). These contacts are either direct contacts between the vitreal pole of the synaptic body of an α-receptor and the conical surface of the synaptic body of a β-receptor, or the contacts are brought about through thin branchlets or short extensions from the synaptic bodies of β-receptors, which approach the vitreal pole of an adjacent synaptic body to end blindly in contact with the surface of the latter. The appearance of the contact area is similar to the contact conditions in synaptic

contacts in general. No Müller's cell cytoplasm separates the end surface of the synaptic branchlet from the plasma membrane of the adjacent synaptic body. With this exception, the synaptic bodies are completely separated by Müller's cell cytoplasm. These synaptic branchlets have so far only been observed originating from the large, conically shaped synaptic bodies, the β-receptor synapses. Through such branchlets, each β-receptor appears to be connected with a great number of surrounding synaptic bodies of the α-receptors. Each α-receptor, on the other hand, receives such branchlets from several β-synapses. So far three to four such connections have been traced from three to four different sources, presumably β-receptor synaptic bodies, to the same α-receptor synapse.

The width of these branches is 0.1–0.2 μ and the area of the contact surface about 0.25×0.50 μ.

The contact surfaces between the receptor synapses are located very close to the place where the dendritic branchlets of the bipolars pass through the vitreal pole of the synaptic body. The most peripheral part of the receptor branchlets consists of a rather straight part oriented in a vitreal–scleral direction and running parallel to the dendritic branchlets of the bipolars. A complex bundle consisting of dendritic branchlets from the bipolars, branchlets from the receptor synaptic bodies and Müller's cell extensions, which are interposed between the dendritic branchlets, is formed at the vitreal pole of each synaptic body.

The contacts between β-synapses and the dendrites. The synaptic bodies of the β-cells show a more complicated inner structure due to the fact that they contain several pairs of synaptic vacuoles, where each pair is associated with one synaptic ribbon. The number of such components seems to be adjusted to the number of dendritic branchlets from the bipolars that make a synaptic contact with these receptors. As many as four pairs of synaptic vacuoles have been observed.

In addition to the regular type of synaptic contact between the β-cells and the dendritic branchlets, which is structurally identical to that between the α-cells and their dendrites, there are two more types of contacts between the synaptic bodies of the β-cells and the surface of the dendrites. The branches, which extend from the synaptic bodies of the β-cells to those of the α-cells, are in contact with the dendrites entering the vitreal pole of the α-cells just below this pole. Furthermore, the surface of the synaptic bodies of the β-cells makes contact with rather wide, horizontally oriented dendrites. These dendrites might extend from horizontal cells (Figs. 4–7). The synaptic bodies of the β-type receptors are also in direct mutual contact.

Description of the Electron Micrographs of a Series of Forty Sections

Section No. 2, Fig. 1, of the serial sections cuts through several synaptic bodies (*R*1–*R*4, *R*6–*R*7) and dendritic branchlets, two of which are indicated by *D*3

and *D*4. Interposed between these components, regions of cytoplasm belonging to Müller's cells, *MC*, are visible, characterized by their granulated appearance. Receptors *R*1, *R*6 and *R*7 are of the α-type with ovoid-shaped synaptic bodies. Receptors *R*2 and *R*4 are of the β-type with conically shaped synaptic bodies and several branches. *R*3 represents a branchlet, the origin of which has been assumed to be a synaptic body of a receptor of the β-type. This conclusion is based on the fact that this branch appears morphologically identical to the branches originating from β-cell receptors. The two arrows, *A* and *B*, point to direct contacts between receptors *R*4 and *R*7 and receptors *R*2 and *R*6. The synaptic body of receptor *R*1 is presented in three-dimensional reconstruction in Figs. 24–34. Dendrite *D*3 is a large dendrite extending in a horizontal direction. It might belong to a horizontal cell. *D*4 indicates a dendrite containing granules which show some similarity to the synaptic granules. Receptor *R*4 is in direct contact with this dendrite. Magnifications of all EMG's, · 40,000.

In *section No. 8*, Fig. 2, the two parts belonging to receptor *R*4 have fused. Furthermore, several of the structural components located inside the synaptic body of receptor *R*1 can be observed. These components are two of the synaptic vacuoles (*V*1 and *V*3) and the synaptic ribbon (*Ri*). *D*2 indicates a tangentially sectioned part of the bounding membrane of one of the dendrites that make synaptic contact with receptor *R*1. *N*, in the lower right-hand corner, indicates a part of the cytoplasm of a bipolar cell.

In *section No. 9*, Fig. 3, another part of dendrite (*D*2) has appeared inside the synaptic body (*R*1).

Section No. 10, Fig. 4, shows clearly the part of dendrite *D*2 that is located outside the vitreal pole of the synaptic body of *R*1.

In *section No. 11*, Fig. 5, the first traces of synaptic vacuole *V*2 have appeared in *R*1. Notice further the close contact relations between receptors *R*2 and *R*4 at arrow *A* and between receptor *R*4 and dendrite *D*3 at arrow *B*.

Section No. 13, Fig. 6, is characterized by the appearance of the first traces of the end vesicle of dendrite *D*1 inside *R*1 as a tangentially sectioned part of its bounding wall.

In *section No. 14*, Fig. 7, the outer and inner parts of dendrite *D*2 show indications of fusing. Receptor *R*2 sends a branch towards receptor *R*6. Notice the small vesicular elements in dendrite *D*3.

The inner and outer parts of dendrite *D*2 have fused in *section No. 15*, Fig. 8.

FIGS. 1–23. Electron micrographs from a series of serial sections consisting of forty sections through the synaptic region of the retinal receptors in the guinea pig eye. For description, see p. 129. · 40,000.

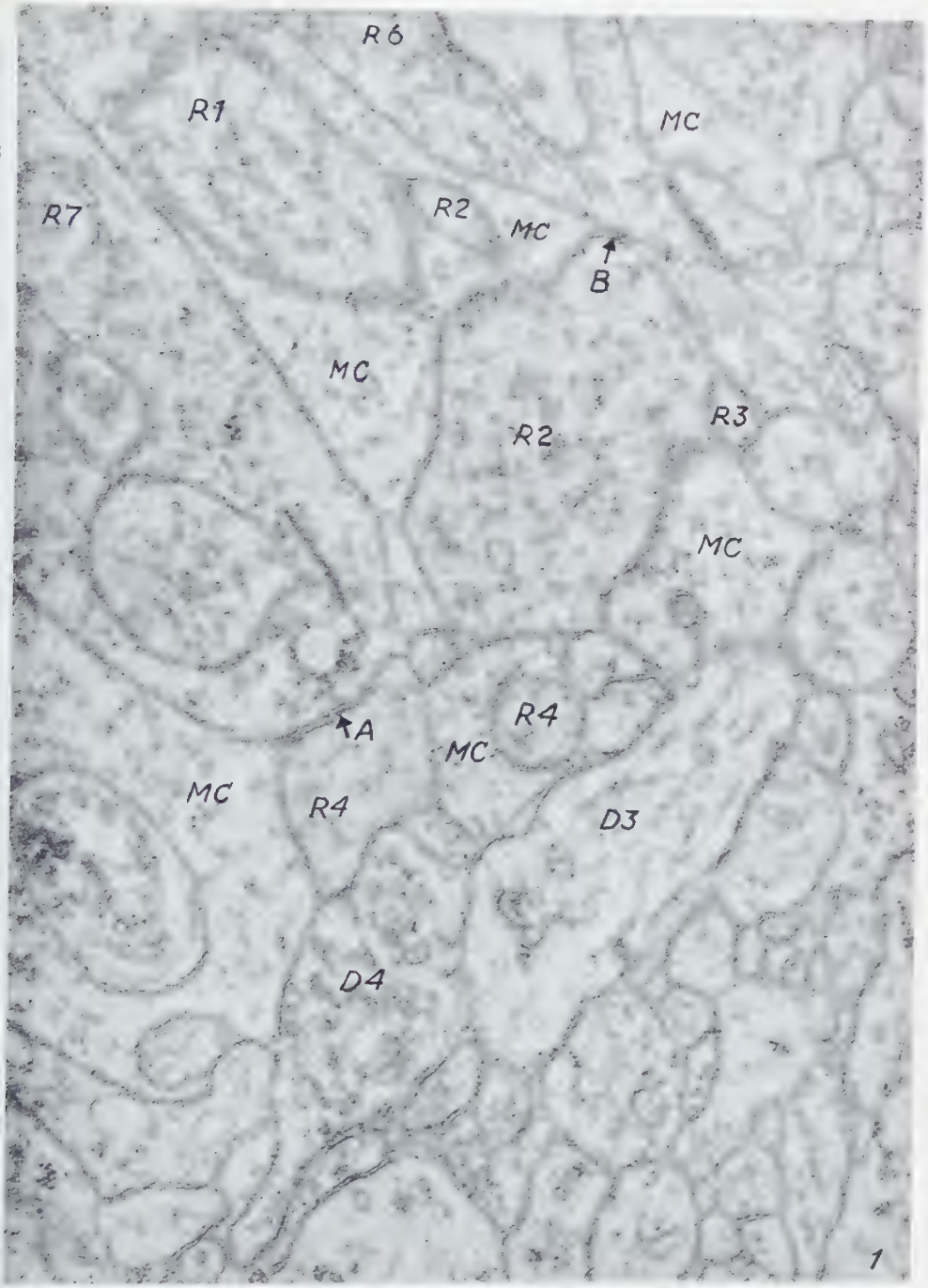
R6
R1
MC
R7
R2
MC
B
MC
R2
R3
MC
A
R4
MC
MC
R4
D3
D4
1

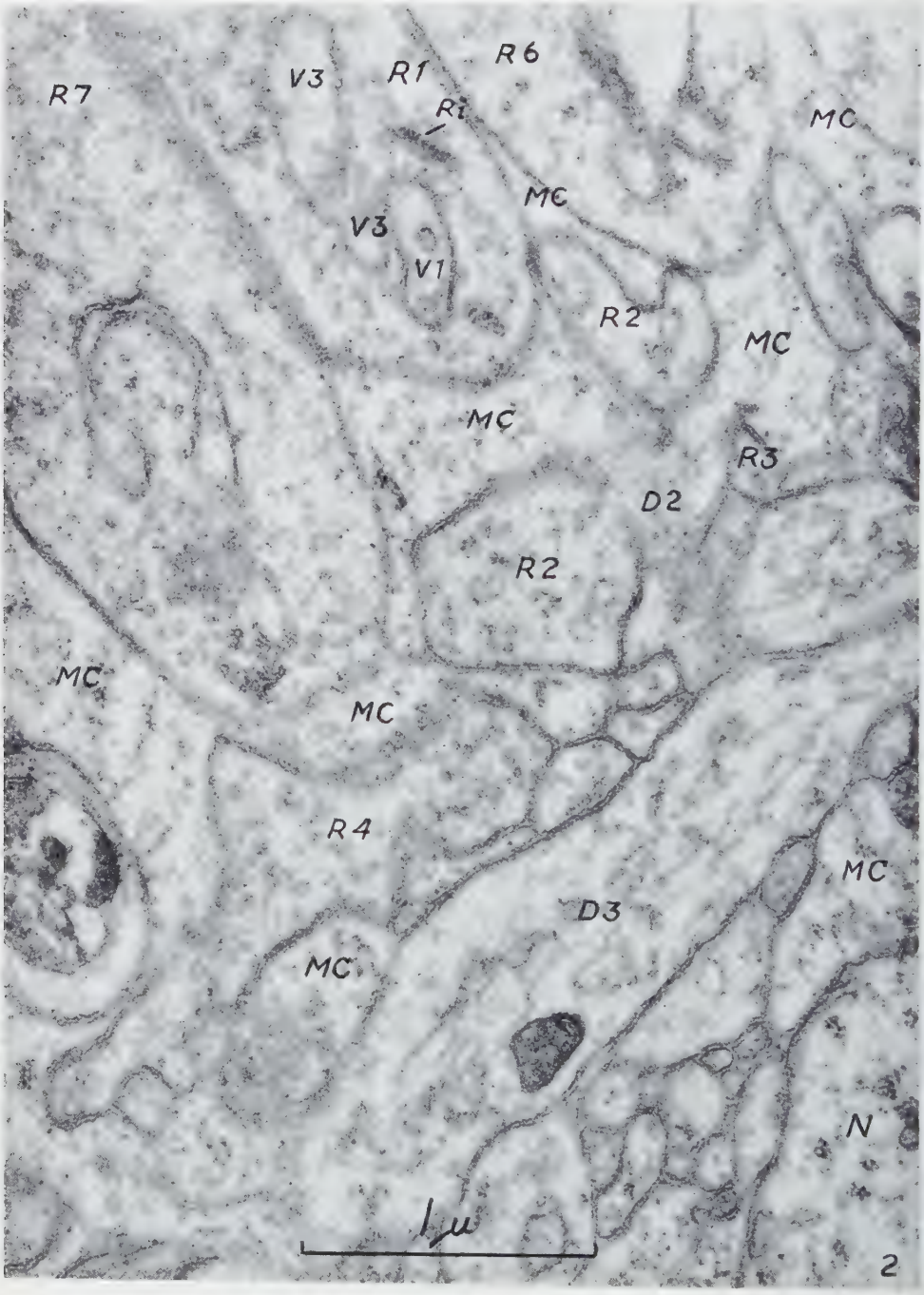
R7
V3
R1
R6
Ri
MC
MC
V3
V1
R2
MC
MC
R3
D2
R2
MC
MC
R4
MC
D3
MC
N
1μ
2

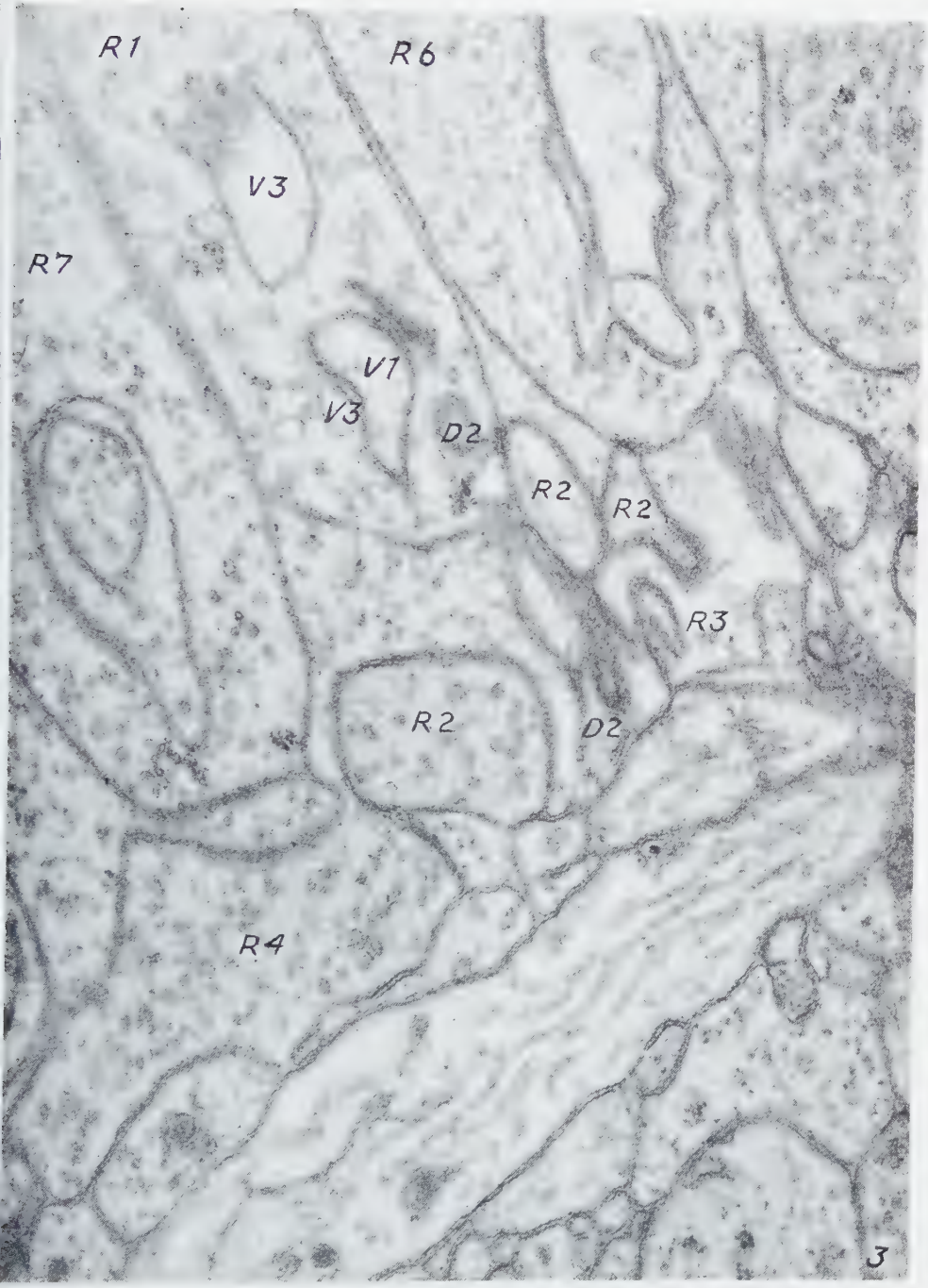
R1
R6
V3
R7
V1
V3
D2
R2
R2
R3
R2
D2
R4
3

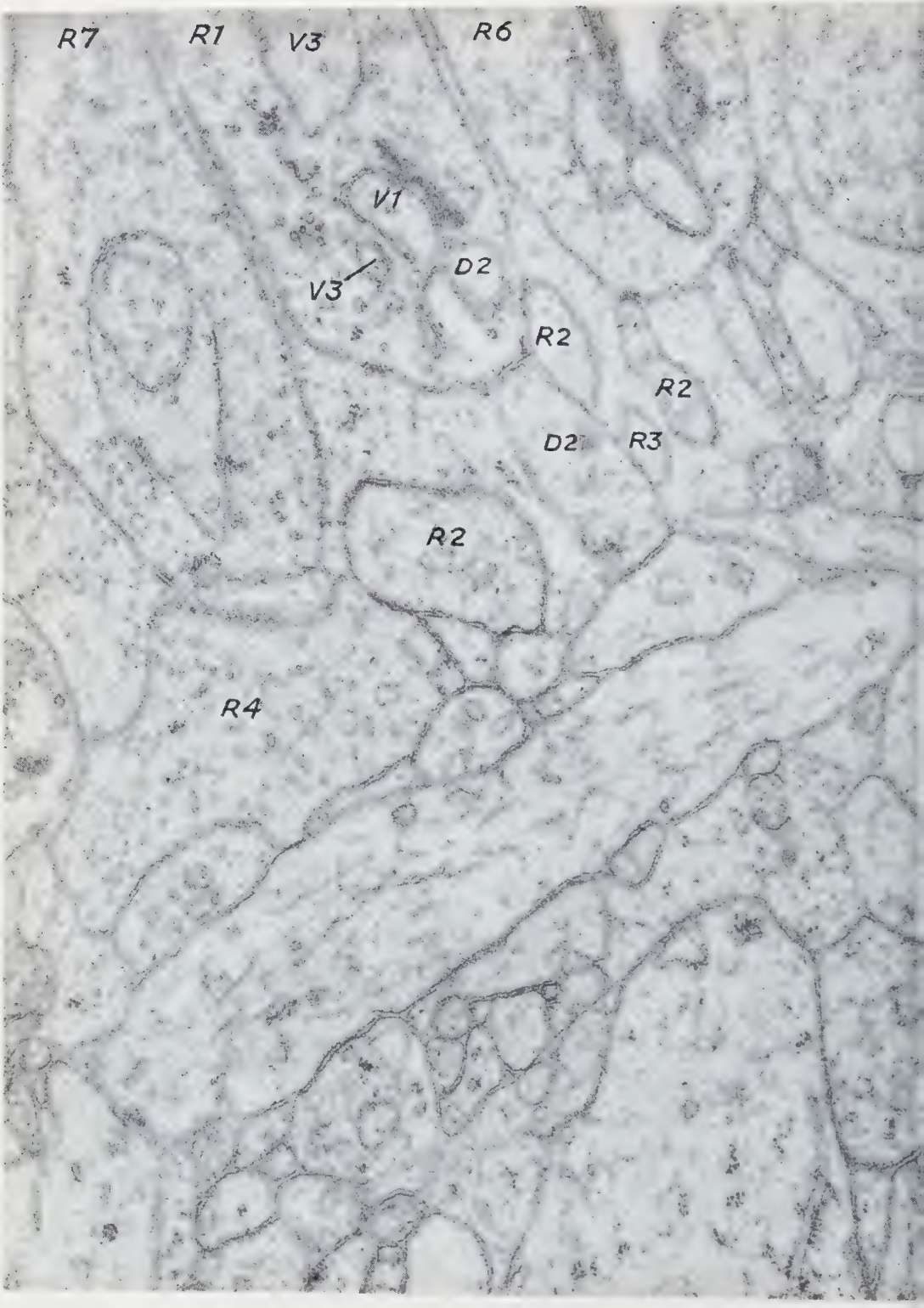
R7
R1
V3
R6
V1
V3
D2
R2
R2
D2
R3
R2
R4

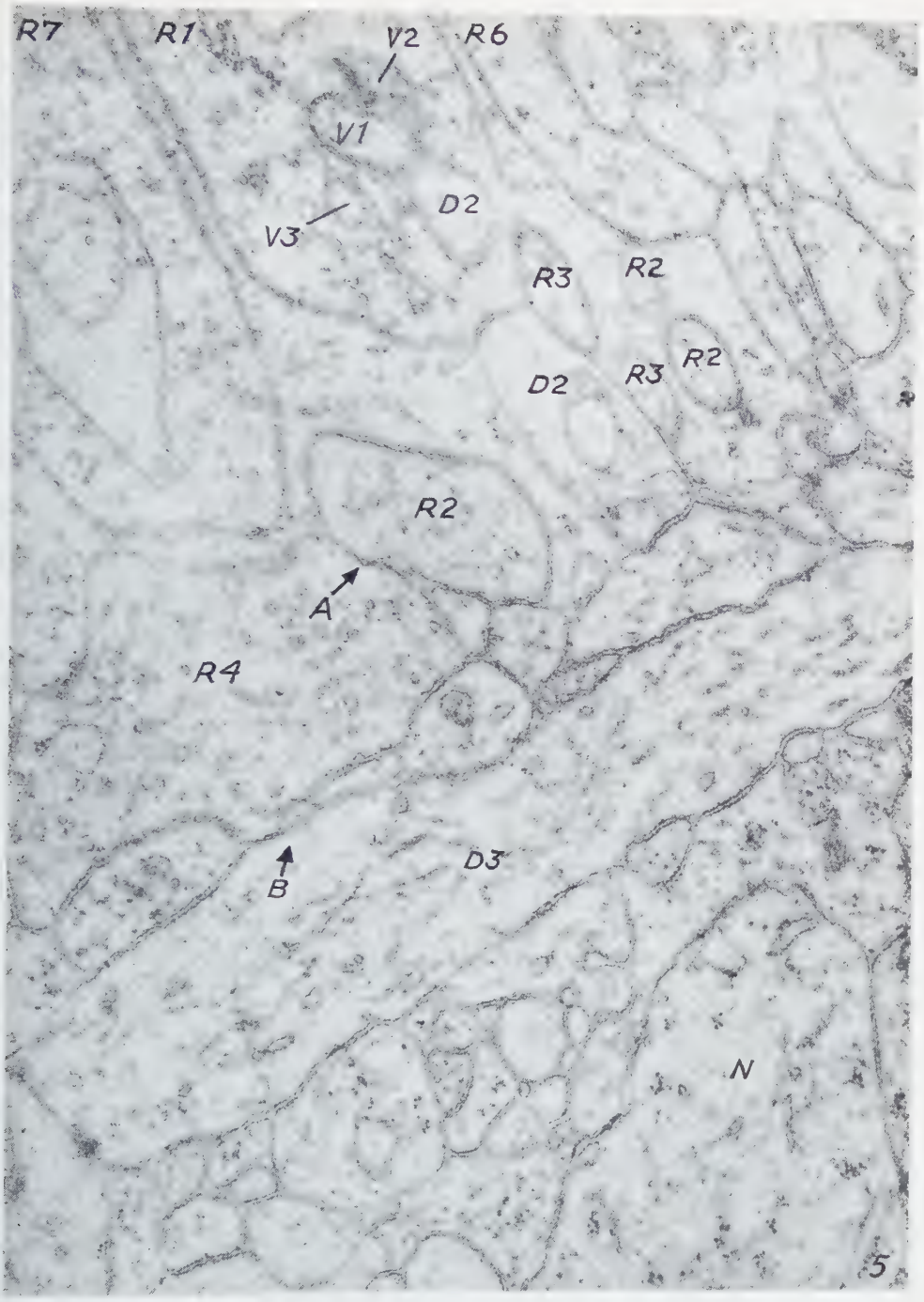
R7
R1
V2
R6
V1
D2
V3
R3
R2
D2
R3
R2
R2
A
R4
B
D3
N
5

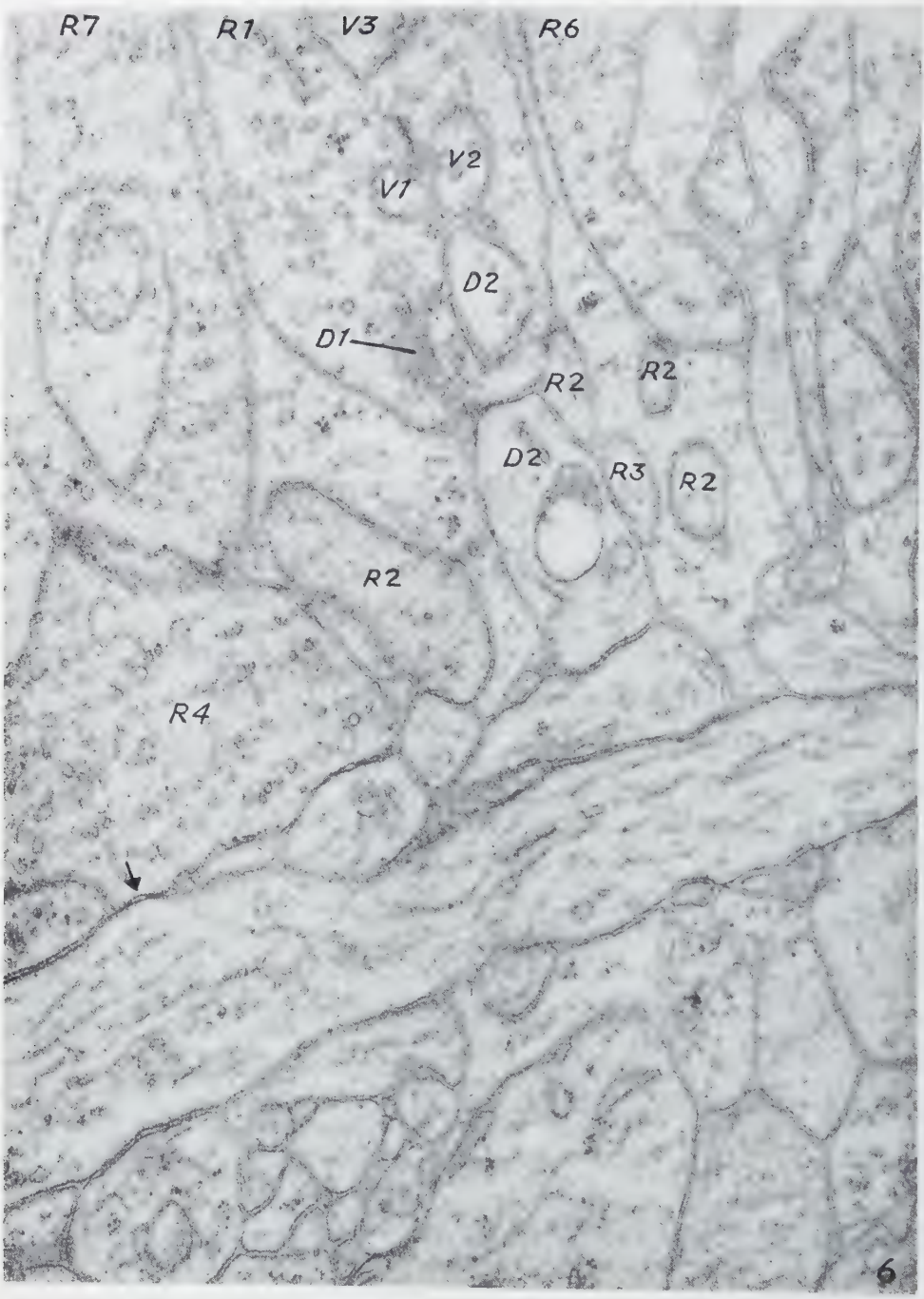
R7
R1
V3
R6
V2
V1
D2
D1
R2
R2
D2
R3
R2
R2
R4
6

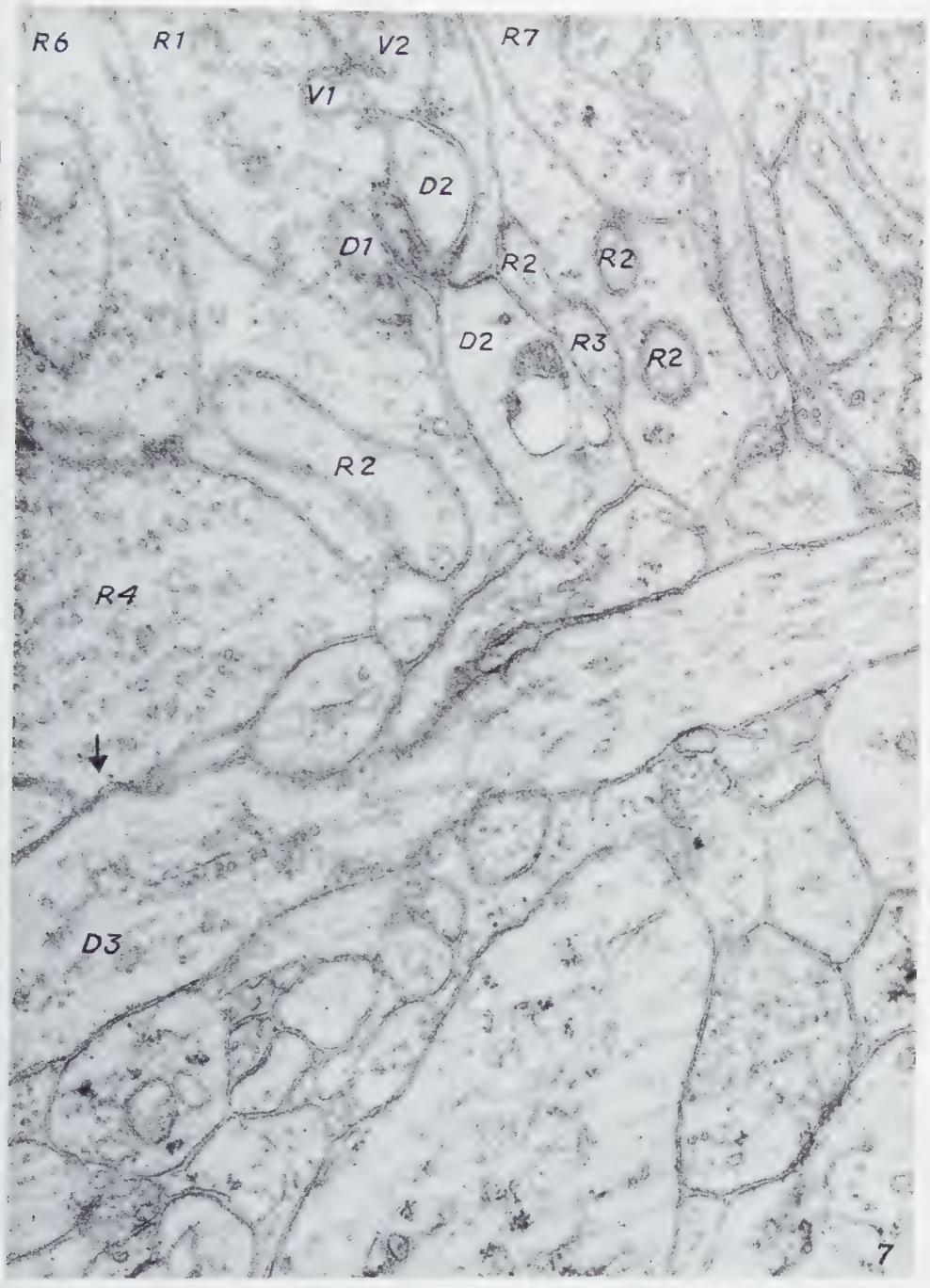
R6
R1
V2
R7
V1
D2
D1
R2
R2
D2
R3
R2
R2
R4
D3
7


R7
R1
V3
R6
V2
V1
V2
V2
D2
D1
R2
R2
R2
D2
R3
R2
R4
R2
D2 ?

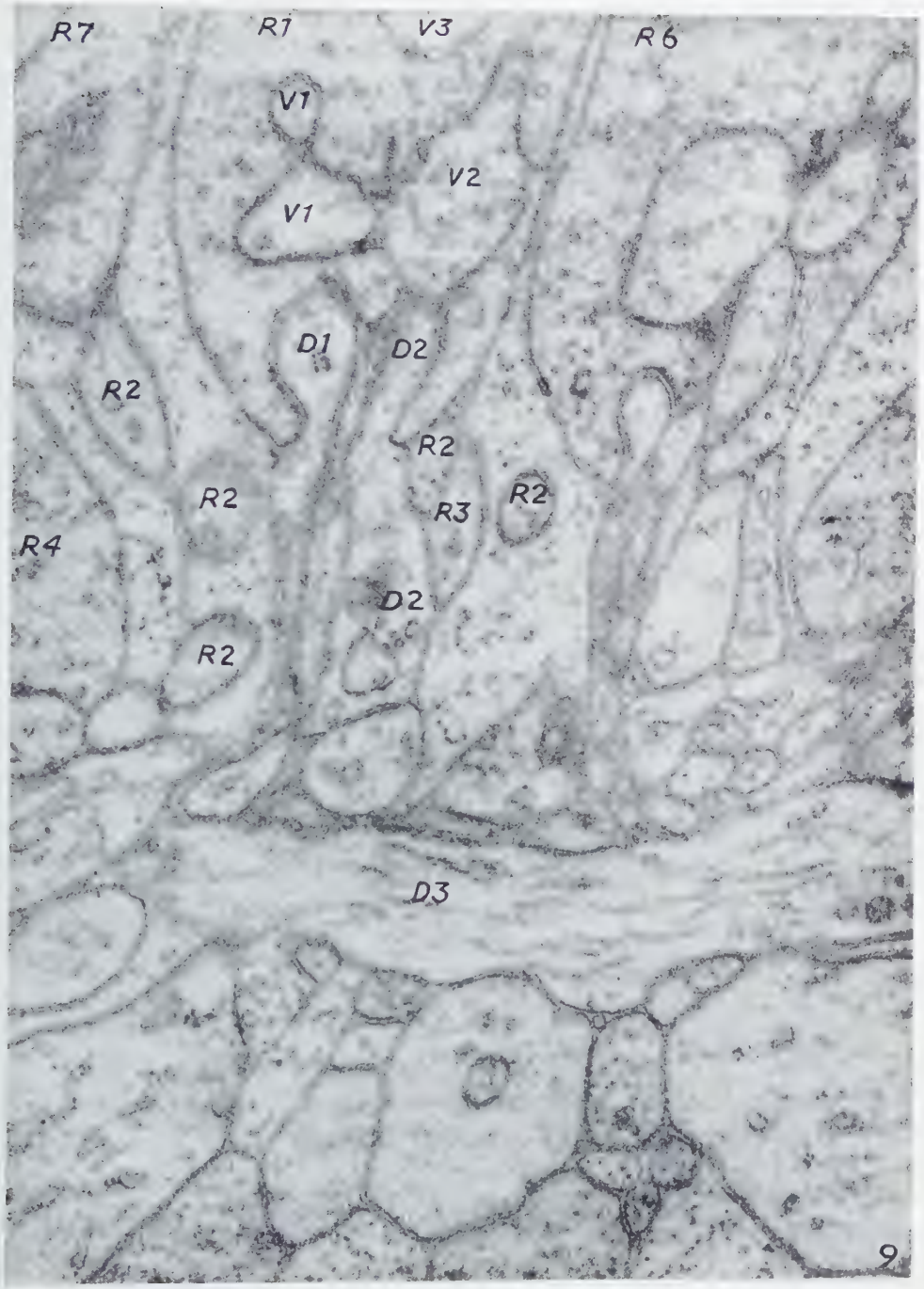
R7
R1
V3
R6
V1
V2
V1
D1
D2
R2
R2
R2
R3
R2
R4
D2
R2
D3
9

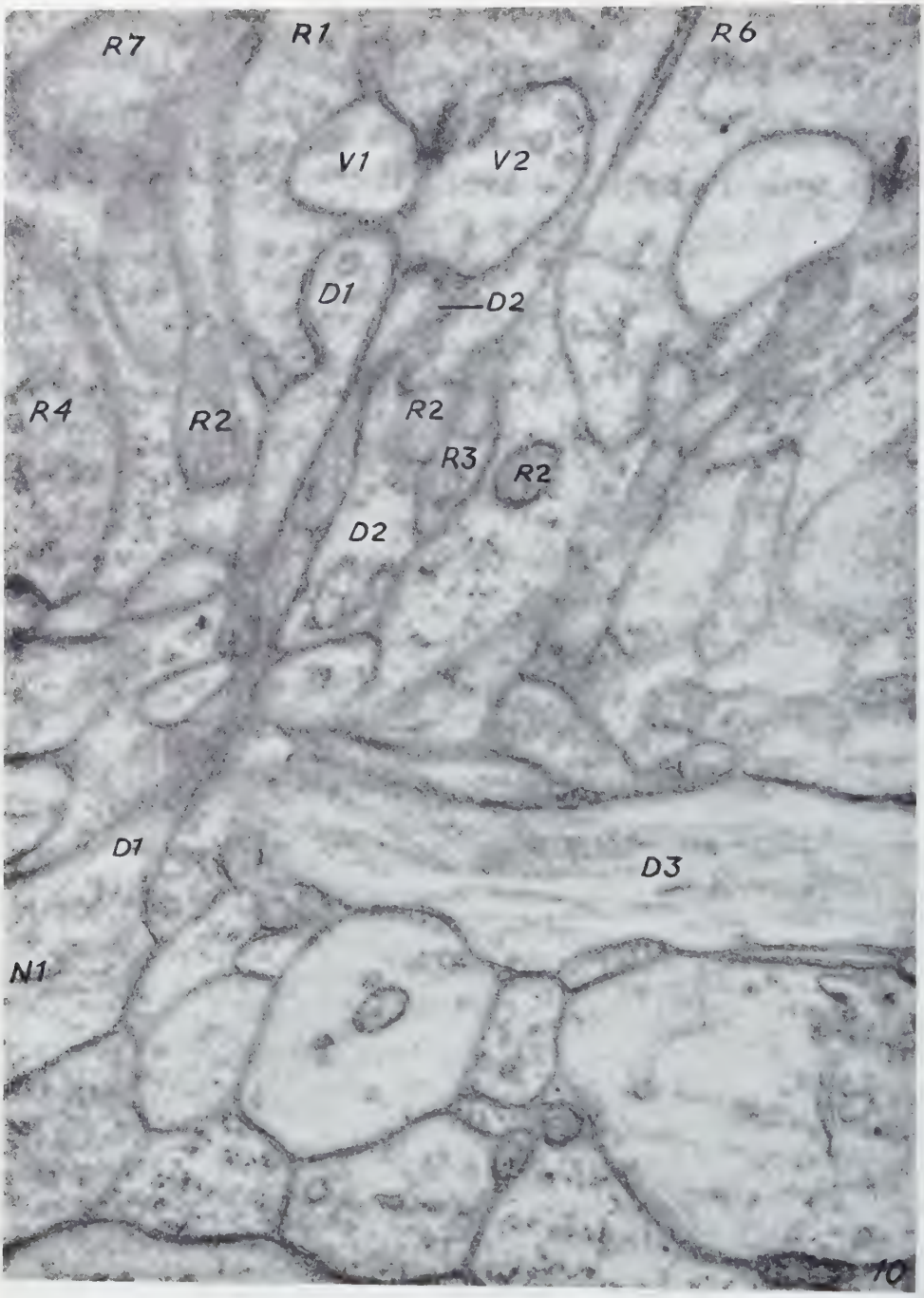
R7
R1
R6
V1
V2
D1
D2
R4
R2
R2
R3
R2
D2
D1
D3
N1
10

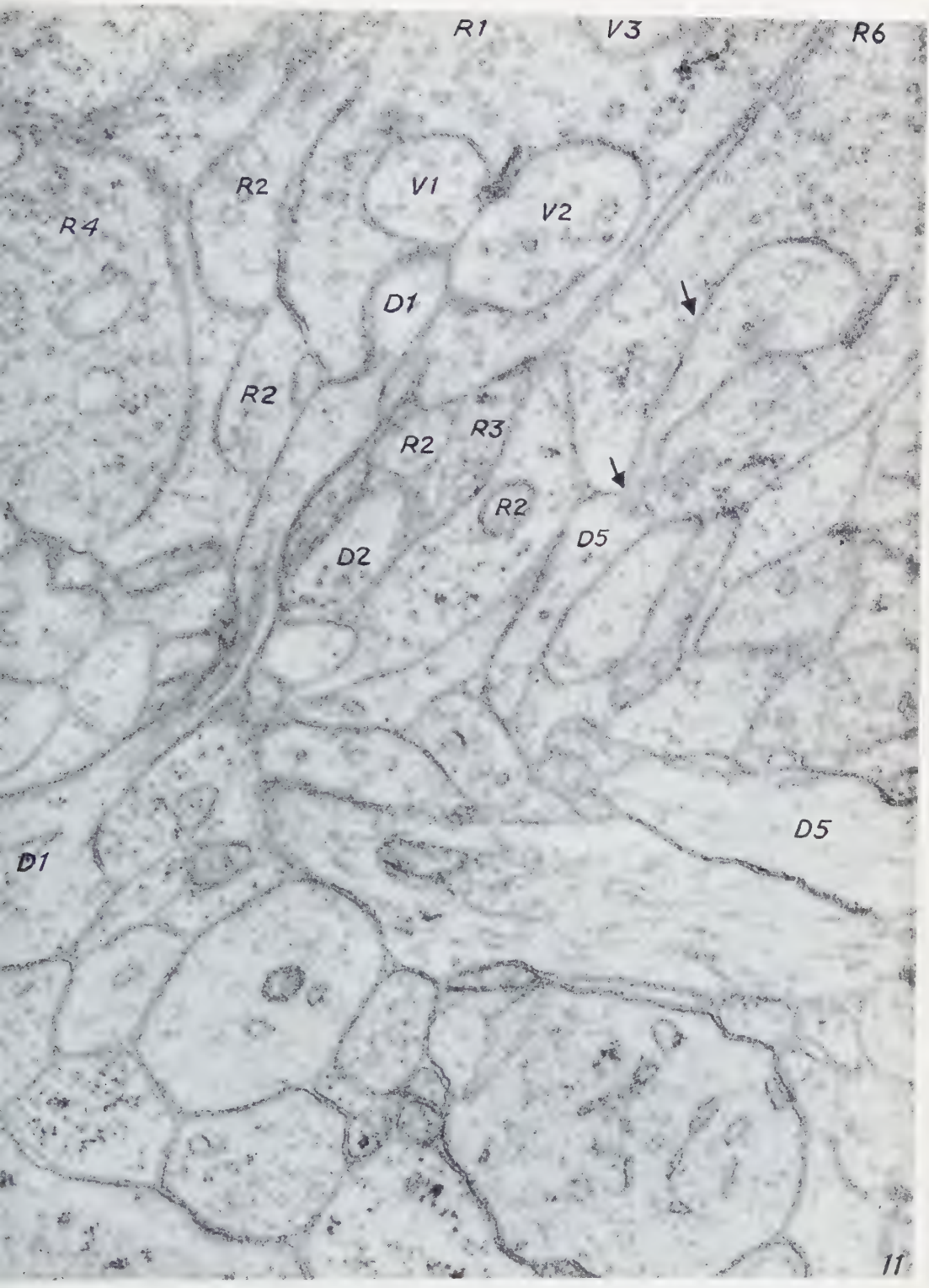
R1
V3
R6
R2
V1
V2
R4
D1
R2
R3
R2
R2
D5
D2
D5
D1
11

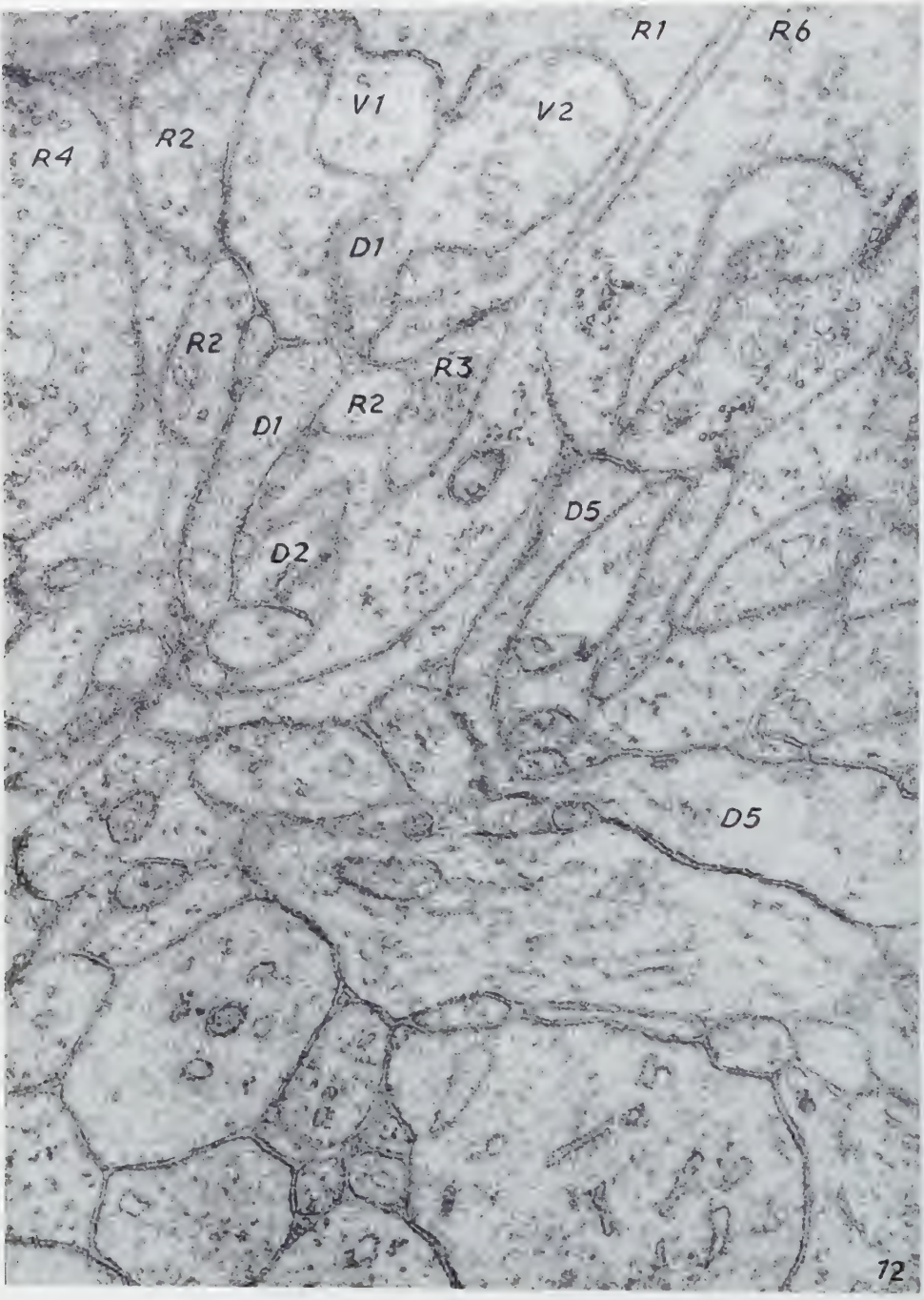
R1
R6
V1
V2
R4
R2
D1
R2
R3
R2
D1
D5
D2
D5
72

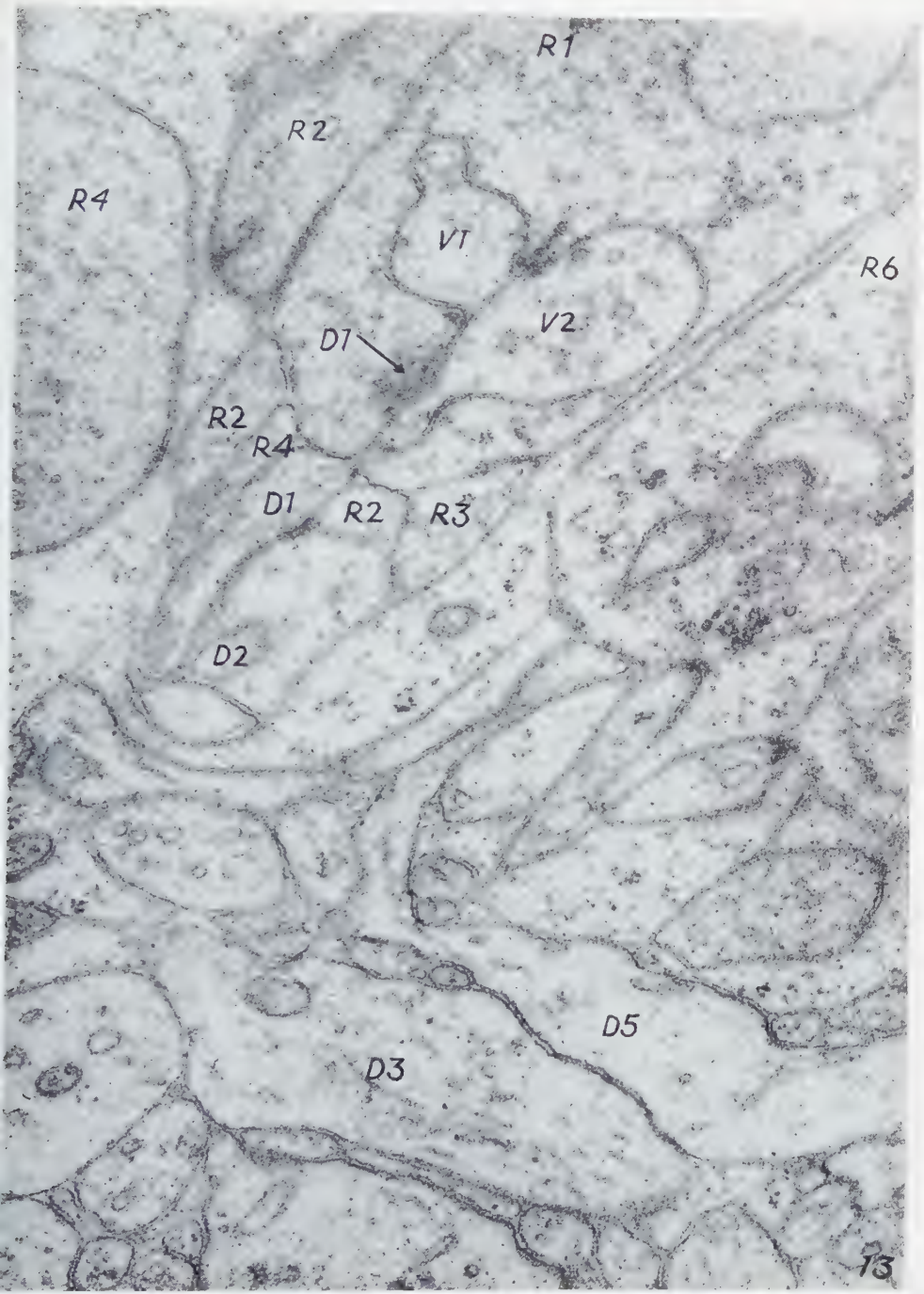
R1
R2
R4
V1
R6
V2
D1
R2
R4
D1
R2
R3
D2
D5
D3
13

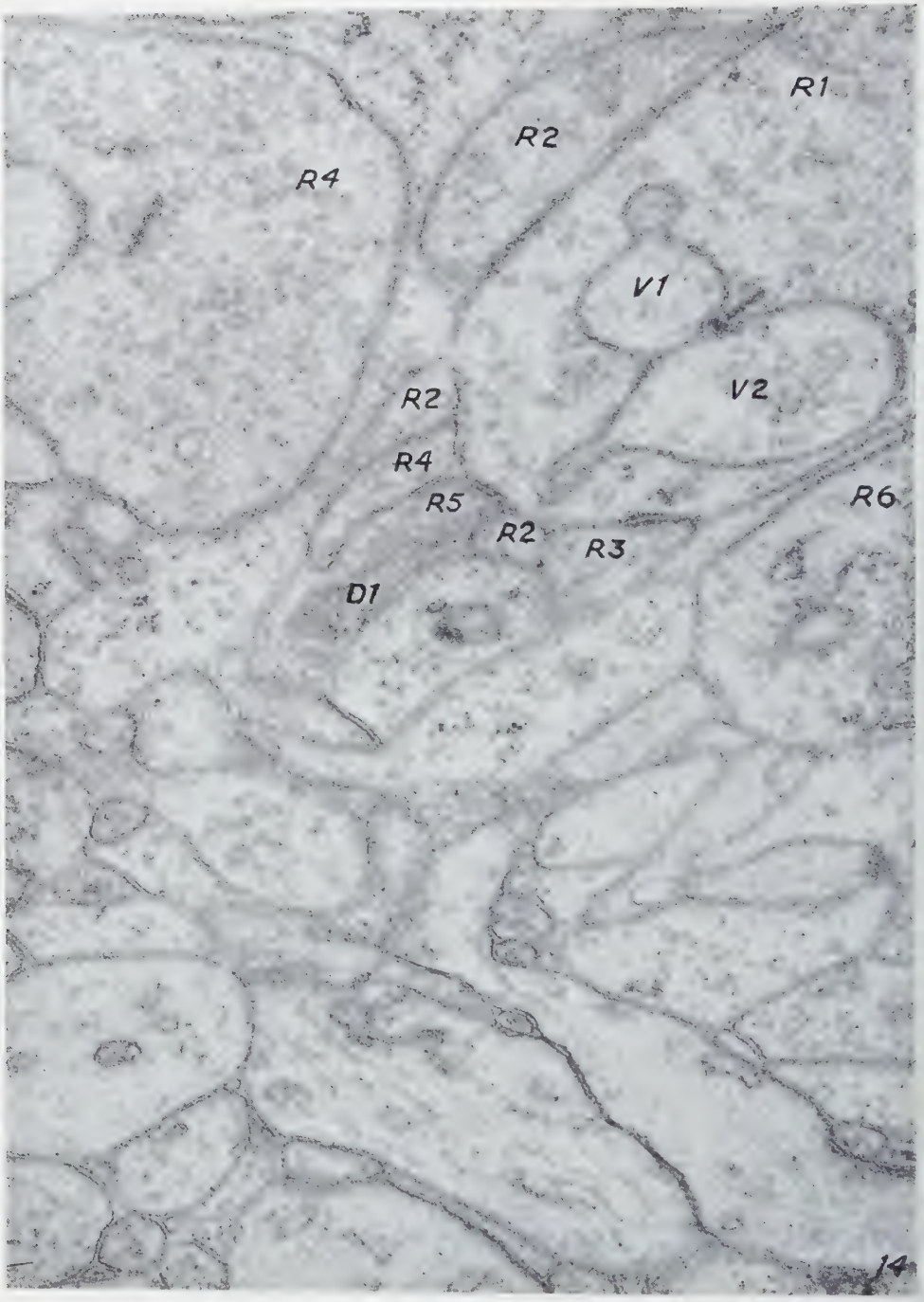
R1
R2
R4
V1
V2
R2
R4
R5
R2
R3
R6
D1
14

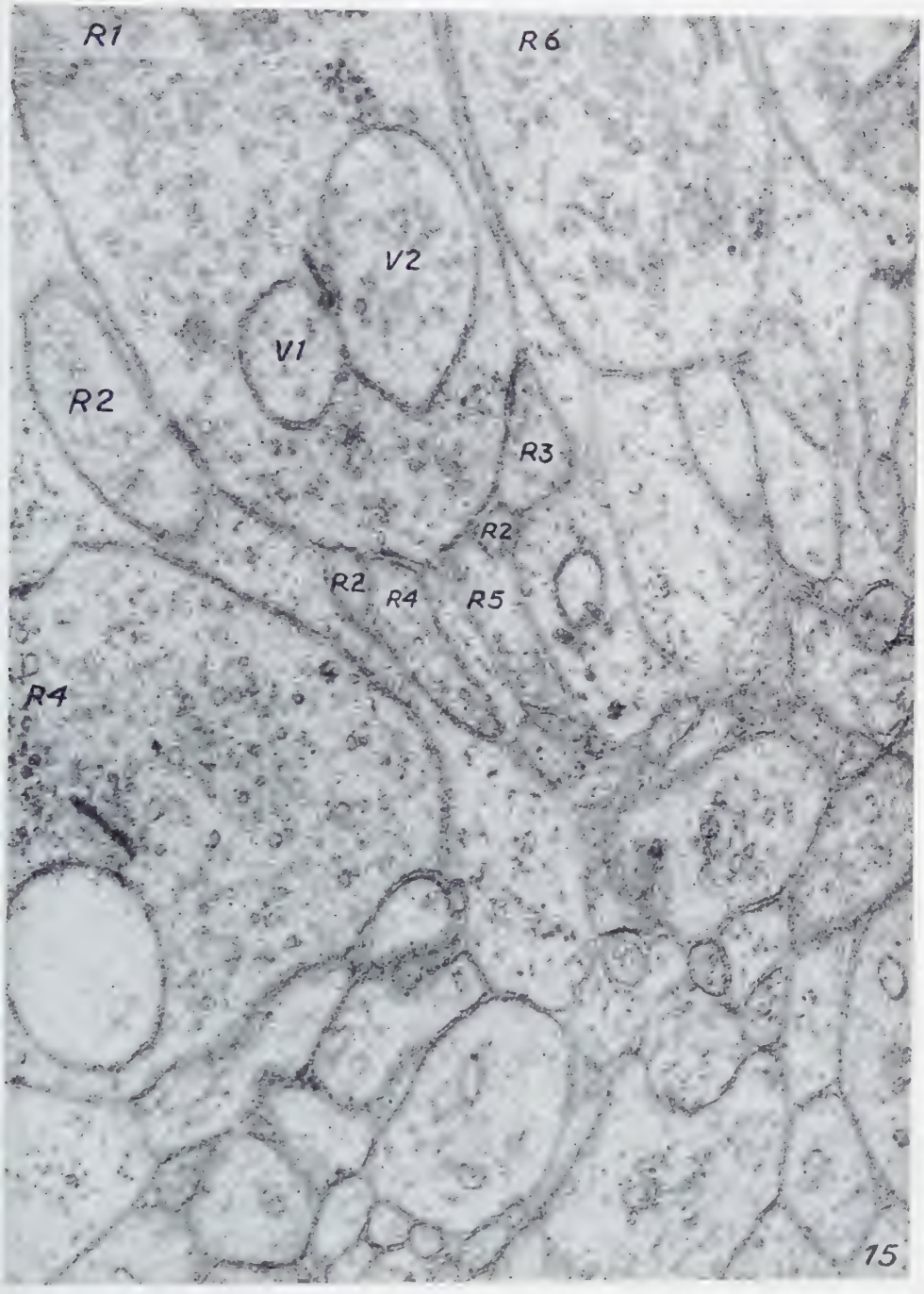
R1
R6
V2
V1
R2
R3
R2
R2
R4
R5
R4
15

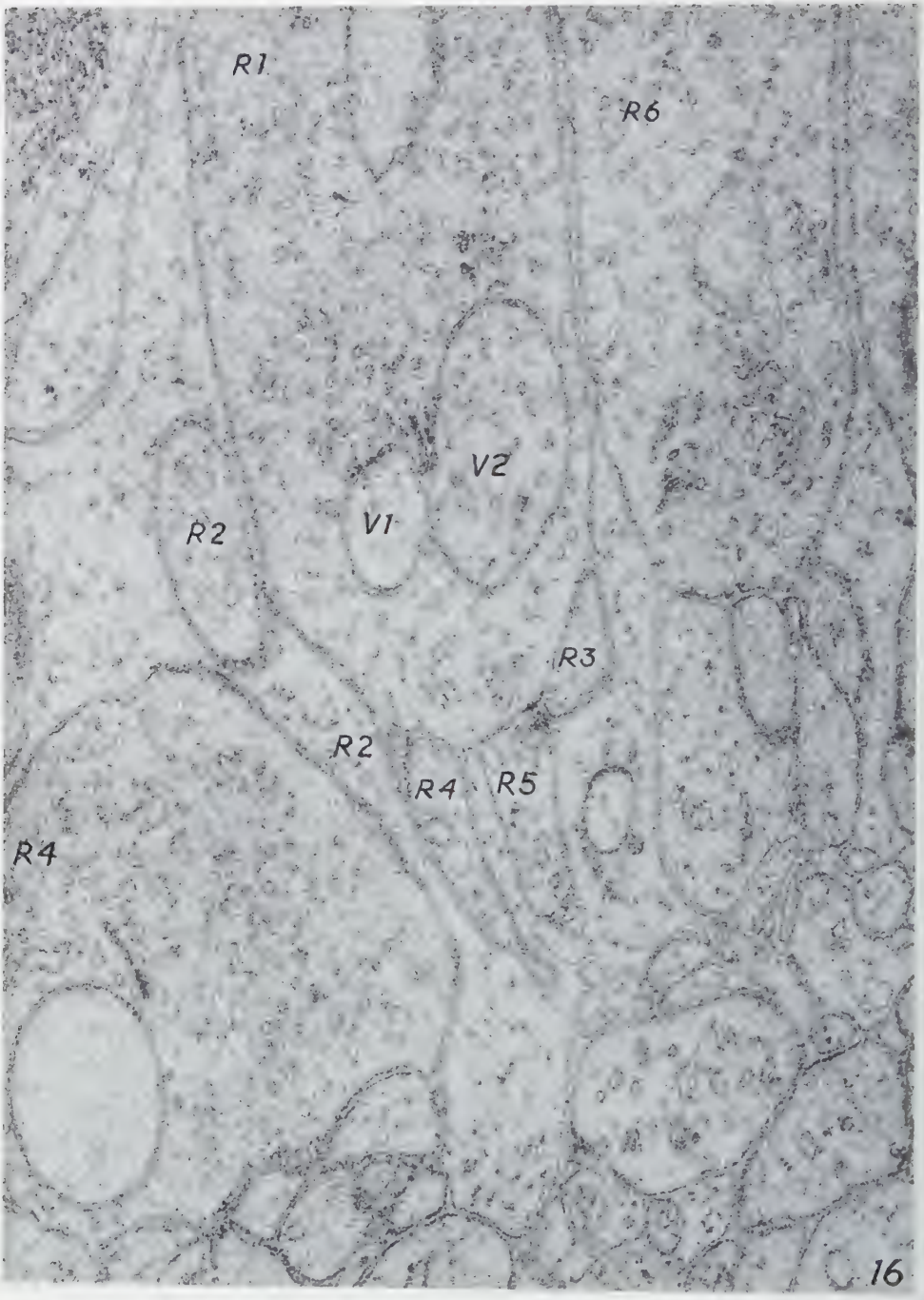
R1
R6
V2
V1
R2
R3
R2
R4
R5
R4
16

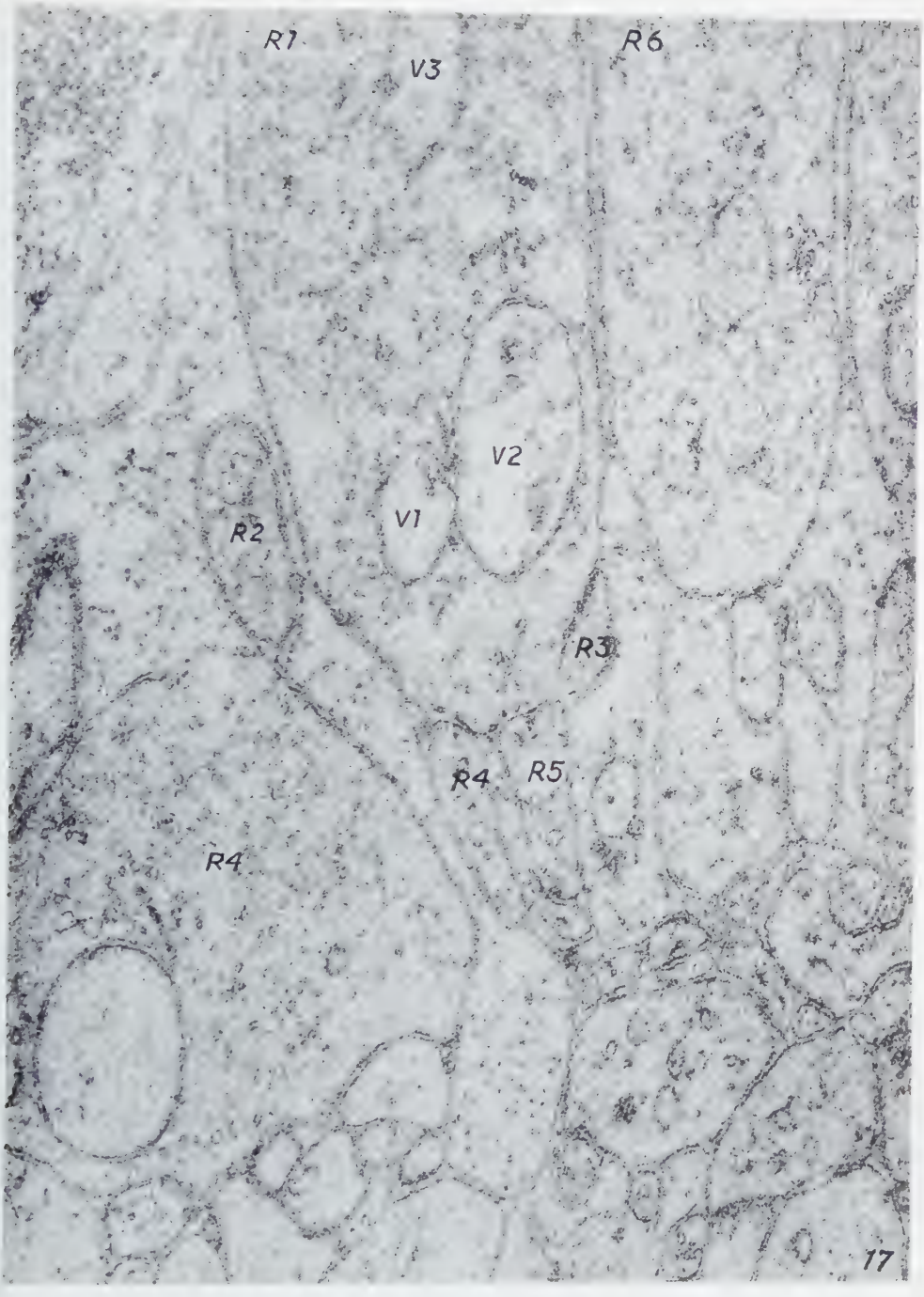
R1
V3
R6
V2
V1
R2
R3
R4
R5
R4
77

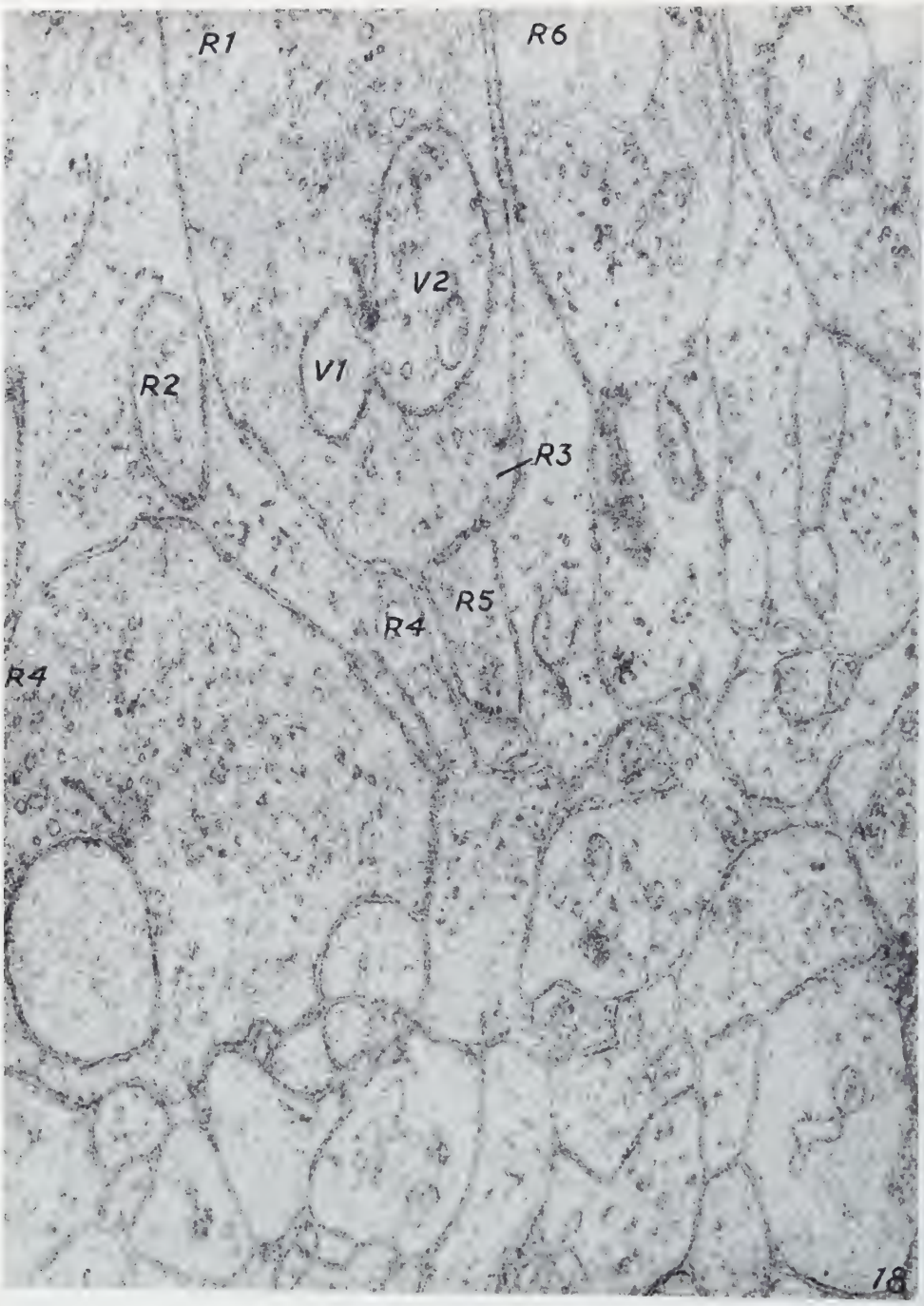
R1
R6
V2
V1
R2
R3
R5
R4
R4
18

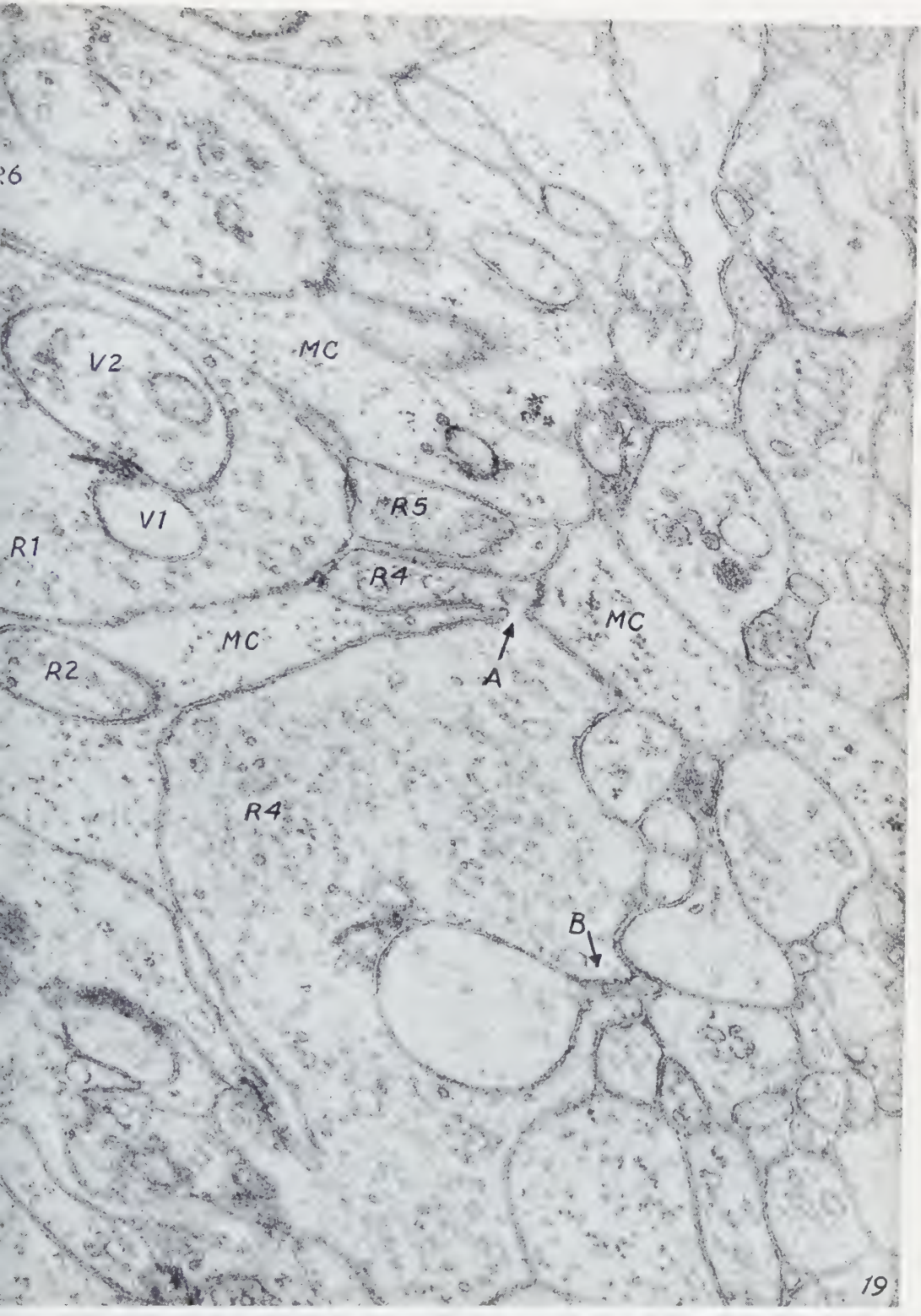
26
V2
MC
V1
R5
R1
R4
MC
MC
R2
A
R4
B
19

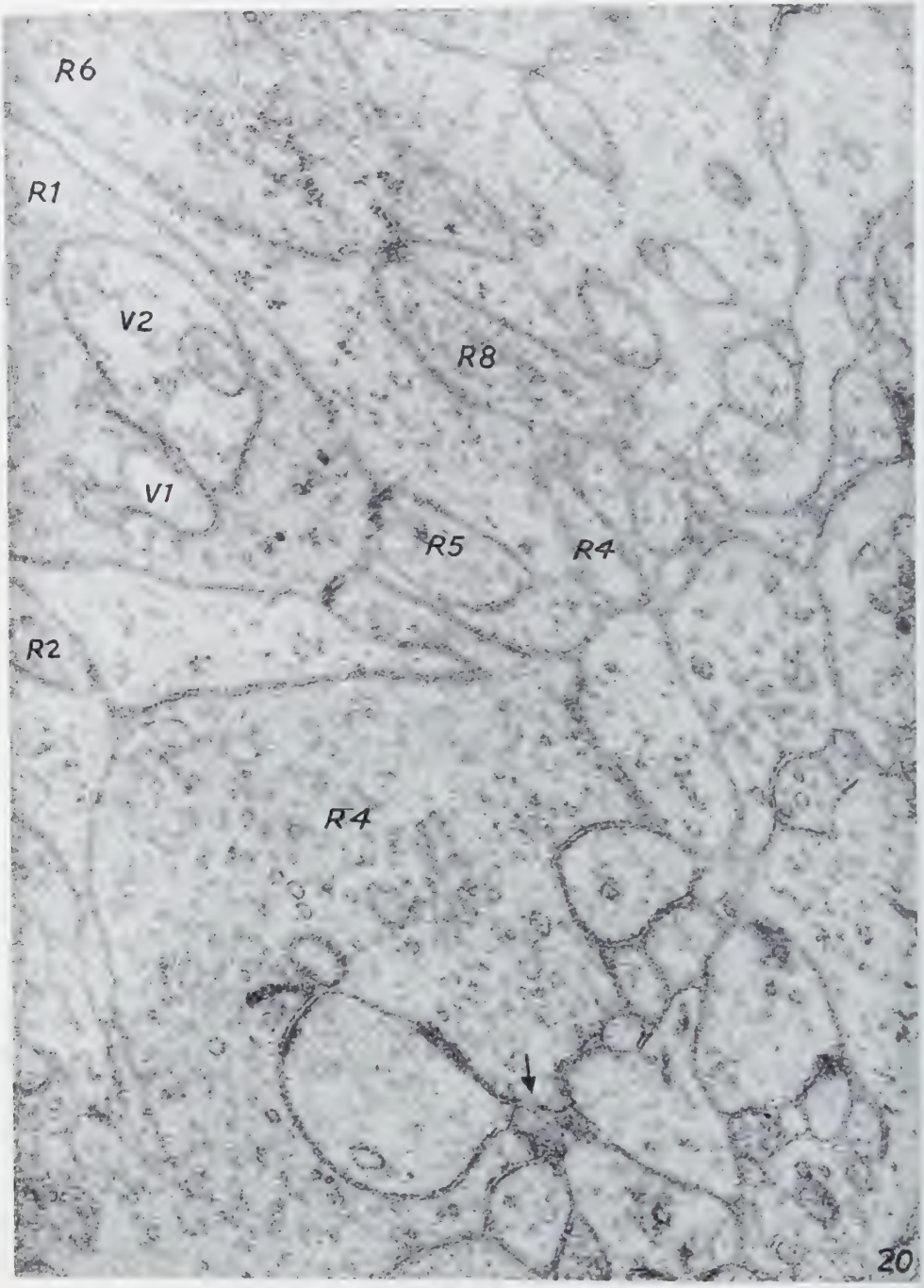
R6
R1
V2
R8
V1
R5
R4
R2
R4
20

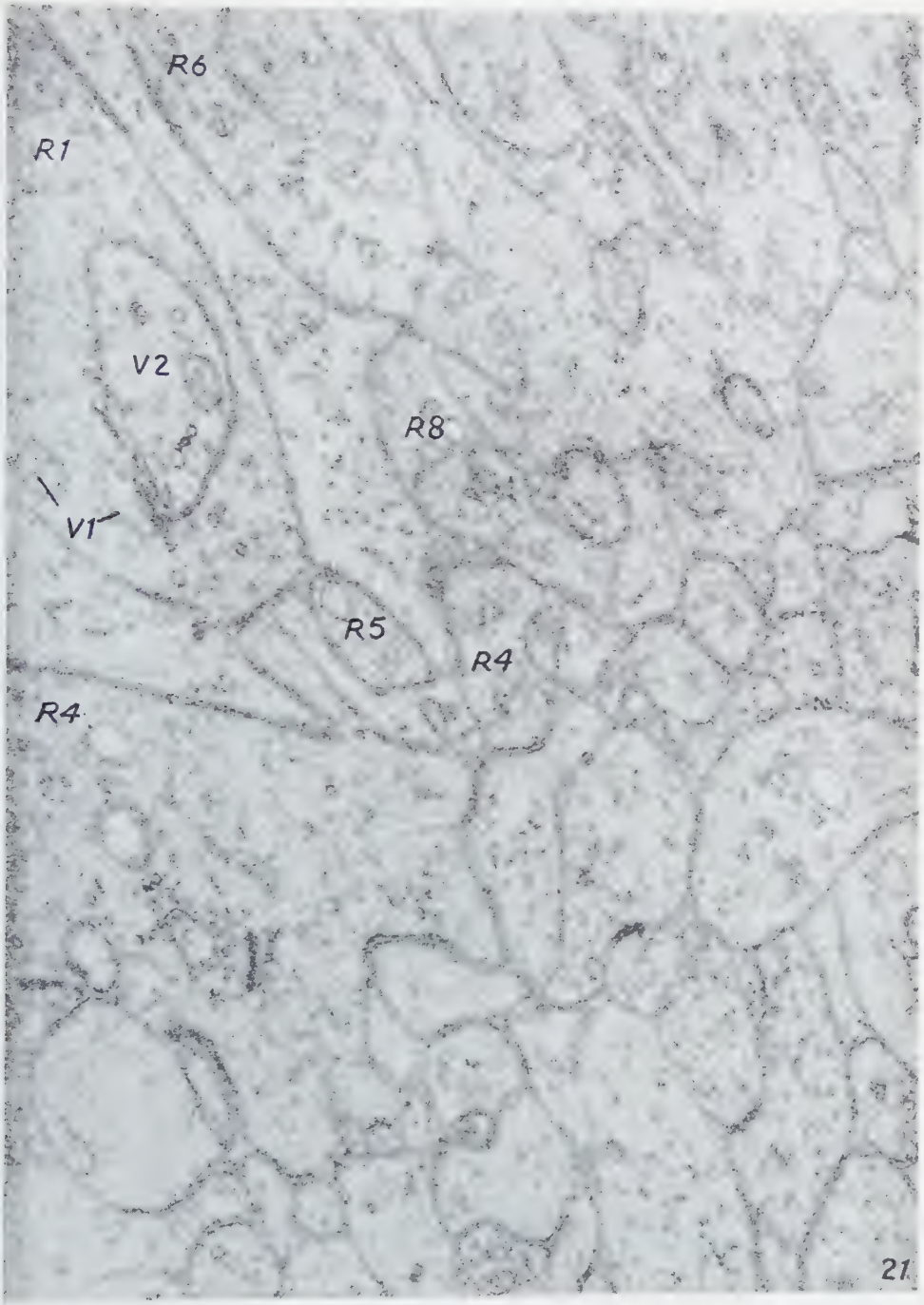
R6
R1
V2
R8
V1
R5
R4
R4
21

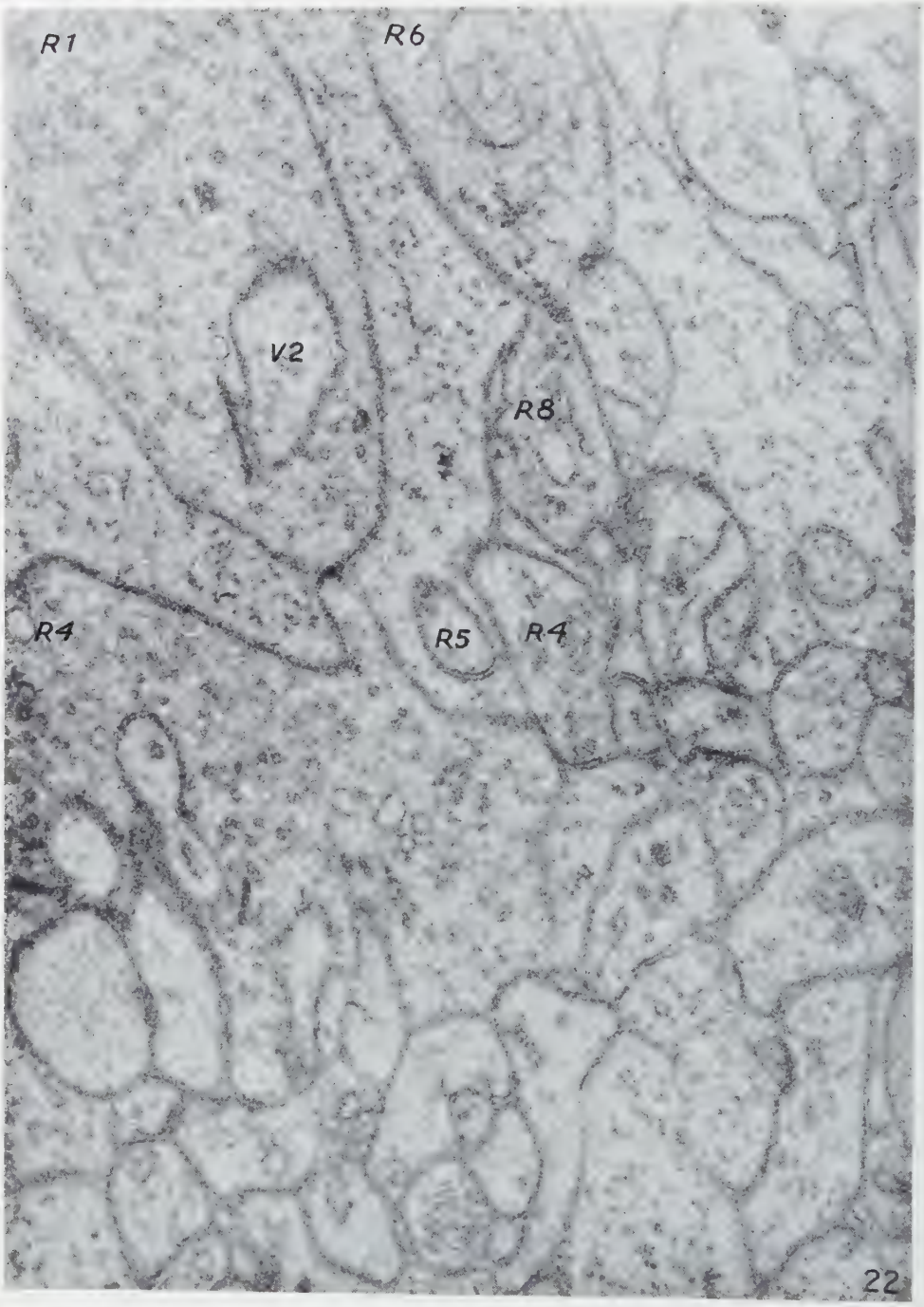
R1
R6
V2
R8
R4
R5
R4
22

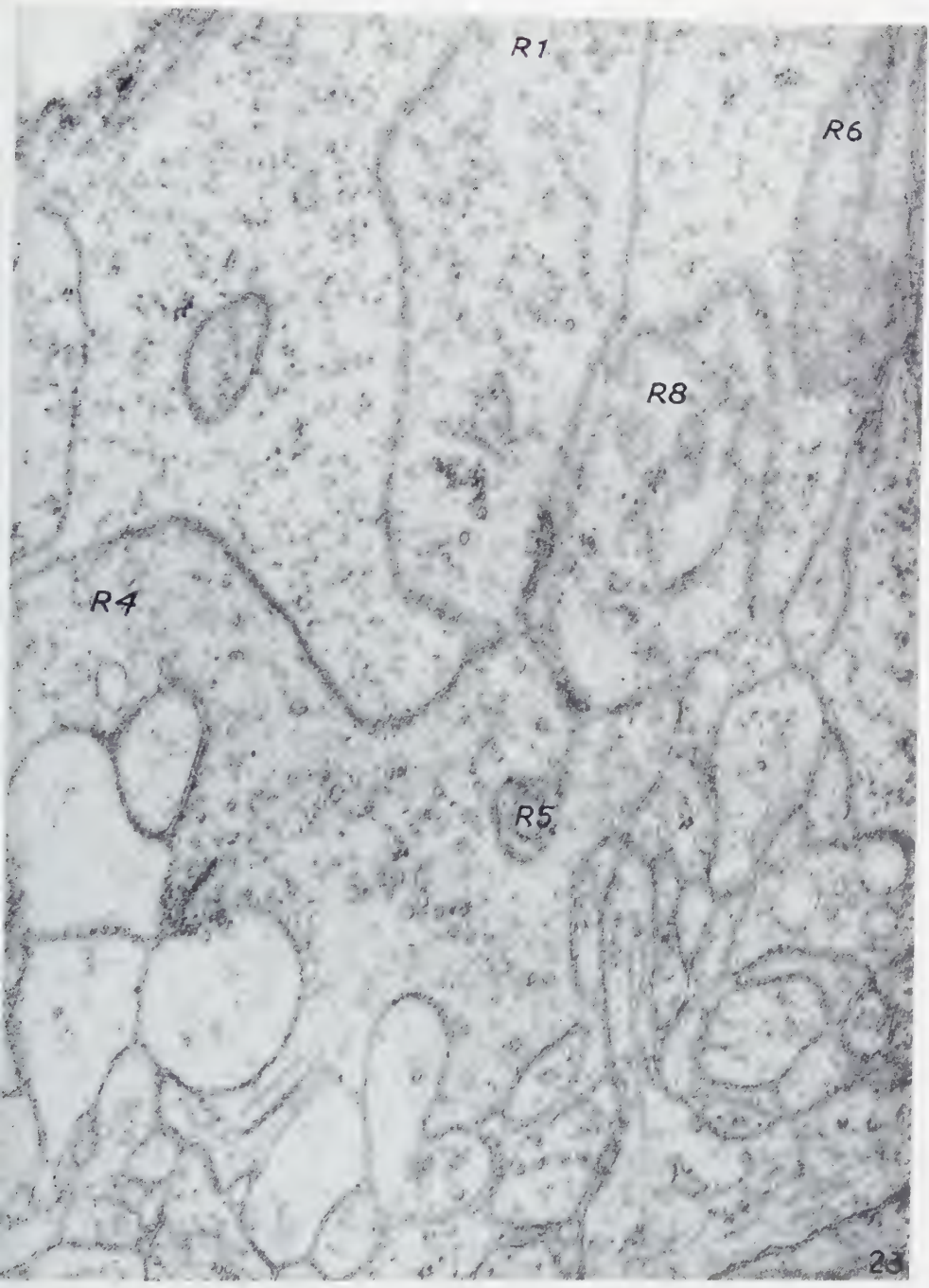
R1
R6
R8
R4
R5
23

In *section No. 17*, Fig. 9, the end vesicle of dendrite *D*1 communicates with traces of the extrasynaptic part of the dendrite. A layer of cytoplasm (Müller's cell cytoplasm?) separates the two dendrites *D*1 and *D*2.

The extrasynaptic part of dendrite *D*1 is still more visible in *section No. 18*, Fig. 10. The intrasynaptic part of dendrite *D*2 is represented by a tangentially sectioned part of its bounding wall. This section represents the thickest section in the whole series, and the discreteness of the details is therefore reduced appreciably as compared to the other sections of the series. Fortunately, the main features of the various structural components that have been analyzed can still be observed.

In *section No. 20*, Fig. 11, dendrite *D*1 can be traced all the way from the cell body of a bipolar cell, part of which is visible at the left-hand lower part of the picture, to the synaptic body *R*1. The two arrows point to a synaptic vacuole in the synaptic body of receptor *R*6 which reaches the surface of the synaptic body at the point where one dendritic branchlet approaches its vitreal pole. No definite signs point to a continuity between the dendrite and the synaptic vacuole. It appears more likely that *D*5 ends with a dendritic end vesicle inside *R*6.

In *sections No. 21 and 22*, Figs. 12 and 13, the dendritic vesicle of *D*1 is represented by tangential or almost tangential sections through its wall. Notice the stalk of synaptic vacuole *V*2. In section No. 22 and the following sections, a branch from receptor *R*4 can be seen extending to the vitreal pole of the synaptic body of receptor *R*1.

In *section No. 23*, Fig. 14, as well as in sections No. 21 and 22, a branch from receptor *R*2 makes contact with the lateral surface of the synaptic body of receptor *R*1. In section No. 23, the first indication of a branchlet from receptor *R*5 is observed as a tangential section through its wall.

In *sections No. 24–40*, Figs. 15–23, the continuity between the main part of the body of receptor *R*4 and that part which, in the preceding sections, appeared as a fragment located at the vitreal pole of *R*1 is demonstrated (see section No. 29, Fig. 19, arrow *A*).

In *section No. 29*, Fig. 19, at arrow *B*, the stalk of one synaptic vacuole of receptor *R*4 is observed reaching the vitreal surface of the synaptic body. The unclear structural relations at this point are demonstrated in *section No. 31*, Fig. 20. However, in no case has it so far been possible to observe any continuity between any synaptic vacuole and a structural component located outside the synaptic body.

In section No. 31 and the following sections, another synaptic body belonging to a receptor (*R*8) appears. Furthermore, a new extension from receptor *R*4 can be seen which appears as an individual component in *sections No. 31–35*, Figs. 20–22, but as a branch from the synaptic body of receptor *R*4 in *section No. 40*, Fig. 23. The branch from receptor *R*5 is completely surrounded by parts of receptor *R*4

in section No. 40. The identification of $R5$ as a branch from a synaptic body of a receptor is not conclusive because this component has not been traced all the way to its origin. It leaves the series of sections in section No. 40. The assumption that it belongs to a receptor is based on its similarity morphologically to the other branches which have definitely been identified as belonging to receptors. The drift, which is observed in the last electron micrographs of the sections of the series, depends on a rupture of the supporting film.

The Construction of Three-Dimensional Models of the Receptor Synapses

Two methods were tried in order to achieve an idea regarding the three-dimensional arrangement of the synaptic bodies. For the first, a large number, about 1000, synaptic bodies were studied in sections cut at different angles through the retina. Especially sections cut perpendicularly and those cut in a tangential direction to the retina were instructive. They revealed that, in spite of a great variation in the structural patterns observed, there was sufficient repetition of certain features to make it obvious that a definite basic pattern common to all synaptic bodies could be suspected.

When cutting sections in an approximately tangential direction through the retina, the plane of the sections always becomes oriented obliquely to the layers of the retina. This is obvious from the fact that the retina has a curved form. This means that a number of synaptic bodies will be cut through at various levels. Assuming an identical structural organization of all synaptic bodies and an identical orientation of the structural components, this would mean that information similar to that obtained from serial sectioning would be obtained from such oblique sections. The individual variations are, however, sufficient pronounced to introduce a great uncertainty in evaluating these patterns.

From the analysis of roughly transversal and longitudinal sections through the synaptic bodies, a model representing the main structural organization was worked out. This model was then made in plasticine by free hand. The model was divided by sections oriented at various levels and at different angles. The patterns observed in the cut surfaces were compared to those observed in the electron micrographs and the model modified until most of the latter patterns could be explained as sections through a body basically of the form presented by the model.

This part of the analysis clearly showed that the strongly osmiophilic material located close to the paired vesicles formed a continuous ribbon-shaped component. When lining up the sections obtained by serial sectioning, the synaptic ribbon therefore was used as a reference structure (see further below).

The second method for revealing the three-dimensional form of the synaptic bodies was identical to the classical method used in light microscopy for an identical

FIGS. 24–34. Three-dimensional reconstruction of the synaptic body of a rod cell of the retina in the guinea pig eye and of its connections with adjacent synaptic bodies of retinal rods. The reconstruction has been made from a series of forty serial sections by drawing the outlines of each section on sheets of celluloid and cutting out the contours of the various components according to the classical method for three-dimensional reconstructions from series of sections. For description, see p. 160.

purpose, that is, three-dimensional reconstruction from series of sections. A careful reconstruction was made from *inter alia* a series of 40 ultrathin sections through the layer of the synaptic bodies, the layer of the dendrites of the bipolars and part of the layer of the bipolars.

The contours of the structural components in each section were drawn in India ink on sheets of transparent cellophane, a method proposed by Bang and Bang (*2*).

26

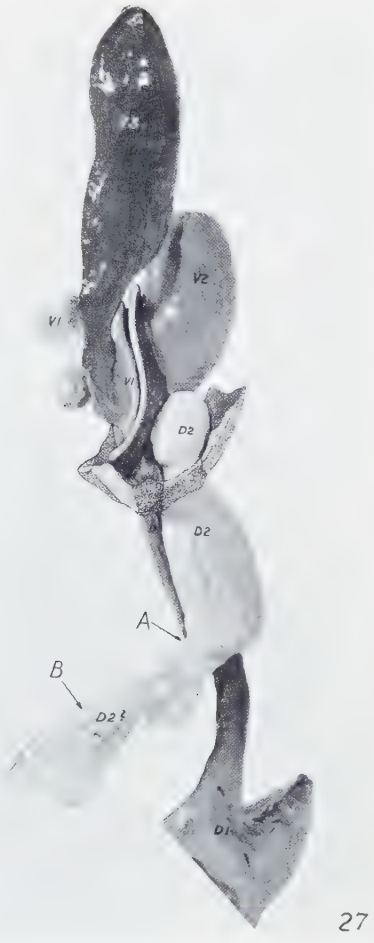

27

Two sets of such drawings were made. The sheets of cellophane were then piled up on top of each other. In the one set of drawings, all the sheets of cellophane were glued together with small drops of acetone. Then the pile was divided into eight parts each one containing five sheets. The five sheets of cellophane in these eight series were then carefully glued together by wetting their surfaces with acetone. By means of a dentist's drill (Dentalair)[1], the various components were cut out rather crudely in such a way that all components were kept mutually in the original orientation. Bridges of cellophane were left to secure this orientation of the various

[1] Generously put at the author's disposal by Atlas Copco Inc., Stockholm.

components. Then the eight series of "sections" were glued together and the shape of the various components smoothened.

A long series of ultrathin sections represents sections that vary in thickness to a certain extent. These variations must not be too large for two reasons. First, only very thin sections make it possible to obtain clear-cut electron micrographs of the various structural components. In the present case, the dimensions of these components are many hundred Ångström units which would indicate that a particularly good resolution would not be necessary. However, these components appear in the pictures because they are bounded by a surface membrane. It is all the time these surface membranes that are made use of for plotting the structural pattern. Further-

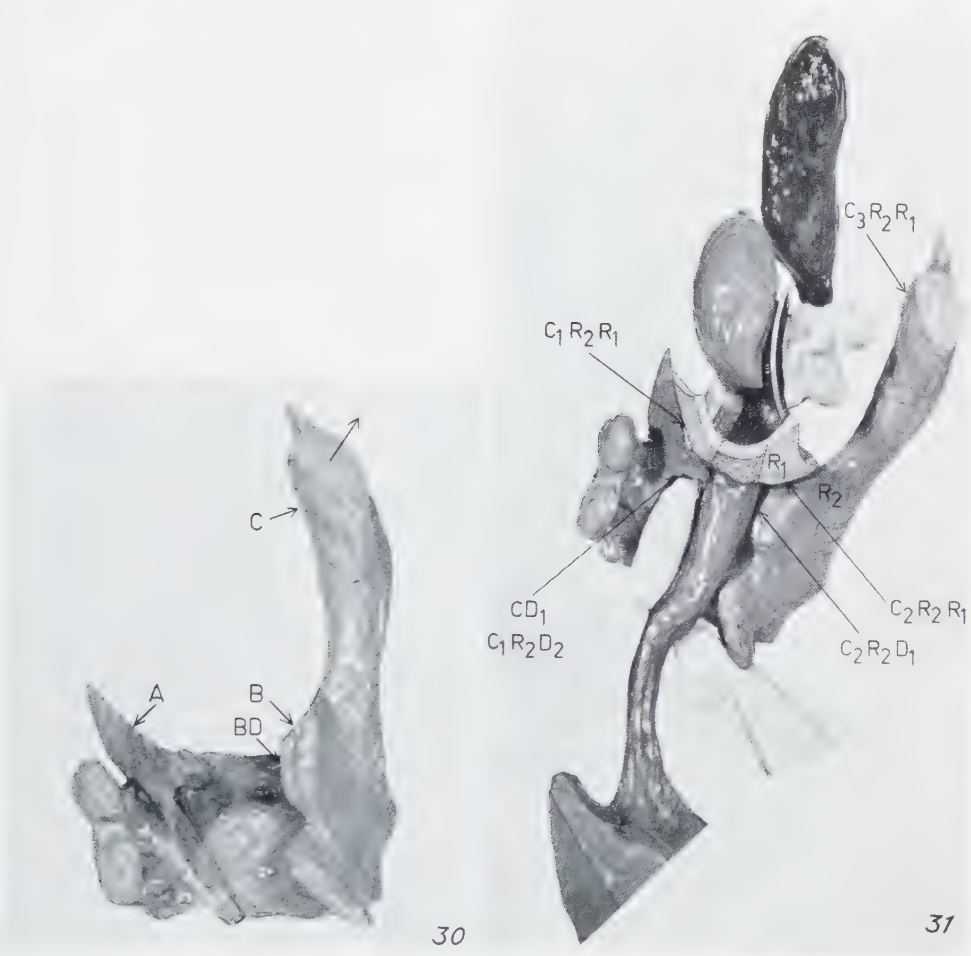

more, it is only the 40–60 Å thick, osmiophilic layer of this surface membrane that can be directly observed. Such a layer is easily recognized when oriented perpendicularly to the plane of the section due to the favourable contrast conditions. However, when these layers are oriented obliquely to the plane of the section, it is necessary to have access to very thin sections in order to see the layer. The superposition effect, which interferes when dealing with insufficiently thin sections, spoils the chances for a reconstruction.

For the second, the variation in thickness is associated with a variation in the "compression" of the sections in a direction parallel to the relative movement of the knife edge and the tissue block. This factor means that the dimensions of the structural

components, when measured in this direction, are more or less distorted. The variation in distortion, when comparing the sections in a series, obviously depends on the variation in their thickness and, therefore, on the performance of the microtome. It is of importance that, within the whole field from which a reconstruction is being made, the variations are definitely smaller than the size of the smallest structural components included in the reconstruction. In the reconstructions made during this study, the surface of the various components has been smoothened to represent approximately the average position of the contours in the drawings.

When making three-dimensional reconstructions in light microscopy it is recommended to include an external indicator which can be used when mutually orienting the series of drawings or wax cut outs made from the microscope pictures of the sections. This has not been considered necessary in the present case and seems to be practically impossible to realize. The variation of the "compression" of the sections makes it more difficult to make reconstructions the larger the area that the reconstruction will cover. An external indicator would introduce a large error because it would have to be placed in a position rather far from the region in the tissue block that is of interest.

The problem of orienting the drawings made from the sections in relation to each other is simplified in the present case by the fact that we are dealing with membranes, the orientation of which is clearly indicated in the pictures. Furthermore, we know that the plasma membrane is a continuous structure. It is therefore rather useful as an internal index for orienting the sections. The synaptic ribbon represents another component that is ideally suited for this purpose.

When orienting the drawings of the sections in the present study, the part of the plasma membrane of the synaptic bodies, which is covering the region at its vitreal pole, and the synaptic ribbon were used for orienting the drawings in relation to each other. This means that two lines, which in most pictures are oriented at right angle to each other, were used for orientation. In no case, the orientation was influenced by any assumption regarding the mutual relations of any other components. Their form and arrangement were considered definitely as unknown.

The reconstructions have been made at 40,000 times magnification, and the thickness of the sheets of cellophane has been one millimeter corresponding to an average thickness of the original sections of 250 Å. From the form of the synaptic bodies, as shown in the reconstructions, this value for the assumed average thickness appears to be quite realistic.

Description of the Three-Dimensional Reconstruction Made from Serial Sections

Fig. 24 shows the three-dimensional model of the synaptic body with two dendrites attached to its vitreal pole. Through a window in the surface membrane, the internal

32

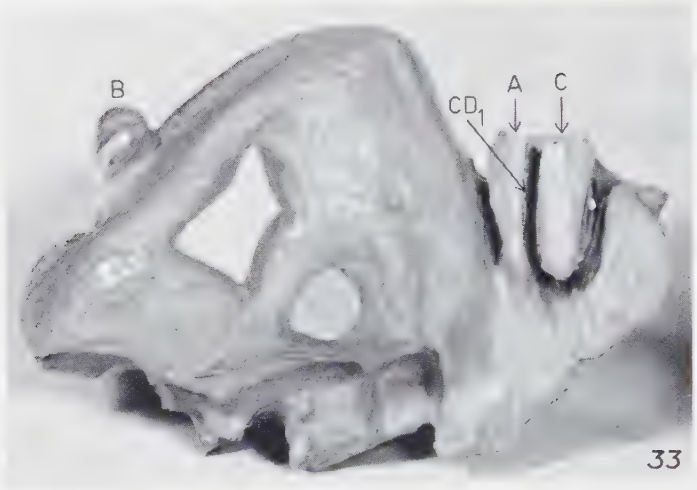

structural components are vaguely observed. After removing most of the surface membrane (Fig. 25), the end vesicles of the dendrites (*D*1 and *D*2), the three synaptic vacuoles (*V*1, *V*2 and *V*3) and the synaptic ribbon (*Ri*) are observed. The dendrites (*D*1 and *D*2) with their end vesicles are located close together. The scleral top surface of the end vesicles of the dendrites is in contact with the paired synaptic vacuoles. The synaptic ribbon (*Ri*) is located in the scleral furrow between the two paired vacuoles. One of these vacuoles (*V*2) is larger with a smooth rounded form with the exception of one process pointing sclerally. The other (*V*1) of the paired vacuoles has a rather irregular form with several outpocketings. A narrow extension of the first-mentioned vacuole almost reaches the plasma membrane close to the vitreal pole of the synaptic body. The third synaptic vacuole (*V*3) extends far in a scleral direction. The widened parts of the dendrites at the vitreal pole are seen. Dendrite *D*1 has been safely traced all the way to its nerve cell body as can be seen from Fig. 11. Dendrite *D*2, on the other hand, has not been traced with certainty further than to the constriction at *A* (Fig. 27). The part *B* cannot be proven to belong to this dendrite. The difficulties in tracing the extension of such components in serial sections are great when the branches are narrow, obliquely cut and surrounded by several profiles of a similar dimension.

In Fig. 26, we observe the model turned about 90° in relation to Fig. 25. The end vesicles of dendrite *D*1 is observed partly covered by vacuole *V*1. The extension of vacuole *V*3 is revealed. The narrow extension from vacuole *V*1, which approaches the vitreal surface of the synaptic body, can be seen at the right side of the end vesicle of dendrite *D*1. The synaptic ribbon can be seen in the scleral furrow between the paired vacuoles.

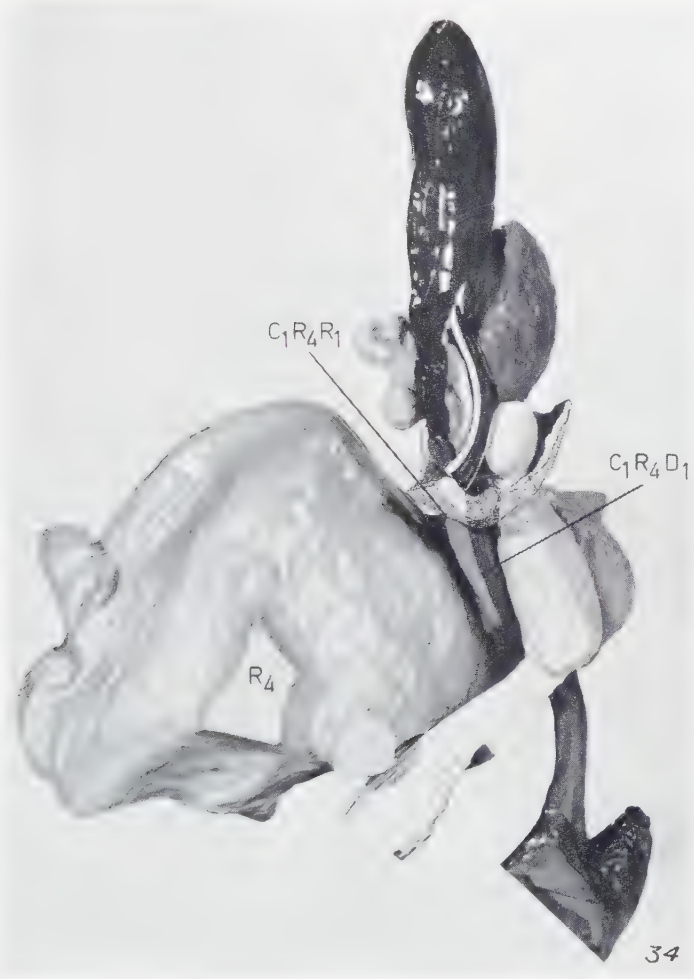

In Fig. 27, the relation between dendrite $D2$ and vacuole $V2$ is observed as well as the uncertain branching off of vacuole $V3$ from vacuole $V1$. The synaptic ribbon shows a twisted course. The parts of the dendrites located below the vitreal pole of the synaptic body offer contact surfaces for the branchlets from the synaptic bodies of receptors $R4$ and $R5$. In Fig. 28, the model has been tilted to show more clearly the arrangement of vacuole $V1$.

Fig. 29 shows the model turned 90° in relation to Fig. 27.

Fig. 30 shows the side of the synaptic body of receptor $R2$ which faces the synaptic body of receptor $R1$. The extensions A and B make contact with the surface

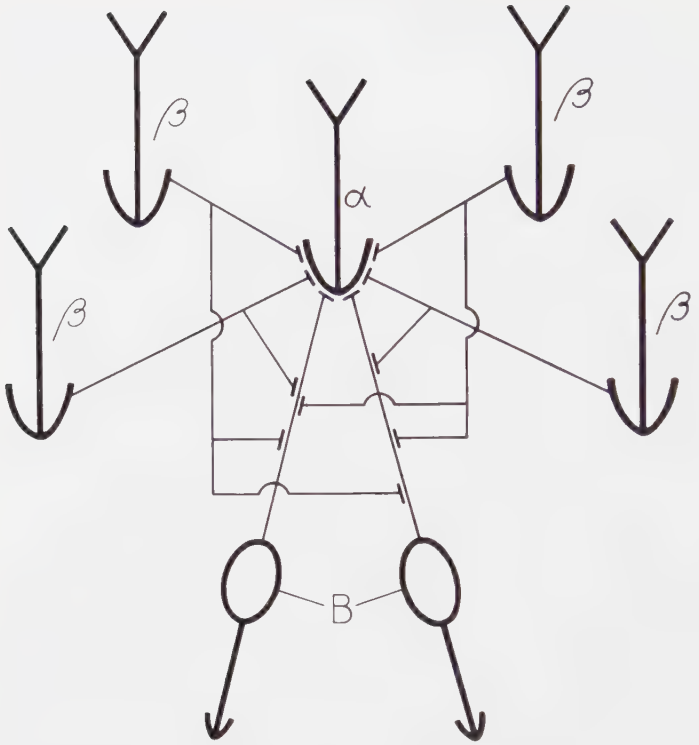

FIG. 35. Schematic presentation of the contact relations of a receptor of the α-type with those of the β-type and with bipolars (*B*).

of the synaptic body of the latter, and *B*, in addition, contacts dendrite *D* 1 (*BD*). At *C*, a fairly large branchlet from receptor *R* 2 extends in a scleral direction and enters into a direct contact relationship with the synaptic body of receptor R 1 above its vitreal pole. The final station of this branchlet could not be revealed because it passed out of the region covered by this series of sections. In Fig. 31, the synaptic body of receptor *R* 2 has been adjusted in its original relation to receptor *R* 1. In Fig. 32, a branchlet presumably belonging to another receptor (*R* 3) makes contact with receptor *R* 1. It has been assumed that this branchlet does not belong to receptor *R* 2 because it passes in a grove in the surface of the synaptic body of receptor *R* 2 in direct contact with its surface for a fairly long distance without showing any tendency to fuse with the latter.

Fig. 33 shows the surface of the synaptic body of receptor *R* 4 which faces receptor *R* 1. It shows two branchlets, *A* and *B*, which make contact with two other receptors, branchlet *A* with receptor *R* 1, at its vitreal pole. Furthermore, it enters into

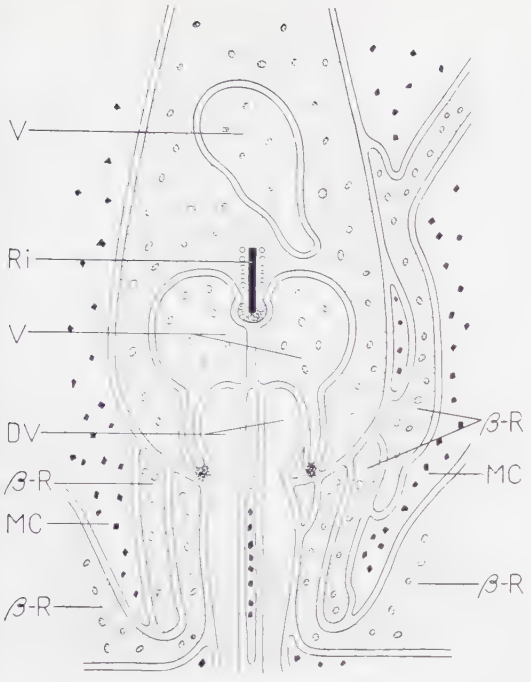

36

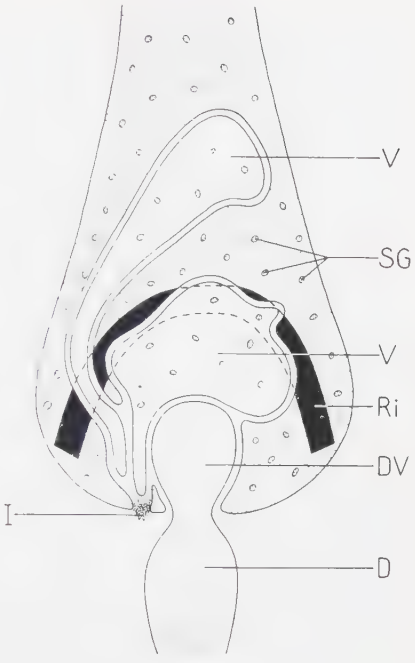

37

FIGS. 36 and 37. Schematic drawings illustrating the main features of the synaptic bodies of retinal rods of the α-type in the guinea pig retina. *V*, synaptic vacuoles; *Ri*, synaptic ribbon; *DV*, dendritic end vesicles; *β-R*, receptor cell of the β-type making contact with the synaptic body of the α-type; *MC*, Müller's cell cytoplasm; *SG*, synaptic granules or vesicles; *I*, site of invagination of the plasma membrane in connection with the synaptic vacuoles; *D*, dendrite from a bipolar. Fig. 37 shows the component of the synaptic body in a projection at 90° as compared to Fig. 36. The drawings show the characteristic arrangement of the plasma membranes of the various components.

contact relation with dendrite *D* 1 along part of its vertical surface. *C* is a branchlet from still another receptor (*R* 5) which passes through a part of the synaptic body of receptor *R* 4 and makes contact with receptor *R* 1 at its vitreal pole as well as with dendrites *D* 1 and *D* 2.

In Fig. 34, the reconstructed fragment of receptor *R* 4 has been arranged in its original relation to receptor *R* 1. The receptor *R* 4 makes one contact with receptor *R* 1 ($C_1 R_4 R_1$) and also with dendrite *D* 1 ($C_1 R_4 D_1$).

A schematic drawing (Fig. 35) illustrates the contact relations at the receptor *R* 1. This drawing represents a first attempt to present what might be considered a "circuit diagram" for the first link in the visual pathway.

In the schematic drawings presented in Figs. 36 and 37, the arrangement of the plasma membranes and the various components of the receptor synapses is illustrated.

DISCUSSION

The synaptic bodies of retinal receptors exhibit a complicated structural organization involving several well defined structural components. In addition to synaptic contacts between receptors and the bipolar cells, an extensive system of interreceptor contacts has been observed. The receptor bipolar cell contacts are mainly located within the synaptic bodies due to the fact that the dendritic branchlets pass through the vitreal pole of the synaptic bodies covered by what appears as an invagination of the plasma membrane of the receptor cell. Within the same invagination, we find the synaptic vacuoles which are partially in contact with the ends of the dendritic branchlets. This arrangement has been characterized as an intracellular synapse (*20*, *23*), a terminology that has been criticized by De Robertis and Franchi (*6*). This criticism is justified if this terminology would give the impression that it referred to a continuity of the cytoplasm of the receptor cell and of the dendrites. Any such continuity has not been observed and has not been assumed. A triple-layered membranous structure always separates the two cytoplasmic territories. This triple-layered component can be interpreted as representing the two plasma membranes of the receptor and the dendrite in close contact or separated by a narrow interspace. This interspace could be supposed to correspond to an extracellular space as has been proposed by Robertson (*16*) in connection with the axon–Schwann cell relations in the peripheral nerve fibers. Triple-layered structures with two osmiophilic layers separated by a less osmiophilic interspace appear frequently in connection with various cytoplasmic components. For this frequently repeated pattern, another interpretation was tentatively proposed (*21*, *25*, *27*); for a detailed discussion, see (*26*). According to this interpretation, the opaque layers would mainly correspond to protein layers, and the less opaque interspace to layers of oriented lipid molecules. In the case where two plasma membranes are closely associated, this interspace could accommodate two double layers of lipid molecules. The main argument for interpreting this interspace as filled with some kind of "cementing" material is the constancy of its width in spite of the drastic treatment of the tissue in connection with fixation, dehydration and embedding. The actual dimension points to lipid molecules as a possible material. In a study by Fernández-Morán and Finean (*7*) on the myelin sheath of peripheral nerves where a repetition of this layered pattern occurs, the nerve tissue was treated with different lipid solvents. These experiments were interpreted in agreement with the proposal made by Sjöstrand (*22*) regarding the distribution of lipids and proteins in the layered pattern of the myelin sheath.

The opaque layers of the plasma membrane of the dendritic branchlets and of the invagination of the synaptic surface measure 60 Å in thickness and the less opaque interspace 100 Å. The latter figure shows a relatively limited variation. Obviously we

find the same arguments as described above for interpreting the less osmiophilic layer as consisting of some cementing material, alternatively the lipid molecules or mucopolysaccharides of the plasma membranes. A colloid gel has been proposed by Robertson (*17*). It would be possible to accommodate for two double layers of lipid molecules in this interspace if we assume the same dimension of these double layers as the one estimated from electron micrographs for the myelin sheath. This interpretation does not exclude the possibility that the two double layers are separated by an ionic milieu of low ohmic resistance in the living intact tissue which might well function as an intercellular space.

We find identical structural conditions at the boundaries between the receptor cells and the Müller's cells, the dendrites and the Müller's cells, and the bipolar nerve cell bodies and the Müller's cells.

Furthermore, the synaptic vacuoles are bounded by a surface membrane which forms an identical triple-layered structure together with the invagination of the synaptic surface and with the ends of the dendritic branchlets. The precision with which the same dimension appears in all these connections is remarkable.

The synaptic vacuoles are located in the same invagination as the dendritic branchlets (Figs. 8 and 36). No observations have so far made it possible to interpret these vacuoles as continuous with any structural component present on the cytoplasmic side of the invagination or with the end vesicles of the dendritic branchlets. One narrow extension of each paired vacuole reaches, or almost reaches, the vitreal surface of the synaptic bodies. At the tip of this extension, the plasma membrane of the receptor cells forms the invagination in which the vacuole is wrapped. Some opaque material separates the synaptic vacuoles from the structural components located at the outer surface of the synaptic body.

The term "intracellular synapse" distinguishes this type of synapse from other known synapses in stressing the fact that the synaptic contact is shielded off from the surrounding structures through the cytoplasm of the synaptic body of the receptor cell. Agreeing with the criticism of De Robertis and Franchi (*6*), this term can be considered improper. The term "invaginated synapses" might be preferable.

The fact that the synaptic vacuoles are localized in what appears to represent invaginations of the plasma membrane of the synaptic bodies would raise the question whether these components should be considered extracellular components. However, it seems likely that the structural integrity and the metabolism of these components are secured by the receptor cell. This might justify to consider them functionally as components or satellites of the receptor cell. The invagination means that the vacuoles communicate with an eventual extracellular space or with the Müller's cells.

If any extracellular space exists in the retina, this space must be confined to what appears in fixed preparations as a 100 Å wide interspace between the osmiophilic

layers of the plasma membranes of receptor cells, neurons and Müller's cells or to a part of this interspace. This extracellular space might well have been reduced in dimensions during fixation, dehydration and embedding. If the reduction would be considerable, there would, however, be some difficulties in understanding the extremely uniform shrinkage of this space. If this space contains a high concentration of inorganic ions (Na^+), the ohmic resistance along this space would be low and this space might eventually represent the outside of the depolarizable membrane of receptors and neurons.

According to the second possibility, the plasma membrane of the Müller's cells would be included in the system. The combination of receptor or neuron plasma membrane and the Müller's cell plasma membrane would then represent the depolarizable membrane and the cytoplasm of the Müller's cells the "outside" milieu.

The interreceptor contacts observed so far represent contacts between the β-cells and the surrounding α-cells. The structural characteristics of these contacts make it justified to assume that they are synaptic contacts. From a morphological point of view, conditions are therefore fulfilled for an extensive interference between the receptor cells in connection with their stimulation. It is characteristic that these interreceptor synapses are predominantly located at the vitreal pole of the α-cells immediately at the place where the dendritic branchlets from the bipolars enter the synaptic body. This fact might be interpreted as an adaptation of the synaptic contacts to a timing of the effects transmitted to the bipolar cells and those provoked through the interreceptor interference. Each α-cell is presumably in synaptic relation with 3–4 β-cells, as far as has been observed in the present material. So far no direct interreceptor contacts have been observed between the α-cells. In this connection, it is justified to point out that it has not been possible to follow all branches, which make contact with the individual synaptic bodies, to their origin. The reason is that still larger regions have to be included in the reconstructions in order to cover the complete course of these branches. However, in no case has it so far been possible to trace any such branch to any other origin than the synaptic bodies of the receptors of the β-type.

The branchlets extending from the synaptic bodies of the β-cells to the vitreal pole of the α-cells also enter into a direct contact relation with the dendritic branchlets from the bipolars. The widened part of the latter branchlets, which is located at the vitreal pole of the receptor, offers a fairly large surface area for such contacts. It seems justifiable to assume that the widening of the dendrite represents a structural adaptation for these extensive receptor–dendrite contacts.

According to the analysis presented above, two β-cells are in contact with both dendrites at the vitreal pole of the α-cell, and two β-cells are in contact with only one of the dendrites.

The functional significance of the interreceptor contacts can only be the object for speculations. These contacts presumably mean that the activity in a β-cell receptor can affect the transmitting of impulses from the α-cells to the bipolars. If we assume that the β-cells can exert an inhibitory effect on the α-cells through these contacts, such an effect would very well result in an increase of the contrast in the picture recorded by the retina and would explain at least certain features of the simultaneous brightness contrast. Inhibitory interaction along the visual pathway was postulated by Fry (*8*) to explain many properties of the simultaneous brightness contrast. Bright areas projected onto the retina would activate β-cells that would suppress the impulse transmission of the α-cells. This effect would mean an inhibition of the adjacent α-cells located just outside the boundary of the bright field. On the other hand, the α-cells located at this boundary on the bright side would be less inhibited than those further inside the boundary. The latter cells would namely be inhibited by all β-cells surrounding the α-cell but the α-cells at the boundary only by those adjacent β-cells located in the bright field. The effect would be that the dark field would appear darker and the bright field brighter at the boundary.

A mutual inhibition has been recorded by Hartline *et al.* (*10*) from the compound lateral eye of *Limulus*. The discharge of impulses in the axon of the eccentric cell of one ommatide was inhibited by illumination of other ommatides in its neighbourhood. Unfortunately, the technical difficulties of recording from single receptors in the vertebrate eye have so far excluded any similar observations in vertebrates.

With the technique applied in this study, it seems possible in the future to reveal in detail the basic synaptic patterns of the retina. Such information seems to be a prerequisite for drawing a detailed circuit diagram of the retina. A first trial in this respect, which only covers the synaptology of the α-cells based on the analysis of a few cells, is shown in Fig. 35. With these patterns worked out further, it would be possible to test various alternative modes of interaction in model experiments.

The functional significance of the complex internal structure of the synaptic bodies is obscure, and a morphological analysis alone does not present any basis for an interpretation.

The synaptic granules or vesicles in the receptor synapses appear similar to those observed in, for instance, the nerve endings of the motor end plates (*15*). However, according to a recent study in our laboratory by Andersson-Cedergren (*1*), this component in the motor end plates appears definitely as vesicular. Del Castillo and Katz (*3*) have assumed that the motor end plate vesicles would contain acetylcholine, and De Robertis and Bennett (*5*) have proposed that the synaptic granules or vesicles contain transmitter substances. It might well be that the surface membrane bounding these vesicles or granules represents the site of synthesis of these com-

ponents and that the synthetized transmitter is stored in the granules. Such speculations have to be tested by direct biochemical analysis of the isolated granules.

De Robertis and Franchi (*6*) claim to have observed a reduction in size of the synaptic granules after prolonged exposure to strong light. However, their study was based on only one experimental animal in each experiment, and the normal variations in control animals were not analyzed.

The author is very much indebted to Mrs. A. Kajland for excellent technical assistance. This study has been supported by grants from the Swedish State Medical Research Council, the Wallenberg and the Rockefeller Foundations.

REFERENCES

1. Andersson-Cedergren, Ebba, under preparation.
2. Bang, B. G. and Bang, F. B., *J. Ultrastructure Research* **1**, 138 (1957).
3. Castillo, J. del and Katz, B., *Progr. in Biophys. and Biophys. Chem.* **6**, 137 (1956).
4. Carasso, Nina, *Compt. rend.* **245**, 216 (1957).
5. De Robertis, E. and Bennett, H. S., *J. Biophys. Biochem. Cytol.* **1**, 47 (1955).
6. De Robertis, E. and Franchi, C. M., *J. Biophys. Biochem. Cytol.* **2**, 307 (1956).
7. Fernández-Morán, H. and Finean, J. B., *J. Biophys. Biochem. Cytol.* **3**, 725 (1957).
8. Fry, G. A., *Am. J. Optom. and Arch. Am. Acad. Optom.* **25**, 162 (1948).
9. Gay, H. and Anderson, T. F., *Science* **120**, 1071 (1954).
10. Hartline, H. K., Wagner, H. G. and Ratliff, F., *J. Gen. Physiol.* **39**, 651 (1955/56).
11. Latta, H. and Hartmann, J. F., *Proc. Soc. Exptl. Biol. Med.* **74**, 436 (1950).
12. Newman, S. B., Borysko, E. and Swerdlow, M., *J. Research Natl. Bur. Standards* **43**, 183 (1949).
13. Palade, G. E., *J. Exptl. Med.* **95**, 285 (1952).
14. Polyak, S. L., The Retina. The University of Chicago Press, Chicago, 1941.
15. Robertson, J. D., *J. Physiol. London* **137**, 6 (1957).
16. —— *J. Biophys. Biochem. Cytol.* **3**, 1043 (1957).
17. —— *ibid.* **4**, 349 (1958).
18. Sjöstrand, F. S., *J. Cellular Comp. Physiol.* **42**, 15 (1953).
19. —— *ibid.* **42**, 45 (1953).
20. —— *J. Appl. Phys.* **24**, 1422 (1953).
21. —— *Nature* **171**, 30 (1953).
22. —— *Experientia* **9**, 68 (1953).
23. —— *Z. wiss. Mikroskop.* **62**, 65 (1954).
24. —— *Proc. 3rd Intern. Conf. Electron Microscopy, London*, 1954, p. 428. Royal Microscopical Society, London, 1956.
25. —— *Intern. Rev. Cytol.* **5**, 455 (1956).
26. —— *Ergeb. Biol.* **21**, 128 (1958).
27. Sjöstrand, F. S. and Rhodin, J., *Exptl. Cell Research* **4**, 426 (1953).

NOTICE TO AUTHORS

Journal of Ultrastructure Research publishes papers dealing with the ultrastructural organization of biologic material as analyzed by means of electron microscopy, X-ray diffraction techniques, X-ray microscopy, and polarization optical analysis. Papers dealing with techniques and instruments which are of importance for the development of this field will also be accepted. The field covered by the journal extends from the structure of molecules which are of biologic interest to the level of cell and tissue organization at the limit of the range of light microscopy.

Address: The author's complete address should be placed on the manuscript.

Manuscript: Manuscripts should be sent to the Editorial Office, Department of Anatomy, Karolinska Institutet, Stockholm 60, Sweden. Manuscripts in English, French or German are accepted. The manuscripts should be typed double-spaced on one side of the paper only. Footnotes should be avoided, but if used they must be numbered consecutively and placed on a separate sheet at the end of the manuscript. Authors are requested to conclude their manuscripts with a brief summary not exceeding 150 words, and to indicate an *abbreviated running title* on the title page. Descriptions of technique and sections of minor importance will be printed in small type.

Manuscripts should be submitted in complete and final form for publication. The policy of the editors will be as prompt a publication as is possible. Papers will be published within three to six months after the date of receipt of the manuscripts by the Editors. Galley proofs will be sent to the authors who are requested to return them together with proofs of the figures immediately by air-mail to the Editorial Office. The point of insertion of each figure should be indicated.

Tables and Figures: The dimensions of the printed page, $5'' \times 7''$ or 125×175 mm, should be kept in mind in preparing figures and tables for publication. Each table should be typewritten on a separate sheet and all figures and tables should be identified with the author's name. Figure legends should be typed in sequence on a separate sheet. Graphs and diagrams should be carefully drawn in black ink on white paper or blue coordinate paper, and all drawings should be so prepared and lettered that they can stand a reduction of 50 per cent. No illustrations in color will be accepted unless the author is prepared to cover the cost of reproduction. All figures, whether photographs or drawings, should be numbered consecutively as Fig. 1, Fig. 2, etc. Other illustrations, such as diagrams, should be called Chart 1, Chart 2, etc. Tables should be numbered with roman numerals.

Note: Do not draw on photographs or attach labels directly to them. Labels should be drawn on a transparent sheet of paper or cellophane covering the electron micrograph. The structures etc., to which the labels refer, should be indicated by lines or arrows. The exact position of this sheet in relation to the electron micrograph should be shown by drawing the outlines of the latter on the sheet.

Literature cited: Papers referred to in the manuscript should be listed on a separate page and headed "References". The journal, volume, page number, and year of publication should be indicated. The system of abbreviation given in "List of Periodicals" in *Chemical Abstracts* **50** (1956) should be followed. The references should be arranged in alphabetical order according to the (first) author's surname. They should also be numbered so that each may be referred to in the text by number only. Please follow carefully the following style for punctuation and order of listing:

1. LACY, D., *Nature* **173**, 1235 (1955).
2. PRICE, G. R. and SCHWARTZ, S., Physical Techniques in Biological Research, Vol. III, p. 91. Academic Press, Inc., New York, 1956.
3. SZENT-GYÖRGYI, A. G., MAZIA, D. and SZENT-GYÖRGYI, A., *Biochim. et Biophys. Acta* **16**, 339 (1955).

Reprints: Authors will be furnished, free of charge, with fifty reprints without covers. Additional reprints may be obtained at cost. Order forms will be submitted with the galley proofs. These should be filled in, indicating shipping and billing instructions, and returned with the proofs.

Abstracts: Authors are requested to provide an abstract for *Biological Abstracts* on a special form which is submitted with the galley proofs.

THE BIOLOGY OF HAIR GROWTH

Proceedings of the International Conference on the Biology of the Hair Follicle and the Growth of Hair held in London under the Auspices of the British Society for Research on Ageing

Edited by WILLIAM MONTAGNA and RICHARD A. ELLIS

Arnold Biological Laboratory, Brown University, Providence, Rhode Island

September 1958, 520 pp., illus., $15.00

CONTENTS:

THE STRUCTURE AND FUNCTION OF SKIN

By WILLIAM MONTAGNA, *Brown University, Providence, Rhode Island*

1956, 356 pp., illus., $8.80

CONTENTS:

ACADEMIC PRESS INC., *Publishers*

111 FIFTH AVENUE, NEW YORK 3, NEW YORK, U.S.A.

British Office: Academic Books Ltd., 129 Queensway, London W. 2
German Agency: Minerva, G.m.b.H., Holbeinstr. 25-27, Frankfurt am Main
Indian Agency: Asia Publishing House, Nicol Road, Ballard Estate, Bombay 1

CONTENTS

Printed in Sweden

Uppsala 1958. Almqvist & Wiksells Boktryckeri AB 583563